Novel clinical perspectives of cardiac computed tomography

Thesis

Doctor of the Hungarian Academy of Sciences

Dr. Pál Maurovich Horvat

Semmelweis University

Heart and Vascular Center

Budapest

2018

Table of Content

Abbreviations

ACC	American College of Cardiology
ACS	Acute coronary syndrome
AHA	American Heart Association
AIT	Adaptive intimal thickening
AUC	Area under the receiver-operator characteristics curve
BMI	Body mass Index
BP	Blood pressure
CAD	Coronary artery disease
CAD-RADS	Coronary artery disease - reporting and sata system
CAV	Cardiac allograft vasculopathy
CI	Confidence interval
CFD	Computational fluid dynamics
CM	Contrast media
CNR	Contrast to noise ratio
CP	Calcified plaque
CT	Computed tomography
CTA	Computed tomography angiography
CV	Coefficient of variation
CX	Circumflex coronary artery
DICOM	Digital imaging and communications in medicine
DZ	Dizygotic
EAT	Epicardial adipose tissue
ECG	Electrocardiogram
EDS	Effective luminal diameter stenosis
EDTA	Ethylenediaminetetraacetic acid
EFA	Early fibroatheroma
ELISA	Enzyme-linked immunosorbent assays
ESS	Endothelial shear stress
FBP	Filtered back projection
FDA	Food and Drug Administration
FFR	Fractional flow reserve
Fib	Fibrous plaque
GLCM	Gray level co-occurrence matrix
GLRLM	Gray level run length matrix
GWAS	Genome-wide association studies
H&E	Hematoxylineosin
HIR	Hybrid iterative reconstruction
HR	Heart rate
HU	Hounsfield units
hsCRP	High-sensitivity c-reactive protein
HTX	Heart transplantation
ICA	Invasive coronary angiography
ICC	Intraclass correlation coefficient
IMR	Iterative model reconstruction
IQR	Interquartile range
IRB	Institutional review board
IV	Intravenous

IVUS	Intravascular ultrasound
LAD	left anterior descending artery
LDL	Low-density lipoprotein
LFA	Late fibroatheroma
LM	Left main coronary artery
MACE	Major adverse cardiovascular event
MCP-1	Monocyte chemoattractant protein 1
MDCT	Multidetector-row computed tomography
MESA	Multiethnic Study of Atherosclerosis
MI	Myocardial infarction
MZ	Monozygotic
NCP	Non-calcified plaque
NCEP ATP	National Cholesterol Education Program Expert Panel on Detection, Evaluation, and Treatment of High Blood Cholesterol in Adults
NICE	National Institute for Health and Care Excellence
NRS	Napkin-ring sign
OR	Odds ratio
OCT	Optical coherence tomography
OFDI	Optical frequency domain imaging
PAI-1	Plasminogen activator inhibitor-1
PAP	Plaque attenuation pattern
PCP	Partially calcified plaque
PIT	Pathological intimal thickening
RCA	Right coronary artery
RIA	Radiomics Image Analysis
ROC	Receiver operating characteristics
ROI	Region of interest
SAP	Stable angina pectoris
SCCT	Society of Cardiovascular Computed Tomography
SD	Standard deviation
SE	Semmelweis Egyetem
SIS	Segment involvement score
SISi	Segment involvement score index
SSS	Segment stenosis score
SSSi	Segment stenosis score index
TCFA	Thin-cap fibroatheroma
TNFα	Tumor necrosis factor α
TUKEB	Tudományos és Kutatásetikai Bizottság
VAT	Visceral adipose tissue
VH-IVUS	Virtual histology intravascular ultrasound

1 Introduction

Atherosclerosis of the coronary arteries is the leading cause of morbidity and mortality in industrialised nations.[1] The most dreadful manifestation of coronary artery disease (CAD) is myocardial infarction (MI) or sudden cardiac death with the underlying mechanism of vulnerable plaque rupture and subsequent intracoronary thrombus formation. Acute MI and sudden cardiac death remain the first manifestations of CAD in the majority of the population.[2] Most individuals do not, therefore, experience any symptoms or warning signs before the coronary event (acute coronary syndromes [ACS] or sudden cardiac death) occurs.

The number of people who die from cardiovascular diseases, mainly from coronary heart disease and stroke, will increase to reach 23.3 million by 2030 from an estimated 17.3 million deaths in 2008. Cardiovascular diseases are projected to remain the single leading cause of death by 2030 globally.[3] Cardiovascular diseases are the largest single cause of death, accounting for about 3.8 million deaths each year, or 45% of all deaths across European Society of Cardiology member countries. Ischemic heart disease was the leading cause, responsible for 1.7 million deaths (20% of all deaths) with stroke responsible for 970 391 deaths (11% of all deaths). After cardiovascular diseases, cancer was the next most common cause of death accounting for 1.9 million cases or 23% of all deaths.[4]. The age-standardised death rates per 100 000 from ischemic heart disease is approximately 400 in Hungary, whereas the death rate is below 100 in France.[4]

Diseases of the heart and circulatory system have major human as well as economic costs, mainly due to the fact that cardiovascular disease are being responsible for the largest number of premature deaths before the age of 75 years. Importantly, cardiovascular disease causes a greater proportion of deaths among women (51%) than men (42%) overall. Almost half of these deaths were due to coronary heart disease alone. Coronary artery disease is estimated to cost the European economy €60 billion a year. Of the total cost of CAD in the European Union, around 33% is due to direct health care costs, 29% to productivity losses and 38% to the informal care of people with CAD.

Considerable efforts are ongoing to predict where acute coronary events will happen on an individual plaque level. Histological investigations have revealed three distinct features of plaques associated with acute coronary events: rupture; erosion; and calcified nodule.[5] Two-thirds of luminal thrombi in acute events result from ruptured atherosclerotic lesions characterized by a necrotic core covered by a thin layer of fibrous cap.[5] Plaques vulnerable to

rupture might have the same morphological characteristics as ruptured plaques, but with an intact thin fibrous cap.[6] These lesions - termed thin-cap fibroatheroma (TCFA), with a cap thickness of <65 μm—are considered to be the precursor lesions of plaque rupture, and referred to as 'vulnerable plaques'.[5]

Preventing acute coronary events by identifying patients at risk seems to be the only effective strategy to reduce the burden of cardiovascular disease and improve mortality and morbidity rates. The mechanisms leading to adverse events from atherosclerotic disease are clearly more complex than initially assumed, explaining our difficulties in accurately predicting myocardial infarction at an individual level. Traditional risk assessment strategies such as the Framingham risk score has been shown to predict 10-year risk of MI; however, the prediction at an individual level is quite poor. Furthermore, it is challenging for the clinicians and patients alike to conceptualise and act upon a 10-year risk estimate. Therefore, we must strive for personalized risk assessment that integrates specific imaging information on the atherosclerotic plaques and systemic factors that increase the risk for disease activity and vascular thrombosis. Next generation CAD phenotyping using advanced imaging techniques could improve our understanding of the atherosclerotic disease process and enable efficient triaging of patients into treatment categories ranging from continued risk factor control to coronary arterial revascularization.[7,8] Therefore, the main goals of my research work reflect these notions. In all research projects that I have been involved with or lead since my PhD degree have focused on four main topics: 1) improving the quality and safety of coronary CTA imaging, 2) improving the ability of coronary CTA to identify the high-risk plaque and high-risk patients, 3) assessing complex interactions between adipose tissue compartments and coronary artery disease and 4) improving the communication of coronary CTA results with referring physicians. The structure of my doctoral thesis follows this course of thoughts and reflects my research path.

2 Background

2.1 Cardiac CT: technical developments and challenges

After the first description of CT angiography (CTA) in 1992,[9,10] further technological advances, such as: more powerful X-ray tubes, faster gantry rotation times, multiple parallel detector rings and decreased slice thickness were introduced,[11,12] that allowed the visualization of the coronary arteries.[13] Coronary CTA has emerged as a non-invasive alternative to invasive coronary angiography (ICA) for the diagnosis of obstructive CAD. With its excellent sensitivity and negative predictive value,[14,15] coronary CTA is a robust diagnostic test to rule out severe coronary stenosis and it is widely used as a "gate-keeper" for ICA.[16,17] Multidetector-row CT (MDCT) permits imaging of calcified coronary atherosclerotic plaque using native scan and the additional detection of noncalcified plaque and luminal narrowing by using contrast-enhanced image acquisition.[18] The newest MDCT technology with gantry rotation times of 240-350 milliseconds, temporal resolution of 75-106 milliseconds, coverage in z-direction of 3.2-16 cm, and isotropic resolution of 0.4 mm now provides technical prerequisites for coronary atherosclerotic plaque imaging. Thus, research targeting the qualitative and quantitative assessment of coronary plaque, including assessment of plaque size, composition, and remodelling became feasible.

Coronary CTA permits the non-invasive evaluation of the coronary atherosclerotic plaque, not just the coronary lumen.[19] Coronary CTA provides information regarding the coronary tree and atherosclerotic plaques beyond simple luminal narrowing and plaque type defined by calcium content.[18,19] These novel applications will improve image guided prevention, medical therapy, and coronary interventions. The ability to interpret coronary CTA images beyond the coronary lumen and stenosis is of utmost importance as we develop personalized medical care to enable therapeutic interventions stratified on the basis of CAD characteristics.

Coronary CTA with its high sensitivity and high negative predictive value is an established diagnostic tool for the evaluation of coronary artery disease.[20] Despite the great advances in scanner technology, the image quality remains highly dependent on heart rate (HR) and the regularity of cardiac rhythm.[21,22] Current guidelines recommend that HR should be <65 beats/min and optimally <60 beats/min to achieve excellent image quality and low effective radiation dose.[23] Metoprolol is the first-line intravenous (IV) β-blocker for HR lowering in

patients undergoing coronary CTA.[24] However, a recent survey has revealed that 50% of centers allow an HR >70 beats/min for coronary CTA, mainly because of concerns regarding potential side effects of β-blocker administration (mainly hypotension and bradycardia).[25] The half-life of IV metoprolol is approximately 3 to 7 hours; therefore, if adverse effect occurs as a result of the HR-lowering medication, it may debilitate the patient for hours. These data indicate the need for a safe, short-lasting HR control in the scanner rooms.[20]

Esmolol is an ultrashort-acting cardioselective IV β-receptor blocking agent with a rapid onset (within 2-3 minutes) and ultrashort duration of action (mean half-life [$t_{1/2}$]= 9 minutes).[26] The rapid onset and offset of effects of esmolol provide an element of safety not previously available with longer-acting β-adrenoceptor antagonists.[27] During coronary CTA, short and effective HR control is desirable; therefore, esmolol might be a good alternative to the standard of care metoprolol. There is a lack of evidence regarding the efficacy and safety of IV esmolol administered in a body weight-independent simplified protocol. Furthermore, no direct comparison of esmolol vs metoprolol administration for HR control during coronary CTA is available.

The other crucial factor in coronary CTA image acquisition is the proper iodinated contrast media (CM) enhancement of the coronaries and the left side of the heart. Therefore, high flow rate injection, high concentration and relatively large volume of CM is used in daily practice. However, the highly viscous iodinated CM and the high injection flow rate increase the risk of vessel wall injury resulting in CM extravasation. Contrast media extravasation is a well-known complication of CTA, with an incidence rate of 0.3–1.3%.[28-33] In case of CM extravasation, image quality is deteriorated due to insufficient intraluminal attenuation, leading to an increased number of repeated CTA examinations, which results in extra radiation doses, additional CM load and increased costs.[34,35] Extravasation usually resolves without any serious complications; however, in some instances it can lead to severe injuries.[36] CM has toxic effects on perivascular tissues that may trigger acute and chronic local inflammatory response, tissue necrosis or compartment syndrome.[31,32,37,38] It has been shown that female gender, elderly age, history of chemo- or radiotherapy, low muscle volume and peripheral locations other than the cubital region as injection site increase the risk of CM extravasation.[29,30,39] Three-phasic CM injection-protocol is widely used to achieve optimal attenuation during coronary CTA, which results in high contrast enhancement in the left side of the heart and in a lower enhancement in the right.[40,41] The traditional three-phasic injection-protocol starts with a high flow rate CM injection (>5 ml/s), continues with a mixture of CM and saline, and finishes with a saline chaser

bolus. The relatively large quantity of high viscosity CM could place an increased strain on the vein's wall, which increases the risk of extravasation. Extending the three-phasic injection-protocol with an initial slower saline flux of pacer bolus right before CM administration may open the possibly collapsed vein lumen with less stress on the vessel wall, thus when the contrast material enters the lumen with a higher flow rate, the already pre-dilated lumen is less likely to rupture.

The third factor that greatly influences coronary CTA image quality is linked to the image reconstruction techniques. Image quality is especially important in quantitative plaque assessment. Automated plaque quantification with coronary CTA allows highly reproducible assessment of plaque dimensions, however its performance is influenced by image quality.[42-44] Most coronary CTA studies have been reconstructed with noise prone filtered back projection (FBP). With hardware evolution, vendors facilitated the introduction of computationally intense iterative image processing techniques, potentiating low-dose CT imaging with improved image quality.[45-48] Hybrid iterative reconstruction (HIR) utilizes statistic-model based denoising both in raw and image domains, providing up to 55% noise reduction for cardiac image acquisition at standard tube settings.[49] Moreover, two recent studies demonstrated that HIR has no significant effect on plaque morphology assessment.[50,51] Three-dimensional raw data based reconstruction techniques were introduced with forward modelling of system geometry (focal spot size, shape of X-ray beam, interactions of emitted photons with tissue and detector) additionally to statistical modeling.[52] Preliminary data showed the potential of model based iterative reconstruction techniques to achieve more robust noise reduction and/or improved image quality of coronary CTA.[53,54] There is a growing body of evidence regarding the prognostic value of quantified coronary plaque volume for adverse events. Our study group previously demonstrated significant changes in coronary calcium scores using novel iterative reconstruction algorithms.[55] Novel model based iterative reconstruction could influence measured plaque volumes that ultimately influence individual risk assessment.

The image quality and radiation dose of coronary CTA in patients who underwent heart transplantation (HTx) is of great importance. Cardiac allograft vasculopathy (CAV) is the leading cause of death during the first year HTx. The overall frequency of CAV at 1, 5, and 10 years after transplantation is 8%, 30%, and 50%, respectively.[56] CAV is characterized by diffuse concentric intimal hyperplasia.[57] Because of the denervated transplanted hearts, patients do not experience symptoms related to ischemia; therefore, early diagnosis of CAV is challenging. International guidelines recommend annual or biannual invasive coronary

angiography for the assessment of coronary status. However, invasive coronary angiography has limited diagnostic accuracy to detect CAV because of the diffuse and concentric manifestation of the disease. Furthermore, invasive coronary angiography does not provide information regarding the coronary wall; therefore, intravascular ultrasound (IVUS) or optical coherence tomography (OCT) is suggested as a complementary imaging test.[58] The combination of invasive coronary angiography with intravascular imaging techniques increases sensitivity, but their routine use increases costs and rates of procedural complications; therefore, it is considered optional for CAV assessment.[59] In addition, the International Society for Heart and Lung Transplantation consensus statement does not recommend the routine use of intravascular ultrasound for CAV assessment.[58]

Coronary CTA allows non-invasive visualization of the coronary artery wall and lumen with a high diagnostic accuracy.[18] It can detect 1.5-2 times more coronary segments with coronary atherosclerotic plaques than does invasive coronary angiography.[60] Notably, the absence of parasympathetic and sympathetic innervation of the transplanted hearts results in higher resting HRs, which may compromise the diagnostic performance of coronary CTA. Moreover, because of their higher HRs, retrospective ECG-gating has been used for HTx recipients, which results in higher radiation dose. These concerns precluded the widespread use of coronary CTA in HTx recipients.[61] Prospectively ECG-triggered coronary CTA would be desirable because of its low radiation dose, but it requires a low HR (generally <65 beats/min). The HTx recipients have higher but steady HR with minimal HR variability because of the lack of autonomous innervation. The steady HR of HTx recipients might provide a unique opportunity to scan these patients with low radiation dose and achieve good image quality.

2.2 Imaging coronary artery disease with computed tomography

The identification of patients at high risk of developing acute coronary events remains a major challenge in cardiovascular imaging.[62-64] Current diagnostic strategies focus predominantly on the detection of myocardial ischaemia and haemodynamic luminal narrowing, but not the detection and characterization of coronary atherosclerotic plaques.[2,65] This strategy is based on the evaluation of symptomatic patients and ignores the larger problem of a major adverse coronary events occurring as the first (and only) manifestation of CAD.

In post-mortem studies, most acute coronary events are found to be caused by sudden luminal thrombosis due to plaque rupture.[6,66,67] The morphology of atherosclerotic plaques that

are prone to rupture is distinct from stable lesions (Figure 1a), which provides a unique opportunity for non-invasive imaging to identify high-risk plaques before they lead to adverse clinical events.[68,69] Moreover, the assessment of coronary plaque composition and size are potentially more important than traditional detection of luminal stenosis for predicting devastating acute coronary events.[67,70-72]

Histological investigations have revealed three distinct features of plaques associated with acute coronary events: rupture; erosion; and calcified nodule.[5] Two-thirds of luminal thrombi in acute events result from ruptured atherosclerotic lesions characterized by a necrotic core covered by a thin layer of fibrous cap (Figure 1b).[5] Plaques vulnerable to rupture might have the same morphological characteristics as ruptured plaques, but with an intact thin fibrous cap.[6] These lesions – termed thin-cap fibroatheroma (TCFA), with a cap thickness of <65 μm – are considered to be the precursor lesions of plaque rupture.[5] The spatial resolution of current CT scanners (≈400 μm) precludes the morphometric analysis of fibrous cap by coronary CTA.[73] Histopathological investigations suggest that plaques prone to rupture are enlarged in all three spatial dimensions.[5,74] In TCFAs the necrotic core length is ~2-17 mm (mean 8 mm) and the area of the necrotic core in 80% of cases is >1.0 mm^2.[5] These dimensions are over the plaque detection threshold (>1 mm plaque thickness) for coronary CTA.[75] Moreover, the majority of TCFAs occur in the proximal portions of the main coronary arteries, where vessel diameter is largest, and coronary CTA has the highest image quality and accuracy for the plaque detection.[5,76] In modern CT scanners, the detection and quantification of some features of high-risk lesions might, therefore be feasible.

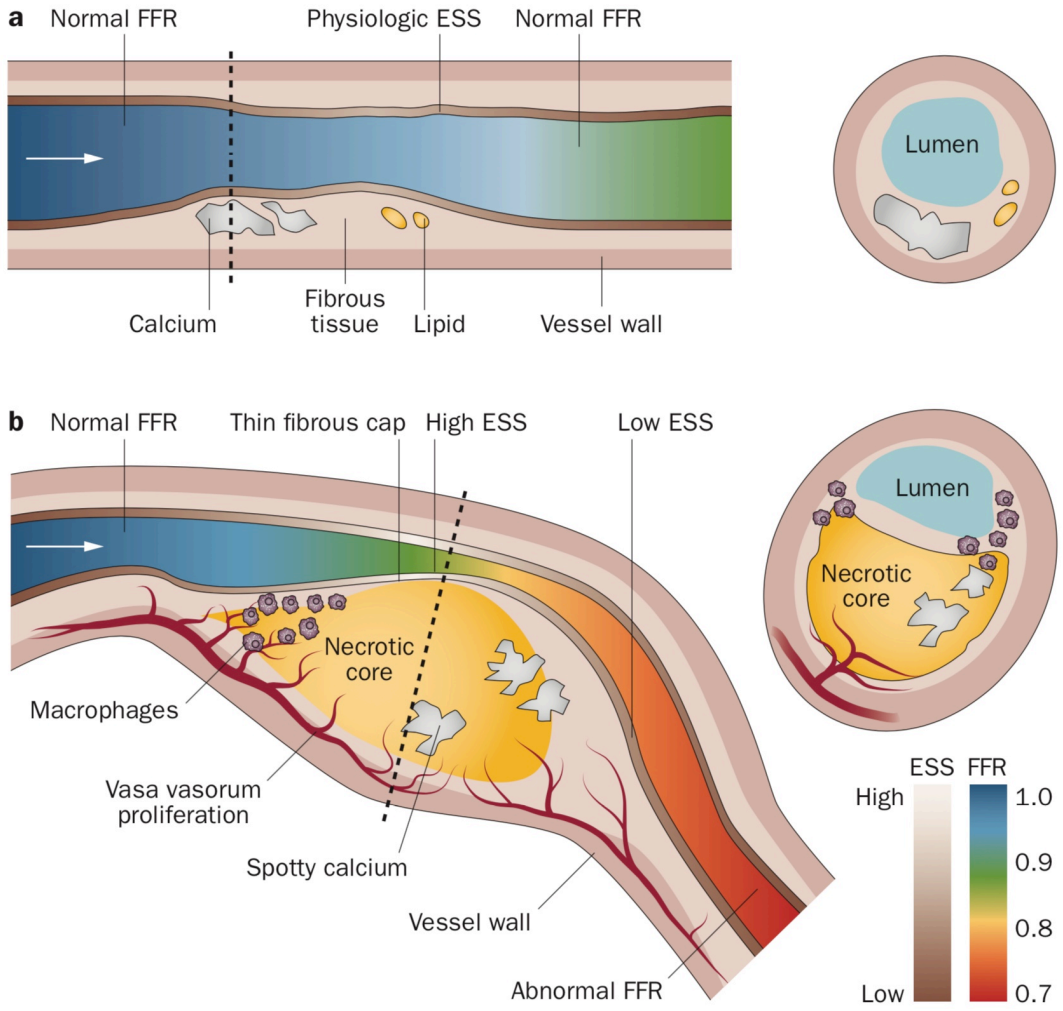

Figure 1 | The morphology and functional characteristics of stable and vulnerable plaques. a | Stable fibrocalcific lesion with calcification and small lipid pools. The plaque leads to mild narrowing of the lumen; and there is no ischaemia after the lesion (FFR >0.8; green). ESS near the plaque is in the normal physiological range indicating undisturbed flow. b | Rupture prone vulnerable plaque with a large lipid-rich necrotic core, thin fibrous cap, neovascularization, spotty calcium and presence of inflammatory cells. Despite the positively remodelled vessel wall at the site of the plaque, the lesion causes severe luminal narrowing and ischaemia (FFR <0.8; red). The downstream plaque region with low and oscillatory ESS promotes plaque growth, whereas the upstream low ESS at the shoulder regions is more inflamed (indicated by presence of macrophages), which might lead to plaque destabilization. High ESS at the most stenotic part can trigger plaque rupture. Abbreviations: ESS, endothelial shear stress; FFR, fractional flow reserve.

2.2.1 Morphologic plaque characteristics

Low attenuation plaques

Lesions leading to ACS often have a large necrotic lipid-rich core; therefore, the CT differentiation between plaques containing lipid-rich material and plaques with predominantly fibrous components is desirable for prediction of ACS.[69] Traditionally, coronary CTA classifies plaques according to the presence or absence of calcified components, thereby differentiating

between calcified (CP), partially-calcified or mixed (PCP), and non-calcified plaques (NCP). The differentiation between CP components and NCPs was feasible even with early multidetector CT technology (such as 4-slice CTs used in the late 1990s).[77,78] However, the classification of NCPs into lipid-rich and fibrous lesions on the basis of CT attenuation values (measured by HU) remains challenging.

Some investigators have correlated coronary CTA plaque assessment with the clinical reference standard IVUS, and report low CT attenuation on average for lipid-rich plaques.[79] Non-calcified plaques with high CT attenuation correlated with fibrous tissue and those with low densities correlated with necrotic core and fibrofatty tissue as assessed by VH-IVUS.[80] In histogram analysis of the intraplaque pixel CT numbers, lipid-rich plaques have a higher percentage of pixels with low HU values compared with plaques of predominantly fibrous components.[81] This observation was validated in an *ex vivo* study that showed that the relative area (area >25%) of intraplaque pixels with <60 HU could accurately detect lipid-rich atherosclerotic lesions (sensitivity, 73%; specificity, 71%).[82] Moreover, low CT numbers were measured in TCFAs identified by optical coherence tomography (OCT; the standard clinical reference for fibrous cap thickness measurements and necrotic lipid-rich core detection) compared with stable lesions (35-45 HU versus 62-79 HU; P <0.001).[83,84] However, the variability of CT values within plaque types is wide. Despite the differences in mean densities between fibrous plaques and lipid-rich plaques, almost all investigators have reported a substantial overlap of densities, which prevented the reliable sub-classification of NCPs.[79,80] Furthermore, CT measurements of coronary plaques are influenced by several factors, such as the concentration of adjacent intraluminal iodinated contrast agent, plaque size, image noise, tube voltage, slice thickness, and the reconstruction filter.[18,85-87] The reliable differentiation between lipid-rich and fibrous lesions made solely on the basis of CT attenuation is, therefore, not yet feasible.[19] New automated plaque quantification software tools, with scan specific adaptive attenuation threshold settings, can potentially overcome some of these limitations and might improve CT number-based plaque component quantification.[88,89] Despite the challenges associated with CT attenuation-based plaque characterization, low CT numbers seem to be a consistent feature of lipid-rich plaques. Low-density plaques, defined by <30 HU average attenuation, were more often seen in patients with ACS than in those individuals with stable angina pectoris (SAP) (79% versus 9%; P <0.0001).[90] The same investigators compared the characteristics of ruptured fibrous cap culprit lesions in patients with ACS with the intact fibrous cap plaques of patients with SAP. Again, the low plaque attenuation was defined as <30 HU, and 88% of ruptured plaques had a low CT attenuation, compared with 18% of the stable

lesions (P <0.001).[91] Similarly, other investigators have also reported lower mean CT densities of NCPs in patients with ACS versus SAP (40-86 HU versus 97-144 HU; P <0.01).[92-94]

Establishing a simple CT number cut-off value across an entire plaque that permits the reliable differentiation between lipid-rich and fibrous atherosclerotic lesions is difficult. However, quantification of CT number variability and identification of focal areas of low CT attenuation are methods that might aid a more-accurate differentiation of vulnerable plaques by coronary CTA. Moreover, culprit lesions in patients with ACS have significantly lower average CT numbers compared with patients who have SAP, suggesting that low CT attenuation is an established high-risk plaque feature (Figure 2).

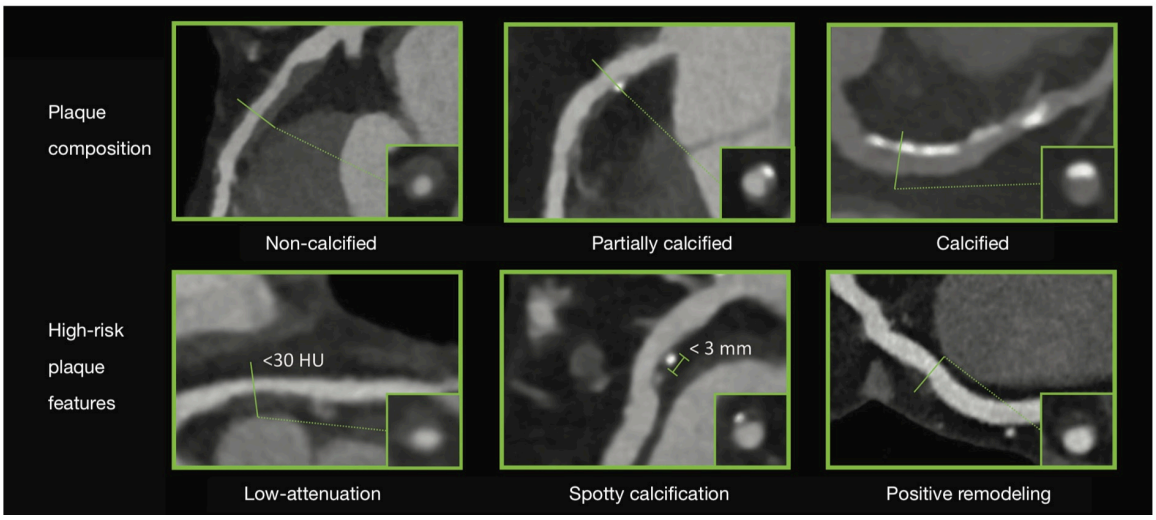

Figure 2 | Representative images of plaque coronary CT angiography-based plaque types

Positive remodelling

Rupture-prone plaques might not lead to significant luminal narrowing, owing to the effect of positive remodelling.[95] Positive remodelling describes the compensatory enlargement of the vessel wall that occurs at the site of the atherosclerotic lesion as the plaque size increases, resulting in the preservation of luminal area.[96] In histopathology studies, positive remodelling is associated with the abundance of macrophages and increased necrotic core.[97] Coronary CTA can measure the outer vessel wall and lumen dimension.[80,98] The remodelling index is calculated as the vessel cross-sectional area at the site of maximal stenosis divided by the average of proximal and distal reference segments' cross-sectional areas.[98] A remodelling index threshold of ≥1.1 was suggested for the definition of positive remodelling visualized by coronary CTA, whereas some authors use ≥1.05 or >1.0 as the cut-off point on the basis of IVUS studies.[99] Automated software now permits the easy quantification of the remodelling

index.[88] The remodelling index assessed by coronary CTA correlates well with IVUS measurements; however, coronary CTA has a trend towards overestimation of remodelling index (95% CI of the mean difference 0.01-0.08; p=0.005).[88,99] Consistent with histopathological data, lesions with positive remodelling on coronary CTA have a higher plaque burden, a larger amount of necrotic core and a higher prevalence of TCFA assessed by VH-IVUS when compared to lesions without positive remodelling.[100]

Furthermore, in two correlative studies comparing coronary CTA with OCT, the CT-derived remodelling index was higher in TCFA compared with non-TCFA lesions classified by OCT (1.14 versus 1.02, P <0.0001; and 1.14 versus 0.95, p<0.0001).[83,84] In a study of 38 patients with ACS and 33 patients with SAP, positive remodelling was strongly associated with culprit plaques in ACS (87%), but not SAP (12%; P <0.0001), and had the best diagnostic performance among other high-risk CT plaque features (low attenuation and spotty calcification) to identify the culprit lesions (sensitivity 87%; specificity 88%).[90] Several other cross-sectional coronary CTA studies have also found a higher remodelling index in patients with ACS compared with patients with SAP (1.14-1.6 versus 0.9-1.2; p=0.001-0.04).[92-94,101] Positive plaque remodelling and/or low plaque attenuation was an independent predictor of ACS in a clinical study with 27 ± 10 months follow-up (HR 22.8; 95% CI 6.9-75.2; p <0.001).[102] Among patients with one of these high-risk CT features, one in five will have an adverse coronary event within 1-3 years, a similar rate to those with a three-feature positive plaque determined by VH-IVUS in the The multicentre Providing Regional Observations to Study Predictors of Events in the Coronary Tree (PROSPECT) trial.[102,103] The remodelling index can be reliably measured by coronary CTA. However, a more conservative remodelling index threshold of 1.1 is preferred in the assessment of coronary CTA (Figure 2).[99]

Spotty calcium in plaques

Calcification is an ever-present feature of advanced coronary atherosclerosis.[104] Coronary calcification assessed by CT is highly associated with plaque burden and related to poor clinical prognosis.[105,106] However, the effect of calcification on plaque instability is controversial.[107-110] Although most acute plaque ruptures in individuals with sudden cardiac death contain some calcification under histopathology, approximately two-thirds have only microcalcification, which is not detectable by CT.[111] In a serial IVUS study, plaques with heavy calcification are clinically quiescent, whereas spotty (small) calcification was associated with accelerated disease progression in patients with SAP.[112] Furthermore, the presence of spotty

calcification was related to culprit plaques in patients with ACS in a study utilizing IVUS imaging.[113] In coronary CTA, spotty calcification is defined as a small, dense (>130 HU) plaque component surrounded by noncalcified plaque tissue. The typical cut-off to define a small calcification in coronary CTA as spotty is <3 mm (Figure 2).[70,90,102]

Spotty calcifications have been further differentiated into small (<1 mm), intermediate (1–3 mm), and large (>3 mm) calcifications.[114] Small spotty calcification has the strongest association with vulnerable plaque features defined by VH-IVUS.[114] Furthermore, in multiple cross-sectional studies in patients with ACS and SAP, spotty calcification is associated with ACS culprit lesions.[92-94] However, results vary widely, and highlight the current uncertainty in the relationship between spotty calcification and plaque rupture.[104] With further improvements in CT technology, detection of microcalcifications, which have been suggested to be a frequent feature in unstable angina, might be feasible.[115]

Semiquantitative coronary plaque burden

Several studies, such as the COURAGE trial (Clinical Outcomes Utilizing Revascularization and Aggressive Drug Evaluation) showed that plaque burden assessment may be more important than ischemic myocardium burden for predicting later major adverse outcomes.[116] Furthermore, Bittencourt et al. demonstrated that patients with extensive CAD (>4 coronary artery segments involved) have similar hazard ratios for developing major adverse events as patients with obstructive disease with less than 5 segments involved, thus also emphasizing the importance of quantifying plaque burden.[117] Min et al. proposed a score system, the Segment Stenosis Score (SSS) and the Segment Involvement Score (SIS) to quantify plaque burden.[118] SSS is calculated by grading all coronary segments as: 0 - No plaque; 1 - < 50% stenosis; 2 - 50-69% stenosis; 3 - ≥ 70% stenosis. SIS is the number of affected segments. Based on 1127 patients, SSS had a hazard ratio of 1.99 (CI: 1.48–2.67), while SIS had a hazard ratio of 1.23 (CI: 1.13-1.34). Similarly, results from the CONFIRM (COroNary computed tomography angiography evaluation for clinical outcomes: an InteRnational Multicenter) registry also showed SIS to be an independent predictor of later major adverse events (hazard ratio: 1.22; CI: 1.03-1.44) [119]. Several other studies have also demonstrated SSS and SIS to be significant independent predictors of later outcomes.[120-123] While SSS and SIS are simple and elegant concepts for describing plaque burden, they are conceptually flawed. SSS and SIS scores assume that plaque burden is additive, meaning that adding one plaque to two diseased segments or 12 diseased segments has the same effect. Furthermore, SSS and SIS

Table 1 Modified Duke Coronary Artery Disease Index for coronary CTA

Extent of coronary artery disease	Points
Stenosis <50%	0
Stenosis ≥50%	
1 vessel	23
2 vessel	37
3 vessel	56
Stenosis ≥50% and proximal LAD stenosis ≥50%	
1 vessel	48
2 vessel	56
3 vessel	74
Left main stenosis	
≥50%	80
≥70%	100

Score system is based on Miller et al. In the Modified Duke Coronary Artery Disease Index patients are assigned to the most severe category. CTA, CT angiography; LAD, left

lose all anatomical information, thus they assume a moderate stenosis on the left main has the same effect as a moderate stenosis on the second diagonal branch, which clearly is not true. Results of the CONFIRM trial also emphasize the importance of lesion characteristics and location. The trial demonstrated that excluding distal segments and only considering the number of proximal segments with obstructive plaques significantly improved their prediction model.[119] Another simple metric for quantifying the magnitude of plaque burden is the 3-vessel score, which counts how many major epicardial vessels (Left anterior descending, Left circumflex, Right coronary) have obstructive stenosis.[118] Andreini et al. demonstrated that having only one major epicardial vessel effected with an obstructive lesion (≥ 50%) has a hazard ratio of 3.18 (CI: 2.16–4.69), if all three vessels are affected, the hazard ratio increases to 7.10 (CI: 4.61–10.93).[120] Similar tendencies have been reported by several studies.[118,121-125] A more quantitative approach originally developed to characterize CAD severity using ICA,[126] later adopted for coronary CTA is the Duke Coronary Artery Disease Index.[118,127] Patients are assigned a risk score between 0-100 based on previously published prognostic data.[126] The score is an extension of the 3-vessel disease score. It also incorporates stenosis severity and calculates with left main stenosis and proximal left anterior descending stenosis (Table 1). Min et al. showed that there was a significant difference between patients' survival for the different scores.[118] Left main plaque with any additional moderate or severe stenosis had the worst outcome, while patients without any disease or only mild CAD had almost no events.

Altogether, plaque burden assessment seems to be a very important concept to describe the severity of CAD and predict adverse outcome.[128,129] Several methods have been proposed to properly quantify plaque burden, indicating the lack of a single best method. Furthermore, as we have seen, not only plaque burden, but plaque localization, stenosis severity, plaque composition and vulnerability features all play a role in later outcomes, thus necessitating a more complex holistic approach, which incorporates as many of these parameters as possible.[72] Based on the clinical outcome studies investigating the risk of plaque features and extension of CAD, several attempts have been made to create composite scores incorporating anthropometric vulnerability with extent of CAD, plaque localization and vulnerability features

as assessed by CTA.

The CONFIRM registry is an international prospective observational cohort currently with seven participating countries.[130] Structured interviews were used to collect information regarding patients' anthropometrics and cardiovascular risk profile. Using this information the National Cholesterol Education Program Expert Panel on Detection, Evaluation, and Treatment of High Blood Cholesterol in Adults (NCEP ATP III),[131] the Framingham[132] and the Morise clinical risk scores were calculated.[133] The 16-segment coronary artery model was used to assess the CTA images.[134] Each coronary segment was evaluated for the presence of plaque. Plaques were classified as calcified, partially calcified or non-calcified. The degree of stenosis was graded as: none (0% luminal stenosis); mild (1% to 49% luminal stenosis); moderate (50% to 69% luminal stenosis); or severe (≥70% luminal stenosis). Overall, 17,793 patients' data was used to create the CONFRIM risk score using multivariate Cox proportional hazard models.[119] The resulting models were evaluated using a separate test set, which consisted of 2,506 patients' data. After separate assessment of clinical risk scores and CTA imaging markers, a combined score was created. The COMFIRM risk score is a combination of the NCEP ATP III score, the number of proximal segments (proximal and mid right coronary artery, left main, proximal, and mid left anterior descendent, proximal circumflex, first obtuse marginal branch) with stenosis greater than 50%, and the number of proximal segments with partially calcified or calcified plaques. Adding these two additional parameters caused 32% of the patients to be reclassified, 22% to a lower risk category and 10% to a higher category. Overall, the combined risk score outperformed all clinical scores and significantly improved prediction of all-cause mortality. A online calculator is available for the CONFIRM risk score.[135]

Originally the Leaman score was established based on ICA measurements. Since plaque features cannot be visualized using ICA, only the localization and the degree of stenosis is used to calculate the score. Obstructions are weighted based on typical amount of blood flow to the left ventricle going through that given segment. On average in case of a right dominant coronary anatomy, the RCA receives 16%, while the left main trunk delivers 84% of the blood flow going the left ventricle.[136] For left dominant coronary systems, all of the left ventricle is supplied by the left coronary artery. Weighting factors are equal to how many times more blood goes through a given segment as compared to the RCA. For left dominant systems, the RCA receives a weighting factor of zero, while the weighting factor of the LM and circumferential segments increases by one.[137] The degree of stenosis was also accounted for. Occlusions receive a multiplication factor of five, 90-99% stenosis receive multiplication factor of three and obstructions between 70-89% receive a multiplication factor of one. Non-obstructive lesion

Table 2 Coronary CTA adapted Leaman score weighting factors

Segments	Dominance		
	Right dominance	Left dominance	Balanced
Proximal RCA	1.0	0	0.5
Mid RCA	1.0	0	0.5
Distal RCA	1.0	0	0.5
R-PDA	1.0	–	0.5
R-PLB	0.5	–	–
Left main	5.0	6.0	5.5
Proximal LAD	3.5	3.5	3.5
Mid LAD	2.5	2.5	2.5
Distal LAD	1.0	1.0	1.0
1st diagonal	1.0	1.0	1.0
2nd diagonal	0.5	0.5	0.5
IM	1.0	1.0	1.0
Proximal LCX	1.5	2.5	2.0
1st OM	1.0	1.0	1.0
Mid-distal LCX	0.5	1.5	1.0
2nd OM	1.0	1.0	1.0
L-PDA	–	1.0	–
L-PLB	–	0.5	0.5
Stenosis severity			
Obstructive	1.000	–	–
Non-obstructive	0.615	–	–
Plaque composition			
Non-calcified or partially calcified	1.5	–	–
Calcified	1	–	–

CTA adapted Leaman-score is calculated by multiplying the weighing factors regarding plaque composition, stenosis severity and location for a given segment. Overall score is calculated by summing up scores for all segments. RCA, right coronary artery; R-PDA, posterior descending artery originating from right coronary; R-PLB, posterolateral branch originating from right coronary; LAD, left anterior descending; IM, intermediate branch; LCx, left circumflex; OM, obtuse marginal; L-PDA, posterior descending artery originating from left coronary; L-PLB, posterolateral branch originating from left coronary.

(<70%) are not accounted for. A patients' Leaman score is equal to the sum of all segment scores for all 16 segments.[134] Coronary CTA adapted Leaman score as proposed by Gonçalves et al.[138] has minor modifications as compared to the original publication of Leaman et al.[137] To account of balanced coronary systems an intermediate value was used for segments where there was difference in weighting factors for left and right dominant systems. Plaque composition was also included. For non-calcified and partially calcified plaques weighting factor of 1.5 is added, while calcified plaques receive a weighting factor of one. Lesions with <50% stenosis receive a multiplication factor of 0.615 which is the relative proportion of the hazard ratios for mortality between obstructive and non-obstructive CAD, as reported by Chow et al. from the CONFIRM registry.[139] A summary of the calculation can be found in Table 2. Mushtaq et al evaluated the CTA adapted Leaman score using a single-center prospective registry including 1,304 consecutive patients.[140] Hard cardiac events (cardiac death and nonfatal myocardial infarction) were considered primary end-points. Using multivariate Cox regression models which included clinical parameters and SSS or SIS or the coronary CTA adapted Leaman score, were all independent predictors of adverse events. The Leaman score had the highest hazard ratio as compared to the other two scores (hazard ratio: Leaman score: 5.39, CI: 3.49 - 8.33; SSS: 4.42, CI: 2.97 - 6.57; SIS: 3.09, CI: 2.00 - 4.75, respectively). The event free survival of patients with

Leaman scores in the highest tercile (score >5) and obstructive CAD was similar to patients with similar Leaman scores but without obstructive CAD (78.6% vs. 76.5%; p=0.627).

Originally the SYNTAX (SYNergy between percutaneous coronary intervention with TAXus and cardiac surgery) score was developed to quantify the complexity of CAD, and to determine optimal revascularization strategies for multi-vessel CAD patients.[141] SYNTAX score incorporates multiple score systems. As opposed to previously described CTA scores, the SYNTAX score is a lesion-based scoring system, rather than a segment-based system, thus multiple lesions can be present and also scored in the same segment. The original 16-segment classification of the American Heart Association[134] is extended based on the Arterial Revascularization Therapies Study,[142] to include additional side branches. Only vessels greater than 1.5 mm and lesions with a stenosis greater than >50% are analysed. The SYNTAX score does not recognize balanced coronary dominance. Each lesion receives the Leaman score values for the segments in which it is present. Each segment score is multiplied by 2 for non-occlusive lesions (50-99%) and by 5 for occlusive lesions (100%). Only one segment is allowed to be occlusive for each lesion. Additional lesion attributes are scored based on the ACC/AHA lesion classification system.[143] Characteristics of occlusions[144], involvement of trifurcations, bifurcations[145,146] and aortal ostium, severe tortuosity, lesion length, heavy calcification, thrombus and diffuse coronary disease are all accounted for. Further adverse lesion characteristics are all additive. Details of the scoring system is described in

Table 3 Scoring system of the SYNTAX score

Characteristics	Points
Stenosis	
Occlusion	×5
Significant lesion	×2
Aorto ostial stenosis	+1
Occlusion characteristics	
Age >3 months or unknown	+1
Blunt stump	+1
Bridging	+1
First segment visible beyond occlusion	+1 per non-visible segment
Side branch	+1
Trifurcations	
1 diseased segment	+3
2 diseased segments	+4
3 diseased segments	+5
4 diseased segments	+6
Bifurcations	
Type A, B, C	+1
Type D, E, F, G	+2
Angulation <70°	+1
Severe tortuosity	+2
Lesion length >20 mm	+1
Heavy calcification	+2
Thrombus	+1
Diffuse disease of affected vessel	+1 per number of segments

SYNTAX score is calculated by multiplying the Leaman score (Table 2) of the segments which contain the given lesion by the stenosis factor. Further lesion characteristics are all additive. Overall, the SYNTAX score is the sum of all individual lesion scores. +, addition; ×, multiplication.

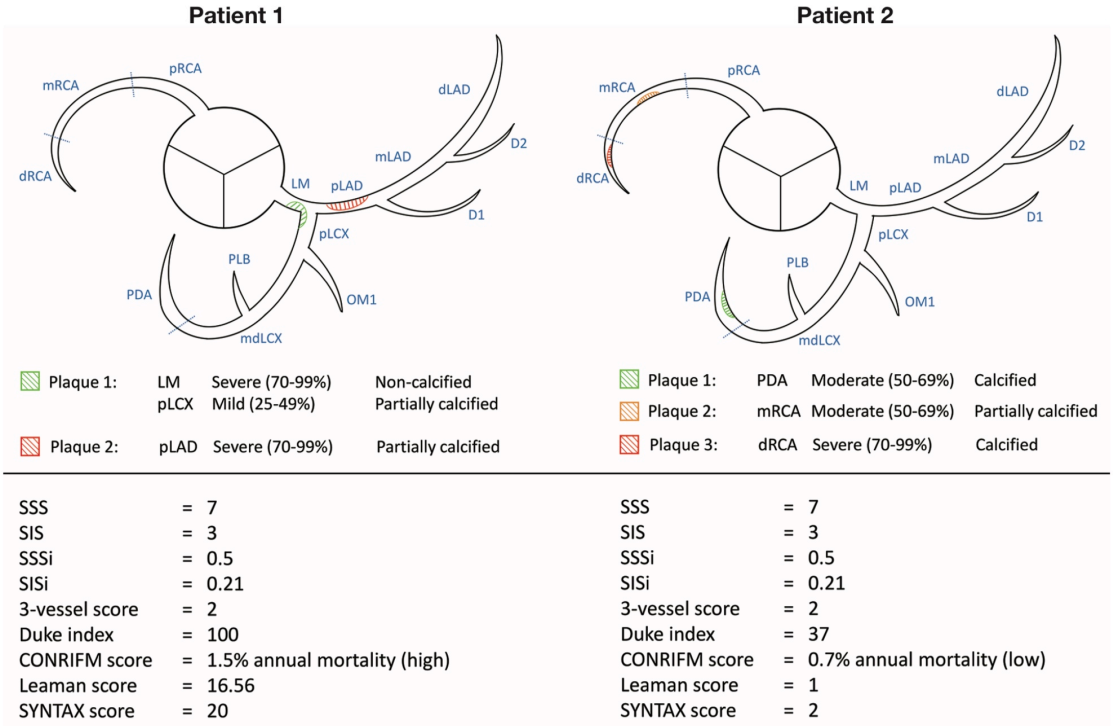

Figure 3 | Representative examples of plaque burdens and composite plaque scores. For the CONFIRM score both patients were assumed to be 65-year-old smoking male patients with 230 mg/dL total cholesterol, 47 mg/dL HDL, 142 mmHg systolic blood pressure using hypertension medication. For the SYNTAX score calculations, the LAD-LCX bifurcation was assumed to be ≥70˚and all plaques were shorter than 20 mm. The example shows, that patients with very different degree of disease can have very similar plaque burden scores. Composite plaque burden scores on the other hand seem to better differentiate between the severity of coronary artery disease. D, diagonal; IM, intermediate branch; LAD, left anterior descending; LCX, left circumflex; PDA, posterior descending artery; PLB, posterolateral branch; OM, obtuse marginal; RCA, right coronary artery; prefixes: d, distal; m, mid; p, proximal.

Table 3. The SYNTAX score includes many vulnerability parameters, thus utilization of the scoring system for long-term prognosis seems rational. Suh et al. evaluated the performance of the SYNTAX score based on 339 patients who underwent both CTA and ICA [147]. Only characteristics assessable by both CTA and ICA were included in the SYNTAX score. Based on univariate Cox regression analysis age, 3-vessel or LM disease on coronary CTA, two-vessel disease or three-vessel or LM disease on ICA, and SYNTAX scores higher than 23 based on ICA were predictors of MACE. On the contrary, multivariate analysis showed that models incorporating the SYNTAX score or simply the number of involved vessels had similar predictive power, both in case of CTA (area under the curve: 0.701 vs. 0.659, respectively) and ICA (area under the curve: 0.706 vs. 0.676, respectively). Recently, the SYNTAX score II has been developed that combines the SYNTAX score with clinical variables.[148] Long term follow-up data are promising based on ICA, but we currently lack CTA-based results. Based on these results, it seems incorporating an exceedingly complex score system, such as the SYNTAX

score, is not justifiable, since it has no proven additive value in risk prediction, as compared to simple CTA based CAD burden scores.

Overall, composite plaque burden scores seem to be a valid concept to determine the severity of CAD.[128] One major limitation of simple plaque burden scores is that very different disease severities can have very similar scores (Figure 3). Composite scores seem to account for this, but one must not forget, that these scores are only useful if they are calculated. The calculation of composite scores can become very complex, adding an additional burden to the clinicians. In the future, with the use of structured reporting platforms, these values can be calculated and evaluated automatically.[149,150] Therefore, these scores could transition from research domain to clinically useful risk stratification systems.[128]

Quantitative coronary plaque burden

Large plaque volume was associated with the diagnosis of ACS in cross-sectional studies, and quantification of NCPs can improve risk stratification and improve the prognostic value of coronary CTA to predict future cardiovascular events. The PROSPECT trial is the first and largest natural-history study of coronary plaques using invasive angiography and IVUS to identify plaques vulnerable to rupture on a per lesion basis.[103] The prospective study included 697 patients with ACS in whom three-vessel grey- scale IVUS and IVUS with radiofrequency backscatter analysis (known as virtual histology IVUS [VH-IVUS]) were performed to characterize non-culprit (that is unruptured) lesions. After a median of 3.4 years follow-up, the strongest predictor of future events was the IVUS-derived plaque burden of ≥70% (HR 5.03; 95% CI 2.51-10.11; P <0.001).[103]

Coronary CTA datasets with sub-millimeter isotropic spatial resolution, and the possibility of CT attenuation-based tissue characterization enable the quantification of total coronary plaque burden and individual plaque components, which is similar to the results obtained with IVUS.[101,151-153] Automated software tools are now available for plaque quantification and characterization (Figure 4). Automated quantification of plaques is desirable to improve the reproducibility, accuracy and efficiency of coronary CTA plaque analysis. The reproducibility of automated 3D quantification software for plaque burden was demonstrated to be excellent, with an ICC value of 0.88 (95% CI 0.74–0.95); excellent agreement was defined as an ICC coefficient of >0.8.[88] The accuracy of automated coronary plaque quantification by coronary CTA was successfully validated against greyscale IVUS and VH-IVUS.[80,88] However, automated plaque quantification software tools have poor inter-platform reproducibility; the

same software should, therefore, be used for serial or comparative assessments.[154]

The culprit lesion (that is ruptured) and vulnerable plaques evaluated by histology or invasive imaging techniques tend to be large in size, leading to the hypothesis that coronary CTA quantification might incrementally improve risk stratification of patients over conventional coronary CTA reading.[69] A cross-sectional clinical investigation demonstrated that the culprit plaques in patients with ACS have larger volume than stable lesions in patients

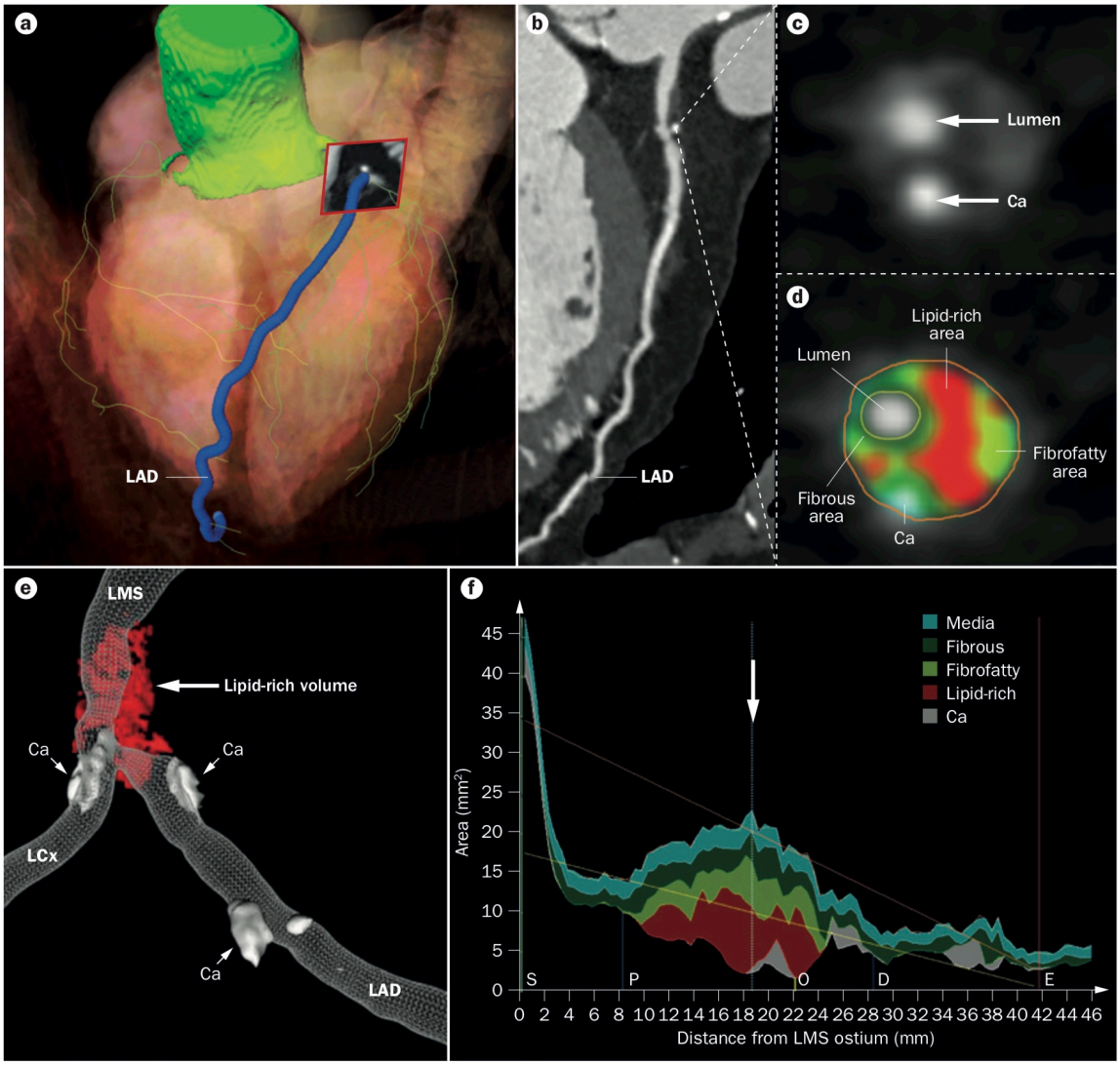

Figure 4 | Example of plaque characterization and quantification using a dedicated automated software tool and coronary CTA data set. a | Segmented whole coronary tree. The LAD is indicated in blue. The coronary centrelines and the aorta are indicated in green. Red box indicates plaque of interest. b | Curved multiplanar reconstruction of the LAD. Dotted lines indicate a partially calcified, positively remodelled plaque in the LMS bifurcation. c | The LMS plaque cross-section from panel b. d | The LMS plaque cross-section with colour overlay derived with adaptive threshold setting. The lipid rich (low CT attenuation) plaque components are shown in red. Fibro-fatty tissue is shown in light-green. Fibrous tissue is shown in dark-green. Calcium is shown in white. e | Volumetric assessment of the lipid rich plaque core is shown in red, and the core's spatial relation to the lumen (grey mesh) and calcium (white). f | The graph illustrates the areas of different plaque components. The colour scheme is identical to panel d. Abbreviations: Ca, calcium; coronary CTA, coronary computed tomography angiography; LAD, left anterior descending artery; LCx, left circumflex coronary artery; LMS, left main stem.

with stable angina pectoris (SAP; 193 mm^3 versus 104 mm^3; p=0.001).[92] In patients with unstable angina, quantitative coronary CTA revealed that plaques with morphological features of plaque disruption (such as intraplaque contrast dye penetration) had a larger volume compared with plaques that had no signs of disruption (313±356 mm^3 versus 118±93 mm^3; p<0.0001). These lesions also contained more low CT attenuation components characteristic to lipid-rich plaques (99±161 mm^3 versus 19±18 mm^3; p<0.0001) than undisrupted plaques.[155] In patients with acute chest pain and obstructive coronary lesions, the total volume of plaques leading to stenosis was not significantly different between those individuals with and those without ACS (212 mm^3 versus 171 mm^3; p=0.24). Interestingly, the volume of NCP with low CT attenuation density, (<90 HU) was significantly larger in patients with ACS compared with patients who did not have ACS (91 mm^3 versus 49 mm^3; p=0.03).[70]

Longitudinal clinical investigations indicate a strong prognostic value of coronary CTA derived plaque volume for future coronary events. In a retrospective study of 1,059 patients with stable chest pain, the coronary plaque volume was larger in those patients who developed ACS compared with patients who did not during a follow-up period of 27±10 months (134.9±14.1 mm^3 versus 57.8±5.7 mm^3; p<0.001).[102] The authors of a study published in 2013 elegantly demonstrated that semiautomatic plaque quantification – whereby plaques are manually identified before automatic segmentation, characterization, and quantification, with optional manual corrections – provided additional prognostic value for ACS over both clinical risk factors and traditional CT reading (including calcium score, segment stenosis score, lesion severity, and number of segments with NCP).[156] The patients who developed ACS had a higher total plaque volume (median 94 mm^3 versus 29 mm^3; p<0.001) and total NCP volume (28 mm^3 versus 4 mm^3; p<0.001) at baseline compared with those individuals who did not develop ACS.[156] The volume of nonobstructive NCP measured by CCTA was a strong predictor of future coronary events in a prospective study of 312 patients with non-ST-segment elevation myocardial infarction who underwent CCTA before invasive coronary angiography.[157] In total, 23 patients had a coronary event after a median follow-up of 16 months and the total volume of nonobstructive NCP was independently associated with the events with an HR of 1.18 per 100 mm^3 plaque volume increase. Interestingly, neither Agatston score, nor calcified plaque volume were associated with an increased risk of coronary event.[157] A subset of patients (n = 32) underwent coronary CTA in the PROSPECT study.[103,158] The authors of this exploratory sub-study observed a higher total atheroma volume at baseline in patients with subsequent cardiac events during the mean 39 months follow-up (970 mm^3 versus 811 mm^3; p<0.01).[158]

However, despite these promising results, further software improvements are warranted

to maximize accuracy, reproducibility, and time-efficiency before automated plaque burden quantification is implemented in the clinic.[82] Moreover, industry standards should be developed to enable reproducible plaque assessments with coronary CTA regardless of the software tool used.[129,154]

Coronary plaque radiomics

Radiologic images are large two-dimensional or three-dimensional datasets in which the quantitative values present in the pixels (or volumetric pixels called voxels) are used to create a picture.[159] Each and every voxel is a measurement itself on the basis of some physical characteristics of the underlying anatomic structure, such as the attenuation of electromagnetic radiation intensity that is used in CT. These values can be assessed by visual inspection, as done in daily clinical routine, or they can be analysed using advanced image analyses. Radiomics is the process of extracting numerous quantitative features from a given region of interest to create large data sets in which each abnormality is described by hundreds of parameters.[159] Some of these parameters are commonly known and used by radiologists, such as the mean attenuation value or the longest diameter of a lesion, whereas others that quantify the heterogeneity or shape

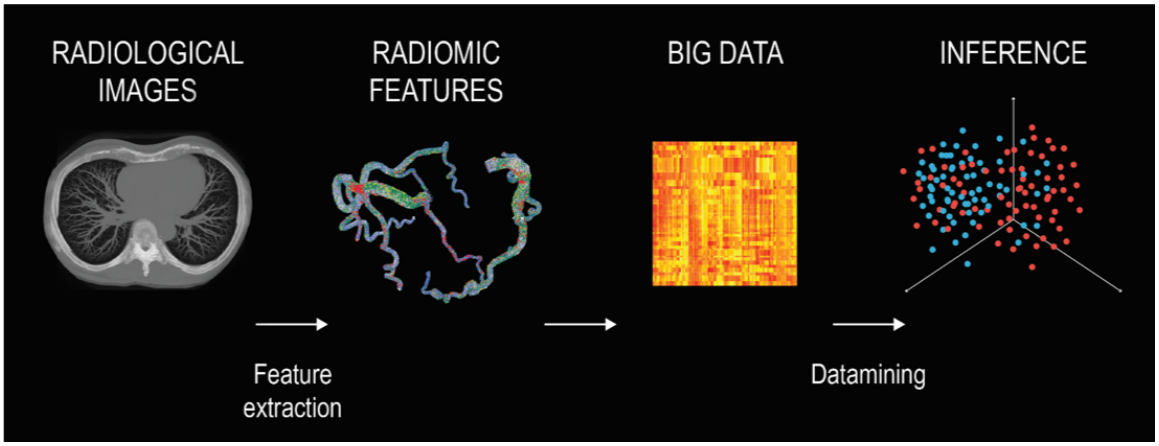

Figure 5 | Pipeline of radiomics-based patient analysis. After image acquisition, new novel radiomics-based image characteristics are extracted to quantify different lesion properties. The hundreds of variables are joined together to create "big data" databases. Data- mining is used to find new meaningful connections between the parameters and the clinical outcome data. On the basis of the results, new imaging biomarkers can be identified that have the potential to increase the diagnostic accuracy of radiologic examinations.

of an abnormality are less apparent. From these values novel analytical methods are used to identify associations between the parameters and the clinical or outcome data. Datamining is the process of finding new, meaningful patterns and relationships between the different variables. From these results, novel imaging biomarkers may be identified that can increase the diagnostic accuracy of radiologic examinations and expand our knowledge of the underlying pathologic processes (Figure 5).[159]

2.2.2 Functional plaque characteristics

Plaques develop at specific areas of coronary arteries where flow is disturbed, such as the outer walls of bifurcations, in side branches, and in the inner curve of arteries, despite risk factors for plaque formation (including smoking, high cholesterol levels, hypertension, and insulin resistance) affecting the whole vascular bed.[160-163] Haemodynamic factors, such as endothelial shear stress (ESS), are pathologically important for the spatial localization and development of atherosclerotic plaques.[164] Low ESS promotes an atherogenic milieu and high-risk plaque formation, whereas high ESS at stenotic vulnerable plaque sites promotes plaque rupture by destabilization of the fibrous cap.[165-167]

In the early 1990s, post-mortem studies indicated that more than two-thirds of infarctions evolve from non-obstructive lesions (that is lesions occupying <70% of the lumen).[168] However, histopathological investigations have now challenged these studies, and a high portion of culprit lesions now seem to cause obstructive luminal narrowing (>75% area stenosis was seen in 70% of plaque ruptures), especially in late stages of plaque development before the disruption of the fibrous cap.[68,71,169] These observations correlate with evidence that patients with ischaemic lesions have a poor prognosis.[170,171] Indeed, increased plaque vulnerability might in part be a consequence of haemodynamic perturbations and altered shear stress owing to abnormal fractional flow reserve (FFR).[172] Invasive FFR is the gold standard method for the identification of lesions that result in ischaemia.[173] The combination of ESS and FFR might, therefore, provide a novel functional dimension in plaque vulnerability assessment.[174] Advances in computational fluid dynamics (CFD) have enabled the simulation of coronary flow and pressure-based metrics on the 3D geometry of the coronary artery tree.[175] When CFD is added to standardly acquired coronary CTA dataset, ESS-CT and FFR-CT coronary maps can be calculated.[174,176]

Endothelial shear stress simulation

The ESS is the tangential force generated by the friction of flowing blood on the endothelial surface of the arterial wall.[177] In coronary artery segments with low and disturbed or turbulent flow - where ESS is low - the endothelial cell gene expression initiates a proatherogenic pattern.[178,179] Persistently low ESS reduces nitric oxide production, increases LDL uptake, promotes endothelial cell apoptosis, and induces local oxidative stress and inflammation, which induce an atherogenic endothelial phenotype and subsequently leads to the development of high-risk lesions.[164,180] By contrast, in straight arterial segments with undisturbed laminar flow - where ESS varies within a physiological range - endothelial cells express atheroprotective genes leading to plaque stability and quiescence.[163,164,177] However, high shear stress at the stenotic portion of the plaque might initiate pathophysiologic processes that promote plaque destabilization and rupture.[163,177] In serial IVUS studies of coronary arteries in diabetic pigs, the majority of vulnerable plaques developed in vessel segments characterized by persistently low ESS.[162,164,181] Furthermore, the magnitude of low ESS at baseline was significantly associated with the severity of high-risk plaque features at follow-up.[164] Another animal study has refined the concept that low ESS promotes coronary plaque growth and vulnerability by demonstrating that dyslipidaemia and low ESS have a synergistic effect leading to the development of vulnerable atheromas.[182] The first natural-history VH-IVUS study in humans assessed the left anterior descending artery in 20 patients with nonobstructive CAD at enrolment and at 6 months follow-up.[166] Low ESS segments developed increased plaque area and necrotic core as well as constrictive remodelling, whereas high ESS segments developed greater necrotic core and regression of fibrous and fibrofatty tissue, and excessive positive remodelling, suggestive of transformation to a

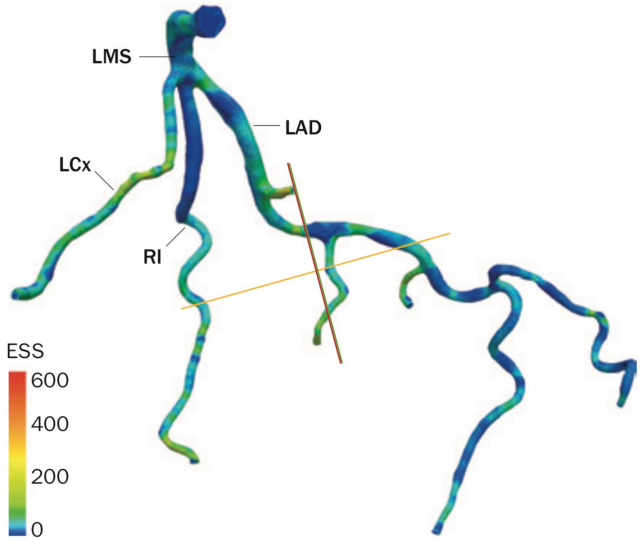

Figure 6 | Time averaged ESS map of a left coronary artery derived by computation fluid dynamics simulation. The ESS values are in dynes/cm2. Dark-blue indicates low ESS values. Turquoise and green colours represent the normal physiological range of ESS. Yellow to red areas are regions of high ESS. Abbreviations: ESS, endothelial shear stress; LAD, left anterior descending artery; LCx, left circumflex coronary artery; LMS, left main stem; RI, ramus intermedius. Permission obtained from Alessandro Veneziani, Emory University, Atlanta, GA, USA.

more-vulnerable phenotype.[166] These observations highlight the importance of low ESS in vulnerable plaque development and high ESS in the destabilization of these plaques.

In the Prediction of Progression of Coronary Artery Disease and Clinical Outcome Using Vascular Profiling of Shear Stress and Wall Morphology (PREDICTION) trial, a total of 506 patients underwent three-vessel IVUS examination and were assessed again at 1-year follow-up.[183] The results demonstrated that large plaque burden and low ESS can independently predict plaques that progressively enlarge and develop substantial lumen narrowing.[183] Three-dimensional coronary geometry visualization by coronary CTA enables CFD to be applied to ESS-CT calculations and subsequent coronary wall behaviour assessment (Figure 6).[184-187] These observations have been confirmed in a study using coronary CTA and IVUS for vascular profiling. Coronary CTA was sufficiently accurate to determine ESS distribution in the main vessels and in the bifurcation regions.[188] The CFD simulations in coronary CTA can be used to remove all plaques in a virtual environment to replicate the healthy vascular wall before the development of atherosclerotic plaques. In an exploratory investigation, static and dynamic parameters of ESS-CT were calculated in a virtual healthy coronary lumen to determine the best haemodynamic predictor of future plaque location. The results of this virtual experiment suggested that low ESS is a prerequisite for plaque formation; however, its presence alone is insufficient to predict future plaque locations. Dynamic factors that describe the time-dependent directional changes in ESS might, therefore, have an incremental prognostic value regarding plaque progression and vulnerability.[189]

Fractional flow reserve simulation

Plaques that rupture cause substantial luminal narrowing at the time of the acute event. Histopathological investigations demonstrated that plaques that rupture but are non-stenotic are very rare.[68,71] The assessment of luminal narrowing at the site of a large lipid-rich plaque might, therefore, be an important addition to high- risk plaque features and could aid the identification of vulnerable plaques.

In a histopathological study of ruptured plaques and TCFAs, 70% produced significant narrowing (>75%) of the cross-sectional luminal area.[71] The remaining 30% of nonobstructive ruptured plaques were further subdivided into those with luminal narrowing of 50–75% and those with luminal narrowing <50% (25% and 5% of lesions respectively).[71] Importantly, the investigators assessed the non-ruptured TCFAs, which are the potential targets for non-invasive imaging, and found 40% also caused luminal narrowing of >75%.[71] Because these lesions are

likely to cause angina, they are more likely to be treated. However, lesions with an intermediate stenosis can be large, but not necessarily associated with symptoms of angina. Vulnerable plaques with a stenosis range of 50–75% (~50% of all TCFAs) are, therefore, the more appropriate targets for non-invasive imaging (Figure 7). Notably, the relationship between intermediate stenosis (50–75% diameter stenosis) and the presence of ischaemia is extremely unreliable - half of the lesions lead to ischaemia and the remaining half do not, as determined by invasive FFR measurement.[190] In an intermediate lesion with abnormal FFR, the flow perturbations, altered ESS, and the physical strain changes placed on the plaque might be responsible for the development of a rupture-prone lesion.[172,191] Furthermore, patients with an obstructive coronary plaque might develop an ACS owing to thrombus formation induced by high EES.[192] In an investigation that included 70 patients with stable CAD, a strong association was observed between inflammatory cytokine activity and FFR; therefore, ischaemia might be involved in plaque progression and destabilization.[193] Moreover, numerous recently published investigations demonstrated a strong link between coronary CTA-visualized adverse plaque features and lesion specific ischemia.[194-197] Vulnerable plaques with intermediate stenosis and positive FFR should be treated; however, the non-invasive identification of these lesions is challenging. Conversely, <1% of patients with a plaque resulting in an intermediate stenosis without ischaemia (FFR ≥0.8) have a myocardial infarction within 5 years, which is similar to a matched control population without diagnosed CAD.[198] Coronary CTA based FFR simulation will help in the identification of lesions with ischaemia and likely improve CT accuracy for the detection of high-risk lesions. Importantly, FFR-CT can be derived from coronary CTA, without the need for additional imaging, extra radiation, or

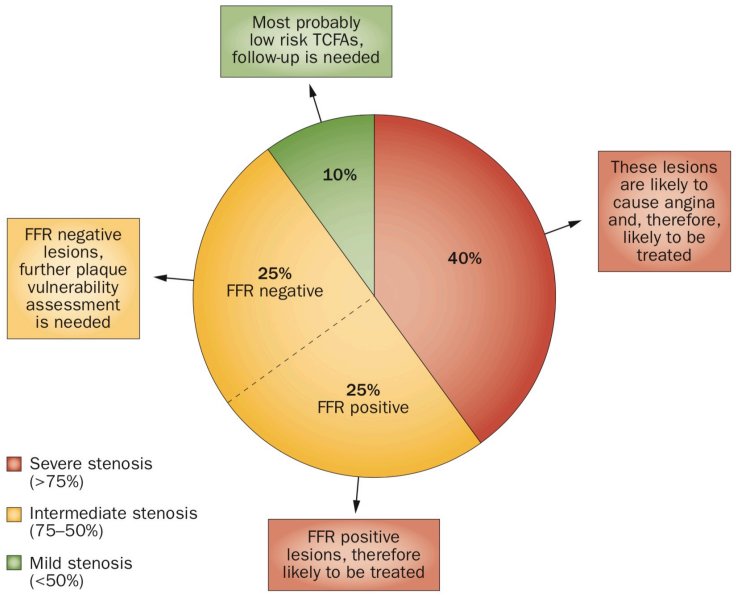

Figure 7 | In histopathological studies of patients who suffered sudden cardiac death, 40% of nonruptured TCFAs also caused >75% luminal narrowing. These TCFAs with significant luminal narrowing (>75%), are likely to cause angina, and therefore be treated. Lesions with an intermediate stenosis can be of danger, as they are large, but are not necessarily associated with symptoms. Vulnerable plaques with a stenosis range of 50–75% (~50% of TCFAs) are the real targets for noninvasive imaging. Abbreviations: FFR, fractional flow reserve; TCFA, thin cap fibroatheroma.

any medication (Figure 8). Furthermore, FFR-CT provides a comprehensive three-vessel FFR from a single coronary CTA, enabling FFR readings at any location of the coronary tree. Three prospective clinical trials have demonstrated that FFR-CT compares favourably to the reference standard invasive FFR measurements.[199-201] In the Diagnosis of Ischemia-Causing Stenoses Obtained Via Noninvasive Fractional Flow Reserve (DISCOVER-FLOW) trial, FFR-CT was compared with invasive FFR, and had a per-vessel accuracy of 84.3%, sensitivity of 87.9%,

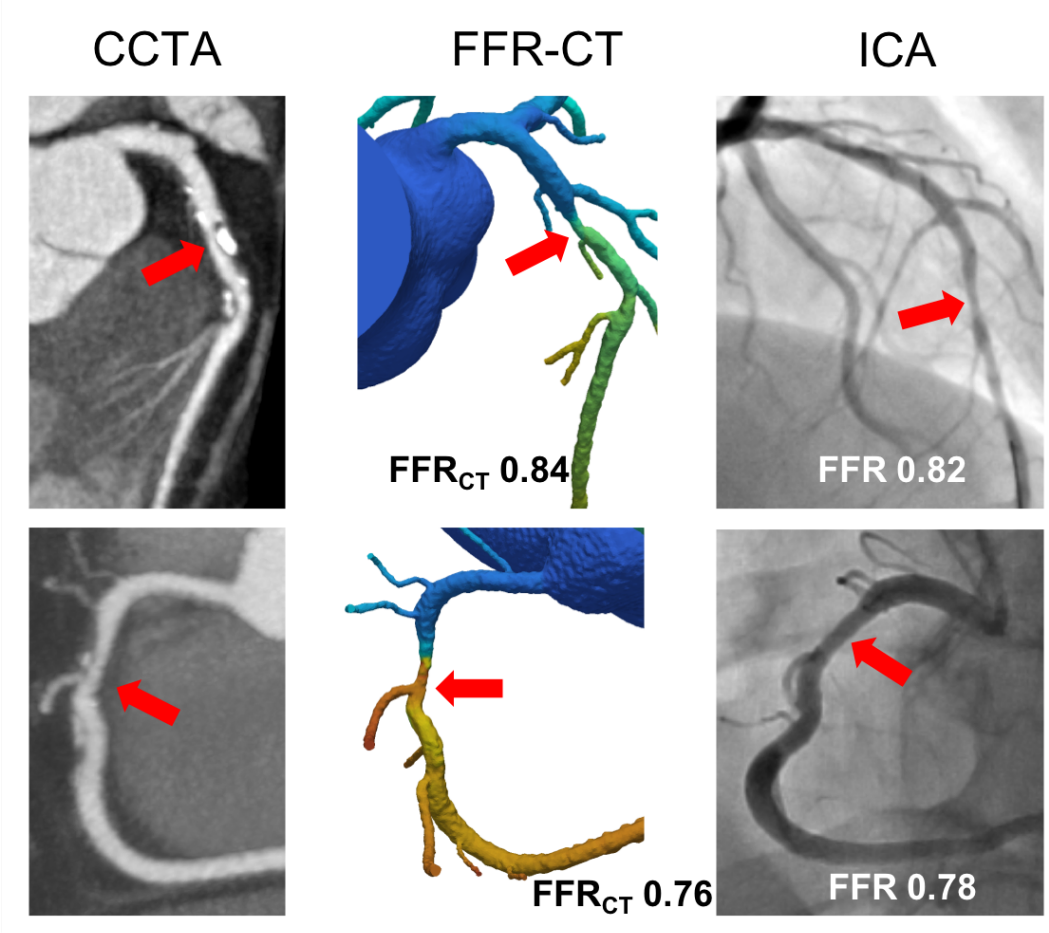

Figure 8 | The first case represents severe (70-90%) proximal LAD stenosis as depicted by CCTA. FFR-CT demonstrates no lesion specific ischemia (0.84), which was confirmed by ICA (0.82). In the second case CCTA demonstrates moderate (50-70%) mid RCA stenosis. The FFR-CT reveals ischemia (0.76), which was confirmed invasively (0.78). Abbreviations: CCTA, coronary computed tomography angiography; FFR, fractional flow reserve; ICA, invasive coronary angiography; LAD, left anterior coronary artery; RCA, right coronary artery. Courtesy of HeartFlow Inc., Redwood City, California.

and specificity of 82.2%.[199] In addition, FFR-CT had better diagnostic performance than coronary CTA when identifying clinically significant coronary lesions; the area under the receiver-operator characteristics curve (AUC) were 0.90 for FFR-CT and 0.75 for coronary CTA (p=0.001).[199] Investigators in the Determination of Fractional Flow Reserve by Anatomic Computed Tomographic Angiography (DeFACTO) trial, a multicentre international study evaluating the diagnostic performance of FFR-CT, enrolled 252 patients.[200] On a per-patient

basis, FFR-CT was superior to coronary CTA in identifying ischaemic lesions (accuracy 73% versus 64%; sensitivity 90% versus 84%; specificity 54% versus 42%). Compared with obstructive CAD diagnosed by coronary CTA alone (AUC 0.68; 95% CI 0.62-0.74), FFR-CT was associated with improved discrimination of coronary stenosis with ischaemia (AUC 0.81; 95% CI 0.75–0.86; P <0.001).[200] Notably, in patients with intermediate stenosis, FFR-CT had more than a twofold increase in sensitivity compared with coronary CTA alone (82% versus 37%; no statistical data was reported), with no loss of specificity (66% versus 66%).[200] In the recently published NXT trial (Analysis of Coronary Blood Flow Using CT Angiography: Next Steps) investigators reported a slightly decreased per-patient sensitivity of FFR-CT comparing to coronary CTA (86% vs. 94%). However, a marked increase in specificity was observed compared with coronary CTA (79% vs. 34%).[201] These studies utilized a commercial laboratory (HeartFlow, Redwood City, CA), which received the routine coronary CTA data and generated an FFR-CT color-coded three-dimensional model of the epicardial coronary arteries. The PLATFORM study (Prospective LongitudinAl Trial of FFRct: Outcome and Resource IMpacts) further demonstrated, that the use of FFR-CT significantly lowered the rate of ICA and used less resources at lower costs. [202-204]

However, current FFR-CT simulations are expensive and time consuming, as the simulations are performed off-site. Recently on-site FFR-CT techniques have been introduced, which are able to calculate FFR-CT in couple of seconds to minutes.[205-208] Further studies are warranted to explore the diagnostic accuracy and utility of these novel on-site algorithms. These observations support the high diagnostic performance of FFR-CT, which might play an important role in the accurate evaluation of lesion-specific ischemia in the near future. A novel application of CFD is the possibility of implanting a stent in a virtual setting to test different stenting strategies and predict functional outcomes by changes in FFR.[209] FFR-CT is an accurate new tool to assess lesion-specific ischaemia in a typically acquired coronary CTA exam and an improvement on the accuracy of CT alone.

2.3 Epicardial adipose tissue

Obesity, especially an increase in abdominal visceral adipose tissue (VAT) quantity, may have an important role in the development of cardiometabolic disease.[210-212] During the last couple of years, a special attention was paid to another fat compartment, namely the epicardial adipose tissue (EAT), as its proximity to the myocardium and coronary arteries might also be of pathophysiological importance.[213-215] Recently, it has been suggested that EAT is a

source of inflammatory mediators affecting the myocardium and coronary arteries, and clinical studies suggested that EAT – through paracrine and vasocrine effects – might have an impact on the development and progression of coronary atherosclerosis.[215,216]

The epicardial adipose tissue is a unique fat compartment located between the myocardial surface and the visceral layer of the pericardium. In physiological circumstances the epicardial fat covers nearly 80% of the heart surface. According to previous observations this fat compartment contributes 20% to the whole heart quantity.[217] Some years ago a hypothesis about the direct role of EAT in the development and progression of coronary atherosclerosis was raised, and paracrine and vasocrine effects of EAT due to close proximity of epicardial fat to coronary arteries was proposed.[218] The hypothesis was indirectly supported by a pathological study in subjects with a myocardial bridge. Namely, no atherosclerosis was observed in coronary segments at the myocardial bridge where surrounding fat around the coronary arteries is lacking.[219]

The relationship of EAT with CAD has been analyzed by several clinical studies.[220,221] In the Framingham and the MESA (Multiethnic Study of Atherosclerosis) epidemiological studies a significant association of epicardial fat with coronary artery calcification was found, which remained significant after adjustment for traditional cardiovascular risk factors.[222,223] The increased epicardial fat proved to be associated with more advanced atherosclerosis and with the presence of non-calcified coronary plaques.[224,225] A significant relationship of increased epicardial fat volume (>130.7 cm^3) with vulnerable plaques was also documented.[226] The relationship of morphological features of vulnerable plaques (positive remodeling, spotty calcifications, and low CT attenuation in the necrotic core) to the pericardial fat was also studied, and the volume of pericardial fat proved to be nearly twice as high in patients with vulnerable plaques as compared to those without CAD.[227] In a systematic review and meta-analysis, an association between the elevated location-specific thickness of EAT at the left atrioventricular groove and obstructive CAD was found.[228]

Fat compartments may differ in embryogenetic origin, physiological and pathophysiological functions.[229] Their accumulation leads to local or systemic adiposity and increase of their quantity is influenced by genetic and environmental factors. Classical twin studies compare monozygotic (MZ) and dizygotic (DZ) same-gender twin pairs to help to evaluate the degree of genetic and environmental influences on body composition.[230,231] Earlier studies demonstrated a predominant genetic effect on body mass index (BMI) and on central abdominal obesity as measured by dual-energy X-ray absorptiometry.[232-234] However, no data are available whether EAT compartment quantity depends predominantly on genetic or

environmental factors. Furthermore, data regarding the heritability of abdominal adipose tissue compartment sizes are scarce and the findings are based on family studies and on measurement methods with limited accuracy.

2.4 Reporting coronary CTA findings

There is a growing trend in diagnostic imaging to structure reports of imaging procedures.[235-238] Structured reporting is important for several reasons. First, structured reporting can improve quality through consistency. Key report elements are less likely to be omitted if the report is structured and elements are listed systematically within a standard template.[150] The development of lexicons standardizes descriptors. Reports convey similar information regardless of the imager's background and are similar throughout and across institutions. Referring physicians have access to an end product from which it is easier to extract the pertinent results because they are in an expected location in the report and in standard defined terminology. In addition, data mining may be facilitated through structure with entries serving as data cells in electronic medical records. Finally, structured reporting also ensures that all required elements for billing purposes are contained within the report. In recent years, the number of coronary CTA examinations increased substantially leading to increased variability in reporting of coronary findings.[239] Performed by cardiologists or radiologists, written in free text or generated by structured reporting platforms, coronary CTA reports should provide a concise, clear description of coronary anatomy and pathologic changes. We have published reporting guidelines and recommendations on behalf of the Hungarian Society of Cardiology and Hungarian Society of Radiology.[240,241] Considering the high variability and inconsistency in coronary CTA reporting, a standardized framework for CAD assessment has long been desired.[235,242,243] In a joint effort, international cardiology and radiology societies proposed a scoring system - the Coronary Artery Disease - Reporting and Data System (CAD-RADS) - for standardized reporting and decision making.[244] This expert consensus document aimed to facilitate interdisciplinary communication of CTA results and provide recommendations on patient management. CAD-RADS holds the potential to substantially improve reporting consistency. Currently there are no data available regarding the use of structured reporting platforms in CAD-RADS classification.

3 Aims

3.1 To improve cardiac CT image acquisition safety and quality

1) To assess if ultrashort-acting β-blocker is at least as efficacious as the standard of care intravenous metoprolol for HR control during coronary CTA.
2) Improve the safety of cardiac CT image acquisition through the development of novel iodinated contrast injection protocols.
3) To assess the effect of novel image reconstruction techniques on plaque volumes.
4) To assess cardiac CT image quality in heart transplanted patients.

3.2 To improve coronary atherosclerotic plaque assessment

1) To identify novel qualitative imaging biomarkers of high-risk atherosclerotic coronary plaques.
2) To develop an attenuation pattern-based plaque classification scheme in coronary CTA to differentiate early and advanced atherosclerotic plaques as defined by histology.
3) To compare invasive and non-invasive imaging techniques to identify high-risk coronary plaques as defined by histology.
4) To compare invasive coronary angiography with coronary CTA to detect coronary atherosclerotic plaques.
5) To develop radiomic techniques to identify high-risk plaques.
6) To assess lesion specific ischemia by using hemodynamic simulations.

3.3 To study atherogenic adipose tissue compartments

1) To investigate the relationship between epicardial adipose tissue, circulating biomarkers and coronary artery disease.
2) To assess the heritability of epicardial adipose tissue compartment.

3.4 To develop novel data collection system for cardiac CT

1) To assess the performance of automated structured reporting tool

4 Methods

4.1 Cardiac CT image acquisition and safety

In the first part of my doctoral thesis, I will focus on research projects aimed at the development of novel techniques to improve the safety and image quality of coronary CTA image acquisition. We have performed three clinical studies at the Heart and Vascular Center, Semmelweis University to optimize HR control, contrast injection protocol and radiation dose. In addition, we have investigated the image quality of heart transplanted patients, who underwent coronary CTA to rule out cardiac allograft vasculopathy.

4.1.1 Heart rate control with ultra-short acting beta-blocker

Study design

In a randomized single-center noninferiority phase III clinical trial we have compared two IV β-adrenergic receptor blockers to reduce HR in patients who undergo coronary CTA due to suspected coronary artery disease (European Union Clinical Trials Register number: 2013-000048-24).[245] The noninferiority margin was set on 10% because we assumed that the difference between the two groups in proportion of responder patients (patients achieving 65 beats/min) less than this is clinically irrelevant. The primary endpoint was the proportion of patients who reached HR 65 beats/min in the esmolol group. The secondary endpoint was the proportion of patients who experienced bradycardia (HR <50 beats/min) and/or hypotension (systolic BP <100 mm Hg) as an effect of β-blockers. We have performed an interim analysis after 45 days to ensure adequate enrolment rate and to assess toxicity as well as adverse events. An adverse event was defined as a change in health condition resulting from the administration of β-blockers, which is not resolving with observation and requires medical intervention.

Study population

Patients who were referred to coronary CTA due to suspected coronary artery disease and had an HR >65 beats/min despite oral metoprolol pre-treatment were enrolled in the study. Patients with history of a coronary intervention and an implanted stent with a diameter ≥3 mm

or previous coronary artery bypass surgery were eligible to participate in the study. Individuals with a heart rhythm other than sinus rhythm, any contraindication against β-blocker (asthma bronchiale, chronic obstructive pulmonary disease, any type of documented atrioventricular block, severe aortic valve stenosis, severe left ventricular dysfunction characterized by ejection fraction below 30%), or a systolic BP<100 mmHg before the coronary CTA scan were excluded from the study.

Drug administration and coronary CTA protocol

Patients received 50-mg oral metoprolol at arrival if the HR was >65 beats/min. If the HR was 80 beats/min, 100-mg oral metoprolol was administered. The HR was re-evaluated 60 minutes after the oral β-blockade, immediately before the coronary CTA examination. Patients presenting with an HR >65 beats/min on the CT table were randomized to IV esmolol or IV metoprolol administration. In both the investigational (esmolol) and the active control (metoprolol) groups, the IV drug was administered by the physician performing the coronary CTA scan. To achieve randomization, we administered IV esmolol on even weeks and metoprolol on odd weeks in an alternating fashion. The IV metoprolol (Betaloc; 1 mg/mL; AstraZeneca, Luton, United Kingdom; 5-mg ampoule) was titrated in 5-mg doses in every 3 minutes until the target HR (65 beats/min) or the maximum dose of metoprolol (20 mg) was achieved. The IV esmolol (Esmocard; 2500 mg/10 mL; AOP Orphan Pharmaceuticals AG, Vienna, Austria) was diluted to 500 mg/10 mL and titrated in ascending 100-, 200-, 200-mg doses in every 3 minutes until the target HR (65 beats/min) or the maximum dose of esmolol (500 mg) was achieved. Blood presure was monitored before every administered drug bolus. If hypotension (defined as systolic BP <100 mmHg) or bradycardia (defined as HR <50 beats/min) was measured, the administration of the β-blocker agent was suspended. Two puffs of sublingual nitroglycerine were given to each patient 3 to 5 minutes before the CT scan to ensure the proper visualization of the coronaries. The HR was recorded at arrival (T1), immediately before coronary CTA (T2), during breath hold, contrast injection, and scan (TS), immediately after scan (T3), and 30 minutes after coronary CTA scan (T4). BP was measured at T1, T2, T3, and T4 time points. The study flow chart is presented in Figure 9.

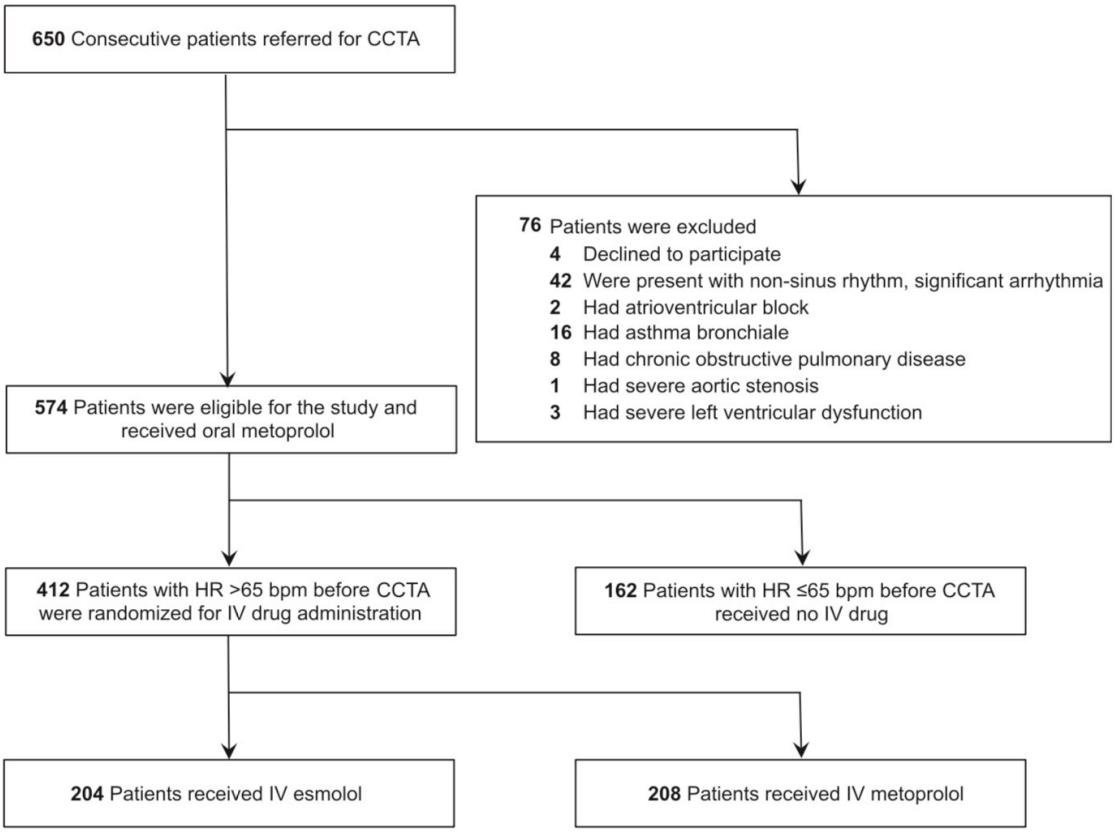

Figure 9 | *Flow chart of the study. bpm, Beats/min; CCTA, coronary CT angiography; HR, heart rate; IV, intravenous.*

All examinations were performed with 256-slice CT (Brilliance iCT 256; Philips Healthcare, Best, the Netherlands). Contrast-enhanced image acquisition was performed in inspiration during a single breath hold in craniocaudal direction. Imaging parameters were used as follows: slice collimation of 128 mm % 0.625 mm, rotation time of 270 ms, tube voltage of 80 to 120 kV, and tube current of 150 to 300 mAs depending on patients' body mass index. The images were acquired using prospective electrocardiogram triggering at 75% to 81% phase (3% padding). The iodinated contrast agent (Iomeron 400; Bracco Ltd, Milan, Italy) was injected into an antecubital vein via an 18-ga cannula using a dual-syringe technique, at a flow rate of 3.5 to 5.5 mL/s depending on patients' body mass index and the tube voltage. Bolus tracking was used with a region of interest placed in the left atrium. Images were reconstructed with a slice thickness of 0.8 mm and 0.4-mm increment.

Statistical analysis

The sample size calculation was based on a recently published study, which showed that

83% of patients who received metoprolol premedication achieved an HR of 65 beats/min during coronary CT angiography.[246] The noninferiority margin was set to 10% because we have assumed that this is a clinically acceptable maximum difference between the responder proportions of the two treatment groups. Degertekin et al. reported that 65% of the patients achieved the target HR of ≤65 beats/min after administration of intravenous esmolol.[247] However, Degertekin et al administered smaller doses; thus, our primary aim to achieve at least 73% responder proportion seemed to be realistic. Dedicated software was used for sample size calculation (East, version 5.4.1; Cytel Inc, Cambridge, Massachusetts). A total of 595 patients, 297 to 298 patients on each treatment arm, were needed to show that the difference between proportion of responders in metoprolol group vs esmolol group is less than the noninferiority margin set at 10% with a power of 90% using a 1-sided p=0.025 level test. The sample size calculation was based on an intention to treat analysis. Continuous variables were reported as mean±standard deviation. Categorical variables are given in frequency. According to the Shapiro-Wilk tests, some of the parameters showed mild deviation from normal distribution. To deal with the non-normality, the groups were compared by robust t tests using 20%-trimmed means with bootstrapping.[248] Differences of categorical variables between treatment groups were analyzed by chi-square tests. With respect to all statistical tests, a 2-sided p-value of <0.05 was considered significant. Statistical analyses were performed with R, version 3.0.2 (R Foundation for Statistical Computing, Vienna, Austria).

4.1.2 Contrast injection protocol optimization

Study design

In this prospective, single-centre, single-blinded, randomized, controlled clinical trial we compared two contrast media injection-protocols in patients who were referred for coronary CTA examination.[249] We randomized patients into two groups: (1) a three-phasic injection-protocol group and (2) a four-phasic injection-protocol group. To achieve randomization, we alternated the use of three-phasic and four-phasic CM administration protocols on a weekly basis: on even weeks, we applied the three-phasic protocol, and on odd weeks we used the four-phasic protocol. The primary endpoint was the occurrence of CM extravasation. CM extravasation was defined as (1) presence of pain and local swelling close to the cannula insertion site occurring after the initiation of CM injection, and (2) absence of CM or minimal CM attenuation in cardiac chambers on the CTA images. Our institutional review board

approved the study and informed consent was waived.

Study population and CTA protocol

We included consecutive patients who were referred for coronary CTA from January 2014 to August 2015. Exclusion criteria were contraindications to iodinated CM, age under 18 years and the presence of a cannula that was not inserted by our radiographers.

Similarly, to the above described study we performed all coronary CTA examinations with a 256-slice multi-detector row CT scanner. Contrast-enhanced image acquisition was performed in inspiration during a single breath-hold in a cranio-caudal direction. The following imaging parameters were used: slice collimation of 128 mm×0.625 mm, rotation time of 270 ms, tube voltage 100–120 kV and tube current 150–300 mAs depending on the patient's weight. The majority of scans (99.8%) were acquired by using prospective ECG triggering at 78% phase of the cardiac cycle with 3% padding. Bolus tracking was used with a region of interest (ROI) placed in the left atrium. Images were reconstructed with a slice thickness of 0.8 mm and 0.4 mm increment.

Contrast media injection-protocol

All patients received the same type of cannula (B. Braun Medical Inc., Melsungen, Germany). All cannulas were inserted by certified radiographers. The preferred location of vein puncture was the right antecubital region. Other distal venous access locations were used if no suitable vein was found in the antecubital region. We registered venipuncture characteristics, such as the side and location of venous access, the size of the inserted cannula and the number of insertion attempts. In all patients the injection site was tested with a 20- ml saline bolus. All patients received a 400 mg/ml concentration iomeprol (Iomeron 400, Bracco Spa, Milan, Italy) CM injected with dual-syringe automated mechanical injector. CM was pre-heated to 37 °C. In patients having more than 80 kg of bodyweight we used a 5.5 ml/s injection rate and 95 ml CM and 120 kV tube voltage. In patients less than 80 kg in bodyweight we used an injection rate of 4.5 ml/s, 80 ml CM and 100 kV tube voltage. In the three-phasic protocol group the injection started with the CM bolus, followed by 40 ml of 75%:25% saline-CM mixture, and finished with 30 ml of chaser saline bolus. With the four-phasic protocol the injection started with the saline pacer bolus of 10 ml, administered with 1.5 ml/s lower flow rate than the CM bolus; specifically, a saline pacer bolus flow rate of 4.0 ml/s if the injection rate of CM was 5.5 ml/s and 3 ml/s if the CM flow rate was 4.5 ml/s and continued with the steps of the three-phasic protocol (Figure 10).

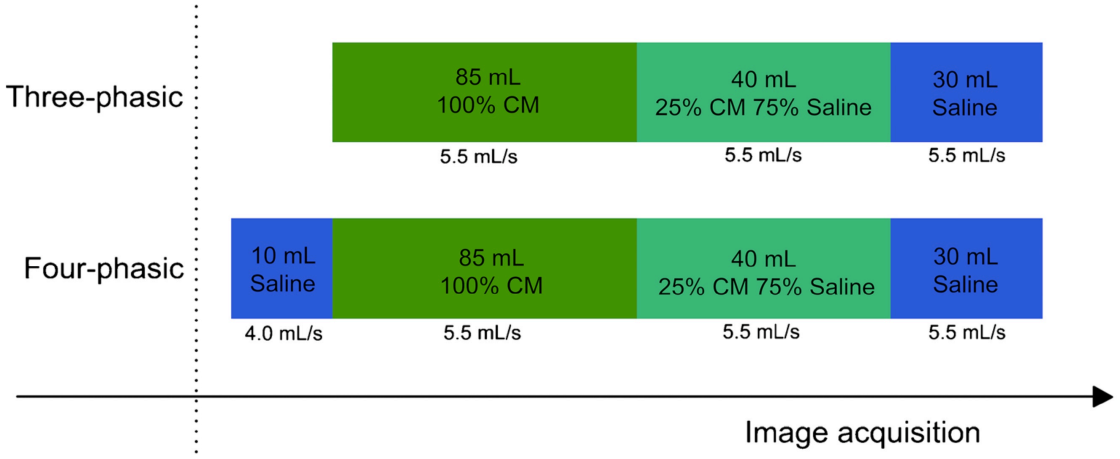

Figure 10 | Schematic representation of the three-phasic and the four-phasic contrast media (CM) injection-protocols. The three-phasic protocol starts with an undiluted CM bolus, followed by a 75%:25% saline and CM mixture and ends with a 30-ml chaser saline bolus. The four-phasic protocol starts with a 10-ml saline pacer bolus, administered at a 1.5 ml/s slower flow rate than the CM bolus, and continues with the three-phasic protocol. The injection rate settings are dependent on the body weight of the patient and on the tube voltage settings.

Statistical analysis

Continuous variables are reported as mean±standard deviation. Based on our relatively large sample size the central limit theorem allows the use of parametric tests, therefore we compared the continuous variables using Student's t-test. To evaluate the differences between categorical variables we used Fisher's exact test. Two-sided p values below 0.05 were considered statistically significant. For risk estimation, we calculated the odds ratio (OR) with 95% confidence intervals (CIs). All statistical data analysis was performed with IBM SPSS (IBM Corp: version 23, Armonk, NY, USA).

4.1.3 Effect of image reconstruction

Study population

We studied 52 consecutive individuals who underwent routine clinical coronary CTA examination due to suspected coronary artery disease.[150,250] Patients who showed calcified and/or partially calcified plaque were included in the further analysis to study plaque characteristics. As we used automated plaque quantification, partially calcified lesions were not further distinguished to predominantly non-calcified or predominantly calcified plaque types, as recommended the Society of Cardiovascular Computed Tomography (SCCT) for qualitative plaque reading.[251] We excluded patients with previous bypass surgery or coronary stent

implantation. To minimize the impact of motion artifact on image quality, patients not in sinus rhythm and/or with a heart rate of ≥65 beat per minute during CTA data acquisition were excluded. Informed consent was waived by the institutional review board (IRB) due to the retrospective design of the study. No additional data acquisition was performed in addition to routine care CTA examinations.

Coronary CTA scan protocol and image analysis

All examinations were performed with a 256-slice scanner with prospective ECG-triggered acquisition mode. Images were acquired in cranio-caudal direction during a single breath-hold in inspiration. The following imaging parameters were used for data cquisition: 128×0.625mm detector collimation, 270ms gantry rotation time, 120 kV tube voltage and 300 mAs tube, field-of-view of 18 cm with a matrix of 512×512. A mid-diastolic triggering was used with 3% padding. Iomeprol contrast media with an iodine concentration of 400mg/ml (Iomeron 400, Bracco Ltd, Milan, Italy) was injected into an antercubital vein via an 18-gauge catheter and dual-syringe system. A triphasic injection protocol (1. saline; 2. 100% contrast; 3. 25% contrast) with 90–95 ml contrast agent was used at a flow rate of 5.0-5.5 ml/s. We used bolus tracking technique with a region of interest (ROI) placed in the left atrium for proper scan timing.

All coronary CTA images were reconstructed with filtered back reconstruction (FBP), hybrid iterative reconstruction (HIR) and iterative model reconstruction (IMR). To ensure data consistency, all three datasets for each patient were generated on an external prototype workstation dedicated for the study. We reconstructed all images with 0.8 mm slice thickness, 0.4 mm increment and medium cardiac kernel. We applied a moderate iteration level for HIR (level 4 of 1-7) and IMR (level 2 of 1-3).

We used a commercially available DICOM viewer (Osirix, version 5.5.1; Osirix Foundation, Geneva, Switzerland) for image quality assessment. Image quality parameters were evaluated blinded to reconstruction type in a random order. For qualitative assessment we reviewed single datasets using fixed window set- tings (window width of 200 HU and window level of 700 HU). For quantitative analysis we displayed the triplets of datasets side by side for each patient to ensure the same level of ROI placement. We transferred the datasets present with any calcified or partially calcified plaque to a dedicated offline workstation (QAngio, version 2.1; Medis Medical Imaging Systems, Leiden, The Netherlands) for further plaque characterization. One reader with 5 years of experience in coronary CTA read all studies. 20 randomly selected datasets were re-evaluated by another reader with 3 years of experience in

coronary CTA to assess intra-observer differences.

We used the guidelines of the SCCT for the assessment of the coronary segments.[251] The proximal and distal segments of the left anterior descending artery (LAD), circumflex artery (CX) and right coronary artery (RCA) were evaluated. As we aimed to assess the differences between proximal and distal coronary segments, middle coronary segments and side branches were not included in our analysis. Four-point Likert-scale was used to rate subjective image quality parameters on axial slices.[252] Overall image quality was defined as a summary of image sharpness, image noise and blooming artifacts, if present and rated as follows: non-diagnostic (0); moderate, considerable artifacts with diagnostic image quality (1); good, minor artifacts (2) and excellent (3) image quality. Subjective noise was further analysed and categorized according to the graininess on the coronary CTA image: severe image noise (0); above average (1); average (2); no image noise (3). Circular regions of interest (ROIs; 3-4 mm^2) were manually placed in the coronary arteries and pericoronary fat to obtain median CT number in HU. ROIs were placed in a homogenous region of the proximal and distal segments of LAD, CX and RCA and the correspondent areas of the pericoronary fat. Artifacts, inhomogeneous regions and plaques were carefully avoided. Median image noise was determined as the standard deviation (SD) of the CT attenuation placed a circular ROI (200mm^2) within the aortic root at the level of the LM coronary ostium. The copy and paste function of the workstation was used to measure exactly the same ROIs at all three reconstruction datasets. Contrast to noise ratios (CNR) were calculated for all segments, as $CNR=(HU_{lumen} - HU_{fat})/noise$; HU_{lumen} and HU_{fat} represents the median CT attenuation in the coronary artery lumen and the pericoronary adipose tissue.[253]

For plaque quantification each dataset was loaded separately and after automated segmentation of the coronary tree the proximal and distal end points of each plaque were set manually. We took screen shots of anatomical fiducial markers to ensure that we analysed the same plaques across the different reconstruction datasets. Fully automated plaque quantification was performed without any manual corrections of boundaries to exclude the influence of observer bias. After automated delineation of the outer and inner vessel-wall boundaries we used the following fixed thresholds: calcified plaque volumes (>130 HU), non-calcified plaque volumes with high attenuation (90-129 HU), intermediate attenuation (30-89 HU) and low attenuation (<30 HU). Overall plaque volume, overall plaque burden (defined for a given lesion as the vessel volume minus the luminal volume, divided by the vessel volume at the site of the plaque), vessel volume and lumen volume was assessed on a per lesion basis for each reconstruction (Figure 11). Overall plaque volume was defined as the sum of calcified and non-calcified plaque component volumes on a per lesion basis.

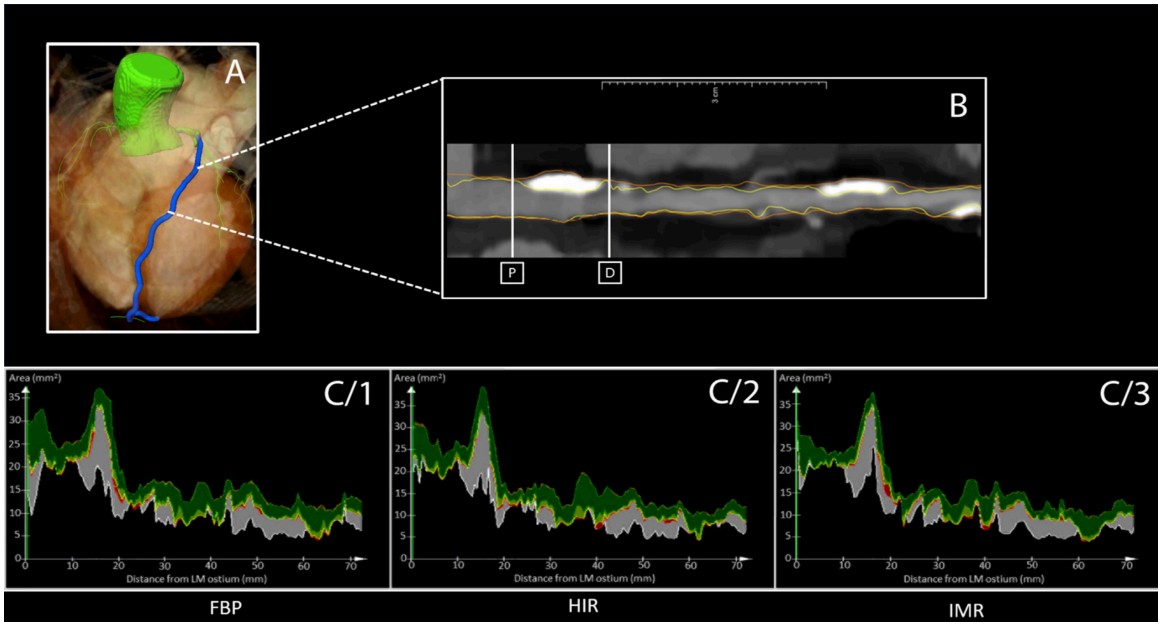

Figure 11 | Plaque quantification with FBP, HIR and IMR technique. Components of a mainly calcified atherosclerotic plaque in the proximal left anterior descending artery (LAD, marked with the blue line on the volumetric 3D reconstruction) are quantified using automated software after coronary segmentation (Panel A.). Consequently, the proximal (P) and distal (D) endpoints of the predominantly calcified plaque were selected on the CT images (Panel B.). After centerline extraction the software automatically detected lumen (yellow) and outer vessel wall (orange) contours. Panel C shows the plaque measurements for all three reconstructions (C/1: FBP; C/2: HIR; C/3: IMR) and the colors are indicated for various plaque components (white: calcified, >130 HU; dark green: non-calcified with high attenuation, 90–129 HU; light green: non-calcified with intermediate attenuation, 30–89 HU; red: non-calcified with low attenuation (<30 HU) Plaque volumes were 156.0 mm^3 for FBP, 148.7 mm^3 for HIR and 133.2 mm^3 for IMR. Calcium volumes were 80.1 mm^3 for FBP, 77.7 mm^3 for HIR and 74.2 mm^3 for IMR, respectively. FBP: filtered back projection; HIR: hybrid iterative reconstruction; IMR: iterative model reconstruction, HU: Hounsfield units.

Statistical analysis

The Kolmogorov-Smirnov test was applied to evaluate normality of continuous variables. Continuous variables are expressed as median with interquartile range (IQR) as appropriate. Categorical variables are expressed as frequency and percentage. The number of assessable segments was compared using chi-square test. Plaque features and image quality parameters (both quantitative and qualitative) of the IMR, HIR, and FBP images were compared by using the Friedman test with Bonferroni-Dunn test for post-hoc comparisons. The Wilcoxon signed rank test was used to assess the difference between image quality parameters of the proximal and distal vessel segments. The inter-reader reproducibility between image quality measurements (median vascular attenuation and CNR) was calculated using Lin's concordance correlation coefficient. The following descriptive scale was used for values of the concordance correlation coefficient: $\rho<0.90$ poor, 0.90-0.94 moderate, 0.95-0.99 substantial, $\rho>0.99$ almost perfect. The reproducibility of visual assessment of two observers was measured with kappa statistics interpreted as follows: $\kappa <0.20$ poor, 0.21-0.40 fair, 0.41-0.60 moderate, 0.61-0.80 good, 0.81-1.00 very good.[254] A p value of 0.05 was considered significant. Statistical analysis was performed using SPSS (IBM Corp, version 22.0, Armonk, NY, USA).

4.1.4 Image quality in heart transplanted patients

Study population

In this retrospective matched case-control cohort study, we evaluated the image quality of coronary CTA performed in patients who underwent heart transplantation (HTx).[255] The institutional review board of Semmelweis University approved the study (approval number SE-TUKEB 173/2016), and because of the retrospective study design, informed consent was waived. The study was conducted in compliance with the Helsinki declaration.

During a 4-year period, 97 coronary CTAs were performed of 57 HTx recipients to rule out CAV. If a patient underwent more than one scan, the scan obtained with the highest HR was selected. Scans with breathing artifacts (n=3), contrast agent extravasation (n=1), and high image noise or insufficient contrast opacification (n=3) were excluded from the study. In total, 50 HTx recipients (HTx group) were included in the study. The image quality of the scans of the HTx recipients was com- pared with that of scans of a control group of patients who did not undergo HTx. The control group was selected from our institutional cardiac CT registry. We

selected the control group according to matching criteria that may influence image quality: age, sex, body mass index (weight in kilograms divided by the square of height in meters), HR, data acquisition phase (systole or diastole), and coronary dominance (Figure 12). For the HR, a maximum difference of ±2 beats/min was allowed; for body mass index and age, a maximum difference of ±10% was allowed. In addition, we matched every pair for coronary dominance. Codominant coronary system was regarded as left dominant.

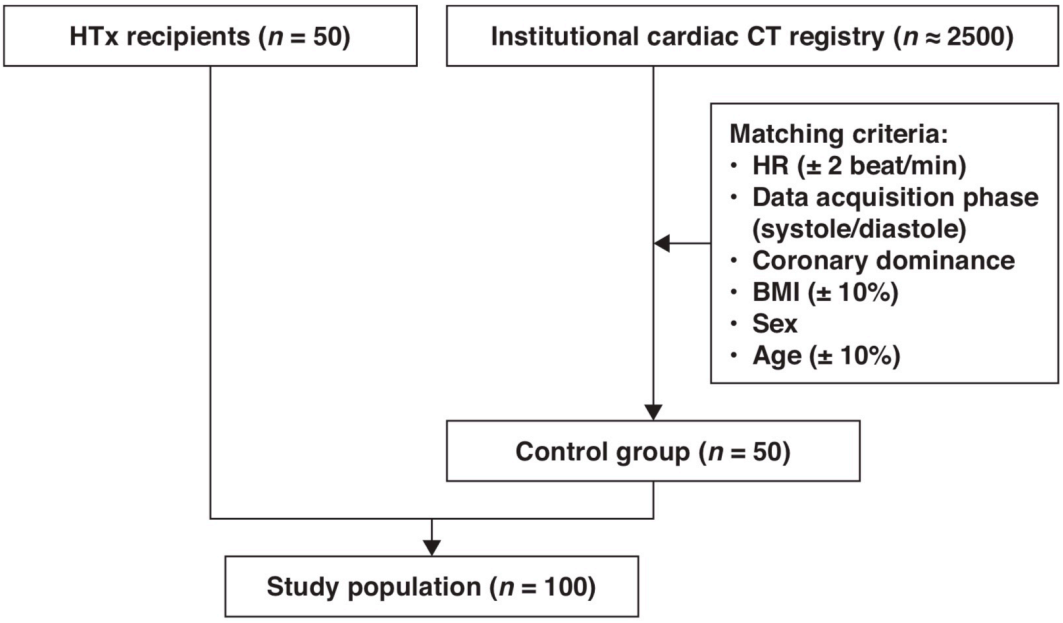

Figure 12 | Flowchart of study population selection. BMI = body mass index (weight in kilograms divided by the square of height in meters), HR = heart rate, HTx = heart transplantation.

Coronary CTA scan protocol and image analysis

All patients underwent imaging with a 256-MDCT scanner (Brilliance iCT 256, Philips Healthcare). Tube voltage was 100–120 kV, and the tube current was set to 100–300 mA depending on the body mass index of the patients. Collimation was 2×128×0.625 mm, with a gantry rotation time of 270 ms. Both the HTx recipients and the control group were scanned with a prospectively ECG-triggered acquisition mode. When the HR was over 80 beats/min, systolic triggering was used at 40% of the cardiac cycle with 3% padding (37-43% of the R-R interval); in all other cases, diastolic triggering was used at 78% of the cardiac cycle with 3% padding (75–81% of the R-R interval).[256] We used a four-phase contrast injection protocol with iodinated contrast agent (iomeprol, 400 mg I/mL; Iomeron 400, Bracco), with a flow rate of 4.5–5.5 mL/s with an extra saline bolus preceding the contrast bolus described in detail in section 4.1.2. A bolus-tracking technique was used with an ROI in the left atrium. For HR

control, we used 7.5-15 mg ivabradine (Procorolan, 5 mg, Les Laboratoires Servier) administered 3 hours before the scan in 90% of HTx recipients and 50–100 mg oral metoprolol and 5–20 mg IV metoprolol (Betaloc, 1 mg/mL, AstraZeneca; 5-mg ampoule) in 58% and 48% of control subjects, respectively. All patients received 0.8 mg of sublingual nitroglycerin (Nitromint, 8 mg/g, EGIS) a maximum of 1 minute before the image acquisition. Images were reconstructed with 0.8-mm slice thickness and 0.4-mm increment using a hybrid iterative reconstruction (iDOSE4, Philips Healthcare) technique.

Reconstructed images were evaluated by two readers (with 5 and 3 years of experience in coronary CTA) using the 18-segment model of the SCCT.[251] Coronary segments with a diameter greater than 1.5 mm were assessed. We used axial images, multiplanar reformations, and maximum intensity projections to evaluate the image quality. Motion artifacts were described in every coronary segment using a 4-point Likert scale: 0, excellent image quality with no artifacts; 1, good image quality with minor artifacts; 2, moderate image quality,

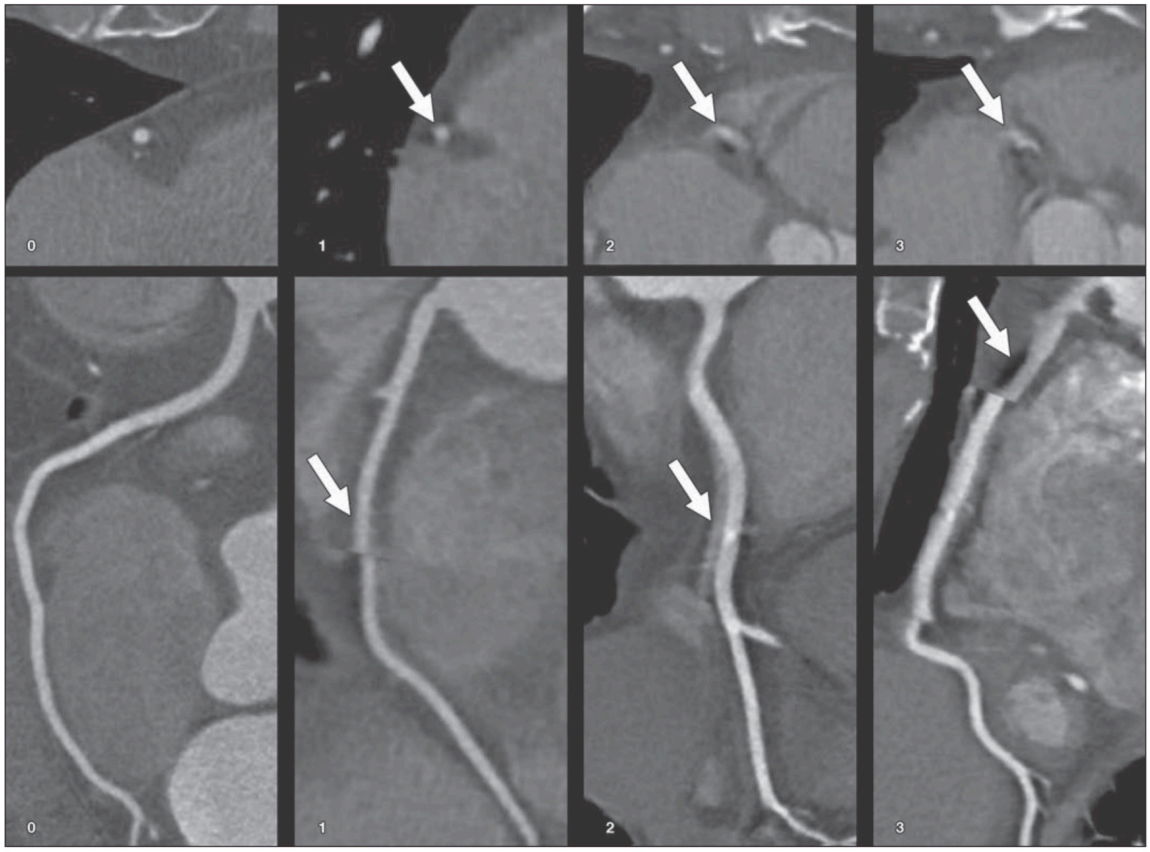

Figure 13 | Examples of 4-point Likert scale of motion artifacts in heart transplant recipients: 0, excellent image quality with no artifacts (62-year-old man); 1, good image quality with minor artifacts (60-year-old woman); 2, moderate image quality, acceptable for routine clinical diagnosis (44-year-old woman); 3, not evaluable, with severe artifacts impairing accurate evaluation (60-year-old man). Upper panels show cross-sectional CT angiography images of right coronary arteries with different motion artifact severities. Lower panels show same vessels in curved multiplanar reconstructions. Arrows indicate motion artifacts.

acceptable for routine clinical diagnosis; and 3, not evaluable, with severe artifacts impairing accurate evaluation (Figure 13).[257,258]

To quantify the total amount of motion artifacts on a per-patient level, we defined the segment motion score, which describes how many segments had motion artifact, and the segment Likert score, which is the sum of the motion severity Likert score of the patient. Because the number of coronary segments affects the total obtainable score, we normalized the scores by dividing them by the number of segments present, which resulted in the segment motion score index and segment Likert score index. To describe how many non-diagnostic segments were present, we defined the segment non-diagnostic score and also divided it by the number of the evaluated segments, which yielded the segment non-diagnostic score index. Furthermore, to assess the effect of systolic versus diastolic triggering, we conducted a subgroup analysis among both HTx recipients and control subjects.

Statistical analysis

The Shapiro-Wilk test was used to assess normality. Because all continuous variables showed nonnormal distribution, continuous variables are expressed as median and interquartile range (IQR). Categoric variables are expressed as numbers and percentages. The Mann-Whitney U test was used to compare continuous data of the HTx and non-HTx groups. Categoric data were compared using the chi-square test. Intrareader and inter-reader reproducibility was assessed on the basis of 20 randomly selected individuals' images using Cohen kappa, interpreted as follows: 1.00-0.81, excellent; 0.80-0.61, good; 0.60-0.41, moderate; 0.40-0.21, fair; and 0.20-0.00, poor.[254] All statistical calculations were done using SPSS software. A $p<0.05$ was considered significant.

4.2 Atherosclerotic plaque imaging by cardiac CT *ex vivo* investigations

In the second part of my Doctoral thesis, I will describe the studies that we have conducted in the field of coronary atherosclerotic plaque assessment. These investigations reflect a continuum of medical research from bench to bedside. The *ex vivo* investigations were performed at the Massachusetts General Hospital, Harvard Medical School in Boston. The clinical studies were performed at the Heart and Vascular Center of the Semmelweis University in Budapest.

4.2.1 The identification of novel signature of high-risk plaques

The heart of a 54-year-old man who died from acute subarachnoidal hemorrhage was investigated.[259] The patient's past medical history included hypertension and hyperlipidemia, which had been diagnosed 5 years earlier and treated since then. The patient did not have any previously known coronary artery disease. The heart was transferred to the Massachusetts General Hospital in Histidine-tryptophan-ketoglutarate solution packed in wet ice. The cold ischemic time was 12 h. The right and left coronary arteries were selectively cannulated and filled with methylcellulose-based iodinated contrast solution to achieve an average attenuation

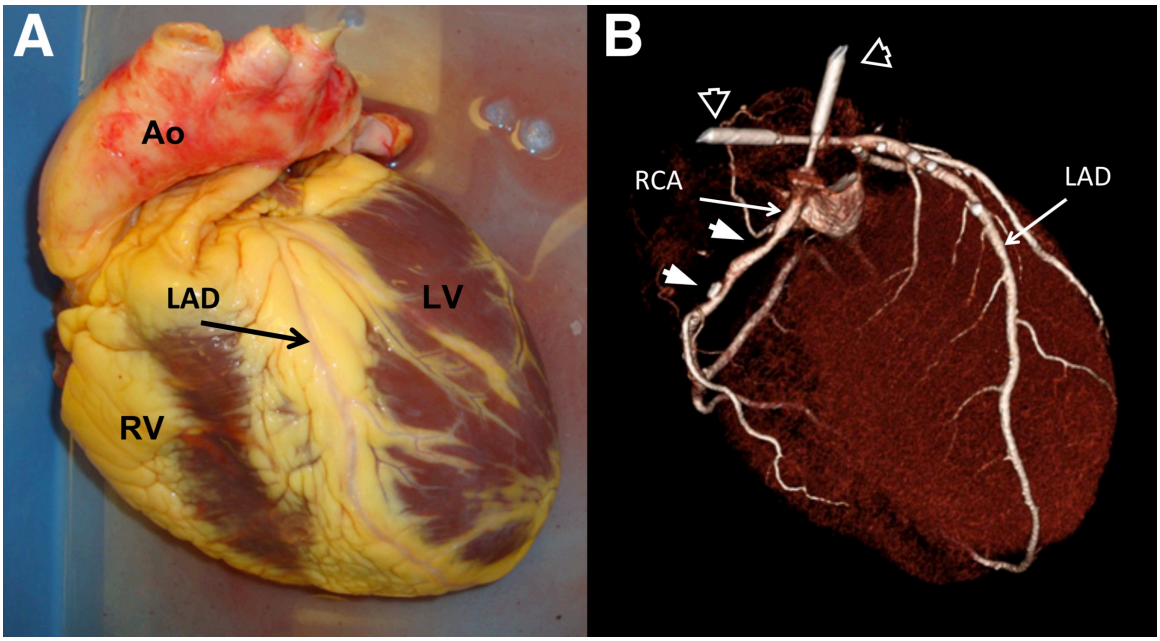

Figure 14 | Ex vivo donor heart and corresponding volume-rendered CT image. The open arrowheads indicate coronary canules; the white arrowheads indicate coronary plaques. Ao: Aorta; CT: computed tomography; LAD: left anterior descending artery; LV: left ventricle; RCA: right coronary artery; RV: right ventricle.

of 250 Hounsfield Units within the coronary vessels (Figure 14). The CT data acquisition was performed with a 64-detector row CT scanner (Discovery High Definition 750, General Electrics, Milwaukee, Wisconsin) using the following parameters for both the nonenhanced and contrast-enhanced scans: 64×0.625 collimation; 0.35 s rotation time; tube voltage of 120 kV; tube current of 500 mAs. A simulated ECG signal was used for prospective triggering. The entire dataset was reconstructed with a 0.625 mm slice thickness and 0.625 mm increment using a clinically available, raw data based adaptive statistical iterative reconstruction with a 0.28 mm × 0.28 mm pixel spacing. Following the CT data acquisition, the coronary arteries were excised and fixed in formalin. Histological sections were obtained in every 1 mm throughout the entire length of the coronary artery. Sections were stained with Movat's pentachrome and H&E. The CT cross sections and the histopathological slides were aligned based on absolute distance measurements and on identification of fiduciary markers (side branches, bifurcations, and vessel wall morphological features).

4.2.2 Attenuation pattern-based plaque classification

All procedures were approved by the institutional ethics committees of the Massachusetts General Hospital and were performed in accordance with local and federal regulations and the Declaration of Helsinki. The donor hearts were provided by the International Institute for the Advancement of Medicine (Jessup, Pennsylvania). The inclusion criteria were the following: donor age between 40 and 70 years, male sex, and history of myocardial infarction or coronary artery disease proven by diagnostic tests. Donors who underwent coronary artery bypass graft surgery were excluded from this study. The maximum allowed warm ischemia time was 6 h, and the maximum allowed cold ischemia time was 15 h. Seven isolated donor hearts (the median age of the donors: 53 years, range 42 to 61 years) were investigated.[260] The cause of death was stroke in 6 cases, and in 1 case, the cause of death was non-natural (suicide).

To prepare donor hearts, the right and the left coronary arteries were selectively cannulated and the coronaries were flushed with saline to remove air bubbles and superficial thrombi. A rubber balloon filled with 50 to 100 ml water was placed in the left ventricle to retain the physiological shape of the heart. The organ was positioned in the center of a canola oil tank to simulate the pericardial adipose tissue layer. The oil tank was secured on the CT table and an in-house prepared contrast agent was injected in the coronary arteries. To achieve

an intraluminal contrast enhancement similar to in vivo coronary CTA, methylcellulose (Methocel, DOW Chemical Company, Midland, Michigan) with 3% iopamidol contrast agent (Isovue 370, Bracco Diagnostics, Milan, Italy) was used. All CT data acquisition was performed with a 64-detector row CT scanner (High- Definition, GE Discovery, CT 750HD, GE Healthcare, Milwaukee, Wisconsin) using a sequential acquisition mode. The scan parameters were the following: 64×0.625 mm collimation; 0.35 s rotation time; tube voltage of 120 kV; tube current time product of 500 mAs. The entire dataset was reconstructed using an adaptive statistical iterative reconstruction technique (ASIR, GE Healthcare,) with a 40% blend with filtered back- projection. All reconstructed coronary CTA images were sent to an offline workstation for further analysis (Leonardo, Siemens Healthcare, Erlangen, Germany). Subsequent to the coronary CTA imaging, the coronary arteries were excised with surrounding tissue and the side branches were ligated. The coronaries were pressure-perfused (130 mm Hg) with 10% buffered neutral formalin solution to achieve tissue fixation. The preparation and the coronary CTA imaging were completed within 4 h after receiving the heart to avoid potential post-mortem changes of the tissue.

Histological analysis and image co-registration

The histological preparation and analysis was performed by experts specialized in cardiovascular pathology. Paraffin sections were obtained in 1.5-mm and in 2-mm increments (382 cuts and 185 cuts, respectively). Coronary artery segments with minimal atherosclerotic disease were sectioned every 5 mm (44 slides). The thickness of a single histological section was 6 μm. All sections were stained with Movat pentachrome. Each cross section was classified according the modified American Heart Association scheme into the following categories: adaptive intimal thickening (AIT); pathological intimal thickening (PIT); fibrous plaque (Fib); early fibroatheroma (EFA); late fibroatheroma (LFA); thin cap fibroatheroma (TCFA).[6] According to a report on atherosclerotic lesion classification from the American Heart Association, the AIT, Fib, and PIT were considered early atherosclerotic lesions, and EFA, LFA, and TCFA were categorized as advanced lesions.[261] The differentiation between early and advanced atherosclerotic lesions is based on histological criteria, where the terms mean both time-dependent development and complexity of atheroma formation. Advanced lesions are associated with vulnerability and with a higher risk of a subsequent clinical event.[261,262]

In addition to the analysis of the individual cross sections, we stratified each of the 21 vessels into individual atherosclerotic plaques. A plaque was defined as at least 1 cross section

with Fib, EFA, LFA, or TCFA and separated (from the next lesion) by at least 1 cross section with AIT or PIT. A plaque was defined as advanced atherosclerotic plaque if it contained at least 1 cross section with EFA, LFA, or TCFA.

An experienced investigator, who did not take part in the image assessment, performed the co-registration of coronary CTA and histology images. A multiplanar reconstruction technique was used to generate coronary CTA images perpendicular to the vessel centerline at the position of the histological cuts. A combined mathematical and anatomical approach was used to match the coronary CTA and histological images. As the first step, we calculated the distance of each image cross section from the 0-reference point (distal end of the plastic luer). Second, we used anatomical markers visible on both coronary CTA and histology, such as side branches, bifurcations, and features of vessel wall morphology (e.g., plaque shape, calcification pattern, orientations of the myocardium and pericardial adipose tissue layer) to match the position and set the rotational orientation of each image.

We formed the qualitative reading of all coronary CTA cross sections and assessed the images for the presence and composition of plaque as will be described. Subsequently we performed the analyses of 100 randomly selected cross sections to calculate interobserver variability. Initially, plaque was characterized as non-calcified plaque (NCP), calcified (CP), or partially calcified plaque (PCP). Specifically, any discernible structure that could be assigned to the coronary artery wall, but with a CT density below the contrast-enhanced coronary lumen and above the surrounding connective tissue, was defined as non- calcified coronary atherosclerotic plaque.[77] Any hyperdense structure that could be visualized separately from the contrast-enhanced coronary lumen (either because it was “embedded” within NCP or because its density was above the contrast- enhanced lumen) and could be assigned to the coronary artery wall was defined as calcified atherosclerotic plaque.[77]

A second qualitative reading was performed to describe the attenuation pattern of NCP in cross sections previously classified as NCP or MP. A plaque cross section was classified as heterogeneous if at least 2 regions of different attenuation could be visually distinguished within the noncalcified portion, whereas the plaque was classified as homogenous if no such distinction could be made. Plaque cross sections with a heterogeneous attenuation pattern were further subclassified into plaques with and without the napkin-ring-sign (NRS) that we have identified previously (described in sections 4.2.1 and 5.2.1).[259] NRS was defined as the presence of low CT attenuation in the center of the plaque close to the lumen surrounded by a rim area of higher attenuation.[259] Heterogeneous plaques were identified as non-NRS plaques if the pattern of low and high attenuation was spatially non-structured or random. Thus, the PAP

classification scheme comprised 3 categories: homogenous plaque; non-NRS heterogeneous plaque; and NRS heterogeneous plaque (Figure 15). All readings were performed with a fixed window setting (700 Hounsfield units [HU] width, 200 HU level).

Statistical analysis

Continuous variables were expressed as mean±SD, and categorical variables were expressed as frequencies or percentages. To determine interobserver variability, an independent reader assessed a random subset of 100 cross-registered coronary CTA images for conventional plaque categories and PAP. The interobserver agreement was evaluated using Cohen kappa statistics that were interpreted as follows. A k value greater than 0.80 corresponded to an excellent agreement, and a kappa value of 0.61 to 0.80 corresponded to a good interobserver agreement.[263]

For all remaining analysis, cross sections containing purely calcified plaque on coronary CTA were excluded. We determined whether the distribution of the PAP categories (homogenous, heterogeneous with and without the NRS) differed between traditional plaque categories (NCP, MP) and whether the frequency of advanced lesions (defined as EFA, LFA, or TCFA) and TFCA differed significantly within PAP categories (homogenous, heterogeneous with and without the NRS) and traditional plaque categories (NCP, MP). To test for statistical significance, Fisher exact test was used for 2×2 tables and chi-squared test for tables with more

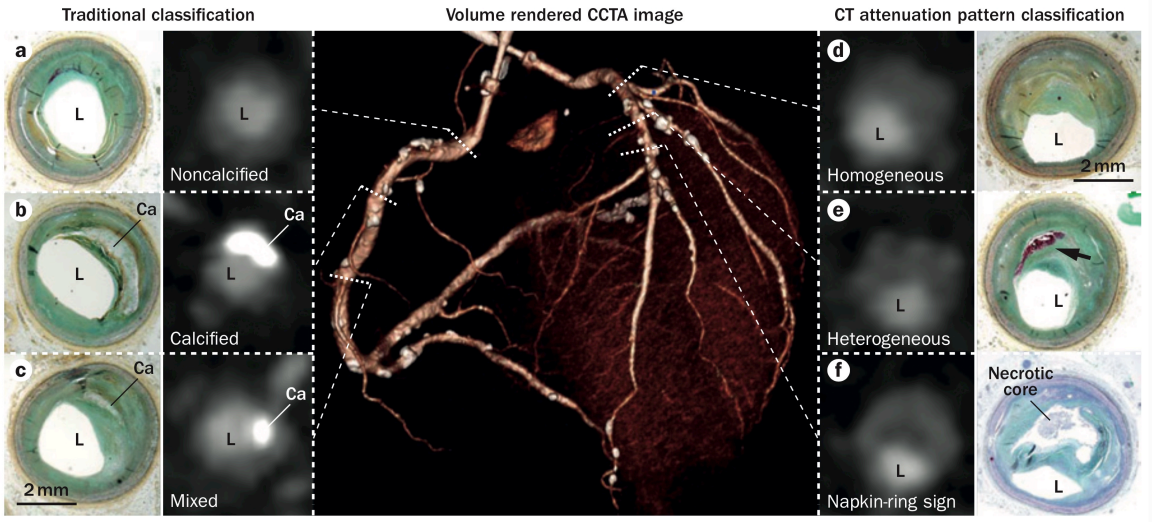

Figure 15 | Conventional and attenuation pattern-based plaque classification schemes in coronary CTA. The centre panel shows a volume-rendered coronary CTA image of a cadaver heart. The traditional plaque classification scheme differentiates between a | noncalcified, b | calcified, and c | partially calcified (mixed) plaques. CT attenuation pattern-based classification (right panel) differentiates between d | homogeneous, e | heterogeneous, and f | napkin-ring plaques. The corresponding histology slides show a | pathological intimal thickening, b | fibrous plaque with sheet calcification, c | pathological intimal thickening with spotty calcification, d | a fibrous plaque, e | early fibroatheroma with intraplaque haemorrhage (arrow), and f | a late fibroatheroma with large necrotic core. Abbreviations: Ca, calcium; L, lumen.

rows or columns.

To determine the diagnostic accuracy of CT-based plaque composition (both conventional and attenuation pattern-based classification) for the detection of advanced lesions and TFCA sensitivity, specificity, negative predictive value, and positive predictive value were calculated from 2×2 contingency tables. We calculated binomial 95% confidence intervals (CI), as well 95% CI adjusted for the correlated data structure on a per lesion level. For this, a SAS (SAS Institute Inc., Cary, North Carolina) macro has been written using a within-cluster correlation estimator.[135,264] Adjusted 95% CI have been reported if not otherwise specified. To assess further the diagnostic capacity CCTA to detect advanced lesions and TFCA, the C-statistic was used. In the first step, the categories for each classification scheme were sorted separately by their likelihood ratio for advanced lesions and TFCA. Next, separated logistic regression models for each scheme were fitted, and C-statistics were derived, which are equivalent to the AUC.[265] The asymptotic 95% CI for the AUC were estimated using a nonparametric approach, which is closely related to the jackknife technique as proposed by DeLong et al. and comparisons in AUC/C-statistics were performed by using a contrast matrix.[266] All statistical tests were performed by using software SAS (version 9.2). A p value of <0.05 was considered statistically significant.

4.2.3 Multimodality plaque imaging

In this investigation we have included three isolated donor hearts with proven coronary artery disease.[267] The coronary CTA protocol was the same as described in the section 4.2.2.. After coronary CTA was completed, the coronary arteries were flushed with saline to remove iodinated contrast medium (Figure 16). Prior to the IVUS imaging, the coronary arteries were connected to a pressure-perfusion system filled with phosphate-buffered saline and perfused with a constant pressure of 130 mmHg. A guidewire with hydrophobic coating (Cougar XT; Medtronic, Minneapolis, MN) was introduced in all three major coronary arteries. IVUS was performed by using a 40-MHz intravascular US catheter (Galaxy; Boston Scientific, Boston, Mass) and motorized pullback (0.5 mm/sec, 30 frames/sec, from distal to proximal). Images were digitized and stored for further analysis on an offline workstation (OsiriX 3.8; the OsiriX Foundation, Geneva, Switzerland).

Optical frequency domain imaging (OFDI) was performed with a prototype clinical system developed at the Wellman Center for Photomedicine at Massachusetts General Hospital.[268] The OFDI system acquired images at 20 frames per second, with a total of 2048 radial scans per circular cross section. Axial resolution was 7 mm in tissue, with a refractive index of 1.4 and a signal-to-noise ratio of 110 dB. Notably, the axial resolution of OFDI can be

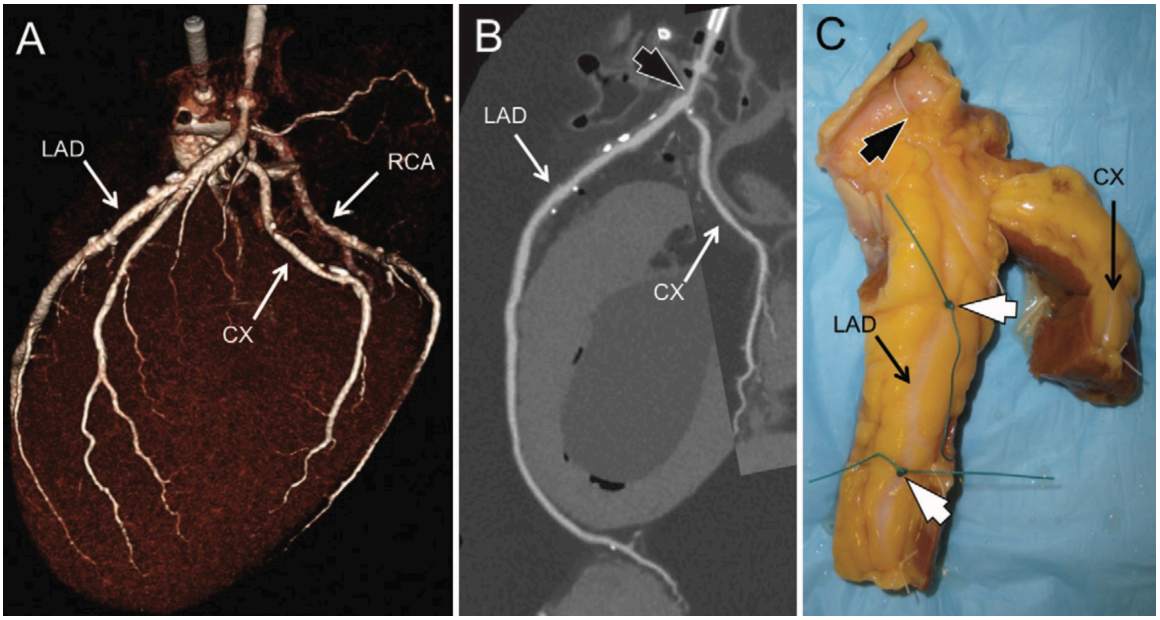

Figure 16 | A, Volume-rendered CT reconstruction of coronary anatomy. CX = circumflex artery, LAD = left anterior descending artery, RCA = right coronary artery. B, Curved multiplanar reconstruction of left anterior descending (LAD) artery and circumflex artery (CX) show air bubble-free and homogeneous luminal enhancement of the vessels. C, After formalin fixation, the coronary arteries were excised. Black arrowheads in B, C = distal end of the plastic luer, which served as the zero reference point for image cross registration. White arrowheads (green surgical knots) in C = 40-mm and 80-mm reference distances.

lower in clinical practice (approximately 10-15 mm).[269] The OFDI catheter had 30-mm transverse resolution with a focal distance of approximately 2 mm. The motorized pullback speed of the optical imaging core was 1 mm/sec, which translated to a 50-mm longitudinal resolution. The OFDI catheter was positioned in the distal portion of the coronary artery to maximize the length of each imaged vessel segment. During OFDI, the coronary arteries were perfused with phosphate-buffered saline. The images were processed at an offline workstation (OsiriX 3.8).

Histologic preparation and analysis were performed as described in section 4.2.2. Briefly, paraffin slices (thickness, 6 mm) were obtained in 1.5 mm increments throughout the entire length of each coronary artery, starting at the zero-reference point (distal end of the luer) and numbered consecutively. The mean analysed vessel length was 60 mm (range, 25-110 mm). The slices were stained with Movat pentachrome and hematoxylineosin (H&E). Images from all three imaging modalities and from histologic examination were coregistered and analysed by using clinically accepted algorithms.

Statistical analysis

Continuous variables were expressed as means 6 standard deviations, and categorical variables were expressed as percentages. The interobserver agreement for plaque differentiation was assessed for each modality (coronary CTA, IVUS and OFDI) by using Cohen κ statistics interpreted as follows: A κ value >0.80 corresponded to excellent agreement, and a κ value between 0.61 and 0.80 corresponded to good interobserver agreement.[263]

To assess the association for each category of coronary CTA, IVUS, and OFDI with early or advanced lesion as defined by histopathologic findings, we used odds ratios (ORs). An OR>1.0 indicated an in- creased probability of a lesion being an advanced lesion, whereas an OR<1.0 indicated an increased probability of a lesion being an early lesion. The Fisher exact test was used to evaluate whether these crude associations were significant. In addition, we recalculated these associations accounting for clustering effects within a lesion by using non-linear mixed-effects models (SAS proc NLmixed; SAS Institute, Cary, NC). All statistical tests were performed by using software (SAS, version 9.2; SAS Institute). A *p* value of less than 0.05 was considered to indicate a statistically significant difference.

4.2.4 Performance of CT versus invasive coronary angiography to detect plaques

Study population

The Genetic Loci and the Burden of Atherosclerotic Lesions (GLOBAL) study enrolled patients who were referred to coronary CTA due to suspected CAD (NCT01738828).[270,271] The study was approved by the Institutional Ethical Review Board, and all participants provided written informed consent for the GLOBAL study. Out of the 883 patients enrolled by our institution into the GLOBAL study, we selected individuals who underwent both coronary CTA and invasive coronary angiography (ICA) within 120 days.[60] Only patients with diagnostic image quality for all coronary segments were selected. In total, 71 patients were included in our analysis. In 58 patients, ICA followed CTA based on clinical findings, while in 13 cases ICA was carried out before CTA. These patients were either referred to CTA after revascularization due to atypical chest pain (seven patients), or were referred to left atrial angiography before radiofrequency ablation (six patients), Table 4.

Table 4 Demographics of study population

Variable	n = 71
Age (years)	61.6 ± 9.0
Female	26 (37 %)
Body Mass Index (kg/m^2)	27.9 ± 4.3
Hypertension	51 (72 %)
Diabetes Mellitus	13 (18 %)
HDL (mmol/l)	1.34 ± 0.4
LDL (mmol/l)	3.0± 1.3
Triglyceride (mmol/l)	1.7 ± 0.8
Cholesterol (mmol/l)	4.8 ± 1.6
Time between coronary computed tomography angiography and invasive coronary angiography (days)	40.2 ± 32.1

Cardiac CT scan and image analysis protocol

All patients underwent a prospectively ECG-triggered coronary CTA scan using a 256-slice multi-detector row computed tomography. Oral β-blockers (metoprolol, maximum dose 100 mg) were administered one hour before the procedure, if the heart rate was above 65 beat per minutes. Coronary CTA images were acquired in axial mode with 270 msec rotation time, 128×0.625 mm collimation, tube voltage of 100-120 kVp at 78% of the R-R interval.

All images were randomly and independently analysed. Semi-quantitative plaque burden quantification of ICA images was performed by an interventional cardiologist (IFÉ with 10 years of experience). A minimum of 5 projections of the left and right coronary systems were acquired in each patient. All coronary segments were analysed blinded to CTA results, using a minimum of 2 projections. Images were analysed using axial thin-slice and multiplanar reformations (Figure 17). For inter-reader reproducibility measures, ICA and CTA images were also analysed by second readers.

A total of 1016 segments were assessed based on the 18-segment SCCT classification with both modalities.[272] We excluded 16 segments due to presence of coronary stents leading to overall 1000 analysed segments. All segments were scored for the presence or absence of plaque (0: Absent; 1: Present) and the degree of stenosis (0: None; 1: Minimal (<25%); 2: Mild (25%-49%); 3: Moderate (50%-69%); 4: Severe (70%-99%) or 5: Occlusion (100%)). In case

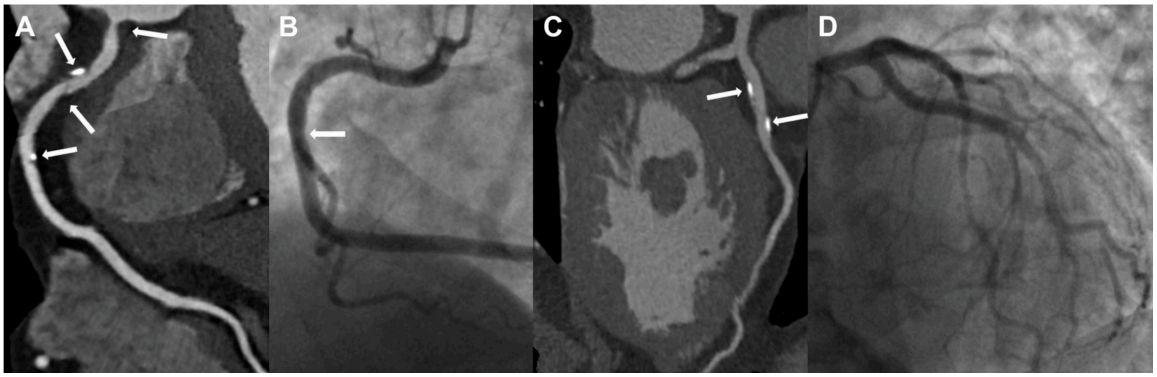

Figure 17 | Representative image showing the difference in plaque burden observed using coronary CTA and ICA images. Coronary CTA and ICA images of a 55-year-old man. (A) Coronary CTA and (B) ICA images of the right coronary artery of the patient. Although coronary CTA showed 4 plaques, ICA only detected 1. (C, D) Coronary CTA and ICA images, respectively, of left coronary artery. Coronary CTA shows 2 plaques that were not detected on ICA.

multiple lesions were present in a segment, the observers recorded the highest degree of stenosis for that segment. In each patient, segment involvement score (SIS) was used to quantify the number of segments with any plaque, whereas segment stenosis score (SSS) was calculated by summing the stenosis scores of each segment. Indexed values were calculated by dividing the SIS and SSS scores by the number of segments: segment involvement score index (SISi) = SIS / number of segments; segment stenosis score index (SSSi) = SSS / number of segments.

Based on Bittencourt et al. the patients were classified as extensive obstructive (SIS > 4 and ≥50% stenosis), extensive non-obstructive (SIS > 4 and <50% stenosis), non-extensive obstructive (SIS ≤ 4 and ≥50% stenosis) or non-extensive non-obstructive (SIS ≤ 4 and <50% stenosis) based on ICA and also CTA results.[117]

Statistical analysis

All continuous variables are expressed as mean±standard deviation (SD), while categorical variables are expressed as frequencies and percentages. Presence of plaque was compared using the chi-square test between modalities. Sensitivity, specificity, positive predictive value and negative predictive value were calculated to assess the diagnostic accuracy of CTA as compared to ICA as reference standard. SIS, SSS and SISi, SSSi were compared using the paired t-test between modalities. Intra-reader and inter-reader reproducibility were

assessed based on 20 randomly selected individuals' images using Cohen's κ for stenosis categories, and intra-class correlation (ICC) for segment scores. Cohen's κ and ICC values are interpreted as: 0.81 - 1.00: Excellent; 0.61 - 0.80: Good; 0.41 - 0.60: Moderate; 0.21 - 0.40: Fair; 0.00 – 0.20: Poor.[263,273] Reclassification rate was calculated by dividing the number of people who shifted groups based on the two modalities by the total study population. All statistical calculations were performed using SPSS software (SPSS version 23; IBM Corp., Armonk, NY). A p-value of 0.05 or less was considered significant.

4.2.5 Coronary CTA based radiomics to identify napkin-ring plaques

Study design and study population

Institutional review board approved the study (SE TUKEB 1/2017) and due to the retrospective study design informed consent was waived. The data and study materials will not be made available to other researchers for purposes of reproducing the results or replicating the procedure due to intellectual property and patient confidentiality. However, we made our analysis software open source and freely accessible for other researchers.

From 2674 consecutive coronary CTA examinations we retrospectively identified 39 patients who had NRS plaques.[274] Two expert readers re-evaluated the scans with NRS plaques. To minimize potential variations due to inter-reader variability the presence of NRS was assessed using consensus read. Readers excluded 7 patients due to insufficient image quality and 2 patients due to the lack of the NRS, therefore 30 coronary plaques of 30 patients (NRS group; mean age: 63.07 years [IQR: 56.54; 68.36]; 20% female) were included in our analysis. As a control group, we retrospectively matched 30 plaques of 30 patients (non-NRS group; mean age: 63.96 years [IQR: 54.73; 72.13]; 33% female) from our clinical database with excellent image quality. To maximize similarity between the NRS and the non-NRS plaques and minimize parameters potentially influencing radiomic features, we matched the non-NRS group based on: degree of calcification and stenosis, plaque localization, tube voltage and image reconstruction.

To assess image quality, we measured the signal-to-noise ratio defined as the mean coronary luminal CT attenuation in Hounsfield units (HU) adjacent to the plaque in a healthy segment divided by the standard deviation of the CT attenuation in the aorta measured in a region of interest at least 2 cm^2 at the level of the left main trunk. Contrast-to-noise ratio (CNR) was calculated as the mean luminal HU minus the perivascular HU at the site of the plaque divided by the standard deviation of the aortic HU. All measurements were performed on a

clinical workstation (IntelliSpace portal, Philips Healthcare, Best, The Netherlands). Detailed patient and scan characteristics are summarized in Table 5.

Table 5 Patient characteristics and scan parameters.

	NRS group (n=30)		non-NRS group (n=30)		p
Demographics					
Age (years)	63.1	[56.5; 68.4]	64.0	[54.7; 72.1]	0.86
Male gender, n (%)	24	(80%)	20	(67%)	0.16
BMI (kg/m^2)	28.1	[25.1; 29.9]	26.9	[23.9; 29.3]	0.34
Cardiovascular risk factors					
Hypertension n (%)	19	(63%)	18	(60%)	0.78
Diabetes mellitus n (%)	25	(83%)	26	(87%)	0.65
Dyslipidemia n (%)	16	(53%)	18	(60%)	0.62
Current smoker n (%)	20	(67%)	21	(70%)	0.80
Scan parameters					
Total DLP (mGy x cm)	362.0	[356.0; 367.0]	358.2	[253.2; 367.0]	0.42
Pixel spacing (mm)	0.41	[0.39; 0.43]	0.43	[0.39; 0.45]	0.30

Conventional and radiomic plaque assessment

All plaques were graded for luminal stenosis (minimal 1-24%; mild 25-49%; moderate 50-69%; severe 70-99%) and degree of calcification (calcified; partially calcified; non-calcified). Furthermore, plaques were classified as having low-attenuation if the plaque cross-section contained any voxel with <30 HU, and having spotty calcification if a <3 mm calcified plaque component was visible. Detailed plaque and imaging information is shown in Table 6. Image segmentation and data extraction was performed using a dedicated software tool for automated plaque assessment (QAngioCT Research Edition; Medis medical imaging systems bv, Leiden, The Netherlands). After automated segmentation of the coronary tree the proximal and distal end of each plaque were set manually. Automatic lumen and vessel contours were manually edited by an expert if needed.[275] From the segmented datasets 8 conventional quantitative metrics (lesion length, area stenosis, mean plaque burden, lesion volume, remodeling index, mean plaque attenuation, minimal and maximal plaque attenuation) were

Table 6 Plaque and image quality characteristics.

	NRS group (n=30)		non-NRS group (n=30)		p
Plaque composition					1.00
Non-calcified, n (%)	19	(63%)	19	(63%)	
Partially calcified, n (%)	11	(37%)	11	(37%)	
Calcified, n (%)	0	(0%)	0	(0%)	
Luminal stenosis					1.00
Minimal (1-24%)	11	(37%)	11	(37%)	
Mild (25-49%)	11	(37%)	11	(37%)	
Moderate (50-69%)	6	(20%)	6	(20%)	
Severe (70-99%)	2	(7%)	2	(7%)	
Stenosis localization					1.00
Left main	2	(7%)	2	(7%)	
Left anterior descending	20	(66%)	20	(66%)	
Left circumflex	2	(7%)	2	(7%)	
Right coronary	6	(20%)	6	(20%)	
Image quality					
Contrast-to-noise ratio	21.94	[18.61; 28.80]	23.42	[18.64; 26.57]	0.70
Signal-to-noise ratio	18.69	[15.84; 24.13]	20.52	[16.33; 22.53]	0.59
High-risk plaque features					
Napkin-ring sign, n (%)	30	(100%)	0	(0%)	<0.0001
Low attenuation, n (%)	26	(87%)	19	(63%)	0.06
Spotty calcification, n (%)	10	(33%)	9	(30%)	0.99
Conventional quantitative metrics					
Lesion length (mm)	13.62	[10.42; 17.02]	13.48	[10.99; 17.71]	0.70
Lesion volume (mm^3)	134.88	[105.68; 190.76]	88.88	[70.02; 143.98]	0.02
Mean plaque burden	0.59	[0.52; 0.66]	0.51	[0.44; 0.59]	0.003
Lumen area stenosis	0.41	[0.15; 0.53]	0.28	[0.19; 0.49]	0.38
Vessel wall remodeling index	1.03	[0.92; 1.46]	1.09	[0.97; 1.20]	0.55
Mean plaque attenuation (HU)	114.67	[85.54; 148.99]	156.75	[138.46; 208.37]	0.002
Minimal plaque attenuation (HU)	-83.00	[-101.75; -58.00]	-60.00	[-84.75; -47.00]	0.10
Maximal plaque attenuation (HU)	523.00	[451.00; 794.50]	634.50	[454.00; 898.00]	0.63

calculated by the software. The voxels containing the plaque tissue were exported as a DICOM dataset using a dedicated software tool (QAngioCT 3D workbench, Medis medical imaging systems bv, Leiden, The Netherlands). Smoothing or interpolation of the original HU values was not performed. Representative examples of volume rendered and cross-sectional images of NRS and non-NRS plaques are shown in Figure 18.

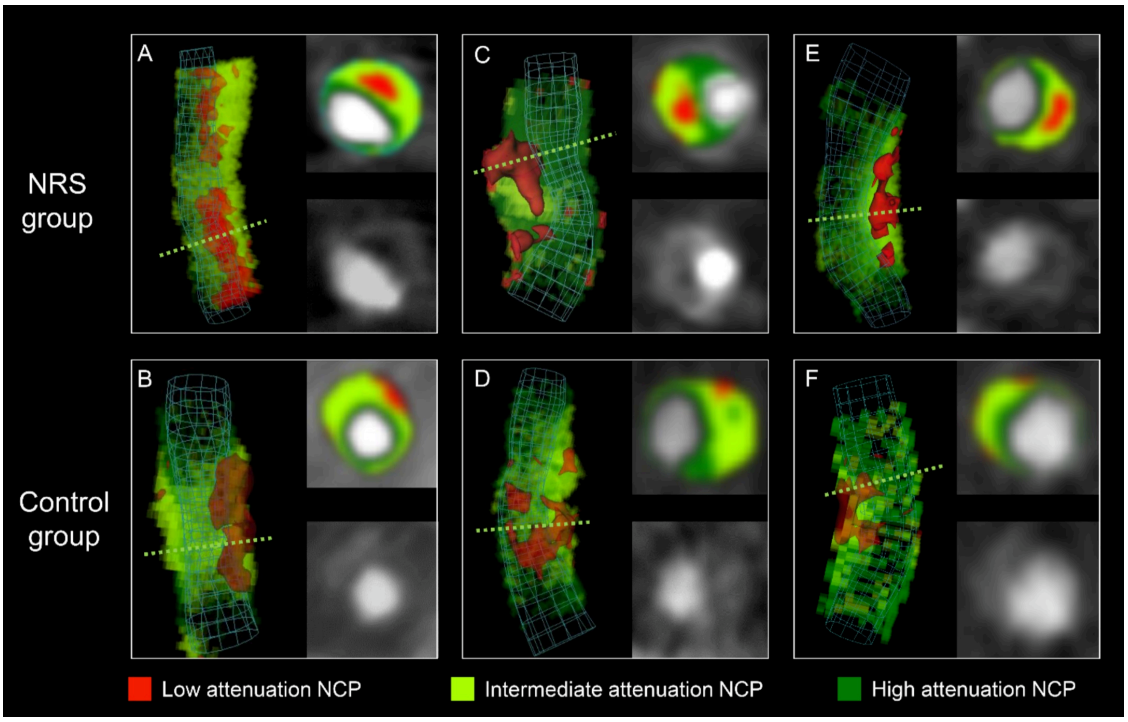

Figure 18 | Representative images of plaques with or without the napkin-ring sign (NRS). Volume-rendered and cross-sectional images of plaques with NRS in the top (A, C, and E) and their corre- sponding matched plaques in the bottom (B, D, and E) are shown. Green dashed lines indicate the location of cross- sectional planes. Colours indicate different computed tomographic attenuation values. NCP indicates noncalcified plaque.

We developed an open source software package in the R programing environment (Radiomics Image Analysis (RIA)) which is capable of calculating hundreds of different radiomic parameters on two- and three-dimensional datasets.[276] We calculated 4440 radiomic features for each coronary plaque using the RIA software tool. Using RIA software package, we calculated 44 first-order statistics, 3585 gray level co-occurrence matrix (GLCM) based parameters, 55 gray level run length matrix (GLRLM) based metrics and 756 geometry based statistics. For first-order statistics 3D arrays containing the HU values were transformed to a 1D vector, from which the statistics were calculated. For GLCM, GLRLM and geometry based analysis images were discretized by dividing the voxel values into 2, 4, 8, 16 and 32 equally probable bins each containing the same number of voxels. This resulted in 5 replicas of the images. The different bin sizes significantly affect the calculated radiomic feature values. Fewer

bins mean more robust values, however result in information loss, while more bins are susceptible to noise, but preserve more information.[277] We conducted our analysis hypothesis free, in a data driven manner by calculating statistics for each discretized image.

GLCM are matrices, where the element in the i^{th} row and j^{th} column represents the probability of finding a voxel with value j next to a voxel of value i in a given direction and distance. Each statistic was calculated for each of the 26 possible directions in 3D space and then averaged to receive rotationally independent measures. All statistics were calculated for distances 1, 2 and 3 voxels.

In the GLRLM matrix the element in the i^{th} row and j^{th} column represents how many times i value voxels occur next to each other j times in a given direction. Each statistic was calculated for each possible run direction in 3D space and then averaged to obtain rotationally independent measures.

Geometry-based statistics were done on raw data as well as discretized images. Surfaces, volumes and radiomic parameters were calculated from the dimensions of the raw image, where the voxels in-plane dimensions were equal to pixel spacing, while the cross-plane dimension was equal to the spacing between the slices. Fractal dimensions were calculated by padding the lesion into an isovolumetric cube with sides equal to the next greatest power of two of the longest dimension of the lesion. Consecutively smaller and smaller cubes were used to cover the lesion and calculate the given statistic.

Statistical analysis

Binary variables are presented as frequencies and percentages, while ordinal and continuous variables are presented as medians and interquartile ranges (IQR) due to possible violations of the normality assumption. For robust statistical estimates, parameters between the NRS and the non-NRS group were compared using the permutation test of symmetry for matched samples using conditional Monte Carlo simulations with 10,000 replicas.[278] For diagnostic performance estimates, we conducted ROC analysis and calculated AUC with bootstrapped confidence intervals values using 10,000 samples with replacement and calculated sensitivity, specificity, positive and negative predictive value by maximizing the Youden index.[279] To assess potential clusters among radiomic parameters, we conducted linear regression analysis between all pairs of the calculated 4440 radiomic metrics. The $1\text{-}R^2$ value between each radiomic feature was used as a distance measure for hierarchical clustering. The average silhouette method was used to evaluate the optimal number of different clusters in our

dataset.[280] Furthermore, to validate our results we conducted a stratified 5-fold cross-validation using 10,000 repeats of the three best radiomic and conventional quantitative parameters. The model was trained on a training set and was evaluated on a separate test set at each fold using ROC analysis. The derived curves were averaged and plotted to assess the discriminatory power of the parameters. The number of additional cases classified correctly was calculated as compared to lesion volume. The McNemar test was used to compare classification accuracy of the given parameters as compared to lesion volume.[281]

Due to the large number of comparisons, we used the Bonferroni correction to account for the family wise error rate. Bonferroni correction assumes that the examined parameters are independent of each other, thus the question is not how many parameters are being tested, but how many independent statistical comparisons will be made. Therefore, based on methods used in genome-wide association studies (GWAS) we calculated the number of informative parameters accounting for 99.5% of the variance using principal component analysis.[282,283] Overall, 42 principal components identified, therefore p values smaller than 0.0012 (0.05/42) were considered significant. All calculations were done in the R environment.[284]

4.2.6 Cardiac CT based FFR simulation

Study design and study population

Patients >18 years old, with no prior history of ischemic heart disease and with symptoms of stable chest pain were prospectively enrolled from two European centers.[285] Subjects were excluded from this study if they could not provide informed consent, were pregnant, had stage IV chronic kidney disease, had a documented allergy to iodinated contrast or had contraindications to betablockers, nitogylcerine or adenosine. Final study selection required high CTA image quality, and an intermediate stenosis severity of between 30-70%. The clinical teams were blinded to the on-site FFR-CT results. ICA was performed on all patients and invasive FFR was performed for the target lesion as determined by CTA and all bystander lesions. Detailed patient demographics are listed in Table 7. The study was

Table 7 Patient demographics

Variable	n = 44
Age (years)	64.6 ± 8.9
Women	15 (34%)
Body Mass Index (kg/m^2)	29.0 [26.0–31.2]
Hypertension	30 (68%)
Diabetes Mellitus	8 (18%)
Dyslipidaemia	33 (75%)
Smoking	11 (25%)
Cerebrovascular event	2 (5%)
Peripheral arterial disease	5 (11%)
Day between coronary CTA and ICA	34 [13–42]
Type of chest pain	
Typical	15 (34%)
Atypical	20 (46%)
Non-specific	9 (21%)

approved by both Institutional Ethical & Research Governance Review Boards, and all participants provided written informed consent.

Image acquisition and analysis

Patients underwent a non-contrast enhanced prospectively triggered CT for Agatston score evaluation followed by a coronary CTA. The CTA was performed using either retrospectively ECG gated tube dose modulated helical protocol on a 64-slice CT (Brilliance 64, Philips Healthcare, Cleveland Ohio, USA) or prospectively ECG triggered CTA using a 256-slice CT (Brilliance iCT, Philips Healthcare, Cleveland Ohio, USA). Local CTA protocols were used for scan acquisition, typically tube voltage was 100-120 kVp depending on the body mass index (BMI) of the patients, while tube current was 600-800 mAs for retrospective gated helical scans, and 200-300 mAs for axial scans triggered prospectively. For heart rate control, oral and intravenous beta-blockade was used if heartrate was >65 bpm. All patients received 0.8 mg sublingual nitroglycerine before the image acquisition. Images were reconstructed with a slice thickness of 0.8 mm at an increment of 0.4 mm using a standard filter.

Patients underwent ICA within 60 days of the coronary CTA. For FFR measurements the pressure wire (St Jude Medical, St Paul Minnesota, USA) was initially calibrated and then passed beyond the stenosis. For tandem lesions, measurements were made by manual pullback for both lesions separately. Hyperemia was induced by means of intravenous infusion of adenosine at 140 μg per kilogram of body weight per minute. FFR values of 0.80 or less were considered to indicate hemodynamically significant stenoses.

Coronary lumen segmentation was performed automatically using a commercially available advanced cardiac application (Comprehensive Cardiac Analysis, IntelliSpace Portal Version 6.0, Philips Healthcare, Cleveland, Ohio, USA). Each of us (an experienced cardiologist from Belfast and myself) independently reviewed the lumen segmentation in all cases, performing corrections as needed. Additionally, I have also reviewed and corrected the lumen segmentation of all the cases after a period of 3 months to assess intra-observer variability. The effective luminal diameter stenosis (EDS) was quantified on curved multiplanar reformatted images using a dedicated software tool by identifying the minimum diameter and the reference diameter for all stenosis (Comprehensive Cardiac Analysis, IntelliSpace Portal Version 6.0, Philips Healthcare, Cleveland, Ohio, USA). The segmented coronary artery tree lumen was used as an input to a research prototype on-site FFR-CT simulation algorithm (Version 1.0.2, Philips Healthcare, Cleveland, Ohio, USA). A representative image of on-site FFR-CT simulation is shown in Figure 19.

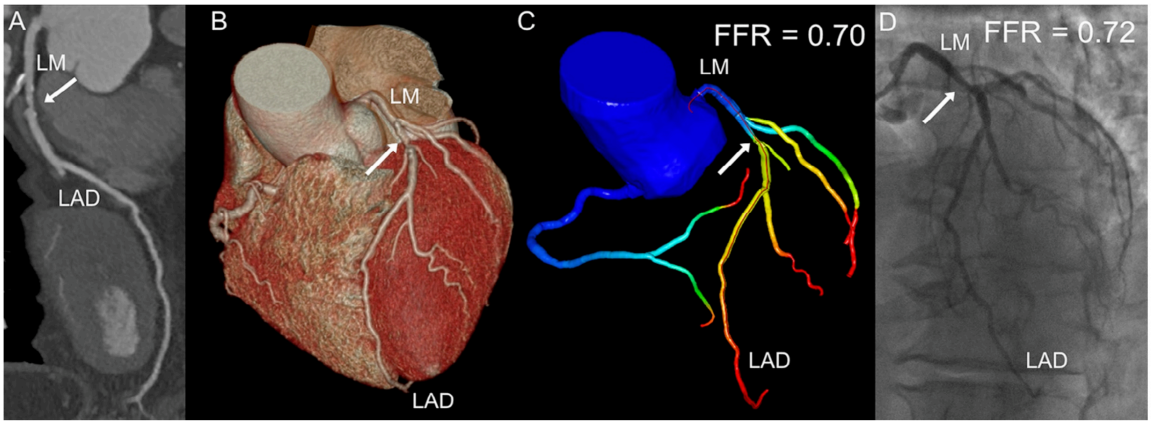

Figure 19 | A representative example of the on-site FFR-CT simulation. Coronary CTA examination showed a partially calcified plaque on the proximal LAD causing moderate stenosis (50% to 69%) (Panels A and B). The FFR-CT simulation demonstrated lesion-specific ischemia with a FFR-CT value of 0.70 (Panel C). The invasive FFR measurement confirmed the ischemia caused by the proximal LAD stenosis with an FFR value of 0.72 (Panel D). CTA = computed tomography angiography; FFR-CT = computed tomography-derived fractional flow reserve; LAD = left anterior descending coronary artery; LM = left main coronary artery.

Statistical analysis

All continuous variables are expressed as mean ± standard deviation (SD) or as median with interquartile range (IQR), as appropriate. Normality was assessed using the Shapiro-Wilk test. Categorical variables are expressed as frequencies and percentages. Invasive FFR values were compared to the on-site FFR-CT values using the Bland-Altman plot.[286] For diagnostic performance analysis of EDS and on-site FFR-CT values, area under the curve (AUC) was calculated using receiver operating characteristics. 95% confidence intervals were calculated using 2000 stratified bootstrap replicates. Sensitivity, specificity, positive and negative predictive values were calculated using a threshold of ≥50% EDS and ≤0.80 FFR-CT value. For reliability measures, intra-reader and inter-reader reproducibility was assessed based on all 60 lesions using the ICC interpreted as: 1.00-0.81: Excellent; 0.80-0.61: Good; 0.60-0.41: Moderate; 0.40-0.21: Fair; 0.20-0.00: Poor.[273] Diagnostic performance values between the readers' FFR-CT values were compared using the DeLong method.[287] All statistical calculations were performed using SPSS software (SPSS version 23; IBM Corp., Armonk, NY) and R (version: 3.2.5). A p-value of 0.05 or less was considered significant.

4.3 Adipose tissue compartments and their heritability

In the third part of my Doctoral thesis, I will elaborate on studies that we have performed to study the relationship between epicardial adipose tissue, circulating biomarkers and coronary

atherosclerotic plaques. In addition, we have studied the heritability of epicardial adipose tissue quantity. The first part of the investigations was performed at the Massachusetts General Hospital, Harvard Medical School in Boston. The heritability studies were performed in collaboration with the Hungarian Twin Registry at the Heart and Vascular Center of the Semmelweis University in Budapest.

4.3.1 Epicardial fat and coronary artery disease

Study design and study population

From May 2005 to May 2007 consecutive subjects were prospectively enrolled as part of the ROMICAT (Rule Out Myocardial Infarction using Computer Assisted Tomography) trial (NCT00990262).[288] The main inclusion criteria were: patients with age >18 years and admitted to rule out myocardial infarction through standard care protocols. The main exclusion criteria were: Elevated troponin I or CK-MB levels in the initial blood sample obtained in the emergency department; new diagnostic ECG changes for myocardial infarction; hemodynamic or clinical instability; history of established CAD, defined as stent implantation or coronary artery bypass grafting. From the 368 patients who underwent 64-slice multi-detector CT, only patients where pericoronary, epicardial, periaortic, and intrathoracic fat (Figure 20) were available for measurements were included in this analysis.[289] We excluded a total of 26 patients who did not have axial images extending caudally to allow for measurement of periaortic fat and thus included a total of 342 patients.

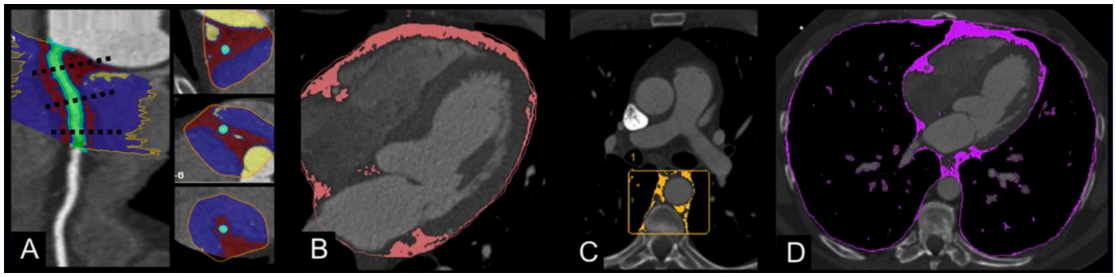

Figure 20 | Depiction of thoracic adipose tissue depots on contrast-enhanced cardiac computed tomography. (A) Pericoronary fat is indicated by red voxels. Green voxels represent the coronary vessel lumen. (B) Epicardial fat (pink) includes all fat contained within the visceral pericardium. Epicardial fat includes all pericoronary fat. (C) Periaortic fat (yellow) includes fat surrounding the descending thoracic aorta. (D) Intrathoracic fat (purple) is the entirety of fat within the thorax including the areas of fat within the pericardium and external to the pericardium.

Imaging protocol and analysis

CT imaging was performed using a standard coronary artery 64-slice multidetector CT (Sensation 64, Siemens Medical Solutions, Forchheim, Germany) imaging protocol using a 330 ms rotation time, 32 x 0.6 mm collimation, tube voltage of 120 kVp, and maximum effective tube current-time product of 850 mAs.[288]

Pericoronary fat volume (Figure 20A) was measured using a method of threshold-based volumetric pericoronary fat volume (cm^3) assessment based on a modified application of software for coronary plaque quantification.[289] Briefly, pericoronary fat measurements started at the ostium of the left main (LM)/left anterior descending coronary artery (LAD), left circumflex artery (LCx), and right coronary artery (RCA) and continued to a distance of 40 mm. Manual tracing was used to circle the region containing pericoronary fat in cross-sectional images perpendicular to the vessel centerline in every 5 mm. The exact pericoronary fat volume within the manually traced region was calculated by the software using Hounsfield unit (HU) based thresholds. Voxels with values between the minimum setting of the SUREPlaque (Vitrea 2, Version 3.9.0.1, Vital Images Inc, Plymouth, MN) tool (-149HU) and an upper threshold of -30HU were used to represent adipose tissue, and the total pericoronary volume was calculated by summing these voxels along the course of each coronary artery.

Epicardial fat volume (Figure 20B), defined as adipose tissue contained within the visceral pericardium, in cm^3 was measured.[290] Measurements were made on axial CT images using a semiautomatic software program (Volume Viewer, Siemens Medical Solutions, Forchheim, Germany) at 10 mm intervals with interpolation of fat volume between the planar regions of interest. Manual adjustment was made when necessary to correct for interpolation errors and tracings were confirmed through use of sagittal and coronal planes. Pixels with HU values of -190 to -30 within the selected region were defined as adipose tissue. Epicardial fat volume used for analysis was calculated as the absolute difference between the measured epicardial fat and pericoronary fat volumes.

Periaortic fat volume (Figure 20C) was measured in accordance with the previously published methods using a semiautomated method on a dedicated offline workstation (Volume Viewer, Siemens Medical Solutions, Forchheim, Germany). [291,292] Briefly, the volume of interest was defined by an approximately 7.0 cm vertical column of fat surrounding the thoracic aorta between the pulmonary artery bifurcation and the diaphragm.[292] Periaortic fat was defined by voxels between -190 and -30 HU within this columnar region of interest, and total periaortic fat volume was determined.

For the calculation of the extracardiac fat volume in cm3 we have subtracted epicardial fat volume from the sum of intrathoracic fat and periaortic fat volumes. Intrathoracic fat volume (Figure 20D) defined as all fat contained within the mediastinum [290]. For intrathoracic fat measurements, the mediastinum was defined as the area bordered by the sternum anteriorly, anterior wall of the descending aorta posteriorly, the center of the right pulmonary artery superiorly, and the diaphragm inferiorly. Pixels from -190 to -30 HU within the mediastinal boundaries were defined as intrathoracic fat. Presence of coronary artery plaque by CT was assessed based on a 17-segment model.[288,293] Extent of coronary artery plaque burden was examined by stratifying patients into 3 groups, those with 0 segments containing plaque, 1-3 segments containing plaque, or >3 segments containing plaque.

Peripheral venous samples for biomarker testing were collected at the time of the CT scan. Samples were collected into ethylenediaminetetraacetic acid (EDTA) coated tubes and non-coated tubes, and immediately centrifuged. The aliquoted plasma and serum were stored in microcentrifuge tubes at -80ºC until assayed. Specimens were tested on the first freeze thaw cycle. All analyses were performed in an independent laboratory (Biomarker Laboratory at the Department of Cardiology, University of Ulm, Germany) in a blinded fashion, irrespective of the clinical and CT findings. Concentration of hs-CRP was measured nephelometrically on a BN II analyzer (Dade-Behring, Marburg, Germany). Enzyme-linked immunosorbent assays (ELISA) from R&D Systems (Wiesbaden, Germany) were used to measure TNF-α, PAI-1, MCP-1, and adiponectin. The intra-assay coefficient of variation (CV) and inter-run CV were ≤10% for all markers.

Statistical analysis

Continuous variables are reported as mean ± standard deviation (SD) or median and interquartile range (IQR), as appropriate. Discrete variables are given in frequency and percentiles. To compare the differences in characteristics between patients with and without CAD, we used t-test or Wilcoxon rank sum test for continuous variables and Chi-square test or Fisher's exact test for categorical variables as appropriate. We used Pearson's correlation to compare the normally distributed fat depots with each other and to BMI. We used the partial Spearman's correlation to assess the strength of association between non-normally distributed biomarker levels and fat compartments, adjusting for presence of coronary plaque. For the association of each of the fat depots to the presence of coronary artery plaque as well as the extent of plaque, we used logistic regression based on a per 10 cm^3 increase. Ordinal logistic

regression analysis was adjusted for age, gender, diabetes, hypertension, dyslipidemia, smoking, BMI, aspirin use, and statin use. A two-tailed p-value of <0.05 was considered significant. All analyses were performed using the SAS software (Version 9.2, SAS Institute Inc, Cary, North Carolina).

4.3.2 Heritability of epicardial adipose tissue quantity

Study population

This study was a prospective, single-center, classical twin study involving MZ and DZ same-gender twin subjects of self-reported Caucasian ethnicity.[294] The total study population consisted of 202 adult twin subjects (101 twin pairs) who were recruited from the Hungarian Twin Registry, of whom 122 were MZ and 80 were same-gender DZ twin subjects. All subjects provided written informed consent. The study was approved by the National Scientific and Ethics Committee (institutional review board number: ETT TUKEB 58401/2012/EKU [828/PI/12], Amendment-1: 12292/2013/EKU [165/2013] and was carried out according to the principles stated in the Declaration of Helsinki.

In the current study we included 180 twin subjects (90 twin pairs; 63.3% female; 57 MZ and 33 DZ same-gender twin pairs); we excluded 11 twin pairs from the original cohort. Twin pairs were excluded when either of them had inadequate image quality or insufficient anatomical CT coverage of any of the investigated fat compartments.

Computed tomography scanning protocol and image analysis

Every subject underwent a non-contrast enhanced CT scan of the heart using a 256-slice CT scanner. Furthermore, a single 5 mm thick slice of the abdomen was acquired at the level of the L3/L4 vertebrae for assessing abdominal SAT and VAT. Further details of the study protocol were reported previously. Importantly, the native CT of the heart and abdomen resulted in a small (0.70 ± 0.16 mSv) radiation dose.

Semi-automated volumetric EAT quantification was performed on a dedicated workstation (CT-viewer, Intellispace Portal Client, Philips Healthcare, Best, The Netherlands). The pericardial layer was manually traced in every slice of the cardiac CT dataset between the level of the right pulmonary artery and the diaphragm. Adipose tissue attenuation was defined between -195 and -45 Hounsfield Units (HU). EAT quantity was assessed with the volumetric reconstruction of any fat tissue between the myocardial surface and the visceral layer of the

pericardium. Abdominal fat compartments were identified and their areas were quantified on the abdominal cross sectional images using a semi-automated software (FAT assessment, Extended Brilliance Workspace, Philips, Best, The Netherlands). The measurements of different fat compartments are illustrated by figures 21 and 22.

Basic anthropometric parameters (weight, height, waist circumference) of every subject were recorded. Brachial blood pressure was measured prior to the CT exam. Questionnaires regarding past medical history and current lifestyle, smoking and dietary habits were recorded for every participant. Fasting peripheral blood draw was performed before the CT examination. Laboratory parameters were investigated by using standard methods in certified laboratory.

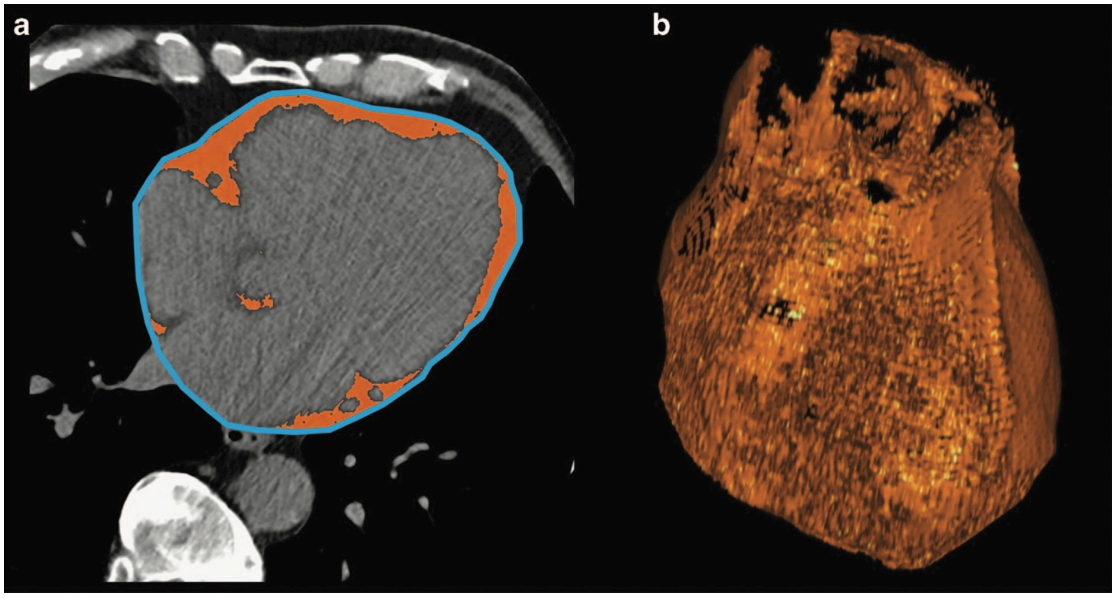

Figure 21 | Measurement of epicardial adipose tissue quantity. (a) Axial CT image of the heart, the pericardial layer is outlined with blue, the epicardial fat is marked with orange colour. (b) Volume rendered reconstruction of the epicardial fat volume.

Statistical analysis

Continuous variables are expressed as mean±standard deviation (SD), whereas categorical variables are expressed as numbers and percentages. MZ and DZ twins were compared using Student's t-tests and Chi-square tests. Correlations were calculated using Pearson correlation coefficients. Intra-reader and inter-reader reproducibility of CT based fat measurements was assessed by two of my PhD students based on 10 randomly selected MZ twin pairs and 10 randomly selected DZ twin pairs images using the intra-class correlation coefficient. Coefficient values are interpreted as: 1.00-0.81: excellent; 0.80-0.61: good; 0.60-0.41: moderate; 0.40-0.21: fair; 0.20-0.00: poor. Descriptive statistics, correlations and

reproducibility measurements were calculated using IBM SPSS Statistics version 23 (IBM, Armonk, NY, USA).

Heritability was assessed in two steps; first, co-twin correlations between the siblings were analysed in MZ and DZ pairs separately. Next, genetic structural equation models were used to model the magnitude of genetic and environmental factors influencing the different fat compartments. All phenotypes are caused by genetic and environmental factors. MZ twins share nearly 100% of their genome, while DZ twins only share half. Genetic similarity is caused by additive genetic components (A). While MZ twins share almost 100% of A, DZ twins only share 50% of A. Environmental components are grouped as common factors (C), which equally effect the siblings, and unique factors (E), which cause differences within families. In our study,

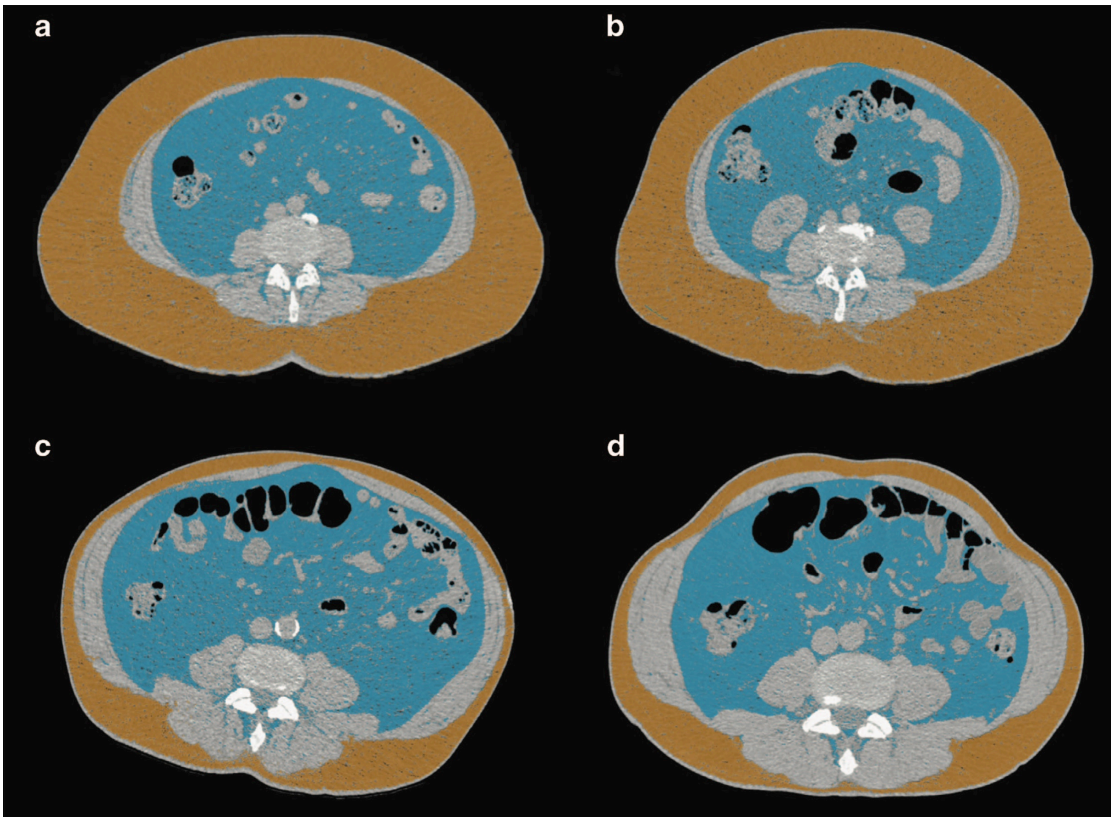

Figure 22 | Abdominal subcutaneous and visceral adipose tissue compartments in monozygotic twin pairs. (a and b) Axial images of the abdomen at the level of the L3/L4 vertebrae. Subcutaneous fat (orange colour) is predominant in this monozygotic twin pair. (c and d) Axial images of the abdomen at the level of the L3/L4 vertebrae. Visceral fat (blue colour) is more prominent in this monozygotic twin pair.

both MZ and DZ twins shared 100% of their C factors and none of their E factors. Covariance between the siblings can be decomposed into A, C and E latent variables using genetic structural equation models. The likelihood ratio test was used to assess the fit of sub-models compared to the full model. If the fit did not decrease significantly by removing one of the parameters, then the more parsimonious sub-model was selected. Furthermore, multivariate genetic models can

be used to further decompose the results of the heritability estimates into common and unique genetic and environmental factors. Common genetic factors refer to genes that are driving the heritability of all three fat components simultaneously (A_c), while common (C_c) and unique (E_c) environmental factors refer to circumstantial factors that affect the heritability of all three phenotypes. The remaining variance then can be attributed to genetic (A_s), common (C_s) and unique (E_s) environmental factors specific of a given phenotype, which are independent of the other phenotypes. Therefore, the heritability of the fat compartments was decomposed to common (A_c, C_c, E_c) and specific (A_s, C_s, E_s) genetic and environmental factors. Independent and common pathway models were used to find the most parsimonious model best describing our data. All calculations were adjusted for age and sex. Log likelihood-based 95% confidence intervals (CI) were calculated for all estimated parameters. All calculations were performed using R version 3.2.5. Twin modelling was performed using OpenMx version 2.5.2. A p value lower than 0.05 was considered significant.

4.4 Structured clinical reporting and data collection

In the fourth part of my thesis, I have described the work that we have performed in order to improve and standardize medical image interpretation. The smart data collection platforms were developed at the Heart and Vascular Center of the Semmelweis University.

4.4.1 Performance of automated structured reporting

Study design and study population

In this single center study we prospectively enrolled 500 patients who underwent coronary CTAs due to stable chest pain between August and December 2016.[150] We included all patients who were older than 18 years. No further inclusion or exclusion criteria were applied to avoid selection bias. Five readers interpreted the coronary CTA images (100/reader) using a structured reporting platform that automatically calculates CAD-RADS based on reader-input. The readers were blinded to the automatically calculated CAD-RADS values. The study was approved by the institutional review board and informed consent was obtained.

Image acquisition and analysis

We performed ECG-gated CTA of the coronaries according to the guidelines of the SCCT.[251] All patients were scanned with a 256-slice CT scanner. We administered oral beta-blocker (metoprolol) if heart rate exceeded 65 beats per minute one hour before the coronary CTA examination. All patients received 0.8 mg of sublingual nitroglycerin shortly prior to the contrast enhanced scan. Intravenous beta-blocker (metoprolol) was administered immediately before the scan if the patient's heart rate was above 60 bpm and systolic blood pressure was higher than 100 mmHg to improve image quality. All coronary CTA images were acquired using prospective ECG triggering, 270 msec rotation time, 128×0.625 mm collimation, tube voltage of 100-120 kVp based on patient's anthropometrics. Images were acquired and reconstructed at diastole (75-81% of the R-R interval) or at systole (37-43% of the R-R interval) if heart rate was still above 70 bpm despite premedication. Axial images were reconstructed with 0.4 mm slice thickness using iterative reconstruction (iDose^4 and IMR, Philips Healthcare, Cleveland, OH, USA). Dose length product (DLP) was registered and converted to an estimated effective radiation dose in millisieverts by multiplying by the k factor of 0.014.[295] All readers assessed the location, type and severity of coronary lesions according to SCCT guidelines using

the 18-segment coronary tree model and also evaluated high-risk plaque features.[72] All reports were generated by a structured reporting platform, which uses single and multiple-choice questions and numeric fields for data input (Figure 23).

All readers recorded the CAD-RADS stenosis categories (0: 0%, 1: 1-24%, 2: 25-49%, 3: 50-69%, 4A 70-99%, 4B: Left main >50% or 3-vessel disease, 5: 100%) and modifiers (N: Non-diagnostic, S: Presence of stent, V: Vulnerable or high-risk plaque features, G: Presence of bypass grafts) according to the CAD-RADS consensus document.[296] Coronary segments

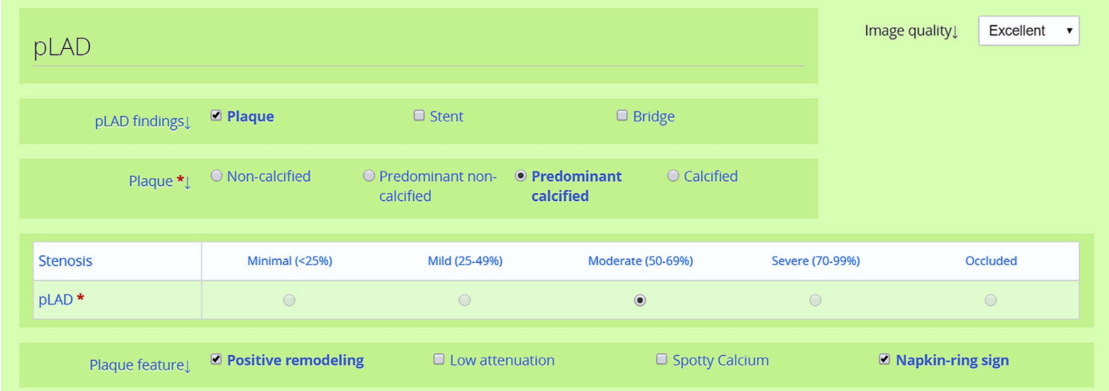

Figure 23 | Representative image of the applied structured reporting platform in clinical routine. The figure demonstrates how plaques were evaluated by the readers including plaque features and stenosis severity using single and multiple choice questions for all coronary segments. The platform includes all components of CAD-RADS assessment. Based on these conditional inputs the CAD-RADS score was automatically calculated (e.g. 3/V) that remain hidden to the readers. We compared the results of the automated score with the manual CAD-RADS classification.

with a diameter of >1.5 mm were analyzed. The reporting platform automatically determined the CAD-RADS score based on the data provided by the readers, which remained hidden to the readers. Readers were able to fill in any score as a free text on the reporting platform. Mismatches between the automated and manually derived scores were re-evaluated by two experienced readers and the correct score was derived by consensus between them. These readers did not take part in the coronary CTA interpretation. We assessed total agreement (both for stenosis categories and modifiers) and also the agreement for every component of the scoring system between the automated and manual classification. Change in management was defined as discrepancy in stenosis categories apart from 0 vs 1 and 1 vs 2 or discrepancy in modifiers among all misclassified cases.

Factors increasing CAD-RADS misclassification rate

We hypothesized that CAD-RADS training, time of the day, clinical load and level of expertise could influence reader's performance when assessing CAD-RADS scores. At the beginning of the study we gave detailed instructions to all readers to ensure proper use of CAD-

RADS and distributed the consensus document for reviewing. Readers were allowed and also encouraged to read the score system regularly or at any time during the study. Additionally, after the first 50 cases each reader received an individual training, which included a short review of CAD-RADS and case evaluations focusing on correcting common mistakes. We also assessed the association of clinical load (defined as ≥5 reports/day) and time of the day (in 6 hours intervals) with reader's performance. We differentiated two groups of readers based on clinical experience (2 readers with 2 years vs 3 readers with 7 years' experience in reading coronary CTAs).

Statistical analysis

Continuous variables are presented as mean and standard deviation, whereas categorical parameters are presented as frequency with percentages. We compared reader's and the structured reporting platform's performance using the McNemar's test for modifiers and the Wilcoxon-rank sum test for stenosis categories. We assessed the effects of clinical load, clinical experience, individual training and diurnal rhythm on agreement by using Fisher exact test for modifiers and Mann-Whitney for stenosis categories. To create a continuous scale for data analysis of stenosis, we separated 4A and 4B into different severity categories. A p value <0.05 was considered statistically significant. All calculations were performed using SPSS software (SPSS version 22; IBM Corp., Armonk, New York).

.

5 Results

5.1 Novel findings regarding CT image quality and image acquisition safety

5.1.1 The efficacy of ultra-short acting β-blocker in heart rate control

In this study we have stopped the patient enrolment early as the interim analysis indicated that IV esmolol is clearly noninferior to IV metoprolol, and in fact, esmolol showed superiority characteristics compared to IV metoprolol in reducing HR during coronary CTA.[245] Between April 2013 and September 2013, in total, 650 consecutive patients referred to coronary CTA were screened, and of these, 574 patients were eligible to participate in the study. In 162 patients no IV drug was administered because the HR before scan was 65 beats/min. In total, 412 patients (with HR >65 beats/min before the scan) were enrolled and randomized into either esmolol or metoprolol group; 204 received IV esmolol and 208 patients received IV metoprolol. There was no difference between the two groups regarding the clinical characteristics (Table 8). In the esmolol group, 53 of 204 patients (26.0%) received 1 bolus (100 mg), 73 of 204 (35.8%) received 2 boluses (300 mg), and 78 of 204 (38.2%) received 3 boluses (500 mg) of esmolol. In the metoprolol group, IV metoprolol was administered in a similar fashion as in the esmolol group but in 5-mg increments. Eighty-three of 208 patients (39.9%) received 1 bolus (5 mg), 45 of 208 patients (21.6%) 2 boluses (10 mg), 53 of

Table 8 Demographic characteristics of study groups.

	esmolol (n=204)	**metoprolol** (n=208)	**p**
age (years)	56.9 ± 10.8	57.6 ± 12.2	0.390
male/female	100/104	111/97	0.377
BMI (kg/m^2)	28.4 ± 4.9	28.2 ± 4.7	0.956
hypertension (%)	67	66	0.889
diabetes (%)	16	14	0.603
dyslipidemia (%)	48	55	0.154
AMI (%)	5	10	0.076
PCI (%)	5	7	0.455
CABG (%)	4	6	0.287
PAD (%)	9	8	0.801
stroke (%)	4	1	0.072
smoking (%)	25	26	0.845
β-blocker (%)	47	48	0.795

AMI, acute myocardial infarction; BMI, body mass index; CABG, coronary artery bypass graft; PAD, peripheral arterial disease; PCI, percutaneous coronary intervention.
Statistics: robust, independent t test and chi-square test.

Table 9 Heart rate

	esmolol (n=204)	**metoprolol** (n=208)	**p**
	mean ± SD	mean ± SD	
T1	78 ± 13	77 ± 12	0.652
T2	68 ± 7	69 ± 7	0.599
TS	58 ± 6	61 ± 7	<0.0001
T3	68 ± 7	66 ± 7	<0.01
T4	65 ± 8	63 ± 8	<0.0001

Heart rate measured (in beats/min) at T1 (arrival), T2 (before scan), TS (during scan), T3 (after scan), and T4 (emission). Statistics: robust, independent t test.

208 (25.5%) 3 boluses (15 mg), and 27 of 208 (13.0%) 4 boluses (20 mg) of metoprolol. Oral metoprolol administration was similar in the esmolol and metoprolol groups (51.2±33.1 vs 52.4±33.6; p=0.71). On average, 325.6±158.4 mg IV esmolol and 10.7±6.3 mg IV metoprolol were administered. The mean HRs of the esmolol and metoprolol groups were similar at the time of arrival (T1: 78±13 vs 77±12 beats/min; p=0.65) and immediately before the coronary CTA examination (T2: 68±7 vs 69±7 beats/min; p=0.60). However, HR during the scan was significantly lower among the patients who received IV esmolol vs patients who received IV metoprolol (TS: 58±6 vs 61±7 beats/min; p<0.0001). On the other hand, HRs immediately after the coronary CTA and 0 minutes after the coronary CTA were higher in the esmolol group than in the metoprolol group (T3: 68±7 vs 66±7 beats/ min; p<0.01; and T4: 65±8 vs 63±8 beats/min; p<0.0001, respectively; Table 9; Figure 24). Systolic and diastolic BPs showed no difference between the 2 groups measured at any time point (Table 10). HR of 65 beats/min was reached in 182 of 204 (89%) of patients in the esmolol group vs in 162 of 208 (78%) of patients in the metoprolol group (p<0.05), whereas HR 60 beats/min was reached in 147 of 204 (72%) of the patients who received esmolol vs in 117 of 208

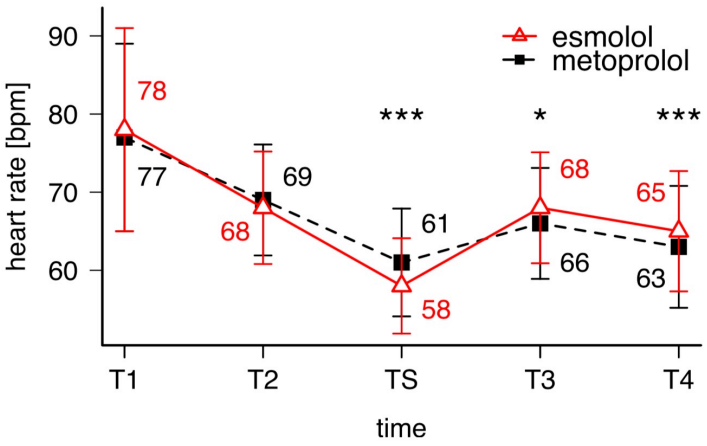

Figure 24 | The figure represents the mean heart rates and their standard deviations in the esmolol and metoprolol groups at different time points. The red triangles represent the mean heart rates in the esmolol group, whereas the black squares indicate the mean heart rates in the metoprolol group. T1, time of arrival; T2, time point before the coronary CT angiography (CTA) scan; TS, coronary CTA scan; T3, time point immediately after the coronary CTA; T4, 30 minutes after the coronary CTA. *p<0.01; ***p<0.0001.

(56%) of patients who received metoprolol (p<0.001; Figure 25). None of the patients developed bradycardia (defined as HR <50 beats/min) after b-blocker administration (minimum HR in group esmolol was 53 beats/min; minimum HR in group metoprolol was 52 beats/min). However, hypotension (defined as systolic BP <100 mm Hg) was observed in 19 patients (9.3%) in the esmolol group and in 8 patients (3.8%) in the metoprolol group right after the scan (T3; p<0.05). Importantly, only 5 patients (2.5%) had a systolic BP<100 mmHg 30 minutes after the scan (T4) in the esmolol group, whereas the number of patients with hypotension remained 8 (3.8%) in the metoprolol group (p=0.418). None of the patients required hospitalization or medical intervention due to hypotension and the systolic BP normalized after a short (maximum 2 hours) observation in every case. Of note, the absolute time spent in the CT unit (T3-T2) did not differ be- tween the esmolol and metoprolol group (21.1±7.5 vs 21.8±7.9 minutes; p=0.428).

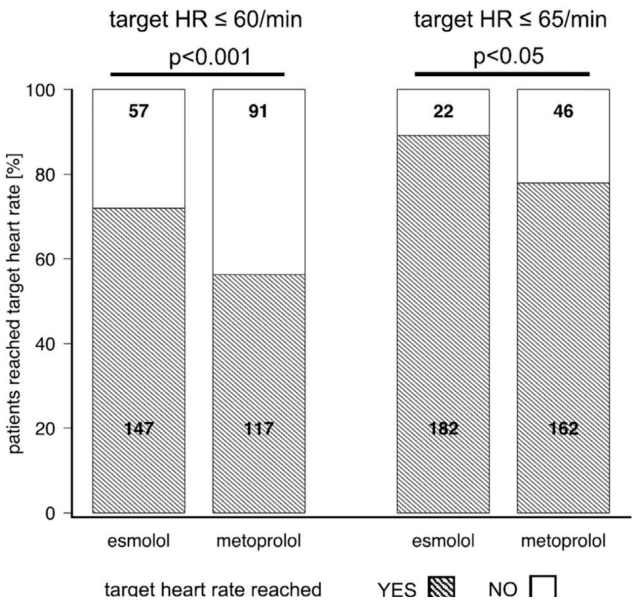

Figure 25 | The bar charts illustrate the proportion of patients that reached a heart rate ≤60 beats/min (left side) and the proportion of patients that reached a heart rate ≤65 beats/min in the esmolol and metoprolol groups.

Table 10 Blood pressure

	esmolol (n=204)	**metoprolol** (n=208)	**p**
	mean ± SD	mean ± SD	
T1			
systole	142 ± 22	146 ± 21	0.195
diastole	87 ± 12	87 ± 12	0.819
T2			
systole	144 ± 21	145 ± 20	0.918
diastole	86 ± 13	87 ± 12	0.945
T3			
systole	128 ± 20	131 ± 19	0.053
diastole	74 ± 12	75 ± 12	0.522
T4			
systole	132 ± 20	134 ± 21	0.414
diastole	79 ± 11	80 ± 12	0.589

Blood pressure (in mm Hg) measured at T1 (arrival), T2 (before scan), T3 (after scan), and T4 (emission).
Statistics: robust, independent t test.

5.1.2 The effect of the novel four-phasic contrast material injection protocol

In total, 2,445 consecutive patients with suspected coronary artery disease were enrolled between 2014 January and 2015 August.[249] The mean age was 60.6 ± 12.1 years and there were less female patients than males (females 43.6%). The clinical characteristics of included patients are summarized in Table 11. Out of the 2,445 patients, 1,229 (50.3%) received a three-phasic and 1,216 (49.7%) a four-phasic CM injection-protocol (Table 12). The overall number of CM extravasation was 23 out of 2,445 patients (0.9%). The CM extravasation rate in the three-phasic group was 1.4% (17/1,229), whereas in the four-phasic group the extravasation rate was 0.5% (6/1,216), p=0.034 (Figure 26). The four-phasic CM injection-protocol resulted in 65% reduction in extravasation rate as compared to the three-phasic CM injection-protocol in coronary CTA (odds ratio (OR): 0.354; CI: 0.139–0.900; p=0.029). The majority of the patients received an 18 G cannula for CM injection (97.2% of all patients). The use of a 20 G cannula did not differ between the two groups (three-phasic protocol group 34 (3.1%), four-phasic protocol group 38 (3.1%), respectively, p=0.63).

Table 11 Clinical characteristics of the patients

	n = 2445
Age (years)	60.6 ± 12.1
Female (%)	1065 (43.6)
Height (cm)	171.2 ± 10.1
Weight (kg)	84.0 ± 17.2
BMI (kg/m²)	28.5 ± 4.8
Hypertension (%)	1605 (65.6)
Diabetes (%)	393 (16.1)
Dyslipidemia (%)	1142 (46.7)
AMI (%)	185 (7.6)
PAD (%)	236 (9.7)
Stroke/TIA (%)	135 (5.5)
Current smoking (%)	990 (40.5)
Total DLP (mGy*cm)	356.8 ± 142.0
Effective dose (mSv)	5.0 ± 2.0
Contrast material (mL)	91.2 ± 7.3

AMI acute myocardial infarction, BMI body mass index, PAD peripheral artery disease, TIA transient ischaemic attack, DLP dose-length product

Besides the CM injection-protocol none of the clinical and vein quality characteristics of patients who had extravasation versus patients with no extravasation showed any differences (Table 12). In the four-phasic group a CM

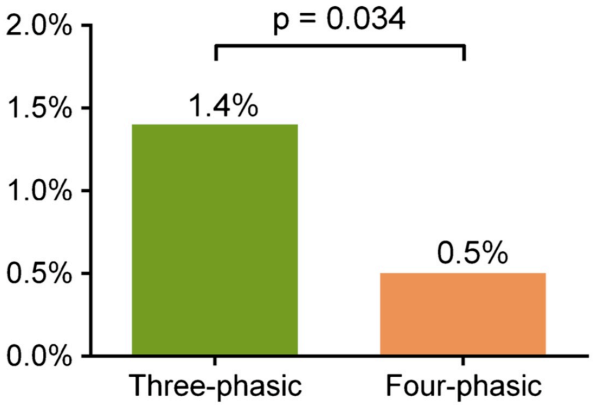

Figure 26 | The contrast media extravasation rate in the three-phasic group was 1.4% (17/1,229), whereas in the four-phasic contrast media injection- protocol group the extravasation rate was 0.5% (6/1,216), p = 0.034

Table 12 Comparison of the extravasation rate, and clinical, vein quality and image acquisition characteristics between the three-phasic contrast media (CM) injection and four- phasic CM injection-protocol groups

	Three-phasic group (n=1229)	Four-phasic group (n=1216)	p
Clinical characteristics			
Age (years)	60.4 ± 12.1	60.8 ± 12.0	0.44
Female, n (%)	529 (44.1)	536 (43.0)	0.63
Height (cm)	171.2 ± 10.0	171.3 ± 10.2	0.88
Weight (kg)	83.8 ± 17.2	84.1 ± 17.2	0.62
BMI (kg/m^2)	28.5 ± 4.9	28.6 ± 4.7	0.76
Hypertension, n (%)	816 (66.4)	789 (64.9)	0.44
Diabetes, n (%)	202 (16.4)	191 (15.7)	0.66
Dyslipidemia, n (%)	582 (47.4)	560 (46.1)	0.54
AMI, n (%)	99 (8.1)	86 (7.1)	0.36
PAD, n (%)	120 (10.6)	116 (10.1)	0.73
Stroke or TIA (%)	62 (5.0)	73 (6.0)	0.33
Smoking (%)	497 (40.5)	493 (40.4)	0.97
Vein quality characteristics			
Venous access side (right %)	1103 (89.7)	1066 (87.7)	0.11
Cubital cannula (%)	1163 (94.6)	1130 (92.9)	0.09
Cannula size			
18 G, n (%)	1195 (97.2)	1178 (96.9)	0.63
20 G, n (%)	34 (3.1)	38 (3.1)	0.63
Cannula size (18 G %)	1195 (97.2)	1178 (96.9)	0.63
Successful cannula insertion at first attempt (%)	1124 (91.5)	1122 (92.7)	0.77
Contrast material characteristics			
Contras material volume	91.3 ± 7.3	91.0 ± 7.4	0.23
Injection flow rate			
5.5 mL/s, n (%)	1121 (91.2)	1075 (88.4)	0.02

AMI acute myocardial infarction, BMI body mass index, PAD peripheral artery disease, TIA transient ischaemic attack, DLP dose-length product

injection rate of 5.5 ml/s was administered in 88.4% (1,075/1,216) of the patients, which was lower than the three-phasic protocol group (91.2%, 1,121/1,229), p=0.02. Even though we found a significant difference between the two groups, this did not influence extravasation rates, since there was no difference in injection rates among patients with extravasation (5.5 ml/s flow rate: 95.7% (22/23)) versus patients who had no extravasation (5.5 ml/s flow rate: 89.8% (2,174/2,422)), p=0.72.

We assessed the effect of the three- and four-phasic CM injection protocols in subgroups considered prone to developing extravasation. Among females, less extravasation events occurred in the four-phasic group compared to the three- phasic group (5.6% (3/533) vs. 23.2% (12/517), respectively p=0.02). Similarly, we could detect significantly less extravasation when

the four-phasic protocol was administered to patients older than 60 years compared to the three-phasic group (4.0% (3/732) vs. 19.4% (14/720), respectively p=0.007). Furthermore, we did not experience any extravasation in patients who received a 20 G cannula.

5.1.3 The impact of iterative reconstruction on calcified plaque burden

The image quality analysis included 468 triplets of coronary artery segments reconstructed with IMR, HIR and FBP.[150] We identified 41 isolated calcified or partially calcified plaques; 25 plaques were located in the LAD, 10 plaques in the RCA, 5 in the LCX and 1 in the left main coronary artery.

Image quality was diagnostic (rated as 1-3) in 453 segments (96.8%) with IMR, 437 (93.4%) with HIR and 407 (87.0%) with FBP (p<0.01). Overall subjective image quality significantly improved with the application of HIR as compared to FBP, and further improved with IMR (p<0.01 all) (Figure 27A). IMR yielded lower image noise by qualitative assessment

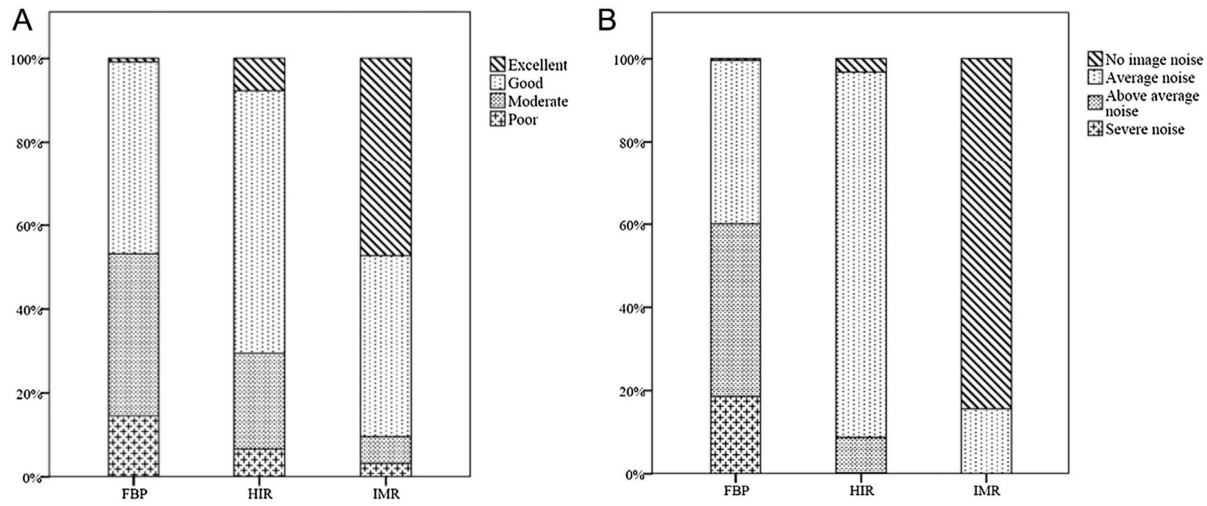

Figure 27 Visual assessment of image quality. Panel A: Overall image quality; Panel B: Image noise.

as compared to HIR and FBP (p<0.01 all). The majority of the coronary segments were rated as having no image noise (395/468, 84.4%), or average image noise (73/468, 15.6%) in the datasets reconstructed with IMR technique (Figure 27B). The inter-reader reliability between the two readers was good for overall image quality (κ:0.71), and image noise (κ:0.73).

Median CT number in the aorta did not differ between the three reconstructions (492.3 [442.7–556.8] for FBP, 492.8 [443.0–556.8] for HIR and 491.3 [442.7–555.0] for IMR, p=1.00). However, higher luminal CT numbers (p < 0.01 all) were revealed in every assessed proximal and distal coronary artery segments with the use of IMR as

Table 13 Comparison of CT attenuation and CNR values between the proximal and distal coronary segments.

	LAD			**CX**			**RCA**		
	Proximal	*Distal*	*p value*	*Proximal*	*Distal*	*p value*	*Proximal*	*Distal*	*p value*
HU_{FBP}	509.6 [445.2-599.4]	492.3 [445.3-564.3]	0.071	506.5 [445.8-598.5]	447.0 [369.5-539.0]	<0.001	523.0 [441.0-601.8]	523.5 [445.8-581.8]	0.655
HU_{HIR}	510.6 [446.3-598.5]	487.9 [442.8-565.8]	0.069	510.5 [444.4-596.1]	434.5 [355.0-538.3]	<0.001	520.9 [441.9-603.0]	524.5 [449.5-581.0]	0.692
HU_{IMR}	534.5 [465.4-633.6]	572.6 [520.3-670.7]	0.001	563.3 [489.6-628.0]	537.6 [474.4-610.1]	0.177	546.5 [471.6-652.0]	561.9 [500.5-636.3]	0.026
	LAD			**CX**			**RCA**		
	Proximal	*Distal*	*p value*	*Proximal*	*Distal*	*p value*	*Proximal*	*Distal*	*p value*
CNR_{FBP}	15.1 [11.7-18.0]	14.2 [11.6-17.7]	0.150	14.5 [11.8-18.0]	12.5 [9.7-16.1]	<0.001	14.6 [11.6-19.1]	14.3 [11.4-18.5]	0.616
CNR_{HIR}	21.5 [17.2-26.3]	20.7 [16.6-25.2]	0.145	20.8 [17.3-26.9]	18.3 [13.5-23.5]	<0.001	21.0 [16.8-27.8]	21.1 [16.9-26.5]	0.372
CNR_{IMR}	50.7 [45.2-59.0]	55.1 [45.4-63.6]	0.001	50.6 [45.3-58.4]	51.2 [38.9-55.5]	0.018	51.2 [43.1-61.3]	53.2 [46.6-62.9]	0.001

Data are presented as medians and interquartile ranges. CT attenuation is presented in Hounsfield units (HU).
Difference between proximal and distal coronary segments was assessed using Wilcoxon signed ranks tests. Utilization of IMR significantly improved CNR values in the distal segments of main coronary arteries.
CNR: contrast-to-noise ratio; FBP: filtered back projection reconstruction; HIR: hybrid iterative reconstruction; IMR: iterative model reconstruction; LAD: left anterior descending coronary artery; CX: circumflex coronary artery; RCA: right coronary artery.

compared to the other two reconstructions (Table 13). No difference was observed between HIR and FBP for the respective coronary segment in HU values. Median attenuation values were similar or lower in the distal coronary segments using FBP and HIR reconstruction, as compared to the proximal coronary parts of the same vessel (LAD: p=0.71 and p=0.69; CX: p<0.01 both, RCA: p=0.66 and p=0.69, respectively).

Interestingly, IMR showed preserved or increased luminal contrast in the distal coronary segments as compared to the respective proximal coronary regions (LAD: p<0.01; CX: p=0.18; RCA: p=0.03) (Figure 28). The CT attenuation values for main coronary arteries are summarized in Table 13. Image noise (SD) in the aorta was significantly different for FBP, HIR and IMR (42.6 [33.2-48.3], 29.4 [23.0-33.1] and 12.4 [11.0-13.8], respectively, p < 0.01 all). Noise reduction achieved by HIR and IMR was 31.5% and 66.9% as compared to FBP, respectively. HIR improved CNR in all assessed coronary segments, as compared to FBP, which was further improved with IMR (p<0.01, both). Inter-observer agreement between quantitative parameters (median attenuation, CNR) was excellent with FBP, HIR and IMR reconstructions (correlation concordance coefficient: 0.97, 0.98 and 0.98, respectively).

The measured lesion length was 24.8 [16.0-28.8] mm, without any significant differences among the three reconstructions. Overall plaque volume was lower with HIR as compared to FBP (p=0.02), and further reduced by IMR (p<0.01 all). Calcified plaque volume was highest with FBP and lowest with IMR (FBP vs. HIR p=0.006; HIR vs. IMR p=0.017; and FBP vs. IMR p<0.001). High attenuation non-calcified plaque volumes with an attenuation ranging 90-129 HU yielded similar values with FBP and HIR (p=0.81), however it was lower with IMR (HIR vs. IMR p=0.002 and FBP vs. IMR p < 0.001). No difference was found between FBP, HIR and IMR in intermediate and low attenuation non-calcified plaque components (p=0.22 and 0.67, respectively). Lumen volumes did not differ between different reconstructions (p=0.23). Overall plaque burden was lowest with IMR and highest with FBP (0.38 for IMR [0.32-0.44], 0.42 for HIR [0.37-0.47] and 0.44 for FBP [0.38-0.50], p<0.05 all). Volumes of various plaque components are summarized in Table 14. As we used a fully automated method for plaque quantification, inter-observer variability was not tested further.

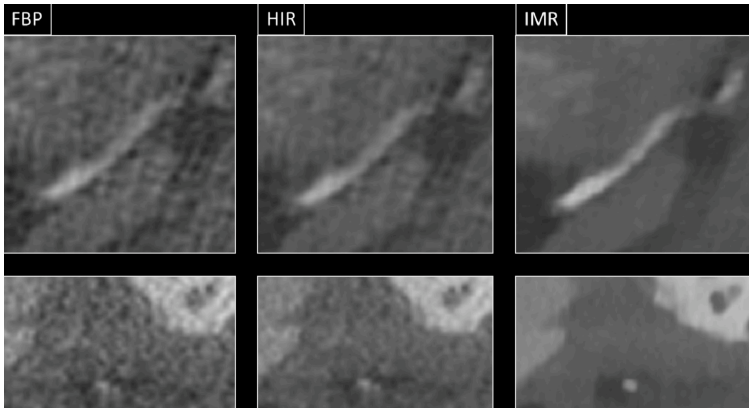

Figure 28 | Representative case demonstrating improved distal coronary visualization using novel IMR algorithm as compared to FBP and HIR

5.1.4 The image quality of coronary CT angiography in heart transplanted patients

In total, 50 HTX patients were included in our study.[255] Every HTX patient had a matched non-HTX pair, therefore in total 100 subjects were evaluated. In the HTX group [11

Table 14 Plaque volume analysis with fixed threshold settings.

				Non-calcified plaque volume			Calcified plaque volume
	Vessel Volume $^{\alpha\beta}$	*Lumen Volume*	*Overall Plaque Volume* $^{\alpha\beta\gamma}$	*<30 HU*	*30-89 HU*	*90-129 HU* $^{\alpha\beta}$	*>130 HU* $^{\alpha\beta\gamma}$
FBP	334.1 [228.1-477.9]	186.0 [126.0-264.5]	147.0 [100.7-183.6]	1.5 [0.3-4.3]	8.2 [2.8-15.3]	10.2 [5.2-20.3]	115.9 [81.7-164.2]
HIR	327.6 [227.6-473.9]	186.6 [129.5-271.6]	138.7 [90.6-191.7]	1.4 [0.4-3.7]	7.7 [3.0-13.2]	9.7 [5.4-18.7]	110.2 [63.8-166.6]
IMR	308.0 [202.7-466.8]	190.9 [102.8-266.3]	121.7 [79.3-168.4]	1.1 [0.3-2.8]	6.0 [3.2-10.3]	7.2 [4.6-16.2]	105.9 [62.1-144.6]

Data are presented as medians with interquartile ranges. Plaque volume values are presented in mm^3. Significant difference for all comparison combinations between the three reconstructions was assessed. Pairwise comparisons are represented between the three reconstructions as follows: α: p<0.05 FBP vs. IMR; β: p<0.05 HIR vs. IMR; γ: p<0.05 FBP vs. HIR.
FBP: filtered back projection reconstruction; HIR: hybrid iterative reconstruction; IMR: iterative model reconstruction; HU: Hounsfield unit

female (22%), 4.3 years post-transplantation] the median age was 57.9 years [IQR: 46.7-59.9], the median HR was 74 bpm [IQR: 67.8-79.3]. We found no significant difference between the HTX and non-HTX groups regarding anthropometric data and scan characteristics (Table 15).

Table 15 Clinical characteristics of study subjects

Parameters	Heart transplant recipients (n = 50)	Control subjects (n = 50)	p
Age (y)	57.9 [46.7 - 59.9]	58.6 [48.5 - 62.1]	0.32
Body mass index (kg/m^2)	25.0 [22.6 - 26.5]	25.0 [23.1 - 28.4]	0.45
Diastolic triggering (n)	31 (62.0%)	31 (62.0%)	1.00
Tube voltage (kV)	120.0 [100.0 - 120.0]	120.0 [100.0 - 120.0]	0.63
Tube current (mAs)	300.0 [250.0 - 300.0]	300.0 [300.0 - 300.0]	0.14
Effective dose (mSv)	3.7 [2.4 - 4.3]	4.3 [2.6 - 4.3]	0.24
Contrast (ml)	90.0 [90.0 - 95.0]	90.0 [90.0 - 95.0]	0.62
Heart rate (bpm)	74.0 [67.8 - 79.3]	73.0 [68.5 - 80.0]	0.58
Coronary dominance, no. (%) of patients			0.91
Right dominant (n)	39 (78.0%)	39 (78.0%)	
Left dominant (n)	11 (22.0%)	11 (22.0%)	

Note - Except where noted otherwise, data are median (interquartile range).

The effective radiation dose was relatively low in both groups (HTX vs. non-HTX groups, 3.7 mSv vs. 4.3 mSv, p=0.24, respectively,).

In total, 1270 coronary segments were evaluated, 662 segments in the HTX group and 608 segments in the non-HTX group. The distribution of motion scores between the two groups is shown in Figure 29. We found a significant difference in the number of segments with excellent image quality between the 2 groups. In the HTX group more segments had excellent image quality than in the non-HTX group (442 (67%) vs. 271 (45%), p<0.001, respectively). Furthermore, in the HTX group the number of non-diagnostic segments were approximately one-third of that of the non-HTX group (38 (5.8%) vs. 104 (17.1%), p<0.001, respectively).

We a found a significant difference between the 2 groups regarding the Segment Likert Score, the Segment Motion Score and the Segment Non-diagnostic Score indices. The Segment Likert Score index of the HTX group was approximately half of the Segment Likert Score index of the non-HTX group (0.4 [IQR: 0.1-0.9] vs. 0.9 [IQR: 0.3-1.6], p=0.003, respectively). Similarly, a nearly twofold

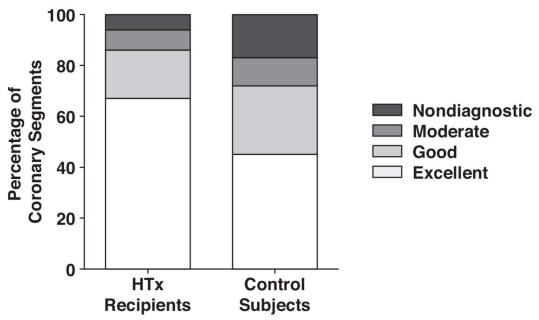

Figure 29 | Proportions of coronary segments with nondiagnostic, moderate, good, and excellent image quality in heart transplantation (HTX) recipients and control subjects.

difference was found between the HTX and non-HTX groups regarding Segment Motion Score index (0.3 [IQR: 0.1-0.5] vs. 0.6 [IQR: 0.2-0.9], p=0.001, respectively). The Segment Non-diagnostic Score index was lower in the HTX group as compared to the non-HTX group (0.0 [IQR: 0.0-0.1] vs. 0.1 [IQR: 0.0-0.3], p=0.004 respectively).

The image quality was better in HTX patients vs. non-HTX patients in the subgroup with systolic triggering. This was reflected by the difference in the Segment Likert Score indices, which was significantly lower in the HTX group as compared to the non-HTX group (0.5 [IQR: 0.4-0.7] vs. 0.8 [IQR: 0.8-0.9], p<0.001, respectively). Furthermore, among scans with systolic triggering we found significantly less motion artifacts and more diagnostic segments in the HTX group; their Segment Motion Score index was almost half of the non-HTX group (0.8 [IQR 0.5-1.1] vs. 1.5 [IQR 1.3-2.1], p<0.001), while their Segment Non-diagnostic Score index was almost quarter of the other group (0.07 [IQR 0.0-0.1] vs. 0.3 [IQR 0.1-0.5], p= 0.001; respectively).

Among diastolic images, significantly better image quality was observed in the HTX scans compared to the non-HTX scans (Figure 30); Segment Likert Score index was significantly lower in the HTX group as compared to the non-HTX group (0.1 [IQR: 0.0-0.3] vs. 0.4 [IQR: 0.1-0.6], p=0.03; respectively). However, among scans with diastolic triggering the degree of motion and the number of non-diagnostic segments did not differ significantly

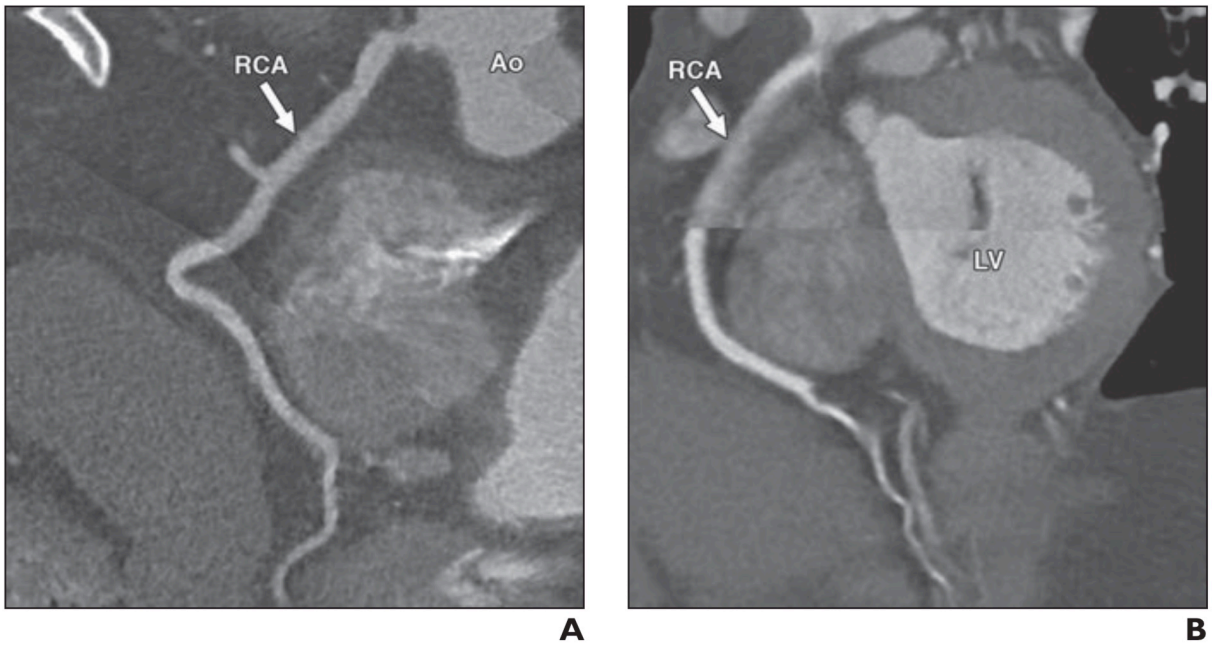

Figure 30 | Coronary CT angiograms of heart transplant recipient and age- and sex-matched control subject.
A, 48-year-old male heart transplant recipient with heart rate of 75 beats/min. No motion artifact is visible in right coronary artery (RCA; arrow) on curved multiplanar reconstruction. Ao = aorta.
B, 48-year-old man with heart rate of 75 beats/min who did not receive heart transplant. Motion artifact (arrow) is visible in proximal segment of RCA on curved multiplanar reconstruction. LV = left ventricle.

between the HTX vs. non-HTX patients; Segment Motion Score and Segment Non-diagnostic Score indices were 0.1 [IQR 0.0-0.4] vs. 0.5 [IQR 0.1-1.1], p=0.05 and 0.0 [IQR 0.0-0.1] vs. 0.0 [IQR 0.0-0.1], p= 0.20, respectively. The median HR of HTX vs. non-HTX patients with systolic triggering was 78 vs. 80 bpm, p=0.86, respectively; and in HTX vs. non-HTX patients with diastolic triggering was 69 vs. 70 bpm, p=0.96, respectively.

Intra-reader and inter-reader agreements of image quality scores were good (κ=0.72; κ=0.62, respectively). Dichotomization of image quality scores to excellent / non-excellent image quality scores resulted in excellent intra-reader (κ=0.83) and good inter-reader reproducibility (κ=0.69). Dichotomization to diagnostic/non-diagnostic image quality scores also showed excellent intra-reader (κ=0.82) and good inter-reader reproducibility (κ = 0.73).

5.2 The main findings of studies on atherosclerotic plaque assessment

5.2.1 The napkin-ring sign

We have identified a novel CT signature of high-risk coronary atherosclerotic plaques with histopathological correlation. We have named this plaque feature as the 'napkin-ring sign'.[259] Our report suggests that the napkin-ring sign (NRS), which can be considered a CT signature of high-risk coronary atherosclerotic plaque, may be caused by the difference in attenuation between a lipid-rich necrotic core (corresponding to the central low attenuation area in CT) and fibrous plaque tissue (corresponding to the rim of high CT attenuation). In this *ex vivo* study, we can exclude the possibility of the high-attenuation representing contrast media uptake, as the CT attenuation values were similar in the non-contrast and contrast-enhanced CT datasets. Interestingly, the average CT attenuation of napkin-ring plaques (50 to 60 HU) was higher than the previously suggested cut-off value (<30 HU) for high-risk lesions (Figures 31-33).

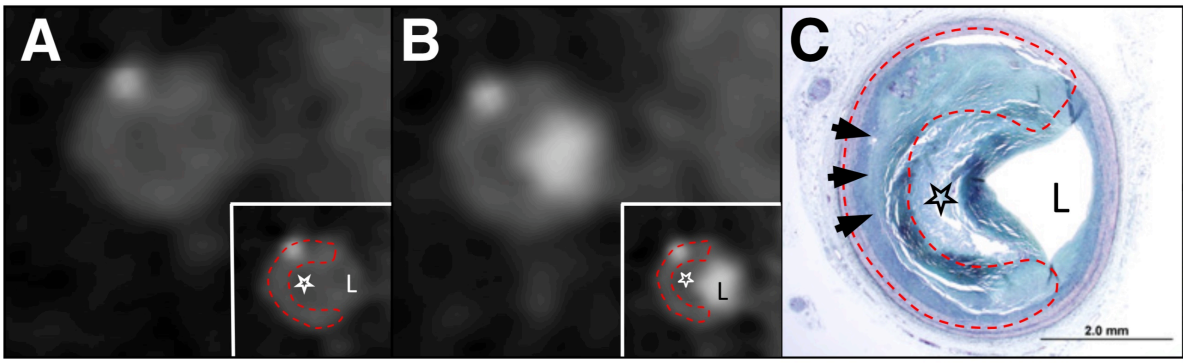

Figure 31 | The cross-sectional CT images show a coronary plaque with napkin-ring-like attenuation pattern and spotty calcification. The circumferential outer rim (red dashed line) of the noncalcified plaque has a higher CT attenuation in both the non-contrast (A) and contrast-enhanced (B) images (44.0 ± 8.8 HU, range 23.0 to 61.0 HU vs. 48.6 ± 5.8 HU, range 34.0 to 60.5 HU; respectively) as compared to the attenuation within the central part of the plaque (27.9 ± 4.2 HU, range 20.7 to 36.4 HU and 31.0 ± 6.6 HU, range 19.0 to 44.0 HU on non-contrast and contrast-enhanced images; respectively). The average noncalcified plaque attenuation on nonenhanced CT was 42.2 ± 9.9 HU versus 43.7 ± 10.0 HU on the contrast-enhanced image. The corresponding histological section (panel C) revealed a late fibroatheroma. The lesion is characterized by a necrotic core (star), which is consistent with the low attenuation core of the plaque and a significant amount of fibrous plaque tissue, which is consistent with the high attenuation rim on the CT images (red dashed line). The arrowheads indicate the vasa vasorum. HU: Hounsfield units; L: lumen

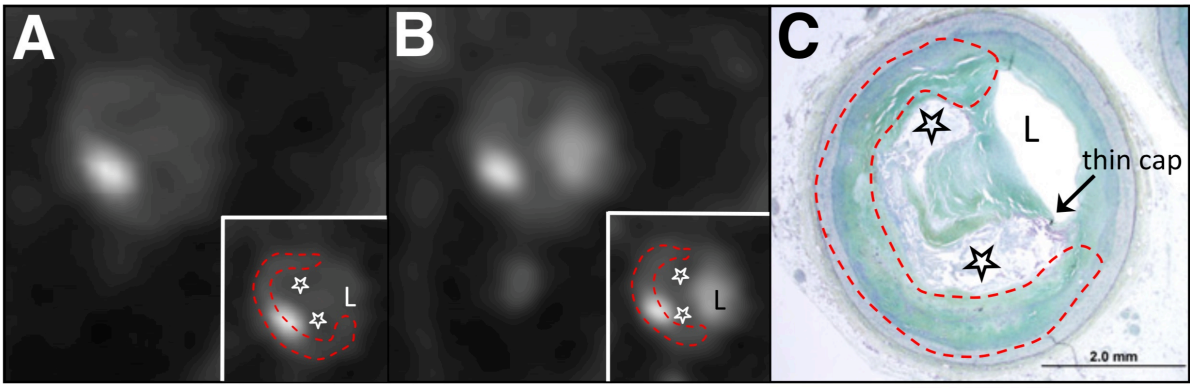

Figure 33 | The CT images show a coronary atherosclerotic plaque cross section with napkin-ring–like attenuation pattern and spotty calcification. The circumferential outer rim (red dashed line) of the plaque has a higher CT attenuation in both the noncontrast (A) and contrast-enhanced (B) images (61.8 ± 9.3 HU, range 42.4 to 74.9 HU vs. 67.3 ± 11.6 HU, range 43.4 to 87.0 HU; respectively) as compared to the attenuation within the central part of the plaque (43.4 ± 7.5 HU, range 35.2 to 62.9 HU and 43.2 ± 14.0 HU, range 21.2 to 72.5 HU, on noncontrast and contrast-enhanced images; respectively). The average noncalcified plaque attenuation on nonenhanced CT was 52.8 ± 10.9 HU versus 58.5 ± 17.1 HU attenuation on the contrast-enhanced image. Histopathology revealed a thin cap fibroatheroma (C and D). Again, the necrotic core (stars) correlates with the low attenuation plaque core on the CT images. The outer rim attenuation (red dashed line) on the noncontrast and contrast enhanced CT images correspond to the fibrous plaque tissue. HU: Hounsfield units; L: lumen.

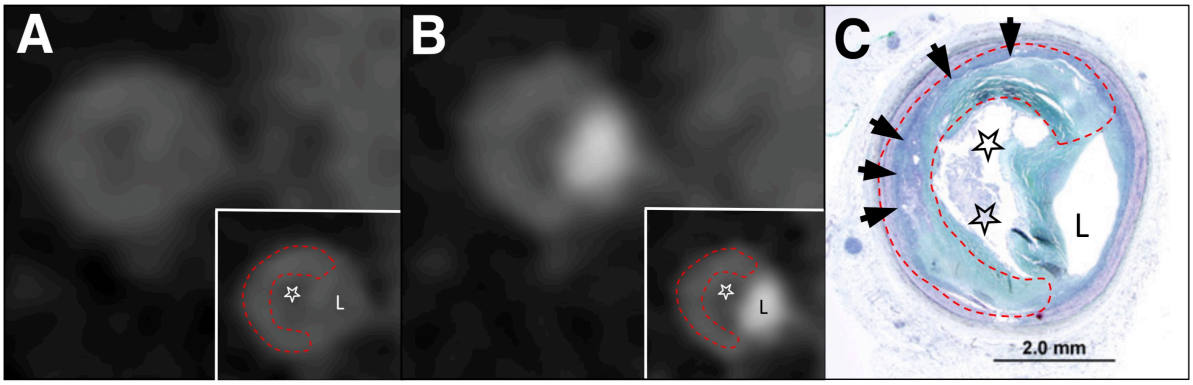

Figure 32 | The CT images show a larger noncalcified coronary plaque with more pronounced napkin-ring–like attenuation pattern as compared to figure 31. The circumferential outer rim (red dashed line) of the plaque has a higher CT attenuation in both the noncontrast (A) and contrast-enhanced (B) images (57.2 ± 8.8 HU, range 40.0 to 81.0 HU vs. 57.9 ± 8.7 HU, range 35.0 to 76.0 HU; respectively) as compared to the attenuation within the central part of the plaque (21.8 ± 4.3 HU, range 13.5 to 31.6 HU and 26.0 ± 2.0 HU, range 22.0 to 31.0 HU on noncontrast and contrast-enhanced images; respectively). The average plaque attenuation on nonenhanced CT was 48.1 ± 14.2 HU versus 52.2 ± 14.0 HU on the contrast-enhanced CT. The corresponding histopathological section (C) demonstrates a late fibroatheroma. Again, the plaque contains a necrotic core (stars), which correlates to the low attenuation plaque core on the CT images. Notably, the necrotic core is larger than in the plaque shown in figure 31, which is in line with the CT morphology. Similar to Figure 31, the outer portion of the plaque (red dashed line) contains a significant amount of fibrous plaque tissue correlating to the high attenuation CT rim. Moreover, the histopathological analysis revealed significant vasa vasorum (C; arrowheads) accompanied by macrophage infiltration in the basal plaque area. HU: Hounsfield units; L: lumen

5.2.2 Attenuation pattern-based plaque classification

As the follow up our first report, we have performed a larger *ex vivo* study. Overall, 611 histological sections from 21 coronary arteries of 7 donor hearts were investigated.[297] The average studied vessel length was 67 mm (range 25 to 110 mm). Of the 611 sections, 71 (11.6%) were identified as AIT, 222 (36.3%) as PIT, 179 (29.3%) as Fib, 59 (9.7%) as EFA, 60 (9.8%) as LFA, and 20 (3.3%) contained TCFA. The proportion of early lesions (AIT, PIT, Fib) versus advanced lesions (EFA, LFA, TCFA) was 77.3% (n=472) versus 22.7% (n=132). All matched coronary CTA cross sections (n=611) were eligible for comparison with histology.

Among the 611 co-registered CT cross sections, no plaque was detected in 134 (21.9%), NCP in 254 (41.6%), MP in 191 (31.3%), and CP in 32 (5.2%) cross sections. Among the 445 cross sections containing NCP or MP, a homogenous pattern of plaque attenuation was found in 207 (46.5%) cross sections (130 for NCP and 77 for MP; 62.8% vs. 37.2%, respectively) and a heterogeneous pattern was found in 238 (53.5%) cross sections (124 for NCP and 114 for MP; 52.1% vs. 47.9%, respectively) (table 16, figure 34). Thus, homogenous plaques were less frequently found among MP than among NCP (p=0.03).

Table 16 Comparison of PAP categories to the conventional CT plaque classification scheme

		Heterogeneous			
	Homogenous	**All**	**Non-NRS**	**NRS**	**Total**
Noncalcified plaque	130 (62.8)	124 (52.1)	105 (52.5)	19 (50)	254 (57.1)
Partially calcified plaque	77 (37.2)	114 (47.9)	95 (47.5)	19 (50)	191 (42.9)
Total	207	238	200	38	445

Values are n (%) or n.
CT: computed tomography; NRS: napkin-ring sign; PAP: plaque attenuation pattern.

Heterogeneous plaques were further classified as non-NRS or NRS plaques (Table 16, figure 34). Among the 238 cross sections with a heterogeneous pattern, non-NRS lesions were identified in 200 (84.0%) cross sections (105 with NCP and 95 with MP; 52.5% vs. 47.5%, respectively) and NRS was identified in 38 (16.0%) cross sections (19 in NCP and 19 in MP, 50% vs. 50%, respectively). Thus, there was no significant difference regarding the distribution of NRS or non-NRS plaques across NCP and MP plaques (p=0.86), suggesting that the presence of NRS was independent of the conventional categories of NCP or MP.

In the subgroup of 100 cross sections, the interobserver agreement between the two CT

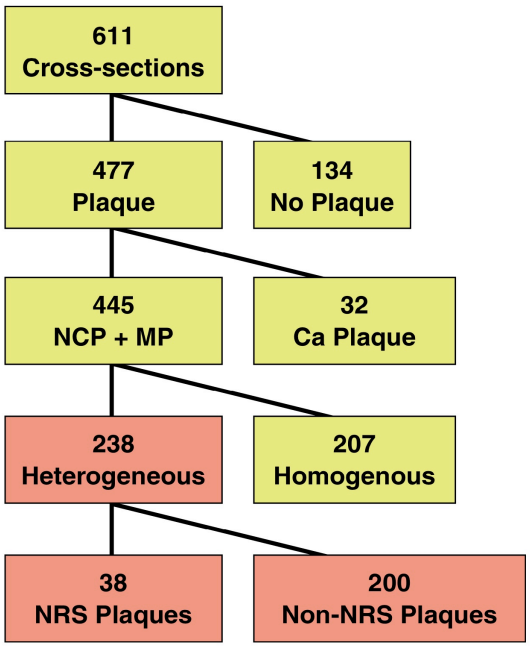

Figure 34 | Among the 611 coregistered CT cross sections, no plaque was detected in 134, noncalcified plaque (NCP) or mixed plaque (MP) in 445, and calcified (Ca) plaque in 32 cross sections. Among the cross sections containing NCP or MP, a homogenous plaque pattern was found in 207 cross sections and a heterogeneous pattern was found in 238 cross sections. Among the 238 cross sections with a heterogeneous pattern, napkin-ring sign (NRS) lesions were identified in 38 cross sections and non-NRS lesions in 200 cross sections. PAP: plaque attenuation pattern.

readers to classify coronary CTA cross sections as no plaque, NCP, MP, or CP was excellent (Cohen kappa=0.83; 95% CI: 0.73 to 0.94) with the majority of the disagreements occurring between a normal vessel wall and the presence of NCP. The interobserver agreement between the two CT readers to classify plaques as no plaque, homogenous plaque, non-NRS heterogeneous plaque or NRS plaque) was good (Cohen kappa=0.61; 95% CI: 0.56 to 0.67) with the majority of disagreements occurring between a normal vessel wall and the presence of a heterogeneous or homogenous NCP. In contrast, the interobserver variability to detect NRS was excellent (Cohen kappa=0.86; 95% CI: 0.76 to 0.96).

Overall, 99.3% (n=133) of CT cross sections without plaque were early lesions according to histology. There was no association between the conventional classification of NCP and MP and early and advanced atherosclerotic lesions as classified by histology (advanced lesions; NCP: 50.8% [n=68] vs. MP: 49.2% [n=66]; p=0.06) (Table 17). In contrast, differences in the distribution of early and advanced atherosclerotic lesions were found when the plaques were classified as heterogeneous and homogenous according to coronary CTA. Overall, 69.4% (93 of 134) of advanced lesions were classified as heterogeneous plaque on coronary CTA and only 30.6% (41 of 134) as homogenous plaque (p<0.0001) (Table 17). Among the 38 heterogeneous plaques classified as NRS, the majority (86.8% [33 of 38]) were classified as advanced atherosclerotic lesions by histopathology (p<0.0001) (Figure 35). In general, these associations were similar for the subgroup of 20

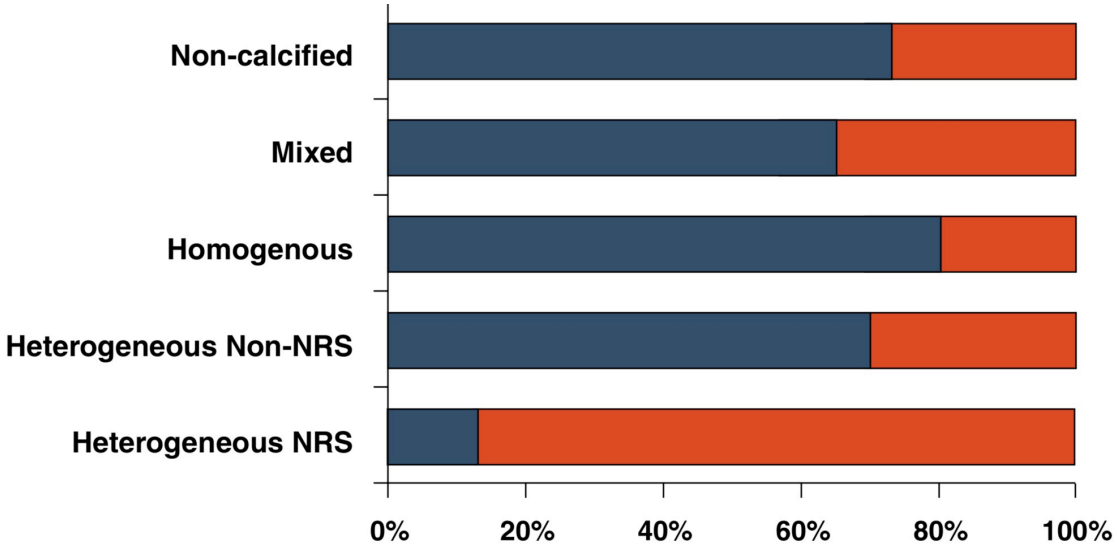

Figure 35 | Percentage of early and advanced atherosclerotic lesions among the conventional and plaque attenuation-based CT plaque Types. The **blue bars** represent early atherosclerotic lesions, whereas the **red bars** represent advanced atherosclerotic lesions. The percentage of advanced atherosclerotic lesions among different CT plaque types: noncalcified plaques: 26.4% (67 of 254); mixed/partially calcified plaques: 35.1% (67 of 191); homogenous plaques: 19.8% (41 of 207); non-NRS plaques: 30.0% (60 of 200); NRS plaques: 86.8% (33 of 38). NRS: napkin-ring sign

plaques (3.3%) characterized as TCFA in histopathology. There were no TCFA present in normal coronary CTA cross sections, and there was no difference between the distribution of TCFA in plaques classified as NCP or MP (p=0.63). In contrast, the frequency of TCFA differed across plaques characterized as heterogeneous or homogenous by coronary CTA with the majority (83.3%) of TCFA being classified as heterogeneous plaques (p=0.01). Among the 15 TCFA lesions described as heterogeneous in coronary CTA, 5 (33.3%) demonstrated NRS (p=0.07).

Table 17 Comparison of conventional plaque classification and intra plaque attenuation pattern-based classification schemes with histology.

	Early	Advanced	Total	p value
No plaque	133 (30)	1 (0.7)	134 (23.1)	
Conventional scheme				0.06
Noncalcified	187 (41.9)	67 (50.4)	254 (43.9)	
Partially calcified	124 (28.1)	67 (48.9)	191 (33.0)	
PAP scheme				<0.0001
Homogenous	166 (37.4)	41 (30.4)	207 (35.8)	
Heterogeneous non-NRS	140 (31.5)	60 (44.5)	200 (34.5)	
Heterogeneous NRS	5 (1.1)	33 (24.4)	38 (6.6)	

Values are n (%).
NRS: napkin-ring sign; PAP: plaque attenuation pattern.

Table 18 Diagnostic accuracy of different qualitative plaque categories for coronary CTA to identify advanced lesions as classified by histology with 95% CI

	Sensitivity % ($n_{TruePos}/n_{DiseasePos}$)	Specificity % ($n_{TrueNeg}/n_{DiseaseNeg}$)	PPV % ($n_{TruePos}/n_{TestPos}$)	NPV % ($n_{TrueNeg}/n_{TestNeg}$)
Any plaque	99.3 (134/135)	30.0 (133/444)	30.1 (134/445)	99.3 (133/134)
Crude 95% CI	95.9-99.9	25.7-34.5	25.9-34.6	95.9-100
Adjusted 95% CI	97.6-100	20.5-39.4	23.1-37.1	94.8-100
PAP classification				
Homogenous	30.4 (41/135)	62.6 (278/444)	19.8 (41/207)	74.7 (278/372)
Crude 95% CI	22.8-38.9	57.9-67.1	14.6-25.9	70.0-79.1
Adjusted 95% CI	14.8-45.9	54.8-70.3	11.0-28.6	65.7-83.8
Heterogeneous	68.9 (93/135)	67.3 (299/444)	39.1 (93/238)	87.7 (299/341)
Crude 95% CI	60.4-76.6	52.8-71.7	32.8-45.6	83.7-90.1
Adjusted 95% CI	53.0-84.8	58.6-76.1	27.3-50.8	82.0-93.3
Non-NRS plaque	44.4 (60/135)	68.5 (304/444)	30.0 (60/200)	80.2 (304/379)
Crude 95% CI	35.9-53.2	63.9-72.8	23.7-36.9	75.8-84.1
Adjusted 95% CI	31.6-57.3	60.2-76.7	18.7-41.3	72.8-87.6
NRS plaque	24.4 (33/135)	98.9 (439/444)	86.8 (33/38)	81.2 (439/541)
Crude 95% CI	17.5-32.6	97.4-99.6	71.9-95.6	77.6-84.4
Adjusted 95% CI	12.1-36.8	97.6-100	62.7-100	76.1-86.2
Conventional plaque classification				
Noncalcified plaque	49.6 (67/135)	57.9 (257/444)	26.4 (67/254)	79.1 (257/325)
Crude 95% CI	40.9-58.3	53.1-62.5	21.1-32.3	74.2-83.4
Adjusted 95% CI	31.0-68.3	50.1-65.6	17.7-35.1	71.0-87.2
Mixed plaque	49.6 (67/135)	72.1 (320/444)	35.1 (67/191)	82.5 (320/388)
Crude 95% CI	40.9-58.4	67.7-76.2	28.3-42.3	78.3–86.1
Adjusted 95% CI	30.8-68.4	64.7-79.4	22.9-47.2	75.5–89.5

Confidence intervals are provided for a crude binomial analysis and adjusted for the within-lesion correlation.
CTA: computed tomography angiography; CI: confidence interval; DiseaseNeg: disease negative; DiseasePos: disease positive; NPV: negative predictive value; PPV: positive predictive value; TestPos: test positive cross section; TestNeg: test negative cross section; TrueNeg: true negative cross sections; TruePos: true positive cross sections; NRS: napkin-ring sign; PAP: plaque attenuation pattern.

Table 18 presents the diagnostic accuracy measures of conventional and pattern-based coronary CTA plaque categories to identify advanced atherosclerotic lesions. The heterogeneous plaque category, showed a good sensitivity, specificity, and negative predictive value to identify advanced lesions (68.9%, 67.3%, and 87.7%, respectively). The NRS category showed the highest specificity value among all coronary CTA plaque categories for the presence of advanced lesions and TFCA in histopathology (98.9%, 95% CI: 97.6% to 100%, and 94.1%, 95% CI: 90.8% to 97.4%, respectively) (Table 18).

Diagnostic accuracy was on average 61% for the conventional plaque categories (56.0% for NCP and 66.8% MP), and it ranged from 55% to 82% for the pattern-based analysis (55.1%

for homogenous, 67.7% for heterogeneous, and 81.5% for NRS plaques). Comparing the diagnostic performance of the 2 different schemes, the plaque classification scheme based on attenuation pattern had a significantly better discriminative power than did the conventional scheme to identify both advanced lesions as well TCFA as defined by histopathology (AUC: 0.761 vs. 0.678, p=0.001, and 0.769 vs. 0.648, p=0.02, respectively) (Figure 36). In addition, we have performed a per plaque analysis. We have identified 95 individual plaques based on histological criteria. Out of this highly diseased sample, 50 plaques were classified as advanced lesions as they contained at least 1 cross section with EFA, LFA, or TCFA; 45 plaques were classified as early lesion because they contained only AIT, PIT, or Fib. Blinded to the histology results, CT readers identified NRS in 38 of 611 cross sections, 18 of 95 individual plaques, and 6 of 7 donor hearts. Notably, all of the individual plaques containing NRS were advanced lesions according to the histology. A per-plaque analysis led to specificity of 100% (95% CI: 92.0% to 100%) and a sensitivity of 36.0% (95% CI: 22.9% to 50.8%) for NRS to identify advanced lesion.

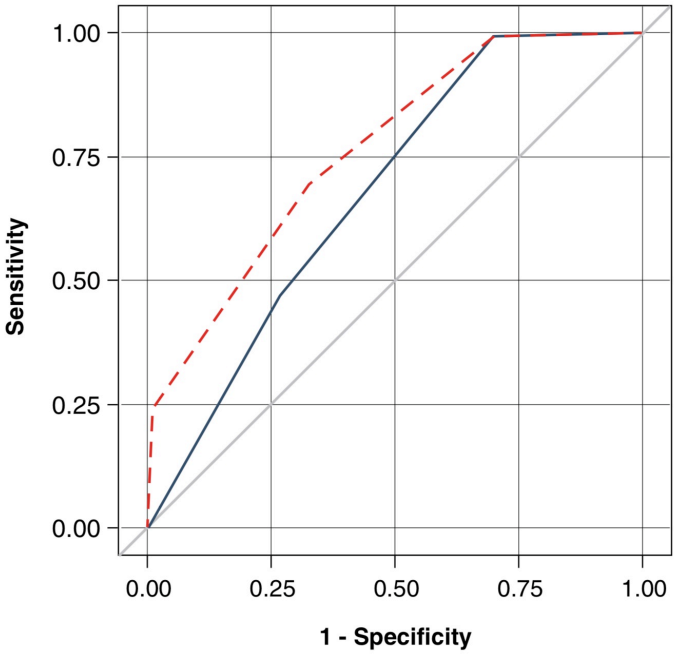

Figure 36 | The area under the receiver-operating characteristic curve was 0.678 for conventional plaque classification scheme (blue line) and 0.761 for plaque attenuation pattern (PAP) scheme (red line). The PAP scheme had a higher diagnostic performance than the conventional plaque scheme does, p=0.001.

5.2.3 Systemic comparison of CT, IVUS and OCT to identify high-risk plaques

Overall, 379 histologic slices from nine coronary arteries of three donor hearts were available for analysis.[298] Among the six histologic plaque types, pathologic intimal thickening (PIT) and fibrous plaques were most frequently detected (163 [43.0%] of 379 and 94 [24.8%] of 379, respectively), followed by late fibroatheroma (LFA) (38 [10%] of 379), early fibroatheroma (EFA) (37 [9.8%] of 379), adaptive intimal thickening (AIT) (30 [7.9%] of 379), and thin-cap fibroatheroma (TCFA) (17 [4.5%] of 379). The proportion of cross-sections that

showed early (AIT, PIT, fibrous plaque) versus advanced (EFA, LFA, TCFA) lesions was similar among the donor hearts (81%-71% vs. 19%-29%, respectively; p=0.45). All matched coronary CT angiography cross sections (n=379) were eligible for comparison with histologic findings; after 22.7% of IVUS and 24.8% of OFDI cross sections were excluded because of large vessel diameter, 293 IVUS and 285 OFDI cross sections remained available for analysis. Additionally, we identified 57 distinct coronary lesions with a median of six cross sections (interquartile range, 4-8). Of these lesions, 29 were advanced and six contained TCFA.

Of the 379 coronary CT angiography cross sections, 91 (24.0%) were classified as showing normal findings, 157 (41.4%) as showing noncalcified plaque, 123 (32.5%) as showing mixed plaque, and only eight (2.1%) as showing calcified plaque (Table 19). Only 1.1% of normal coronary CT angiography cross sections contained an advanced lesion at

Table 19 Plaque composition as assessed by coronary computed tomographic angiography (CCTA), intravascular ultrasound (IVUS), and optical frequency domain imaging (OFDI) within atherosclerotic plaque categories as defined by histopathology.

	Early Lesion			**Advanced Lesion**			
	AIT n (%)	PIT n (%)	Fib n (%)	EFA n (%)	LFA n (%)	TCFA n (%)	Total n
CCTA							
Normal	26 (28.6)	20 (22.0)	44 (48.3)	0 (0)	1 (1.1)	0 (0)	91
Non-Calcified	3 (1.9)	79 (50.3)	33 (21.0)	22 (14.0)	11 (7.0)	9 (5.7)	157
Mixed	1 (0.8)	62 (50.4)	15 (12.2)	14 (11.4)	25 (20.3)	6 (4.9)	123
Calcified	0 (0)	2 (25.0)	2 (25.0)	1 (12.5)	1 (12.5)	2 (25.0)	8
Total	**30 (7.9)**	**163 (43.0)**	**94 (24.8)**	**37 (9.8)**	**38 (10.0)**	**17 (4.5)**	**379**
IVUS							
Normal	4 (66.7)	0 (0)	2 (33.3)	0 (0)	0 (0)	0 (0)	6
Fibrous	0 (0)	3 (42.9)	2 (28.6)	0 (0)	2 (28.6)	0 (0)	7
Fibro-fatty	3 (2.5)	66 (55.46)	29 (24.4)	10 (8.4)	1 (0.9)	10 (8.4)	119
Fatty	5 (6.1)	26 (31.7)	35 (42.7)	9 (11.0)	7 (8.5)	0 (0)	82
Calcified	1 (1.3)	36 (45.6)	13 (16.5)	11 (13.9)	12 (15.2)	6 (7.6)	79
Total	**13 (4.4)**	**131 (44.7)**	**81 (27.6)**	**30 (10.2)**	**22 (7.5)**	**16 (5.5)**	**293**
OFDI							
Normal	0	0	0	0	0	0	0
Fibrous	10 (6.4)	70 (44.6)	70 (44.6)	3 (1.9)	4 (2.5)	0 (0)	157
Fib-Ca	0 (0)	31 (53.4)	21 (36.2)	2 (3.4)	4 (6.9)	0 (0)	58
Lipid-rich	0 (0)	18 (25.7)	1 (1.4)	25 (35.7)	13 (18.6)	13 (18.6)	70
Total	**10 (3.5)**	**119 (41.8)**	**92 (32.3)**	**30 (10.5)**	**21 (7.4)**	**13 (4.6)**	**285**

Note: AIT, adaptive intimal thickening; PIT, pathological intimal thickening; Fib, fibrous plaques; EFA, early fibroatheroma; LFA, late fibroatheroma; TCFA, thin-cap fibroatheroma; n, number of cross-sections.

histopathologic examination (negative predictive value: 98.9%; 95% CI: 94.1%, 99.9%). Most of the 91 normal cross sections at coronary CT angiography were fibrous plaques (48.4%), followed by AIT (28.6%) and PIT (22.0%) (Table 19). Accordingly, the normal coronary CTA cross sections were strongly associated with early plaque (OR=0.01, p=0.0006 [Table 20, Figure 37 A]). Most importantly, normal cross sections at coronary CT angiography excluded the presence of TCFA.

Of the 157 non-calcified cross sections at coronary CTA, 115 (73%) were classified as showing early atherosclerotic plaque at histologic examination, but that association was not significant (p=0.18). Notably, the coronary CTA category of non-calcified plaques contained nine TCFAs (5.7%). The presence of mixed plaque at coronary CTA (Figure 37 B) was associated with a significant increase in the odds of it being an advanced plaque (OR=4.71, p=0.0002). No association was observed between calcified plaques as defined at coronary CT angiography (n=8) and early (n=4) versus advanced (n=4) plaques at histologic examination

Table 20 Association of coronary computed tomographic angiography (CCTA), intravascular ultrasound (IVUS), and optical frequency domain imaging (OFDI) characteristics for early versus advanced plaque as defined by histopathology

		Histological Plaque Stage		**Crude Analysis**		**Accounted for Clustering**	
	Total	Early	Advanced	OR	p	OR	p
CCTA							
Normal	91	90	1	0.02	**<0.0001**	0.01	**0.0006**
Non-Calcified	157	115	42	1.25	0.39	0.59	0.18
Mixed	123	78	45	2.49	**0.0003**	4.71	**0.0002**
Calcified	8	4	4	3.22	0.10	9.39	0.06
Total	**379**	**287**	**92**				
IVUS							
Normal	6	6	0	0.25	0.34	<0.01	0.99
Fibrous	7	5	2	1.33	0.67	9.45	0.10
Fibro-fatty	119	98	21	0.58	0.07	0.34	0.02
Fatty	82	66	16	0.74	0.44	0.49	0.33
Calcified	79	50	29	2.60	**0.002**	3.22	0.01
Total	**293**	**225**	**68**				
OFDI							
Normal	0	0	0	NA	NA	NA	NA
Fibrous	157	150	7	0.06	**<0.0001**	0.04	**<0.0001**
Fibro-calcific	63	53	10	0.59	0.17	0.87	0.78
Lipid-rich	65	18	47	31.2	**<0.0001**	57.15	**<0.0001**
Total	**285**	**221**	**64**				

Data represent absolute numbers. An OR >1.0 indicated an increased probability for being an advance lesion, whereas an OR <1.0 indicated an increased probability for being an early lesion. Having several cross sections within one lesion, we derived OR and *P* values for clustered effect on a per-lesion basis. Owing to multiple testing, significance levels were adjusted by using Bonferroni correction. For modalities with four categories (CT, OFDI), *P* <0.0125 and for modalities with five categories (IVUS), *P* <0.01 was considered to indicate a significant difference. NA = not applicable.

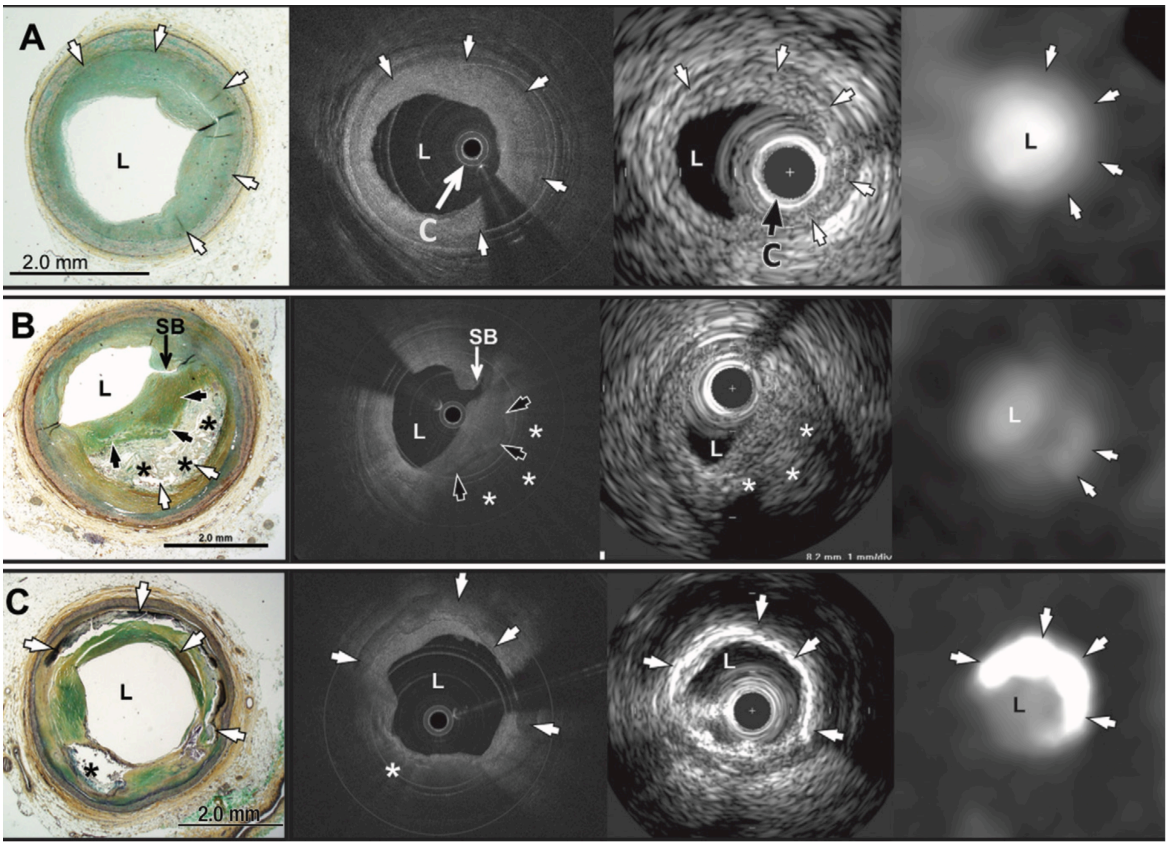

Figure 37 | A, Fibrous atherosclerotic plaque. The invasive modalities (OFDI and intravascular US) correctly depicted the fibrous plaque, whereas the coronary CT angiography cross section depicts normal vessel wall. Arrows = eccentric intimal hyperplasia. B, LFA. Microcalcification (white arrows), a thick fibrous cap (black arrows), and necrotic core (*) are present. The corresponding cross section at OFDI was described as showing lipid-rich plaque with fibrous cap (arrows) and necrotic core (*). Intravascular US shows a fibro-fatty lesion with attenuated areas (*) corresponding to lipid-rich/necrotic areas. Coronary CT angiography depicts a mixed plaque with spotty calcification (arrows). C, TCFA. The necrotic core (*) is covered by a thin fibrotic cap; arrows = sheet calcification. The corre- sponding cross section with OFDI reveals the TCFA, with lipid pool and large calcification. Intravascular US and coronary CT angiography show calcified plaques. C = catheter, L = lumen, SB = side branch.

(Table 20; Figure 37 C). Of the 293 IVUS images, six (2.0%) were classified as normal, seven (2.4%) as showing fibrous plaque, 119 (40.6%) as showing fibrofatty plaque, 82 (28.0%) as showing fatty plaque, and 79 (27.0%) as showing calcified plaque (Table 20). None of the normal IVUS cross sections was classified as showing an advanced plaque. The majority of fibro-fatty and fatty cross sections showed PIT or fibrous plaques, according to results of histologic examination (79.8% and 74.4%, respectively; Table 19, Figure 37 A). However, no significant association was found between fibro-fatty or fatty plaques and advanced plaque at histologic examination (Table 20). Cross sections categorized as calcified corresponded to advanced plaque at histologic examination in 36.7% (29/79) of cases. Thus, the presence of calcification at IVUS was associated in crude analysis with a significant increase in the odds of a plaque being advanced (OR=2.60, p=0.002), but this was attenuated marginally after

accounting for clustered data structure (Table 20; Figure 37 C).

Of the 285 OFDI cross sections, zero (0%) were classified as normal, 157 (55.1%) as showing fibrous plaque, 58 (20.4%) as showing fibrocalcific plaque, and 70 (24.6%) as showing lipid-rich plaque (Table 19). Cross sections defined as showing fibrous plaque at OFDI corresponded to early plaque at histologic examination in 95.5% (150 of 157) of cases (Table 20; Figure 37 A) and were associated with small odds of representing advanced plaque (OR=0.04, p<0.0001; Table 20). The majority of fibrocalcific plaques as defined at OFDI were PIT or fibrous plaques at histologic examination (52 [89.7%] of 58); however, no association was detected between fibrocalcific plaque and histologic plaque stage (p=0.78; Table 20). Notably, none of the fibrous, and fibrocalcific cross sections as defined at OFDI contained TCFA (Table 19). In contrast, lipid-rich plaque was found in 79.7% (51 of 64) of cross sections categorized as showing advanced plaque, corresponding to a high and significant odds ratio for the presence of advanced plaque at histologic examination (OR=57.15, P<0.0001; Table 20). On a cross-section level, OFDI had a significantly better ability (both, p<0.0001) to differentiate early from advanced lesions as compared with IVUS and coronary CT angiography (areas under the curve: 0.858 [95% CI: 0.802, 0.913], 0.631 [95% CI: 0.554, 0.709], and 0.679 [95% CI: 0.618, 0.740], respectively; based on comparing 2 log likelihoods between nested models.

In a sub-analysis accounting for clustering effects, lipid-rich plaque as determined at OFDI yielded a sensitivity of 100% (95% CI: 75%, 100%) and a specificity of 81% (95% CI: 76%, 85%) for the detection of TCFA. In contrast, TCFA composition was heterogeneous and non-discriminatory at IVUS (predominantly fibrofatty, 63%) and coronary CTA (noncalcified plaque, 35%; mixed, 53%; calcified, 12%). In the assessment of individual lesions, OFDI had the best ability to discriminate between early and advanced lesions. The mean percentage of cross sections containing “lipid-rich plaque” was significantly higher in advanced compared with early lesions (43% vs 5%, p=0.04). At coronary CTA, the mean percentage of cross sections containing ”mixed plaque” was significantly higher in advanced compared with early lesions (46% vs 17%, p<0.01). Of note, 42% of early but only 6% of advanced lesions showed no plaque and thus were not detected at coronary CTA (p<0.05). In contrast, no significant difference was detected between the IVUS findings of early and advanced lesions.

The interobserver variability between the two coronary CTA readers for the four categories was excellent (Cohen κ=0.87), with the majority of the disagreements occurring between classification as noncalcified plaque or normal vessel wall. The overall agreement between the two IVUS readers for the five plaque categories was good (Cohen κ=0.66), but

grading of fibro-fatty versus fatty plaque and fibro-fatty versus fibrous plaque was inconsistent. The interobserver variability between the two OFDI readers for the four plaque categories was excellent (Cohen κ=0.85), with disagreement occurring mainly between fibrous and fibrocalcific plaque.

5.2.4 Quantity of plaques by coronary CTA versus invasive coronarography

Coronary CTA detected coronary artery plaque in 49% (487/1000) of the segments, whereas ICA showed coronary plaques in 24% (235/1000) of all segments (p<0.001, Figure 38).[60] Of the 235 positive segments with ICA, corresponding segments on CTA was also positive in 94%. CTA detected atherosclerotic plaque in 35% (266/765) of coronary segments where ICA was negative. 36% (95/266) of these plaques were non-calcified, 38% (102/266) were mixed and 26% (69/266) were calcified plaques on CTA. When considering the severity of coronary stenosis only seen by CTA, 79% of plaques caused minimal or mild luminal stenosis (211/266). Conversely, ICA detected plaque only in 3% (14/513) of segments where CTA was negative. Detailed distribution and quantification of coronary plaques only seen by CTA are shown in Table 21. Regarding segment scores, CTA showed more than two times as many segments with plaque compared to ICA, and also the overall degree of stenosis caused by the plaques was almost twice. Summary of segment score analysis is shown in Table 22. Analysis of diagnostic accuracy revealed high sensitivity with moderate specificity (96% CI: 87-100%; 53 % CI: 28-77%, respectively) with high positive and negative predictive value (87%, CI: 75-94%; 82 %, CI: 48-100%, respectively). Intra-reader agreement of segment-based stenosis categories was excellent for CTA (κ = 0.83) and

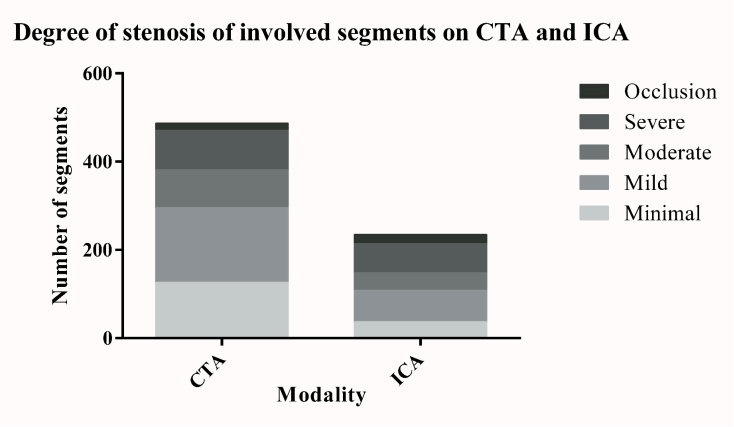

Figure 38 | Distribution of stenosis severity of involved segments on CTA and ICA. Coronary CTA showed 487 plaques, whereas ICA showed 235 coronary plaques in all segments (p<0.001).

Table 21 Number and localization of plaques seen only by coronary CTA and not detected by invasive coronary angiography

	Coronary segments																		
Plaque quantity	LM	prox LAD	mid LAD	dist LAD	D1	D2	IM	prox LCx	md LCx	OM1	OM2	plb LCx	pda LCx	prox RCA	mid RCA	dist RCA	pda RCA	plb RCA	Total
Minimal	22	9	5	8	3	0	1	11	7	3	3	0	0	12	7	10	3	3	107
Mild	15	9	9	8	5	0	1	13	2	5	0	0	1	10	7	12	6	1	104
Moderate	1	4	8	4	5	2	0	4	3	3	0	0	1	7	4	1	0	0	47
Severe	0	0	1	0	3	0	0	0	0	0	1	1	0	0	2	0	0	0	8
Occlusion	0	0	0	0	0	0	0	0	0	0	0	0	0	0	0	0	0	0	0
Total number of involved segments only on CTA	38	22	23	20	16	2	2	28	12	11	4	1	2	29	20	23	9	4	266

Data represent absolute numbers. An OR >1.0 indicated an increased probability for being an advance lesion, whereas an OR Overall coronary CTA showed 487 plaques, of which 266 (54.6%) plaques were not reported on ICA. CTA: CT-angiography, D: diagonal; IM: intermediate marginal, LM: left main, LAD: left anterior descending, LCx: left circumflex, RCA: right coronary artery, PDA: posterior descending artery, PLB: posterolateral branch.

good for ICA (κ = 0.62). Dichotomization of stenosis categories to obstructive (≥50% stenosis) and non-obstructive (<50% stenosis) had an excellent reproducibility for both modalities (CTA: κ = 0.96, ICA: κ = 0.90). Regarding segment scores, intra-reader reproducibility was excellent for both CTA and ICA (CTA: ICC_{SIS}: = 0.97, ICC_{SISi}: = 0.96, ICC_{SSS}: = 0.99, ICC_{SSSi}: = 0.99; vs. ICA: ICC_{SIS}: = 0.96, ICC_{SISi}: = 0.96, ICC_{SSS}: = 0.92, ICC_{SSSi}: = 0.93). Segment-based stenosis categories showed good inter-reader reproducibility for CTA, while ICA showed only moderate results (κ = 0.68; κ = 0.57, respectively). Reproducibility of dichotomized stenosis categories was good for both modalities (CTA: κ = 0.73, ICA: κ = 0.70). For the segment involvement and stenosis scores the ICC values were excellent for both CTA and ICA (CTA: ICC_{SIS}: = 0.90, ICC_{SISi}: = 0.91, ICC_{SSS}: = 0.95, ICC_{SSSi}: = 0.95 vs. ICA: ICC_{SIS}: = 0.88, ICC_{SISi}: = 0.88, ICC_{SSS}: = 0.91, ICC_{SSSi}: = 0.92).

Out of 71 patients, based on CTA results 72% (51/71) was classified as extensive obstructive, 3% (2/71) as extensive non-obstructive, 13% (9/71) as non-extensive obstructive and 13% (9/71) as non-extensive non-obstructive. Using ICA based measurements, 27% (19/71) of the patients was extensive obstructive, 1% (1/71) was extensive non-obstructive, 49% (35/71) was non-extensive obstructive and 23% (16/71) was non-extensive non-obstructive. Overall 52% (37/71) of the patients moved to a higher

Table 22 Segment involvement score and index, segment stenosis score and index values using coronary computed tomography angiography and invasive coronary angiography

	CTA	ICA	p
SIS	6.9 ± 3.0	3.3 ± 2.0	<0.001
SISi	0.5 ± 0.2	0.2 ± 0.1	<0.001
SSS	16.4 ± 8.8	9.4 ± 6.8	<0.001
SSSi	1.2 ± 0.6	0.7 ± 0.5	<0.001

Coronary CTA showed significantly higher segment scores compared to ICA. CTA: CT-angiography, ICA: invasive coronary angiography, SIS: Segment Involvement Score, SISi: Segment Involvement Score index, SSS: Segment Stenosis score, SSSi: Segment Stenosis Score index.

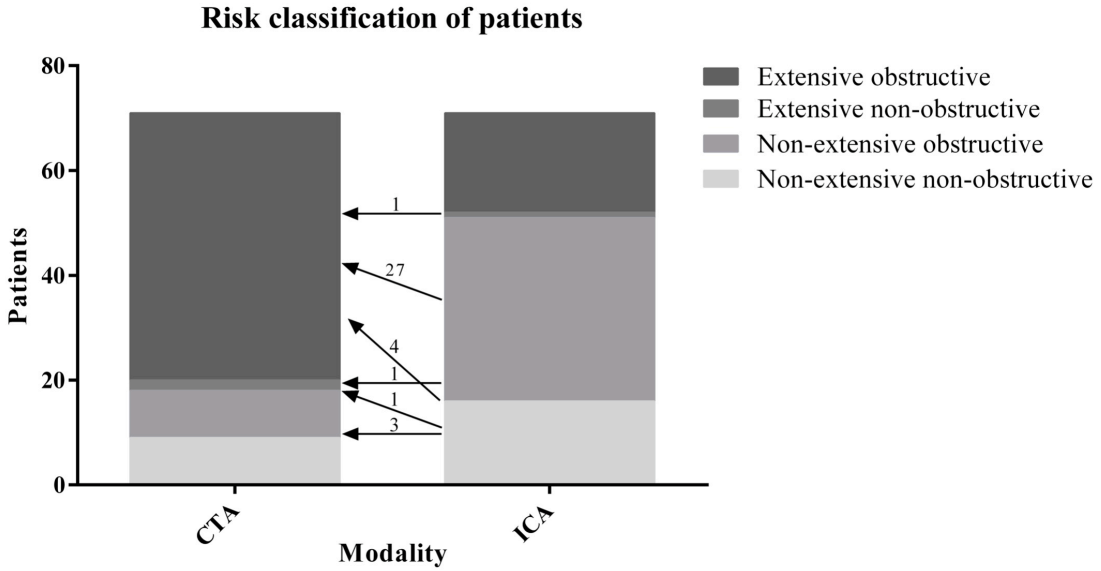

Figure 39 | Risk classification of patients based on coronary CTA and ICA. Overall, 52% of patients moved to a higher risk category. The number of patients switching to higher risk groups are represented by arrows. Only 1% of patients moved to a lower risk category using CTA-based measurements as compared to ICA-based measurements (not shown).

risk category, while 1% (1/71) moved to a lower category using CTA based measurements as compared to ICA based measurements. Graphical representation of the risk groups and exact number of patients moving from one group to another can be found in Figure 39.

5.2.5 Coronary CTA radiomics to identify plaques with napkin-ring sign

There was no significant difference between the NRS and non-NRS groups regarding patient characteristics and scan parameters (Table 23). Furthermore, we did not observe any significant difference in qualitative plaque characteristics and image quality parameters (Table 24) implying successful matching of the two groups. Median number of voxels contributing to the NRS coronary plaques (1928 [IQR: 1413; 2560]) did not show statistical difference as compared to the number of voxels in the non-NRS group (1286 [IQR: 1001; 1768]), p=0.0041.

Table 23 Patient characteristics and scan parameters

	NRS group (n=30)		non-NRS group (n=30)		p
Demographics					
Age (years)	63.07	(56.54 - 68.36)	63.96	(54.73 - 72.13)	0.86
Male gender, n (%)	24	(80)	20	(67%)	0.16
BMI (kg/m²)	28.06	(25.06 - 29.91)	26.93	(23.91 - 29.32)	0.34
Cardiovascular risk factors					
Hypertension n (%)	19	(63)	18	(60%)	0.78
Diabetes mellitus n (%)	25	(83)	26	(87%)	0.65
Dyslipidemia n (%)	16	(53)	18	(60%)	0.62
Current smoker n (%)	20	(67)	21	(70%)	0.80
Scan parameters					
Total DLP (mGy x cm)	362.00	(356.00 - 367.00)	358.20	(253.20 - 367.00)	0.42
Pixel spacing (mm)	0.41	(0.39 - 0.43)	0.43	(0.39; 0.45)	0.30

Data is presented as median with interquartile ranges or frequency and percentage as appropriate.
BMI: body mass index; CTA: Coronary CT angiography; DLP: dose length product; NRS: Napkin ring sign

Among conventional quantitative imaging parameters, there was no significant difference between NRS and non-NRS plaques (Table 24). Furthermore, none of the conventional parameters had an AUC value above 0.8 (Table 25). Overall, 4440 radiomic parameters were calculated for each atherosclerotic lesion. Out of all calculated radiomic parameters, 20.6%

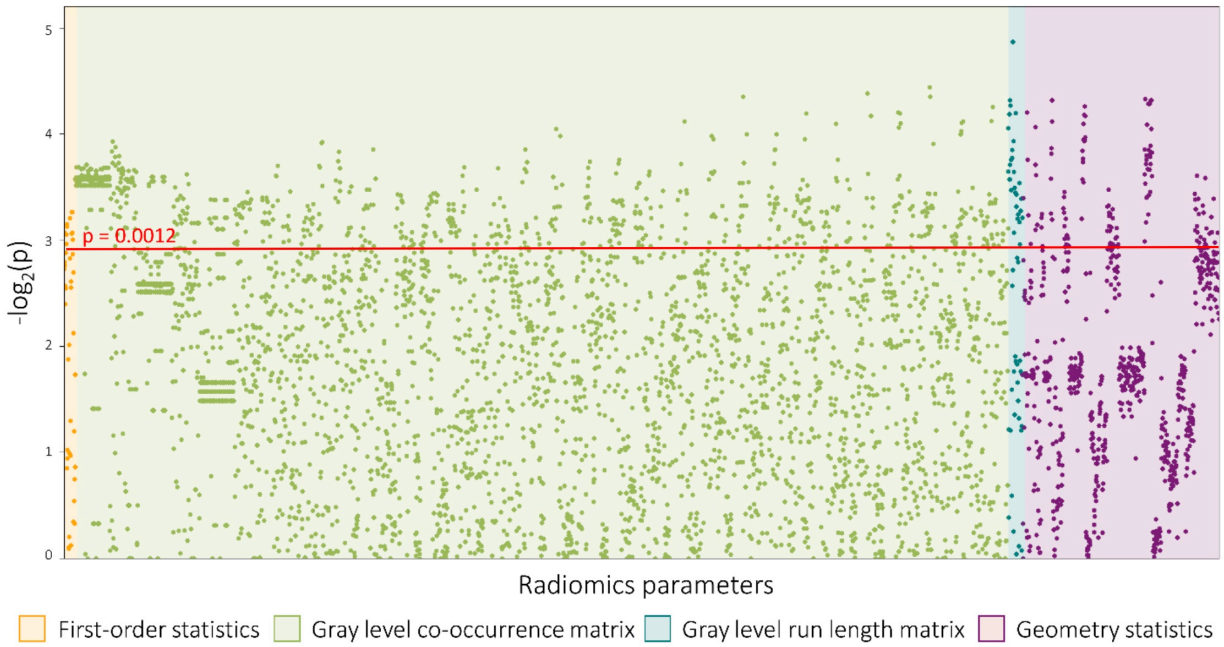

Figure 40 | The Manhattan plot shows all 4440 calculated p values comparing napkin-ring sign (NRS) vs. non-NRS plaques and their distribution among the different classes of radiomic parameters. Radiomic features are lined up on the x axis, while the $-\log_2(p)$ values are plotted on the y axis. The red horizontal line indicates the Bonferroni corrected p value of 0.0012. Radiomic parameters above the red line were considered statistically significant.

(916/4440) showed a significant difference between plaques with or without NRS (all p<0.0012). Of the 44 calculated first-order statistics 25.0% (11/44) was significant. Out of the 3585 calculated gray level co-occurrence matrix (GLCM) statistics 20.7% (742/3585) showed a significant difference between the two groups. Among the 55 gray level run length matrix (GLRLM) parameters 54.5% (30/55) were significant, while 17.6% (133/756) of the calculated 756 geometry based parameters had a p<0.0012. A Manhattan plot of the p values of the calculated radiomic parameters is shown in Figure 40. Among all 4440 radiomic parameters 9.9% (440/4440) had an AUC value greater than 0.80. Out of the 44 calculated first-order

Table 24 Plaque and image quality characteristics

	NRS group (n=30)		non-NRS group (n=30)		p
Plaque composition					1.00
Non-calcified, n (%)	19	(63%)	19	(63%)	
Partially calcified, n (%)	11	(37%)	11	(37%)	
Calcified, n (%)	0	(0%)	0	(0%)	
Luminal stenosis					1.00
Minimal (1-24%)	11	(37%)	11	(37%)	
Mild (25-49%)	11	(37%)	11	(37%)	
Moderate (50-69%)	6	(20%)	6	(20%)	
Severe (70-99%)	2	(7%)	2	(7%)	
Stenosis localization					1.00
Left main	2	(7%)	2	(7%)	
Left anterior descending	20	(66%)	20	(66%)	
Left circumflex	2	(7%)	2	(7%)	
Right coronary	6	(20%)	6	(20%)	
Image quality					
Contrast-to-noise ratio	21.94	[18.61; 28.80]	23.42	[18.64; 26.57]	0.70
Signal-to-noise ratio	18.69	[15.84; 24.13]	20.52	[16.33; 22.53]	0.59
High-risk plaque features					
Napkin-ring sign, n (%)	30	(100%)	0	(0%)	<0.0001
Low attenuation, n (%)	26	(87%)	19	(63%)	0.06
Spotty calcification, n (%)	10	(33%)	9	(30%)	0.99
Conventional quantitative metrics					
Lesion length (mm)	13.62	[10.42; 17.02]	13.48	[10.99; 17.71]	0.70
Lesion volume (mm^3)	134.88	[105.68; 190.76]	88.88	[70.02; 143.98]	0.02
Mean plaque burden	0.59	[0.52; 0.66]	0.51	[0.44; 0.59]	0.003
Lumen area stenosis	0.41	[0.15; 0.53]	0.28	[0.19; 0.49]	0.38
Vessel wall remodeling index	1.03	[0.92; 1.46]	1.09	[0.97; 1.20]	0.55
Mean plaque attenuation (HU)	114.67	[85.54; 148.99]	156.75	[138.46; 208.37]	0.002
Minimal plaque attenuation (HU)	-83.00	[-101.75; -58.00]	-60.00	[-84.75; -47.00]	0.10
Maximal plaque attenuation (HU)	523.00	[451.00; 794.50]	634.50	[454.00; 898.00]	0.63

Data is presented as median with interquartile ranges or frequency and percentage as appropriate. NRS: Napkin ring sign.

statistics 18.2% (8/44) had an AUC value larger than 0.80. Of the 3585 calculated GLCM parameters 9.7% (348/3585) of the AUC values was above 0.80. Among the 55 GLRLM parameters 54.5% (30/55) had an AUC value above 0.80, while out of the calculated 756 geometry-based parameters 7.1% (54/756) had an AUC value above 0.80. Of all radiomic parameters short run low gray level emphasis, long run low gray level emphasis, surface ratio of component 2 to total surface, long run emphasis and surface ratio of component 7 to total surface had the five highest AUC values (0.918; 0.894; 0.890; 0.888 and 0.888, respectively). Detailed diagnostic accuracy statistics of conventional quantitative features and of the five best

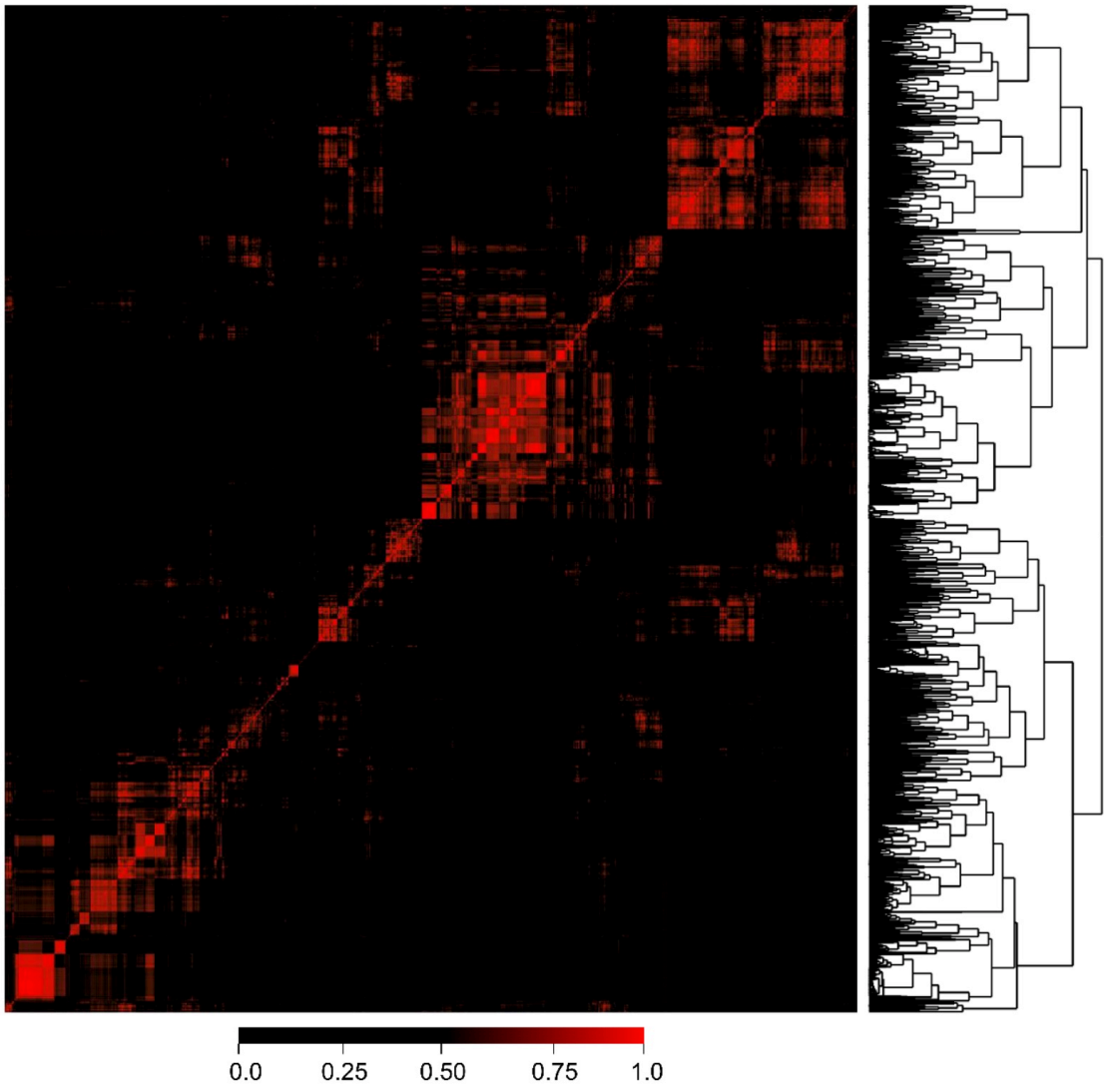

Figure 41 | Heatmap of the covariance matrix of all 4440 radiomic features. Each parameter was compared to all other parameters using linear regression analysis. Features were clustered based on R^2 values of the corresponding regression models and plotted along both axes. R^2 values below 0.5 are black, while greater values are shown in red with increasing intensity. The 1-R^2 values was used as a distance measure between parameters and used for hierarchical clustering. The resulting clustering dendrogram can be seen on the right of the image. Cluster analysis indicated that the optimal number of clusters is 44 based on our radiomics dataset.

Table 25 Diagnostic performance of conventional quantitative parameters and novel radiomic parameters to identify plaques with the napkin-ring sign.

	AUC	CI	Sensitivity	Specificity	PPV	NPV
Conventional quantitative metrics						
Mean plaque attenuation	0.770	[0.643; 0.880]	0.533	0.933	0.889	0.667
Mean plaque burden	0.702	[0.563; 0.826]	0.700	0.667	0.677	0.690
Lesion volume	0.683	[0.543; 0.817]	0.700	0.700	0.700	0.700
Minimal plaque attenuation	0.647	[0.498; 0.788]	0.700	0.700	0.700	0.700
Maximal plaque attenuation	0.553	[0.408; 0.696]	0.700	0.500	0.583	0.625
Remodeling index	0.547	[0.398; 0.700]	0.633	0.633	0.633	0.633
Lumen area stenosis	0.539	[0.389; 0.687]	0.567	0.667	0.630	0.606
Lesion length	0.508	[0.359; 0.654]	0.933	0.133	0.519	0.667
First-order statistics						
30th decile	0.827	[0.716; 0.921]	0.833	0.733	0.758	0.815
First quartile	0.826	[0.712; 0.922]	0.767	0.800	0.793	0.774
Harmonic mean	0.823	[0.708; 0.922]	0.767	0.800	0.793	0.774
Trimean	0.812	[0.696; 0.910]	0.867	0.667	0.722	0.833
Geometric mean	0.803	[0.684; 0.902]	0.633	0.900	0.864	0.711
GLCM						
Interquartile range*	0.867	[0.769; 0.948]	0.700	0.900	0.875	0.750
Lower notch*	0.866	[0.763; 0.948]	0.967	0.633	0.725	0.950
Gauss right focus†	0.859	[0.759; 0.940]	0.767	0.867	0.852	0.788
Median absolute deviation from the mean*	0.856	[0.744; 0.946]	0.867	0.767	0.788	0.852
Sum energy‡	0.848	[0.740; 0.937]	0.967	0.633	0.725	0.950
GLRLM						
Short run low gray level emphasis*	0.918	[0.822; 0.996]	1.000	0.867	0.882	1.000
Long run low gray level emphasis§	0.894	[0.799; 0.970]	1.000	0.733	0.789	1.000
Long run emphasis§	0.888	[0.791; 0.962]	0.933	0.767	0.800	0.920
Run percentage§	0.871	[0.771; 0.951]	1.000	0.667	0.750	1.000
Short run emphasis‡	0.853	[0.747; 0.942]	1.000	0.633	0.732	1.000
Geometry based parameters						
Surface ratio of component 2 to total surface§	0.890	[0.801; 0.960]	0.833	0.833	0.833	0.833
Surface ratio of component 7 to total surface‖	0.888	[0.796; 0.958]	0.933	0.733	0.778	0.917
Surface ratio of component 22 to total surface‡	0.883	[0.787; 0.959]	0.767	0.900	0.885	0.794
Surface ratio of component 14 to total surface†	0.882	[0.790; 0.954]	0.833	0.833	0.833	0.833
Surface ratio of component 3 to total surface*	0.864	[0.767; 0.943]	0.867	0.767	0.788	0.852

Component numbers of the geometric-based parameters refer to the specific attenuation bins created by discretizing the attenuation values to a given number of bins.
AUC: area under the curve; CI: confidence interval; GLCM: gray level co-occurrence matrix; GLRLM: gray level run length matrix; NPV: negative predictive value; PPV: positive predictive value
*: based on discretizing to 4 equally probable bins; †: based on discretizing to 16 equally probable bins; ‡: based on discretizing to 32 equally probable bins; §: based on discretizing to 2 equally probable bins; ‖: based on discretizing to 8 equally probable bins

radiomic features for each group are shown in Table 25. Results of the linear regression analysis conducted between all pairs of the calculated 4440 radiomic metrics are summarized using a heatmap (Figure 41). Hierarchical clustering showed several different clusters where

Table 26 Area under the curve values of stratified five-fold cross-validated receiver operating characteristic curves of the best radiomic and conventional quantitative parameters to identify plaques with the napkin-ring sign.

	AUC	Additional cases classified correctly as compared to lesion volume	p
Short run low gray level emphasis	0. 889	30.6%	<0.0001
Long run low gray level emphasis	0. 866	23.3%	<0.0001
Surface ratio of high attenuation voxels to total surface	0. 848	16.7%	<0.0001
Mean plaque attenuation	0. 754	5.1%	0.0002
Mean plaque burden	0. 709	4.6%	0.0009
Lesion volume	0. 668	-	-

AUC values of averaged ROC curves shown in Figure 42 are presented with the corresponding proportion of additional cases classified correctly by the given parameter compared with the reference lesion volume. *P* values indicate the statistical significance of the increased diagnostic accuracy compared with lesion volume. AUC indicates area under the curve; and ROC, receiver-operating characteristic.

parameters are highly correlated with each other (represented by the red areas in Figure 41), but only have minimal relationship with other radiomic features (represented by the black areas in Figure 41). Cluster analysis revealed that the optimal number of clusters among radiomic features in our dataset is 44. Five-fold cross-validation using 10,000 repeats was used to simulate the discriminatory power of the three best radiomic and conventional parameter. Average ROC curves of the cross-validated results are shown in *figure 42*. Radiomic parameters had higher AUC values (as compared to conventional quantitative features and identified lesions showing the NRS significantly better as compared to conventional metrics. Detailed results are shown in table 26.

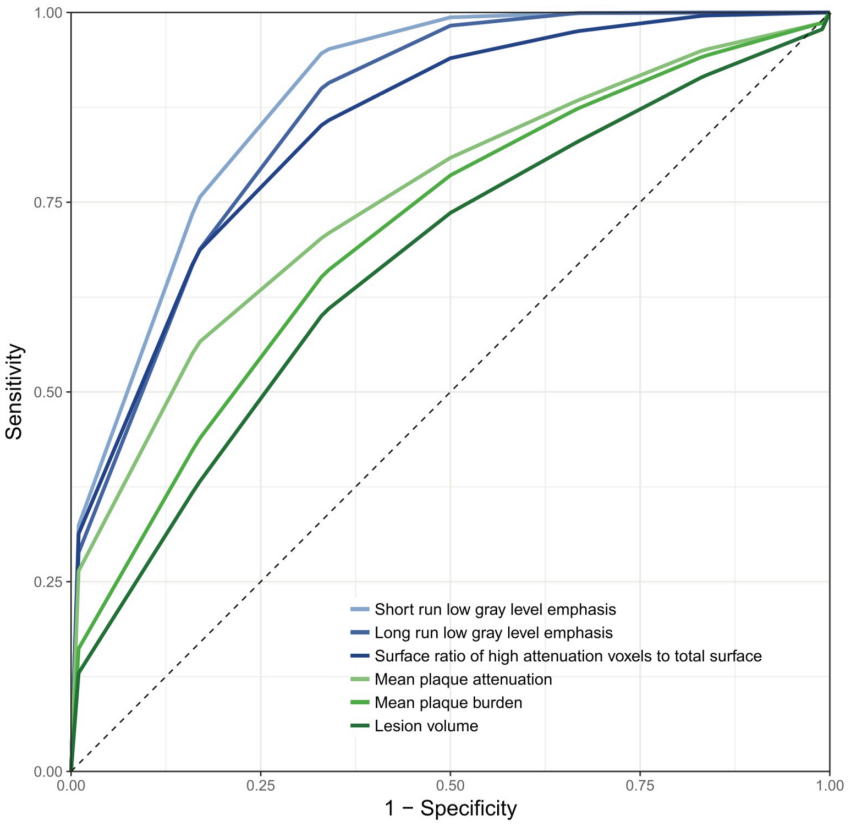

Figure 42 | Stratified 5-fold cross-validated receiver-operating characteristic (ROC) curves of the best radiomic and conventional quantitative parameters. Radiomic parameters (blue) have higher discriminatory power to identify plaques with napkin-ring sign compared with conventional quantitative metrics (green). Detailed performance measures can be found in Table 27.

5.2.6 Diagnostic performance of on-site FFR-CT

Overall, we enrolled 44 patients with 60 lesions.[285] The mean Agatston-score of the patients was: 268 [IQR: 92-834]. There were no left main or ostial stenoses, 68 % of lesions were present in the LAD, 17% in the LCX and 15% RCA. In 5 patients (11%) the vessel demonstrated tandem lesions. The mean EDS was 43.6±16.9%. The average time taken to generate the automatic lumen segmentation of the entire tree was 20 seconds. The lumen segmentation and manual adjustment was performed in 9 minutes, (range: 3-25 min).

Following the review and corrections to the lumen segmentation, the FFR-CT simulation was performed in 5 seconds. The mean on-site FFR-CT value was 0.77±0.15. Bland-Altman plot (Figure 43) revealed that FFR-CT underestimates invasive FFR values by 0.07 ($p<0.001$). Regression of the differences on the average of the 2 methods revealed, that the bias is proportional to the FFR values. Lower FFR values have higher bias, while higher values have lower bias (Standardized $\beta = -0.48$; $p< 0.001$). The ratio of true positive FFR-CT was 32% (19/60 lesions), true negative 47% (28/60 lesions), false positive 18% (11/60 lesions) and false negative 3% (2/60 lesions) (Figure 44). The FFR-CT and EDS values of the true positive patients were 60.7±0.14 and 47.3±14.8%, true negatives 88.4±0.05 and 32.9±12.6%, false positives 70.5±0.1 and 36.6±13,4% and false negatives 84.0±0.05 and 39.5±14.8%, respectively. FFR-CT with a threshold of ≤0.80 showed a high AUC value (0.89 [CI: 0.79-0.96]) with sensitivity of 91%, specificity 72%, positive predictive value 63%, negative predictive value 93% and an accuracy of 78%, while EDS with a ≥50% cut-off showed a moderate AUC value (0.74 [CI: 0.58-0.87]) with a sensitivity of 52%, specificity 87%, positive predictive value 69% and negative predictive value of 77%. On-site FFR-CT demonstrated significantly better

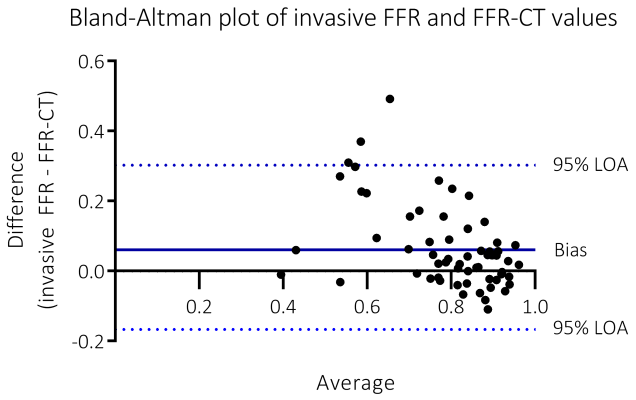

Figure 43 | We compared invasive FFR values with CT-FFR values using a Bland-Altman plot. A bias of 0.07 ($p <0.001$) was found between CT-FFR and invasive FFR values. 95% LOA = 95% limits of agreement; CT- FFR = computed tomography-derived fractional flow reserve; FFR = fractional flow reserve.

diagnostic performance as compared to EDS based assessment (AUC: 0.89 vs. 0.74 respectively; p<0.001). Importantly, the performance of the algorithm was not significantly affected by high calcium scores (defined as Agatston score ≥400). For patients with a calcium score <400 (n=27 lesions) we obtained a sensitivity of 75%, specificity 84%, positive predictive value 68%, negative predictive value 90%, accuracy 81% and an AUC of 0.90, while for patients with calcium score ≥400 (n=28 lesions) the sensitivity was 100%, specificity 69%, positive predictive value 71%, negative predictive value 100%, accuracy 83% and the AUC value was 0.88 (p = 0.87).

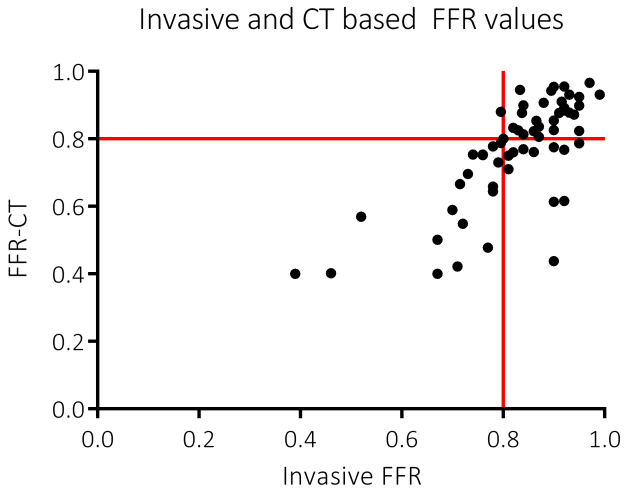

Figure 44 | Scatter plot analysis of invasive FFR and FFR-CT values. We demonstrated a significant correlation between FFR-CT and invasive FFR values (r = 0.73). Overall, 32% (19 of 60) of the lesions were true positive, 47% (28 of 60) true negative, 18% (11 of 60) false positive, and 3% (2 of 60) false negative. FFR-CT = computed tomography-derived fractional flow reserve; FFR = fractional flow reserve.

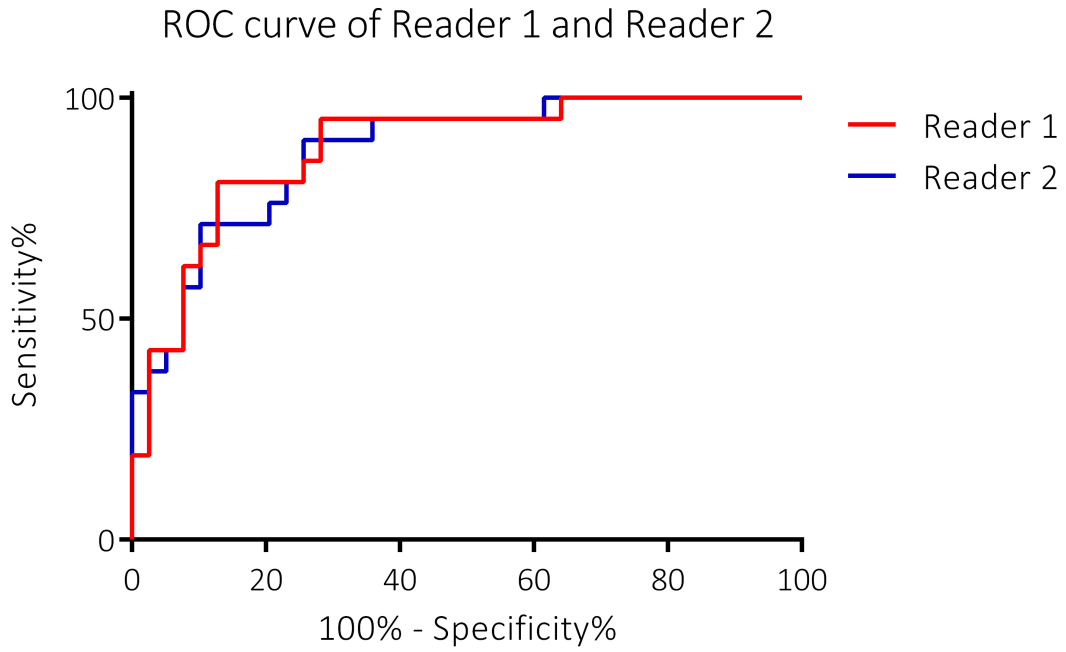

Figure 45 | ROC curve of reader 1 and reader 2. We detected no significant difference between primary and secondary readers' segmentation-based di- agnostic performance values, AUC 0.89 versus 0.88, respectively, p = 0.60. AUC = area under curve; ROC = receiver operating characteristic.

Intra-reader reliability revealed excellent reproducibility for FFR-CT values (ICC=0.95). There was no significant difference between the AUC values calculated based on the primary reader's first and second segmentations (AUC: 0.89 vs. 0.88, respectively; p=0.54). Inter-reader analysis revealed excellent reproducibility for FFR-CT values (ICC=0.90). We found no significant difference between the diagnostic performance values when calculated based on the primary readers' segmentations compared to the secondary readers' segmentations (AUC: 0.89 vs. 0.88, respectively; p=0.74) (Figure 45).

5.3 Findings regarding epicardial adipose tissue compartment

5.3.1 Intrathoracic fat, biomarkers and coronary Plaques

The demographic characteristics of the 342 patients are described in Table 27. Patients with coronary plaque were predominately male and had an increased rate of cardiovascular risk factors such as hypertension, dyslipidemia, and smoking compared to those without CAD, all

Table 27 Patient characteristics of the overall cohort and of subjects with versus without CAD

	Overall Cohort n=342	No Plaque n=173	Plaque n=169	p value
Demographics				
Age, years (±SD)	52.5±11.5	47.6±9.5	57.6±10.4	< 0.0001
Male (%)	210 (61%)	94 (54%)	116 (69%)	0.008
White Race (%)	294 (86%)	143 (83%)	151 (89%)	0.09
BMI, kg/m^2 (±SD)	29.1±5.9	28.7±6.0	29.5±5.7	0.18
Risk factors				
Diabetes (%)	35 (10%)	12 (7%)	23 (14%)	0.05
Hypertension (%)	133 (39%)	44 (25%)	89 (53%)	< 0.0001
Dyslipidemia (%)	128 (37%)	40 (23%)	88 (52%)	< 0.0001
Smoking (%)	171 (50%)	72 (42%)	99 (59%)	0.002
FH of CAD (%)	85 (25%)	37 (21%)	48 (28%)	0.17
Medication				
Aspirin (%)	108 (32%)	46 (27%)	62 (37%)	0.05
Statins (%)	99 (29%)	31 (18%)	68 (40%)	< 0.01
Biomarkers				
hsCRP (IQR)	1.4 (0.6-2.9)	1.1 (0.5-2.4)	1.7 (0.9-3.4)	0.0004
TNFα (IQR)	1.1 (0.7-1.9)	1.0 (0.6-1.8)	1.1 (0.8-2.1)	0.24
PAI-1 (IQR)	12.3 (6.1-24.0)	11.8 (5.6-24.1)	13.1 (7.1-23.7)	0.22
Adiponectin (IQR)	4.9 (2.9-7.7)	4.9 (3.1-7.9)	4.8 (2.6-7.4)	0.33
MCP-1 (IQR)	248.5 (181.0-348.0)	248.0 (178.0-316.0)	252.0 (183.0-367.0)	0.34
Fat Measures in cm^3				
Pericoronary (±SD)	29.9±17.1	24.0±12.9	35.7±18.8	< 0.0001
Epicardial* (±SD)	74.4±37.3	63.5±31.4	85.5 ±39.6	< 0.0001
Periaortic (±SD)	15.5±9.0	12.3±6.7	18.7±10.0	< 0.0001
Extracardiac*(±SD)	99.9±63.2	83.3±59.2	117.0±62.7	< 0.0001

CAD denotes coronary artery disease; SD, standard deviation; BMI, body mass index; FH, family history; IQR, interquartile range; CRP, C-reactive protein; TNFα, tumor necrosis factor alpha; PAI-1, plasminogen activator inhibitor-1; MCP-1, monocyte chemoattractant protein-1. *Epicardial fat compartment excluded pericoronary fat. Extracardiac fat compartment is defined as the thoracic fat volume without epicardial or periaortic fat.

p values p≤0.01.[289] There was no significant difference in race, BMI, prevalence of diabetes, or family history of premature CAD between patients with and without CAD. Table 28 demonstrates that all four fat depots were highly correlated with each other and showed a modest positive correlation with BMI. The largest adipose tissue depot, extracardiac fat (volume 99.9±63.2 cm^3), was most strongly correlated with BMI, (r=0.45, p<0.001). The pericoronary fat depot

Table 28 Correlation among fat measures and body mass index (BMI)

	BMI	Pericoronary	Epicardial	Periaortic	Extracardiac
BMI	-	0.21	0.44	0.44	0.45
Pericoronary	0.21	-	0.70	0.54	0.49
Epicardial	0.44	0.67	-	0.69	0.70
Periaortic	0.44	0.54	0.69	-	0.75
Extracardiac	0.45	0.49	0.70	0.75	-

All p<0.0001.

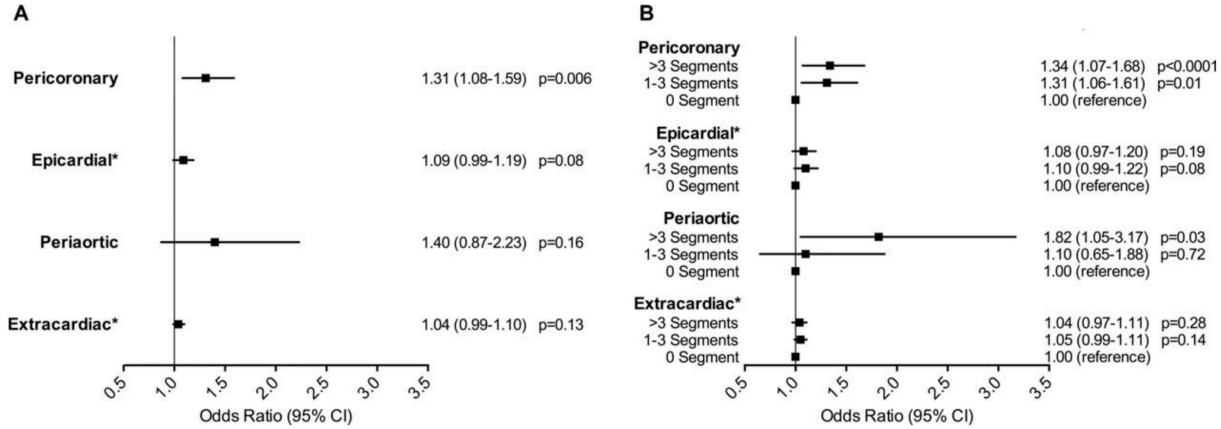

Figure 46 | The relationship of thoracic adipose tissue volumes (per 10 cm^3 increase) to (A) the presence of coronary atherosclerotic plaque and (B) the extent of atherosclerotic plaque by number of coronary segments B. Adjusted for age, gender, diabetes, hypertension, dyslipidemia, smoking, BMI, aspirin use, and statin use. *Epicardial fat compartment excluded pericoronary fat. Extracardiac fat compartment is defined as the thoracic fat volume without epicardial or periaortic fat. CI, confidence interval.

(volume 29.9±17.1 cm^3) was least correlated to BMI (r=0.21, p<0.001). Despite no difference in BMI (p=0.18), patients with coronary plaque had higher volumes of all fat depots as compared to patients without plaque (all p<0.01). We used logistic regression to determine the

Table 29 Relationship of pericoronary fat volume to presence of any plaque on a per patient basis per 10 cm^3 increase in fat volume

	Unadjusted OR (95% CI)	p-value	Adjusted OR (95% CI) [a]	p-value
Pericoronary	1.66 (1.41-1.97)	< 0.0001	1.31 (1.08-1.59)	0.006
Epicardial	1.21 (1.12-1.29)	< 0.0001	1.09 (0.99-1.19)	0.08
Periaortic	2.74 (1.98-3.78)	< 0.0001	1.40 (0.87-2.23)	0.16
Extracardiac	1.10 (1.06-1.15)	< 0.0001	1.04 (0.99-1.10)	0.13

OR, odds ratio; CI, confidence interval.
[a]Adjusted for age, gender, diabetes, hypertension, dyslipidemia, smoking, BMI, aspirin use, statin use.

Table 30 Relationship of adipose tissue volume (per 10 cm^3 increase) to extent of plaque by number of segments

	Unadjusted				Adjusted[1]			
	1-3 Segments vs. 0 Segment		>3 Segments vs. 0 Segment		1-3 Segments vs. 0 Segment		>3 Segments vs. 0 Segment	
	OR (95% CI)	p-value	OR (95% CI)	p-value	OR (95% CI)	p-value	OR (95% CI)	p-value
Pericoronary	1.57 (1.31-1.89)	<0.0001	1.76 (1.46-2.12)	<0.0001	1.31 (1.06-1.61)	0.01	1.34 (1.07-1.68)	<0.0001
Epicardial	1.18 (1.09-1.28)	<0.0001	1.23 (1.14-1.34)	<0.0001	1.10 (0.99-1.22)	0.08	1.08 (0.97-1.20)	0.19
Periaortic	2.04 (1.41-2.96)	0.0002	3.69 (2.53-5.38)	<0.0001	1.10 (0.65-1.88)	0.72	1.82 (1.05-3.17)	0.03
Extracardiac	1.09 (1.04-1.14)	0.0003	1.11 (1.06-1.17)	<0.0001	1.05 (0.99-1.11)	0.14	1.04 (0.97-1.11)	0.28

OR, odds ratio; CI, confidence interval.
[1]Adjusted for age, gender, diabetes, hypertension, dyslipidemia, smoking, BMI, aspirin use, statin use.

association between fat depots and the presence of plaque on a per patient basis. All four fat depots were associated with the presence of any coronary artery plaque in unadjusted analysis, all $p<0.001$ (Table 29). In adjusted analyses only pericoronary fat were found to be independently associated to the presence of coronary artery plaque ($p=0.006$), while epicardial, periaortic and extracardiac fat depots were not (all $p\geq0.08$), Figure 46A. We examined the association between the four fat depots to the extent of plaque and found that pericoronary fat remained associated in adjusted analysis in patients with at least one segment of plaque as compared to those without plaque, irrespective of amount of plaque burden (Figure 46B and Table 30). In addition, periaortic fat showed an association with CAD that affects more than 3 segments of the coronaries ($p=0.03$). We also examined the correlation between the various fat depots and markers of inflammation independent of CAD. Table 31 demonstrates that the circulating hsCRP and PAI-1 levels showed a modest positive correlation with all fat depots (all $p\leq0.003$). Whereas, TNFα level showed a modest positive correlation only with the perivascular fat depots, such as the pericoronary and periaortic fat compartments ($p<0.0001$ and $p=0.02$, respectively). MCP-1 correlated with the fat compartments closest to the heart, pericoronary and epicardial fat compartments ($p<0.0001$ and $p=0.006$, respectively). On the other hand, adiponectin was not associated with the pericoronary fat depot. However, it showed a modest negative correlation with epicardial ($p=0.001$), periaortic ($p<0.0001$) and extracardiac ($p<0.000$) fat compartments.

Table 31 Partial correlation among biomarkers and various adiopose tissue depots with P-values adjusted for the presence of coronary artery plaque

	Pericoronary	Epicardial	Periaortic	Extracardiac
hsCRP	0.21 0.0002	0.22 <0.0001	0.29 <0.0001	0.21 0.0003
TNFα	0.25 <0.0001	0.10 0.07	0.132 0.02	0.07 0.21
PAI-1	0.22 <0.0001	0.27 <0.0001	0.20 0.0003	0.24 <0.0001
Adiponectin	-0.03 0.60	-0.15 0.001	-0.28 <0.0001	-0.27 <0.0001
MCP-1	0.30 <0.0001	0.16 0.006	0.08 0.14	0.09 0.14

5.3.2 Heritability of epicardial adipose tissue quantity

Overall, 180 twins (57 MZ twin pairs, 33 DZ twin pairs) were included from the BUDAPEST-GLOBAL study.[294] Our study population represents a middle-aged, slightly overweight Caucasian population (Table 32).

Table 32 Demographics, clinical-laboratory data and quantity of fat compartments measured in twins

Variables	Total *n = 180*	MZ *n = 114*	DZ *n = 66*	*p*
Demographic, basic hemodynamic characteristics and medical history				
Female (n, %)	114 (63.3%)	68 (59.6%)	46 (69.7%)	0.52
Age (years)	55.8 ± 9.6	54.3 ± 9.7	58.4 ± 8.6	<0.01
Height (cm)	166.4 ± 9.6	166.7 ± 10.1	165.9 ± 8.8	0.63
Weight (kg)	77.2 ± 17.5	77.6 ± 18.3	76.4 ± 16.2	0.67
BMI (kg/m^2)	27.7 ± 5.2	27.7 ± 5.1	27.8 ± 5.4	0.98
Waist (cm)	96.9 ± 14.2	96.8 ± 14.6	96.9 ± 13.6	0.96
Hypertension (n, %)	76 (42.2%)	42 (36.8%)	34 (51.5%)	0.84
Diabetes mellitus (n, %)	15 (8.3%)	9 (7.9%)	6 (9.1%)	0.89
Dyslipidemia (n, %)	80 (44.4%)	46 (40.4%)	34 (51.5%)	0.48
Current smoker (n, %)	28 (15.6%)	17 (14.9%)	11 (16.7%)	0.88
Laboratory parameters				
Fasting blood glucose (mmol/L)	5.35 ± 1.34	5.31 ± 1.48	5.41 ± 1.06	0.66
HbA1c (%)	5.5 ± 0.9	5.5 ± 0.9	5.3 ± 0.9	0.13
Serum total cholesterol (mmol/L)	5.56 ± 1.09	5.63 ± 1.11	5.42 ± 1.07	0.21
Serum LDL-cholesterol (mmol/L)	3.47 ± 0.99	3.52 ± 1.04	3.37 ± 0.89	0.32
Serum HDL-cholesterol (mmol/L)	1.62 ± 0.39	1.61 ± 0.41	1.65 ± 0.35	0.56
Triglycerides (mmol/L)	1.57 ± 1.09	1.62 ± 1.23	1.47 ± 0.77	0.36
Serum creatinine (µmol/L)	80.0 ± 9.0	80.0 ± 9.0	80.0 ± 9.0	0.41
Serum CRP (mg/L)	2.9 ± 4.5	2.7 ± 2.9	3.3 ± 6.5	0.37
Serum leptin (ng/mL)	18.4 ± 17.9	16.2 ± 13.5	22.4 ± 23.6	0.06
CT-based fat measurements				
Epicardial fat (mm^3)	97.1 ± 45.4	94.9 ± 43.2	101.0 ± 49.2	0.38
Subcutaneous fat (mm^2)	217.9 ± 97.4	218.6 ± 90.1	216.7 ± 109.4	0.90
Visceral fat (mm^2)	156.6 ± 87.9	158.9 ± 89.2	152.6 ± 86.0	0.64

Abbreviations: BMI, body mass index; CRP, C-reactive protein; CT, computed tomography; DZ, dizygotic; HbA1c, hemoglobinA1c; HDL, high-density lipoprotein; LDL, low-density lipoprotein; MZ, monozygotic. Continuous variables are presented as mean ± s.d., whereas categorical as n (%). P-values represent two-sided P-values for independent t-tests done between the MZ and DZ twin groups.

Intra-reader agreement showed excellent reproducibility for all CT based fat measurements (ICC_{EAT} = 0.99; ICC_{SAT} = 0.98; ICC_{VAT} = 0.99). We also found excellent reproducibility regarding inter-reader variability (ICC_{EAT} = 0.98; ICC_{SAT} = 0.99; ICC_{VAT} = 0.99). Co-twin correlations between the siblings showed that for all three parameters, MZ twins have stronger correlations than DZ twins, suggesting prominent genetic effects (EAT: r_{MZ} = 0.81, r_{DZ} = 0.32; SAT: r_{MZ} = 0.80, r_{DZ} = 0.68; VAT: r_{MZ} = 0.79, r_{DZ} = 0.48).

For all three fat compartments AE model excluding common environmental factors proved to be best fitting [EAT: A: 73% (95% CI = 56%-83%), E: 27% (95% CI = 16-44%); SAT: A: 77% (95% CI = 64%-85%), E: 23% (95% CI = 15%-35%); VAT: 56% (95% CI = 35%-71%), E: 44% (95% CI = 29%-65%)].

In multi-trait model fitting analysis, overall contribution of genetic factors to EAT, SAT and VAT was 80%, 78% and 70%, whereas that of environmental factors

Table 33 Proportion of common and specific genetic and environmental factors contributing to the phenotypic quantity of computed tomography-based fat measurements

Variable	Epicardial fat	Subcutaneous fat	Visceral fat
Common genetic and environmental factors			
genetic factors (A_C)	35%	18%	70%
environmental factors (E_C)	14%	8%	28%
Specific genetic and environmental factors			
genetic factors (A_S)	45%	60%	0%
environmental factors (E_S)	6%	14%	2%
Overall contribution of genetic and environmental factors			
genetic factors (A)	80%	78%	70%
environmental factors (E)	20%	22%	30%

was 20%, 22% and 30%, respectively (Table 33). Results of the multi-variate analysis suggest that a common latent phenotype is associated with the tissue compartments investigated. Based on our results, 98% (95% CI = 77%-100%) of VAT heritability can be accounted by this common latent phenotype which also effects SAT and EAT heritability. This common latent phenotype accounts for 26% (95% CI = 13%-42%) of SAT and 49% (95% CI = 32%-72%) of EAT heritability. This common latent phenotype is influenced by genetics in 71% (95% CI = 54%-81%) and environmental effects in 29% (95% CI = 19%-46%). Accordingly, the proportion of common and specific genetic and environmental factors contributing to the adipose tissue quantities may differ from each other, for example in case of EAT heritability is caused by 35% common genetic, 45% specific genetic, 14% common environmental, and 6% specific environmental factors. The path diagram of the model is illustrated by Figure 47, and detailed contribution of common and specific genetic and environmental factors for all three fat compartments can be found in Table 33. In addition, our results suggest that none of the phenotypes are independent of the other two (Table 34), thus the heritability of EAT or SAT or VAT phenotype is associated with the remaining two phenotypes.

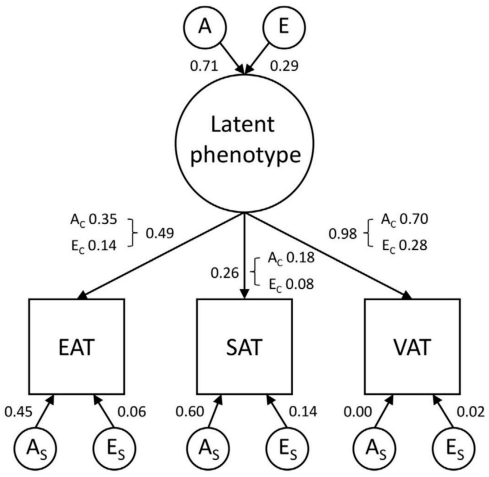

Figure 47 | Proportion of phenotypic variance of CT-based fat measurements. Image shows squared standardized path coefficients of best fitting model 5. The common pathway model calculating with only common genetic and environmental factors proved to be the best. Residual variances were decomposed to specific genetic and environmental factors. In case of VAT only specific environmental factors were considered. A_C, common additive genetic factor; A_S, specific additive genetic factor; EAT, epicardial adipose tissue; E_C, common environmental factor; E_S, specific environmental factor; SAT, subcutaneous adipose tissue; VAT, visceral adipose tissue.

Table 34 Detailed model information regarding multi-trait classical twin models of CT-based fat measurements

Model number	Model name	Estimated parameters	Model *-2LL*	Model *df*	AIC	BIC	Difference to Saturated model *-2LL*	Difference to Saturated model *df*	Difference to Saturated model *p*	Difference to Full model *-2LL*	Difference to Full model *-df*	Difference to Full model *p*
1	Cholesky ACE	24	1047.78	516	15.78	-1274.12	31.38	30	0.40			
2	Cholesky AE	18	1050.47	522	6.47	-1298.43	34.08	36	0.56	2.69	6	0.85
3	Independent pathway AE	18	1050.54	522	6.54	-1298.36	34.15	36	0.56	2.76	6	0.84
4	Common pathway AE 1	17	1052.57	524	4.57	-1305.33	36.18	38	0.55	4.79	8	0.78
5	Common pathway AE 2	16	1052.57	525	2.57	-1309.83	36.18	39	0.60	4.79	9	0.85
6	Common pathway AE SAT-VAT	16	1189.06	525	139.06	-1173.34	172.67	39	$9.66*10^{19}$	141.28	9	$5.61*10^{-26}$
7	Common pathway AE VAT-EAT	16	1110.53	525	60.53	-1251.86	94.14	39	$1.86*10^{6}$	62.75	9	$3.94*10^{-10}$
8	Common pathway AE SAT-EAT	16	1219.96	525	169.95	-1142.44	203.57	39	$3.81*10^{24}$	172.18	9	$2.17*10^{-32}$

Abbreviations: − 2LL, minus 2log-likelihood value; AIC, Akaike information criterion; BIC, Bayesian information criterion; CT, computed tomography; df, degrees of freedom; EAT, epicardial adipose tissue; SAT, subcutaneous adipose tissue; VAT, visceral adipose tissue. Detailed results of calculated multi-trait structure equation models

5.4 Results on structured clinical reporting performance

5.4.1 Structured reporting

In total, 500 consecutive coronary CTAs were included in the analysis (mean age 59.6 ± 12.5 years, 42.0% female gender and mean BMI 28.5 ± 5.0 kg/m^2). Patient characteristics and imaging parameters are summarized in Table 35. We detected a total agreement between manual and automated CAD-RADS classification in 80.2 % of the cases. The agreement in

Table 35 Patient characteristics

	Study population (n=500)
Demographics	
Age (years)	59.6 ± 12.5
Female gender, n (%)	210 (42.0)
BMI (kg/m^2)	28.5 ± 5.0
Blood pressure (Hgmm)	145 ± 19.7
Diamond-Forrester pretest probability	
Very low	28 (5.6)
Low	66 (13.2)
Intermediate	389 (77.8)
High	17 (3.4)
Cardiovascular risk factors, n (%)	
Hypertension	301 (60.2)
Diabetes mellitus	97 (19.4)
Dyslipidemia	207 (41.4)
Current smoker	77 (15.4)
Family history of premature CAD	144 (28.8)
Type of chest pain, n (%)	
Typical	24 (4.8)
Atypical	147 (29.4)
Aspecific	329 (65.8)
Imaging parameters	
DLP (mGy*cm) / effective dose (mSv)	358.4 ± 142 / 5.0 ± 2.0
Contrast agent (ml)	92.5 ± 10.8
Heart rate during scan (1/min)	62.1 ± 13.8
Use of Beta-Blockade, n(%)	368 (73.6)
Use of nitroglycerine, n(%)	494 (98.8)
Agatston score	205 ± 614
SSS	4.0 [1.0 to 9.0]
SIS	3 [1.0 to 5.0]

stenosis categories was 86.8%. In addition, we investigated the agreement in modifiers with the following results: 95.6% for V, 95.8% for N, 96.8% for S, and 99.4% for G. Distribution of modifiers was N: 15.0% vs 17.2%, S: 6.0% vs 9.2%, V: 11.8% vs 15.4%, G: 1.8% vs 2.4%, for manual vs automated, respectively ($p<0.05$ for N, S, V and $p=0.25$ for G).

Readers forgot to assign S in 34.8 % of all patients who had at least one stent, N in 12.8 % of studies with non-diagnostic coronary segments, V in 23.4% of patients with vulnerable plaques and G in 25.0 % among patients with bypass grafts. Importantly, 4.6% of all cases were falsely classified by the readers into non-existing CAD-RADS categories that included 0/N, 1/N 2/N and the stenosis category 4 without assigning A or B (Figure 48). Details of CAD-RADS assessment for stenosis categories and modifiers are shown in Table 36, whereas most common mistakes are summarized in Table 37. Stenosis of 4B (indicating the presence of left main stenosis greater than 50% or three-vessel obstructive CAD) was misclassified in four cases to 4A (0.8%). Discrepancy between the manual and automated classification could have led to changes in patient management recommendations in 13.2% of cases and 15.6% of cases when including discrepancy of the modifier V.

Table 36 Distribution of CAD-RADS based on manual versus automated classification.

	Manual	**Automated**	**p value**
Stenosis, (n, %)			0.008
0	87 (17.4)	90 (18.0)	
1	122 (24.4)	114 (22.8)	
2	100 (20.0)	93 (18.6)	
3	58 (11.6)	61 (12.2)	
4A	32 (6.4)	49 (9.8)	
4B	3 (0.6)	5 (1.0)	
5	19 (3.8)	25 (5.0)	
Non-existing	23 (4.6)	0 (0.0)	
N, (n, %)	75 (15.0)	86 (17.2)	0.027
S, (n, %)	30 (6.0)	46 (9.2)	<0.001
V, (n, %)	59 (11.8)	77 (15.4)	0.001
G, (n, %)	9 (1.8)	12 (2.4)	0.250

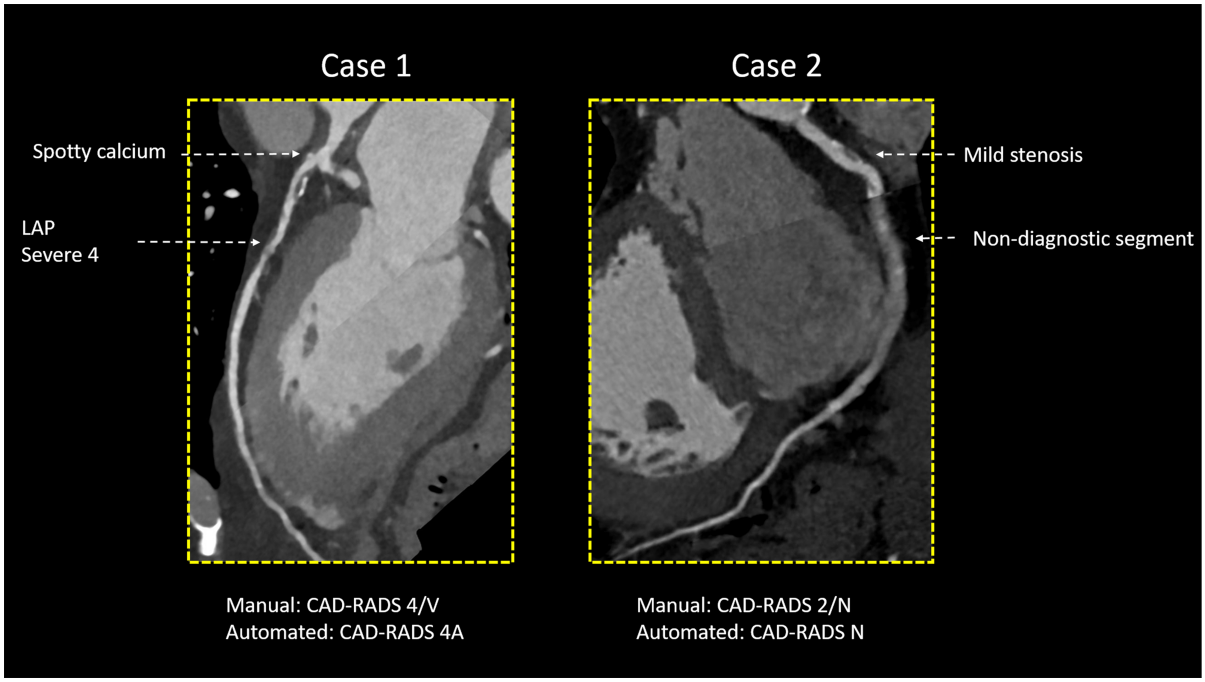

Figure 48 | Pitfalls in CAD-RADS classification that might lead to reporting inconsistency and altered patient management. On the left panel, case 1 is a representative example for plaque vulnerability assessment in CAD-RADS. The reader misclassified this case and assigned V (Vulnerability), although high-risk plaque features were present in two clearly distinct plaques along the proximal and mid segment of the left anterior descending artery (LAD). The CAD-RADS classification requires minimum two high-risk plaque features to be present in a single lesion to apply modifier V. Also, reader forgot to assign A or B to describe lesion severity. Severe lesion in the LAD was marked as 4/V by the reader, whereas the automated tool correctly assigned a CAD-RADS score 4A. The right panel represents another common mistake in classification (case 2). A predominantly non-calcified plaque leading to a mild stenosis was detected in the proximal right coronary artery (RCA), followed by a step artifact and severe motion artifacts on the mid-RCA. Reader assigned a non- existing category (2/N), whereas the automated tool correctly assigned N without stating the stenosis grade.

We detected significantly higher agreement of the modifier "V" after the individual training (first vs. second 50 cases, p=0.047). The agreement of other modifiers and stenosis categories did not show any significant improvement (p>0.05 for all). Time of the day and clinical load (as assessed by ≥5 reports on a given day) did not significantly influence reader's performance (p>0.05 for all). Less experienced readers (1-year experience in coronary CTA) had a higher total agreement with the automated classification as compared to more experienced readers (6 years' experience in coronary CTA) 87.0 % vs 78.0 %, respectively (p=0.011). Also, non-existing CAD-RADS categories were more frequent among more experienced readers as compared to the less experienced clinicians (6.3% vs 2.0%, respectively, p=0.02).

6 Discussion

6.1 Cardiac CT image quality

We have performed two randomized, single-center clinical trials to assess the efficacy of esmolol and to test the efficiency of a novel iodinated-contrast agent injection protocol. We have conducted two additional prospective studies to test the effect of iterative image reconstruction in plaque volumes and to investigate the image quality of coronary CTA in HTX patients.

In our first clinical trial we compared IV esmolol versus IV metoprolol for HR control in patients who underwent coronary CTA because of suspected coronary artery disease. We showed that esmolol with a stepwise bolus administration protocol is at least as efficacious as the standard of care metoprolol to achieve the optimal HR (<65 beats/min) during coronary CTA. Furthermore, we have demonstrated that IV esmolol allows a safe HR control for coronary CTA examination even if it is administered in high doses with a dosage scheme independent of body weight. Esmolol is an ultrashort-acting intravenous β-blocker.

The rapid onset and offset of effects of esmolol make this intravenous drug a potential alternative of the standard of care metoprolol in the daily routine coronary CTA service. Especially, coronary CTA services with no access to cardiology or intensive care background might benefit most of this ultrashort-acting medication. The recommended administration protocol of IV esmolol with infusion pump is relatively complex and precluded its widespread use in the diagnostic facilities. Different dosage schedules have been developed depending on clinical setting and diagnosis. Generally, a loading dose of <500 μg/kg/min over 1 minute is administered followed by a continuous infusion of 25–300 μg/kg/min.[246] We showed that esmolol is safe and efficacious if administered in boli without the subsequent continuous infusion. The “bolus only” administration protocol of esmolol would make this IV β-blocker a real-life alternative of IV metoprolol. In this clinical trial we used a body weight-independent administration protocol with stepwise increments in dose in every 3 minutes. Importantly, the timing of the administration of the IV esmolol boli was similar to the metoprolol administration protocol; therefore, it did not slow down our routine clinical cardiac CT workflow. Our choice of 100-mg IV esmolol for the initial bolus is based on a previous observational study that showed that the dose of 2 mg/kg (for a 70-kg patient this equals 140-mg esmolol) is safe to administer before the coronary CTA examination.[247] If 100-mg dose proved to be ineffective,

thus the patient's HR did not reach the predefined ≤65 beats/min in 3 minutes, we have increased the bolus to 200-mg IV esmolol. Finally, if the HR did not change after an additional 3-minute period (testing during a Valsalva maneuver as well), we administered the third, once again 200-mg, bolus of IV esmolol. We have not added further boluses; thus, the maximum administered IV esmolol was 500 mg during an approximately 6- to 7-minutes time period. Of note, only about one-third of patients have received the full dose of esmolol and two-thirds of patients have reached the target HR with ≤300-mg esmolol dose. We have stopped the patient enrollment early as the interim analysis indicated that esmolol is clearly noninferior to metoprolol; in fact, it showed superiority characteristics as the responder proportion in the esmolol group was 89% vs the metoprolol group's 78%.

Degertekin at al. demonstrated the safety and efficacy of IV esmolol in 391 patients.[247] In this prospective study, HR was reduced from 80±11 beats/min to 63±7 beats/min and HR <65 beats/min was achieved in 65% of the patients. Four of the 391 patients (1%) have experienced a final HR of <50 beats/min; however, all 4 remained asymptomatic and the bradycardia resolved in minutes without any intervention with atropine or temporary pacing. Moreover, Degertekin et al. reported a 0.5% incidence of transient hypotension (systolic BP <100 mm Hg).[247] In our clinical trial, we have reached a higher responder proportion (89.2%) probably because of a more aggressive dosing scheme. Importantly, none of the 204 patients who received esmolol had severe bradycardia (minimum HR was 53 beats/min). On the other hand, transient hypotension (systolic BP <100 mm Hg) was observed in 9.3% of the patients immediately after the scan in the esmolol group, which was significantly higher compared to the metoprolol group's 3.8%. Importantly, 30 minutes after the scan this decreased to 2.5% in the esmolol group, whereas in the metoprolol group the percentage of patients with hypotension did not change (3.8%).

None of the patients had clinically significant adverse event. Thus, the stepwise bolus administration of esmolol is safe and it is well tolerated among patients with normal left ventricular function scheduled to undergo coronary CTA examination. Furthermore, our data show that IV esmolol is at least as efficacious as IV metoprolol to reach optimal HR during coronary CTA. Many centers are reluctant to administer IV medication for HR control during coronary CTA owing to the fear from potential side effects. A recent study by Kassamali et al. reported minor complications (transient hypotension) related to IV metoprolol administration only in 1.47% and major complications (not resolving with observation of analgesia) in 0.44% of patients who underwent coronary CTA.[299] These results demonstrate that IV metoprolol is a safe drug to use for this purpose in patients with normal left ventricular function although the

study was underpowered to assess for rare major complications. Esmolol is metabolized via rapid hydrolysis by red blood cell esterases, independent of the hepatic and renal function.[300] It is routinely administered during perioperative intensive care and before laryngoscopy and tracheal intubation procedures to prevent hypertension and tachycardia.[301,302] In this clinical trial, we have excluded patients with contraindications to β-blockers such as asthma. However, it has been demonstrated previously that esmolol is safe in bronchospastic diseases.[303]

There are some limitations of our study we have to consider. This is a single-center study; therefore, the efficacy and safety of the described esmolol bolus protocol has to be evaluated in a multi-center randomized controlled trial. As the administration protocols and the injected volumes were different for the IV metoprolol and IV esmolol groups, it was not feasible to blind the physicians to the drug they were administering. The combined use of oral and IV β-blocker protocols for HR control might limit the generalizability of our results for IV-only protocols. Owing to the oral metoprolol pretreatment, our findings do not demonstrate that esmolol IV alone vs metoprolol IV is as or more effective for HR control. However, it is important to note that the combined use of oral and IV β-blockers is a widely used and effective strategy for HR lowering before coronary CTA.[23,304] In this scenario, esmolol is at least as efficacious as IV metoprolol. The response rate to oral metoprolol was relatively low in our study (162 of 574 [28%]), which might have been higher with the use of a more aggressive administration regime (eg, 100-mg oral metoprolol if HR >65 beats/min).[246] Furthermore, we did not test smaller doses of esmolol (eg, 50–100 mg), which might be equally efficacious. Moreover, it is important to note that esmolol is more expensive than IV metoprolol. However, the effective and short duration of HR control achievable with esmolol might result in wider usage of this IV β-blocker in cardiac CT labors, which would increase the percentage of patients scanned with optimal HR and improve the diagnostic performance of CTA. A larger multicenter trial is warranted to adequately explore the cost-effectiveness of esmolol use in the coronary CTA laboratories.

In our next randomized clinical trial we have demonstrated that the novel four-phasic contrast injection protocol developed by us, resulted in a 65% reduction of the extravasation rate as compared to the conventionally used three-phasic CM injection-protocol in coronary CTA. The addition of a saline pacer bolus to the three-phasic CM injection-protocol is easy to implement at no additional cost. We found an overall extravasation rate of 0.9%, which is similar to that in the published literature (0.3–1.3%).[28-32]

Interestingly, from the comprehensive review of Cohan et al. published in 1996 through recent publications, the same range of extravasation rate is reported, which suggests that no

effective strategy is available to reduce the risk of CM extravasation.[29] To the best of our knowledge our study is the first to describe the four-phasic CM injection-protocol, in which a saline pacer bolus is added to the conventional three-phasic CM protocol to reduce the risk of extravasation. We detected a statistically significant difference between the three- and four-phasic group regarding contrast injection rates (5.5 ml/s: 91.2% (1,121/1,229) vs. 88.4% (1,075/1,216), respectively, p = 0.02); however, we did not find any difference in injection flow rates among patients with versus without extravasation (5.5 ml/s flow rate: 95.7% (22/23) vs. 89.8% (2,174/2,422), respectively, p = 0.72).

In a study by Federle et al., the effect of contrast bolus flow rate was evaluated in 5,106 patients who received CM for CTA examination, and they detected no correlation between extravasation and injection flow rate.[30] The mean CM injection flow rate was 2.8 ml/s (range 1-5 ml/s) and they observed an overall extravasation in 0.9% of the scans. Although the authors used low flow rates, they still experienced the same percentage of extravasation independent of the injection speed as we did in our study. This suggests that instead of the flow rate other characteristics, such as CM viscosity and collapsed vein wall, might play a role in extravasation.

We adjusted the CM injection rates according the tube voltage setting. In case of 120 kV we used a higher injection rate (5.5 ml/s) in order to achieve higher intracoronary attenuation. In case of 100 kV we used lower injection rates (4.5 ml/s), due to the increased iodine x-ray absorption at lower tube voltages. Davenport et al. assessed whether extrinsic warming of low- and high-osmolality CM affects the extravasation rate.[305] They could not detect any beneficial effect of preheating on low-osmolality CM extravasation rates (preheated: 0.30% (32/10,831), non-heated: 0.23% (23/10,064); p = 0.64); however, pre-heating of high-osmolality CM decreased extravasation rate as compared to non-heated (0.27% (5/1,851) vs. 0.87% (18/2,074), respectively; p = 0.05. Similar to these findings, in a prospective study of 4,457 patients iodine concentration and flow rate did not show any association with CM extravasation.[31] In these studies, besides the injection flow rate, the CM injection-protocol was not described in detail, rendering direct comparisons with our study difficult. Other studies have identified several risk factors of CM extravasation that are unrelated to CM administration protocols and are not modifiable. These risk factors are mainly associated with the fragility of the patients' vasculature, such as atherosclerosis, diabetes, chemo- or radiotherapy, and autoimmune diseases.[29,39] Female gender and elderly age (>60 years) were predictors of CM extravasation in a study by Shaquan et al.[37] Our results suggest that four-phasic protocol reduces extravasation rate independently of these risk factors.

Contrast media extravasation may cause severe complications due to the toxic effects

of iodinated CM on the perivascular tissues.[29,32] Furthermore, it may lead to repeated CTA exams with a consequently higher radiation dose, increased CM load and higher costs. Therefore, the reduction of CM extravasation is of importance. It seems that the beneficial effect of a four-phasic CM injection-protocol is due to the saline pacer bolus, which opens the vein before the high flow-rate CM injection and reduces the risk of vessel wall injury and extravasation, and reduces the risk of vessel wall injury and extravasation. Some state-of-the art power injectors offer 'keep vein open' functionality with an intravenous saline drip that is flowing just enough (e.g. 0.25 ml every 30 s) to keep the vein open for a longer time period and prevent coagulation or clot formation at the injection site. Intuitively, this technique might also reduce the risk of extravasation to some extent. However, it is unlikely that the slow drip of saline prevents extravasation as effectively as the saline pacer bolus described in our study, although this needs further investigation.

Furthermore, it is important to note that the four-phasic CM injection-protocol is vendor independent and can be programmed with all power injectors. It is important to note that with the introduction of novel CT technologies, the amount of CM needed to achieve diagnostic quality has markedly decreased. In a recently published study by Kim et al., CM volume usage in coronary CTA performed with 320-row CT could be decreased from 60 to 40 ml with preserved image quality and diagnostic accuracy.[306] In addition, Felmly et al. demonstrated that with the latest generation dual source CT a comprehensive transcatheter aortic valve replacement planning was feasible with reduced CM volumes.[307] In line with these findings, Mangold et al. demonstrated that the use of automated tube voltage selection and CM volume adjustment reduces CM volumes and provides excellent image quality and optimal intravascular attenuation.[308] The effect of novel CT technologies and reduced CM volumes on extravasation rate warrants further investigation. This study has some limitations, which should be acknowledged. First, this was a single-centre study, which might limit the generalizability of our results. We used a deterministic method for randomization, which involves open allocation based on odd and even weeks. This might potentially influence recruitment. However, in our study we enrolled all eligible patients, therefore the risk of selection bias is minimized. In addition, we did not perform a power calculation. However, during the 20-month study period we enrolled the maximum number of patients. Furthermore, we defined extravasation based on local symptoms and the inadequate CM enhancement in CTA images. To further objectivize extravasation events a dedicated extravasation monitor system or pressure monitoring would have been beneficial; however, at the time of the study this was not available at our site.

In our prospective observational study on image quality we demonstrated that IMR improves both qualitative and quantitative coronary CTA image quality parameters over HIR and FBP. We found IMR to improve CNR in the proximal, as well in the distal coronary artery segments. By quantitative coronary plaque assessment, we found a significant reduction in overall plaque volume and calcified plaque volume with the use of IMR as compared to HIR and FBP techniques. Interestingly, the image reconstruction technique did not influence non-calcified plaque volume, except for high-attenuation volume ranging 90-129 HU, which was reduced with IMR, but no difference was found between HIR and FBP.

To the best of our knowledge our study provides the first evidence for reduced calcified atherosclerotic plaque volumes in the coronaries as quantified with IMR and compared to HIR and FBP technique. Only a few studies evaluated the image quality of IMR for the evaluation of the coronary arteries in a clinical setting up until today.[309-311] By using analogous scoring systems for overall image quality and image noise, all previous studies reported improved qualitative image quality parameters, similarly to our findings.[309-311] Quantitative analysis confirmed our subjective findings, as we revealed a substantial decrease in image noise as measured in the aorta using IMR as compared to HIR and FBP. The overall noise reduction of 66.9% with IMR and 31.5% with HIR in our study is comparable with the results of other research groups, which reported a noise reduction of 56.0-78.3% for IMR and 34.1-55.5% for HIR.[309,310]

Similarly, we observed increased CNR values in every assessed coronary segment with HIR as compared with FBP, which further improved with IMR. This finding is in line with other recent studies evaluating the performance of IMR in the cardiac setting.[309,310] Interestingly, while median CT numbers were preserved in the aorta independent of applied image reconstruction technique, HU values in vessels with smaller caliber – proximal and distal segments of the coronary arteries – were higher with IMR as compared to the other two reconstructions. The median CT numbers did not differ between HIR and FBP in the respective coronary segments. Comparing the median values of attenuation in the distal coronary segments to the proximal ones of the same vessel, we found preserved or even increased median attenuation values using IMR. However, with HIR and FBP technique, the HU values were similar, or rather decreased from proximal to the distal coronary segments. A tendency for better visualization of the distal coronary segments was already described by Oda et al., though no difference was found in CT numbers among the three reconstructions between the proximal and distal coronary parts.[310] In the study of Yuki et al. a clear drop of CT number was observed from proximal to distal, independent of image reconstruction.[309] However, the lower tube

voltage settings applied in these studies might have influenced the CT number variations.[309,310]

Interestingly, using model based iterative reconstruction of a different vendor at 120 kV tube voltage setting in an *ex vivo* model, Scheffel et al. also found higher median luminal CT numbers in the coronaries, as compared to HIR and standard FBP, while difference between HIR and FBP was not observed either.[252] Our findings for the median attenuation in the proximal, and distal segments of the coronary arteries are more in line with the study of Scheffel et al. and differ from those of Oda et al.[310] Smaller structures are typically more affected by the partial volume effect. More ideal point spread function, greater edge-enhancement kernels and subsequently improved CNR ratio allowed by IMR might support the imaging of small structures (e.g. coronary branches), which are not always adequately evaluable with noisier image reconstructions. The enhanced spatial resolution with IMR could influence the median HU values in ROIs drawn close to the edge of small structures, since these ROIs are likely to be influenced by the point spread function effect on the edge. On the other hand, ROIs drawn in the middle of larger structures such as aorta are not close to the edges and hence are not affected and provide the median HU values that are comparable to FBP and HIR techniques.

In clinical routine, standard reading of coronary stenosis is highly dependent on image quality and image noise. The utilization of IMR allows an excellent image quality by decreasing "graininess" of the CTA images, and also improves distal vessel visualization. As images remain of high diagnostic quality using IMR, significant dose reduction may be achieved, as reported by other studies. The improved spatial resolution achieved with IMR was also reflected in our results of plaque volume quantification. HIR decreased calcified plaque volume as compared to FBP, which was further reduced by IMR. High attenuation non-calcified plaque volumes were also lower with IMR. These result a reduced overall plaque volume measured with IMR. Low and intermediate attenuation non-calcified plaque volumes were not altered by the type of image reconstruction. Although currently qualitative analysis is used for clinical decision making in coronary CTA, automated plaque assessment is desirable for long term monitoring of plaque burden changes in individual patients. Only a few studies have evaluated the effect of recently introduced iterative reconstruction techniques for this purpose. We used a software tool validated against intravascular ultrasound for fully automated volumetric plaque assessment.[88]

Contrary to our findings, two recently published studies demonstrated that HIR did not affect volumetric plaques assessment, while improved image quality as compared to FBP.[50,51] Although, in the detailed analysis by Fuchs et al., who analysed the plaque volume components in different HU strata, a significant decrease in calcified plaque components was reported with

CT numbers between 401 and 500 HU.[51] Moreover, our previous investigation demonstrated the improved feasibility of automated plaque assessment with model-based iterative reconstruction, while it reduced the vessel-wall delineation incongruences, especially at the site of calcified plaques.[312] This supports our hypothesis, that the decreased plaque volumes measured with IMR results mainly from the improved delineation of the calcified coronary atherosclerotic plaques. Recent studies have demonstrated controversial results regarding the impact of novel iterative reconstruction techniques on CAC scoring.[313,314]

We and others have shown a significant reduction in CAC scores using novel iterative reconstruction algorithms as compared to FBP, which resulted in net reclassification rate of approximately 6-10%.[55,315,316] Thus, novel image reconstruction techniques should be carefully implemented in the clinical setting when assessing patients' risk using CAC or plaque volumes. There are some limitations of this study that we have to consider. During the past decade all vendors have introduced hybrid and model type iterative reconstruction techniques to improve image quality. The results of current study are derived from two different Philips iterative reconstruction algorithms (Philips, Best, The Netherlands), therefore it might not apply for all other vendor's iterative reconstruction. Although FBP, HIR and IMR datasets were reconstructed using the same raw data to ensure data consistency, imaging parameter settings might be different, if data acquisition is optimized for a certain reconstruction type (e.g. tube voltage and tube current settings and contrast protocol). Our strict exclusion criteria have also evaded individuals with higher-heart rates and thus, our findings of image quality might not be generalized for everyday clinical setting. Though, current guidelines recommend sufficient premedication with a target HR<65 bpm during coronary CTA and we wanted to avoid the concomitant effect of motion artifacts. The subjective scoring system used for image quality analysis might show individual differences by readers and the different visual appearance of reconstruction types (e.g. "blotchy" images of IMR) does not enable truly blinded analysis. However, the good-to-excellent inter-observer reproducibility of the qualitative scoring supports the reliability of our data. Moreover, we demonstrated an excellent inter-reader reproducibility of quantitative image quality analysis. The applied plaque quantification method might be also considered as a limitation of our study. The manual setting of plaque start- and endpoints might introduce some errors in plaque volume measurements, however excessive care was taken to ensure that exactly the same lesion was measured by the different reconstruction techniques. Although any observer related bias was avoided using an automated plaque quantification, this can be inaccurate in case of motion artifacts or certain vessel path characteristics. Accordingly, manual correction might be necessary in datasets of patients with

higher HRs during data acquisition and this might introduce observer related differences in plaque volume quantification. Last, there might be an overlap between plaque components and our findings need to be validated against reference standard (e.g. intravascular ultrasound).

In our other clinical study on image quality, we found that scans of HTX recipients had better coronary CTA image quality than did scans of a matched control group with similar HRs. Despite the relatively high HR of HTX recipients, the number of non-diagnostic segments was low (5.8%), suggesting that coronary CTA with prospective ECG- triggering is a robust diagnostic tool with low radiation dose in this patient population. The subgroup analysis comparing the image quality of the two groups among scans with systolic and diastolic triggering showed similar results. The HTX recipients had better overall image quality compared with the control subjects both with systolic and diastolic triggering. However, the segment motion score index did not show any difference between the two groups among the scans triggered in diastole, which is most probably due to the lower HR of patients undergoing coronary CTA with diastolic triggering.

Cardiac allograft vasculopathy is among the top three causes of death 1 year after HTX. Invasive coronary angiography is considered the reference standard method to diagnose CAV. However, it has been found that diagnosis based on a single invasive coronary angiography is challenging because of the concentric intimal hyperplasia; furthermore, the interobserver variation is high.[317] Numerous studies investigated the diagnostic performance of coronary CTA to identify CAV.[318-321] Von Ziegler et al. studied 26 consecutive patients with a mean (± SD) HR of 86 ± 13 beats/min using 64-MDCT.[320] They found that 81.4% of the segments had diagnostic image quality. According to their results, coronary CTA has high negative predictive value (99.7%), and they concluded that coronary CTA is a reliable diagnostic tool to rule out CAV in HTX recipients.[320] Similar results were shown by Mittal et al., who evaluated 130 HTX recipients (mean HR, 82.7 ± 4 beats/min) with 64-MDCT.[318] Most of the evaluated segments (98%) had diagnostic image quality. They concluded that coronary CTA has high sensitivity, specificity, and excellent negative predictive value for the diagnosis of CAV in HTX recipients in comparison with invasive angiography.[318] A meta-analysis published by Wever-Pinzon et al. showed that the combined overall weighted mean sensitivity, specificity, positive predictive value, and negative predictive value of CT for detection of CAV were 97%, 81%, 78%, and 97%, respectively.[322] Importantly, these studies used retrospective ECG-gating, because of the higher resting HR of HTX recipients, which resulted in higher radiation dose (10.2-17.5 mSv).[318,323] The reduction of radiation dose is of utmost importance for HTX recipients who undergo repeated scans and take immunosuppressant therapy, which substantially increases

cancer risk. We found that HTX recipients can be scanned with a prospective ECG-triggering scan mode with a low radiation dose (mean effective radiation dose, 3.7 mSv). Furthermore, we found that scans of HTX recipients with median HR of 74.0 beats/min have significantly better image quality than scans of control subjects with a similar HR (73.0 beats/min). In addition, the number of segments with excellent image quality was higher for HTX recipients than for control subjects. In accordance with these results, the ratio of non-diagnostic segments was lower among HTX recipients. Our observations might be explained by the loss of autonomous neural control. The surgical denervation after heart transplantation causes chronotropic incompetence, which results in elevated resting HR and nearly absent HR variability.[324,325] According to Stolzmann et al. and Brodoefel et al., HR variability has a significant effect on the image quality in prospectively triggered coronary CTA.[326,327] Therefore, the lack of autonomous neural control and the consequent regular and steady HR seems to be optimal for prospectively ECG-triggered coronary CTA. Despite the excellent diagnostic accuracy and low radiation dose of modern CT scanners, the routine use of coronary CTA for follow-up of HTX recipients has not become widely accepted in daily practice.

The guidelines of the International Society for Heart and Lung Transplantation and the recommendations of the European Association of Cardiovascular Imaging and Cardiovascular Imaging Department of the Brazilian Society of Cardiology raise concerns regarding the higher HR of HTX recipients and the excess ionizing radiation.[58,61] However, contemporary scanner technology allows coronary imaging at ever decreasing radiation doses, and with modern scanners, the radiation dose generally does not exceed that associated with invasive coronary angiography. Therefore, we believe that, in experienced centers with contemporary CT scanners, coronary CTA is a promising alternative to invasive coronary angiography for follow-up of HTX recipients. This study has some limitations that we have to acknowledge. First, coronary segments with a diameter smaller than 1.5 mm were excluded from the study because of the limited accuracy of coronary CTA in distal coronary segments and small-caliber side braches. Nevertheless, the evaluation of small coronary segments remains a challenge even with invasive techniques. Second, because of the specific postoperative appearance of the extracardiac structures (e.g., sternal sutures and great vessel anastomoses) of HTX recipients, the readers could not be blinded to the compared groups (HTX recipients vs control subjects), which might represent a potential bias that affects quality rating. Furthermore, we acknowledge that this HTX study was a single-center single-vendor study using a 256-MDCT scanner, which might limit the generalizability of our findings.

In these four clinical investigations we have demonstrated that, 1) ultrashort acting β-

blockers might be a safe alternative of metoprolol in heart rate control before coronary CTA, 2) by implementing innovative CM injection protocols the CM extravasation rate can be reduced significantly, 3) the new reconstruction algorithms improve coronary CTA image quality and 4) despite the higher heart rates in HTX patients the coronary CTA image quality is excellent.

6.2 Imaging coronary atherosclerotic plaques

6.2.1 Ex vivo studies

One of the most important findings of our coronary plaque imaging projects was the identification of a novel radiological sign that we have named as 'napkin-ring sign'.[259] The NRS is a qualitative plaque feature and can be defined in a noncalcified plaque cross-section by the presence of two features: a central area of low CT attenuation that is apparently in contact with the lumen; and a ring-like higher attenuation plaque tissue surrounding this central area.[72] Interestingly, NRS was present in both native (that is non-contrast-enhanced) and contrast-enhanced *ex vivo* CT images, suggesting that the feature is the result of differences in CT attenuation between the large necrotic core (a central low CT attenuation) and fibrous plaque tissue (ring-like higher attenuation). However, in vivo, some additional factors (such as the vasa vasorum) might influence the development of NRS.[328] We have demonstrate that the area of necrotic core can be over twice the size in NRS plaques compared with non-NRS plaques (median 1.10 mm^2 versus 0.46 mm^2; P = 0.05).[298] These values correlate with other histopathological observations that demonstrate the area of necrotic core in vulnerable plaques is >1.0 mm^2 in the majority (~80%) of cases.[5]

The current clinically used coronary CTA classification of coronary atherosclerotic plaque composition is based on the presence or absence of calcification and was initially suggested in early coronary CTA studies using 4-slice multidetector CT technology with limited spatial and temporal resolution.[18,78] Although this classification has demonstrated that presence of NCP has some incremental value over the detection of CP in predicting adverse cardiovascular events, its ability to distinguish individual plaques that may be at higher risk for cardiovascular events is limited.[18,86] Therefore, as a next step we have developed a novel plaque classification scheme, which differentiates three types of non-calcified plaques: napkin-ring sign, heterogeneous and homogenous plaque. Our data demonstrates that a qualitative assessment of the attenuation pattern of NCP by coronary CTA under *ex vivo* conditions

significantly improves diagnostic accuracy for the detection of advanced plaque and TCFA as determined by histopathology compared with the conventional assessment of plaque composition ($p<0.05$ for both). Remarkably, both heterogeneous appearances of NCP and NRS are highly specific for the presence of both advanced plaque and TFCA in histopathology (specificity: 98.9% and 94.1%, respectively). Previous studies demonstrated the inability of density measurements within the plaque to differentiate reliably between lipid-rich and fibrous plaques because of a significant overlap in attenuation values (30,39–41).[79,85,329,330] Significant progress in CT technology with an improvement of spatial resolution reaching 0.3 mm in-plane, allows a more differentiated assessment of the noncalcified portion of plaque. Recent studies suggest that low attenuation (<30 HU) is a hallmark of both culprit lesions in acute coronary syndromes and is more frequently found in plaques that are at high risk for rupture.[84,328,331] In addition, higher spatial resolution may mitigate the "masking" of NCP by CP, which appears at least 4× larger in CT than its actual size due to blooming artifacts.[332]

Our results demonstrate the increased ability of coronary CTA to differentiate individual plaque characteristics that are specific for advanced atherosclerotic lesions associated with increased vulnerability and subsequent adverse cardiovascular events.[5,6,261,262] Whereas the current clinically used classifications of partially calcified and NCP are unable to predict the presence of advanced plaques, NRS demonstrated a 98.9% specificity to identify advanced lesions and a 92.3% specificity for identifying TCFA. Our finding that the frequency of NRS was similar in MP and in NCP may help to resolve some contradictions in published studies, some of them reporting that MP rather than NCP indicates a higher risk for future cardiovascular events.[90,102,333-336] Our data suggest that certain qualities of NCP irrespective of the presence of calcium are associated with advanced atherosclerotic lesions.

Prospective clinical studies are warranted to determine the prognostic value of PAP assessment to identify patients with the highest risk of developing cardiovascular events.[337] Whereas quantitative analysis of NCP has been described before, we pursued a qualitative approach to plaque characterization based on initial encouraging findings. The qualitative plaque pattern assessment may be more feasible and easier to implement in clinical practice or large studies. In addition, the quantitative assessment of plaque attenuation might be significantly altered by the coronary lumen enhancement, the reconstruction kernel, and the size and number of regions of interest used for the attenuation assessment.[18,85] The *ex vivo* coronary CTA imaging was performed in an ideal, motion-free experimental setting. This might limit the direct translation of our findings into in vivo circumstances. However, it is important to note that some recently published studies observed a ring like attenuation pattern similar to

that of NRS in patients presenting with acute coronary syndromes.[338,339] These observations indicate that the qualitative PAP assessment might be feasible in clinical scenarios. Further improvements in acquisition and post-processing techniques (e.g., iterative reconstruction techniques) in combination with reduction in radiation dose may further enhance the ability of coronary CTA to differentiate between individual plaque components and broaden the applicability of coronary CTA for the evaluation of coronary atherosclerosis.

In our third *ex vivo* investigation, we have described a robust approach for data acquisition, co-registration, and systematic comparison of non-invasive (coronary CTA) and invasive (IVUS and OFDI) imaging modalities with the standard of reference (histologic examination). In this study we have demonstrated that (a) Various imaging features of plaques are associated with early plaque (normal cross section at coronary CT angiography and fibrous at OFDI) and advanced plaque (mixed at coronary CT angiography, any calcified plaque at intravascular US, and lipid-rich plaque at OFDI); (b) The overall performance of OFDI for differentiating early from advanced plaque is significantly better than that of IVUS and coronary CTA; (c) We found excellent interobserver agreement for OFDI and coronary CTA and good agreement for IVUS.

Overall, the performance of each modality for differentiating early from advanced plaques reflects the differences in the physics behind these imaging methods. Not surprisingly, OFDI, with its excellent spatial resolution and tissue characterization, rendered the strongest associations with histologic examinations as compared with IVUS and coronary CTA. This is reflected by several significant associations between plaque type at OFDI and histopathologic examination. At OFDI, fibrous plaques were associated with early lesions, while lipid-rich plaques were associated with advanced lesions. In addition, OFDI yielded a sensitivity of 100% and a specificity of 81% for identifying TCFA, confirming the previously described potential of OFDI to help identify or confirm high-risk lesions.[340-342] In contrast, TCFA composition was heterogeneous and non-discriminatory at intravascular US and coronary CTA. Normal IVUS findings precluded the presence of TCFA at histologic examination. However, the overall modest association of IVUS-based plaque composition with early or advanced plaques emphasizes the known limitations of gray-scale IVUS for tissue differentiation using the conventional classification scheme.[343-345] Hence, IVUS has a higher potential in plaque size and volume assessment than for the presence of high-risk plaque.[346,347] However, the newest IVUS methods, using, for example, virtual histologic examination techniques, and more advanced plaque classification may overcome these limitations.[344,348] Our data suggest that conventional IVUS and coronary CT angiography are not significantly different in their ability to help predict

lesion stage at histologic examination. Importantly, both *ex vivo* studies demonstrated that the absence of plaque in coronary CTA excludes the presence of advanced atherosclerotic lesion or TFCA. This finding is consistent with clinical studies demonstrating the rarity of cardiovascular events in patients without coronary artery disease as described by coronary CTA.[90,101,349,350]

Although non-invasive imaging is evolving rapidly, IVUS and OFDI still offer the highest accuracy regarding the differentiation of plaque components, and IVUS remains the clinical standard of plaque burden assessment. However, coronary CTA is able to reliably help exclude relevant coronary artery disease and offers a high sensitivity for the detection of significant coronary artery stenosis.[351] Furthermore, as the presence of mixed plaques and other high-risk plaque features are associated with the presence of advanced coronary atherosclerotic lesions at histologic examination.[90,102,259,350]

It is important to note that these studies were performed in an ideal *ex vivo* setting providing motion-free image-based plaque characterization in a limited number of hearts. Thus, our results cannot be directly translated to *in vivo* circumstances. At histopathologic examination, a modified nomenclature for coronary atheroslcerosis was applied.[6] We believe that the modified stratification is useful as it differentiates plaques that have a higher risk of causing cardiac events from those with lower risk while accommodating the limited spatial and contrast resolution of intravascular US and of coronary CT angiography. Moreover, our experimental setup resulted in no exclusion of vessel segments because of artifacts and allowed the analysis of 379 histologic cuts from three donor hearts. In contrast, previously published *ex vivo* studies included a much higher number of cadaver hearts (11-30 hearts), on the other hand because of methodologic limitations and air bubble formation, much fewer cross sections were suitable for analysis (17-312 sections).[352-354] Furthermore, the generally used plaque classification schemes for coronary CTA, IVUS, and OFDI were developed independently; thus, a direct comparison between modalities is limited.

A sequential imaging strategy using coronary CTA to identify high-risk plaque features such as the NRS, followed by invasive imaging tools to confirm the presence of vulnerable plaques might provide a framework suitable to identify individuals with the highest risk to develop acute coronary syndromes. Further *ex vivo* and *in vivo* research is warranted to assess the generalizability of our findings.

6.2.2 In vivo studies

In a prospective clinical study we have demonstrated that ICA sees only half as many segments with plaque and underestimates plaque sizes compared to coronary CTA in patients with moderate, mild, and minimal plaques. These differences might have a significance in patient risk stratification and patient management. Butler et al. reported even larger differences when analyzing the results of 37 patients who underwent both imaging modalities.[355] In their patient population, even larger differences were observed between the methods (CTA: 67%; ICA: 24%), which resulted in greater percentage of segments only seen stenotic on CTA (57%). To assess the clinical significance of discrepancy in the number of stenotic segments seen by CTA and ICA, we classified patients as proposed by Bittencourt et al.[117] In 78% of reclassified subjects, reclassification was solely caused by CTA classifying the patients as extensive compared to ICA, which classified them as non-extensive, whereas in 22%, it was caused by CTA overrating the degree of obstruction. One patient who changed to lower risk category was due to that coronary CTA underestimated the degree of stenosis.

Bittencourt et al. calculated hazard ratios associated with the patient categories: extensive obstructive: 3.9, extensive non-obstructive: 3.1, non-extensive obstructive: 3.0, whereas non-extensive non-obstructive did not show any association with any increase in rate of events. Using hazard ratio values of the risk groups, average hazard ratio of ICA-based measurements was lower than CTA-based calculations (2.7 vs 3.3, respectively). Current identification of patients prone to major adverse cardiovascular events is based on anthropometric and blood test information. In recent years with the development of imaging techniques, significant efforts have been invested into finding morphologic features unique to vulnerable plaques. This paradigm shift from risk factors to lesion-based phenotypic risk assessment showed promising results, but longitudinal studies question the predictive value of a single high-risk plaque at a given time point.[356] Kubo et al. demonstrated using intravascular ultrasound-virtual histology that 75% of vulnerable plaques lost high-risk characteristics by thickening of the fibrous cap or by transforming to fibrotic plaques.[357] Only 25% showed vulnerable characteristics after 12-month follow-up.

It seems that the identification of vulnerable patients is more than identifying high-risk plaques. Invasive coronary angiography is accepted as the reference standard of stenosis quantification in daily clinical practice. Although the coronary lumen is depicted with high temporal and spatial resolution, the coronary wall is imperceptible with ICA; therefore, the identification plaques that cause minimal and mild stenosis is challenging. In contrast, coronary

CTA is capable of visualizing not only the lumen but also the coronary wall and atherosclerotic plaques. It has a high diagnostic accuracy to identify obstructive lesions; however, it has a tendency to overestimate stenosis severity. Because of the high CT attenuation values of calcium, coronary CTA shows a superior sensitivity to identify calcified plaques. The identification of noncalcified plaque is more challenging, and it requires excellent image quality. The CONFIRM registry demonstrated the importance of the presence of mild and minor plaques, as the hazard ratio increases by 1.22 for each segment with any plaque.[119] Thus, differences in the number of diseased segments observed by different imaging techniques can have a major impact on risk assessment. Hence, ICA and coronary CTA are not interchangeable. Invasive coronary angiography is superb at detecting obstructive coronary disease but is inferior to CTA in plaque detection. Therefore, ICA might underestimate patient risk because of the insufficient recognition of nonobstructive plaques.

In our subsequent retrospective case-control study we demonstrated that coronary plaques consist of sufficient number of voxels to conduct radiomic analysis. Importantly, 20.6% of radiomic parameters showed a significant difference between plaques with or without napkin-ring sign, whereas conventional CT metrics (such as plaque volume, positive remodelling) did not show any difference. Furthermore, several radiomic parameters had a higher diagnostic accuracy in identifying NRS plaques than conventional quantitative measures. Cluster analysis revealed that many of these parameters are correlated with each other; however, there are several distinct clusters, which imply the presence of various features that hold unique information on plaque morphology. Cross-validation simulations indicate that our results are robust when assessing the discriminatory value of radiomic parameters, implying the generalizability of our results.

Radiomics uses voxel values and their relationship to each other to quantify image characteristics. On the basis of our results, it seems not only do radiomic features outperform conventional quantitative imaging markers but also parameters incorporating the spatial distribution of voxels (GLCM, GLRLM, and geometry-based parameters) have a better predictive value than first-order statistics, which describe the statistical distribution of the intensity values. Among GCLM parameters, the interquartile range, the lower notch, the median absolute deviation from the mean of the GLCM probability distribution, Gauss right focus, and sum energy had the 5 highest AUC values. NRS plaques have many low-value voxels next to each other in a group surrounded by higher density voxels. This heterogeneous morphology results in an unbalanced GLCM and therefore higher inter-quartile rank values, which also means smaller lower notch values and bigger deviations from the mean. Gauss right focus and

sum energy both give higher weights to elements in the lower right of the GLCM, which represents the probability of high-density voxels occurring next to each other. Because NRS plaques do not have many high-value voxels next to each other, they received smaller values, whereas non-NRS plaques have higher values, which resulted in excellent diagnostic accuracy.

Among GLRLM statistics, long- and short-run low-gray-level emphasis, long- and short-run emphasis, and run percentage had the best predictive value. Run percentage and long-run emphasis give high values to lesions, where there are many similar value voxels in 1 direction, whereas long-run low-gray-level emphasis adds a weight to the previous parameter by giving higher weights when these voxel runs contain low Hounsfield unit values. NRS plaques' low-density core has many low CT number voxels next to each other in 1 direction; therefore, NRS plaques have higher values compared with non-NRS plaques, which results in excel- lent diagnostic accuracy. In case of short-run emphasis and short-run low-gray-level emphasis, the contrary is true, which results in NRS plaques receiving low values, whereas non-NRS plaque have higher values also leading to high AUC values.

Among geometry-based parameters, the first 5 with the best diagnostic accuracy all represent the surface ratio of a specific subcomponent to the whole surface of the plaque. In all cases, the ratio of high-density subcomponents (e.g., sub-component 2 when the plaque was divided into 2 components) to the whole surface had excellent diagnostic accuracy. Because each subcomponent is composed of equal number of voxels because of the equally probable binning, the difference in surfaces is a result of how the high-intensity voxels are situated to each other. In case of NRS plaques, extraction of low attenuation voxels leaves a hollow cylindrical shape of high CT number voxels, which has a relatively large surface. Non-NRS plaques on the contrary do not have such voxel complexes; therefore, the surface of the high attenuation voxels is smaller, and, therefore, the ratio compared with the whole surface is also smaller.

This kind of transition from qualitative to quantitative image assessment was initiated by oncoradiology. Because studies showed that morphological descriptors correlate with later outcomes, reporting guidelines such as the Breast Imaging Reporting and Data System started implementing qualitative morphological characteristics into clinical practice.[358,359] However, despite all the efforts of standardization, the variability of image assessment based on human interpretation is still substantial.[360] Radiomics, the process of extracting thousands of different morphological descriptors from medical images, has been shown to reach the diagnostic accuracy of clinical experts in identifying malignant lesions.[361] Furthermore, radiomics can not only classify abnormalities to proper clinical categories but also discriminate between

responders and non-responders to clinical therapy and predict long-term outcomes.[362,363]

However, there are major concerns on the generalizability of radiomics. Several studies have shown that imaging parameters, reconstruction settings, segmentation algorithms affect the radiomic signature of lesions.[364,365] Furthermore, it has been shown that the variability caused by these changeable parameters is in the range or even greater than the variability of radiomic features of tumor lesions.[366] Little is known about cardiovascular radiomics. Several studies will be needed to replicate these results in the cardiovascular domain. The potential of radiomics is extensive; however, the problem of standardized imaging protocols and radiomic analysis need to be solved to achieve robust and generalizable results.

Despite our encouraging results, our radiomics study has some limitations that should be acknowledged. All of our examinations were done using the same scanner and reconstruction settings. It is yet unknown how these settings might affect radiomic parameters and therefore influence the applicability of radiomics in daily clinical care. Furthermore, our results are based on a case-control study design. The true prevalence of the NRS is considerably smaller compared with non-NRS plaques in a real population. Therefore, our observed positive predictive values might be higher, whereas our negative predictive values might be smaller than that expected in a real-world setting. Moreover, our limited sample sizes might not allow the accurate assessment of the diagnostic accuracy of the different parameters. However, we performed Monte Carlo simulations and cross-validated our results to achieve robust estimates. Radiomics is a promising new tool to identify qualitative plaque features such as the NRS. Because the number of CT examinations increases, we are in dire need of new techniques that increase the accuracy of our examinations without increasing the workload of imaging specialists. We demonstrated that radiomics has the potential to identify a qualitative high-risk plaque feature that currently only experts are capable of. Furthermore, our findings indicate that radiomics can quantitatively describe qualitative plaque morphologies and therefore have the potential to decrease intra- and inter-observer variability by objectifying plaque assessment. In addition, we observed several different clusters of information present in our data set, implying that radiomics might be able to identify new image markers that are currently unknown. These new radiomic characteristics might provide a more accurate plaque risk stratification than the currently used high- risk plaque features. Radiomics could easily be implemented into currently used standard clinical workstations and become a computer-aided diagnostic tool, which seamlessly integrates into the clinical workflow and could increase the reproducibility and the accuracy of diagnostic image interpretation in the future.

In these *ex vivo* and *in vivo* investigations, we have assessed morphological

characteristics of CAD. However, the functional aspects of coronary plaques, i.e. the presence or absence of lesion specific ischemia have important therapeutic and prognostic implications. Therefore, in our prospective two-center study we evaluated the diagnostic accuracy of a new rapid on-site FFR-CT algorithm.

We have demonstrated that this algorithm has a good diagnostic accuracy when compared with the reference standard invasive FFR. The FFR-CT algorithm showed excellent intra- and inter-reader reproducibility. Additional procedure time was short and acceptable for integration into a clinical service workflow. Our results demonstrate the feasibility of a rapid on-site FFR-CT approach for patients in whom referral for ICA was considered appropriate. Off-site algorithms have recently been approved by the Food and Drug Administration (FDA) and are currently being appraised by the National Institute for Health and Care Excellence (NICE). Based on early work in a range of clinical scenarios, the feasibility and diagnostic accuracy of FFR-CT has been established.[176,199-201] Recently, the PLATFORM study demonstrated that when compared with standard of care, an FFR-CT strategy could reduce the normalcy rate of invasive catheter angiography by 61%.[202] Furthermore, there is some evidence to suggest that FFR-CT may be cost-effective and could improve the quality of life of patients who underwent investigation.[203] We have demonstrated that the diagnostic performance of FFR-CT was better than that of anatomic quantitative stenosis assessment based on EDS measurements alone. If the FFR-CT results were available to the referral team it is possible that nearly 50% of ICA referrals may have been avoided. Although further evaluation is required, this would be consistent with the conclusions of the previously published PLATFORM trial.[202]

We also found that lower FFR-CT values had higher bias, whereas higher values had lower bias. This characteristic might increase the false-positive rate, but in contrast, this increased the safety margin of on-site FFR-CT simulation as the false negative rate was low. Finally, the specificity of our algorithm was lower than other off-site techniques, but it is comparable with previously published on-site simulations.[367,368] Although the workflow used here is very similar to other on-site algorithms, they differ in the underlying solver and the patient-specific boundary conditions.[369,370] The approach used by Coenen et al. uses 2 different vessel models (full-order in stenotic and reduced order for healthy regions) to simulate blood flow and boundary conditions for rest and stress where a total blood flow proportional to the myocardial mass is distributed according to Murray's law over the segmented coronaries.[205] In contrast, the lumped parameter model approach used in our work uses a consistent vessel model based on a tree of lumped elements to simulate blood flow along the coronaries and boundary conditions that use a microvascular resistance scaled according to a physical law derived by

Huo and Kassab.[371] For widespread adoption of a new technology, it must complement existing care pathways, be accurate, reproducible, easy to use, cost-effective, and provide additional beneficial diagnostic information. On-site FFR-CT demands excellent image quality and additional operator time for semiautomated 3D coronary lumen segmentation; therefore, fully automated lumen segmentation could greatly improve the workflow.[369]

6.3 Adipose tissue and coronary artery disease

We have conducted two studies aiming to decipher the role of adipose tissue compartment in the development of coronary artery disease and assess the heritability adipose tissue quantities. In our first study we have provided a mechanistic view on various fat compartments located in the thorax and their relationship to coronary artery plaque and systemic markers of inflammation.

We found that all four thoracic fat depots (pericoronary, epicardial, periaortic and extracardiac adipose tissue) were higher in patients with coronary plaque compared to those without despite no difference in BMI. Correlation of the fat depots to BMI was moderate for epicardial, periaortic, and extracardiac fat depots and it was modest for the pericoronary fat compartment. The strength of association to coronary plaque was dependent on the proximity of the fat depot to the coronary arteries. Furthermore, we found an association between higher volumes of perivascular fat depots and the presence of plaque, and more specifically between pericoronary fat and the presence of CAD irrespective of the extent of CAD. Despite being the least correlated to BMI, pericoronary fat, which is one of the smallest fat depots yet closest in proximity to the coronary vasculature, was most consistently associated with CAD. Interestingly, the fat depots farther from the coronary vasculature (epicardial, periaortic, and extracardiac) attenuated in their association to CAD after adjustment for cardiovascular risk factors.

Furthermore, circulatory biomarkers of inflammation showed the strongest positive correlation with fat compartments closest to the coronary arteries. Interestingly, adiponectin was not associated with pericoronary adipose tissue, and it showed a negative correlation with the other intrathoracic fat depots. It has long been understood that increased adipose tissue volume and elevated BMI is associated with increase in cardiovascular disease risk.[372] Our study further extends the data regarding the relationship of the local fat volumes closest to the heart and their relationship to CAD. Our findings that increased volume of thoracic fat depots

closest to the coronary vessels are associated to presence of coronary plaque are consistent with previous studies that showed that pericoronary fat is associated with coronary atherosclerosis in the local underlying coronary segment in patients with known or suspected CAD.[373]

We found that the adipose tissue depot in closest proximity to the coronary artery vessels (pericoronary fat compartment) remained independently associated to the presence of coronary plaque even following adjustment for BMI and other CAD risk factors. Notably, pericoronary adipose tissue was found to be the least correlated to BMI in our analysis. This further suggests the presence of a local atherogenic effect of adipose tissue. These results suggest that coronary atherosclerosis might be influenced by the fat depot in closest proximity to the coronary vasculature. Furthermore, to account for systemic inflammation, which is a well-known risk factor of CAD, we have assessed the levels of several inflammatory biomarkers. The intrathoracic fat depots showed an association with circulating inflammatory biomarker levels irrespective of CAD. The strongest correlations were present between hsCRP and PAI-1 and the fat depots. These findings are consistent with previous studies describing increased inflammatory status and the predisposition of thrombosis in patients with increased adipose tissue volumes.[374] Adiponectin was not associated to the pericoronary fat tissue and it showed an inverse relationship with all other intrathoracic fat compartments.

Mechanistically, this finding is consistent with the results of a previously published meta-analysis, which showed no association between adiponectin and CAD.[375] It has been suggested that locally acting perivascular fat depots such as pericoronary fat may contribute to the development of cardiovascular disease through the modulation of vascular tone, oxidative stress, and inflammation.[376,377] Thoracic fat located close to the coronary arteries has also been shown to be associated with the presence of calcified plaque in large population based studies such as the Multi-Ethnic Study of Atherosclerosis.[223] Importantly, epicardial and pericoronary fat depots are most probably consisting of the same type of metabolically active adipose tissue, however their difference in proximity to the coronary wall what renders potentially different pathophysiologic roles in the process of atherogenesis. The mechanism of action of local perivascular fat depots on the development of CAD is currently under investigation, and multiple studies have shown that visceral fat secretes a variety of inflammatory cytokines including interleukin-6, adiponectin, and TNFα.[218,378-381] Adipocytokines secreted by local fat tissue may diffuse into the vessel wall promoting the development of atherosclerosis independent of the effects of total body fat stores or systemic levels of inflammation. In addition, a genome wide association study has recently shown a specific genetic locus to be associated with the ectopic deposition of fat, further emphasizing the unique role of the adipose

tissue located within the pericardium.[382] Taken together, our study supports the current literature suggesting that there is a local effect of pericoronary adipose tissue on the development of CAD. Our results also suggest that there is a gradient in terms of CAD risk from extracardiac fat compartment towards the pericoronary adipose tissue depot. Furthermore, the circulatory markers of inflammation were correlated to the intrathoracic fat compartments irrespective of CAD, which underscores the endocrine organ-like functions of adipose tissue.

In our classical twin study, we demonstrated that genetics have substantial, while environmental factors have only a modest influence on EAT, SAT and VAT volumes. Our findings show that common and specific genetic effects both play an important role in developing these phenotypes. None of the phenotypic appearance of EAT, SAT and VAT proved to be completely independent of the other two. To the best of our knowledge, this is the first clinical study to evaluate the genetic and environmental dependence of EAT quantity and assessed simultaneously the joint heritability of EAT, SAT and VAT in twin pairs. In the total cohort, SAT quantity was higher (217.9 mm^2) than VAT quantity (156.6 mm^2). The mean volume of EAT (97.1 cm^3) was in the range of middle-aged healthy subjects.[215] It is of note that SAT and VAT was planimetrically, whereas EAT was volumetrically measured in our cohort. Importantly, there was no significant difference in the assessed fat volumes comparing MZ with DZ subjects.

We used advanced statistical methods to decipher the ratio of genetic and environmental effects on EAT, SAT and VAT quantities. In addition to single trait analysis, we performed multi-trait models to explore the complex interactions of multiple quantitative traits. This method has been recently used to dissect genetic mechanisms underlying complex diseases such as obesity.[383,384] We demonstrated that common genetic effects predominated over common environmental influences on the latent phenotype (71% versus 29%). On the other hand, although the latent phenotype markedly influenced VAT (98%), its effect was minimal on SAT (26%) and its impact on EAT was intermediate (49%). This relationship was reflected by the stronger phenotypic correlation between VAT and EAT, than between VAT and SAT. Latent phenotype could be related to BMI, obesity or total fat depot. However, the co-linearity between BMI (which represents all fat compartments) and specific adipose tissue quantities precludes the independent analysis of BMI in our multi-trait models. Regarding the whole distribution of variance of CT-based fat measurements, it seems that the phenotypic appearance of EAT, SAT and VAT quantities are driven by common and specific genetic and environmental factors. Furthermore, we found that none of the fat compartments' heritability was independent of the other two.

Taken together, an interplay between common and specific genetic effects and environmental influences may be hypothesized, but the magnitude of their relative impact on different adipose tissue compartments varies. We demonstrated a relatively strong genetic dependence of EAT, which has not been described previously. The genetic dependence of anthropometric parameters (weight, height and BMI) has been well documented in former twin studies.[385-387] Heritability of different ectopic fat compartments (hepatic lipid accumulation) was also investigated in twins, and in this case environmental factors predominated over genetic influences.[388] Hence, heritability of different adipose tissue compartments and that of ectopic fats may vary.

The presence of strong genetic predisposition does not automatically translate to the development of clinical disease phenotype. Considering this fact, early and continuous preventive efforts should be implemented. In case of obesity, intervention should be initiated as early as possible and all modifiable risk factors should be addressed with diet, physical activity and behavioural interventions starting as early as preschool age.[389,390] Importantly, weight loss and exercise training may reduce EAT and abdominal adipose tissue volumes in adult subjects with obesity.[391,392] Non-contrast enhanced CT scan was used to evaluate quantities of various fat compartments, although other non-invasive methods (echocardiography and magnetic resonance imaging) have been used previously. Echocardiography has several disadvantages including poor reproducibility and high dependence of investigator's experience.[393] Magnetic resonance imaging provides accurate area measurements but is not as widely available in routine clinical practice as CT. Furthermore, it is more expensive and has poorer spatial resolution compared to CT.[394] The CT-based volumetric measurements in our study were highly reproducible. In addition, it is important to note that to the best of our knowledge, our study represents the first investigation using CT phenotyping of fat compartments in twins.

6.4 Structured reporting

The utilization of structured reporting platforms in reading and reporting of coronary CTA findings allows the implementation of automatic classification into medical reporting, which substantially reduces human error and thus improves data integrity.[149] The most widely used classification is coronary CTA reporting is the CAD-RADS scheme, developed by the Society of Cardiovascular Computed Tomography. Our study underlined the use of structured reporting with built in automatic classification algorithms. The CAD-RADS categories were

mis-classified by clinicians in approximately one fifth of the patients.

The implementation of the CAD-RADS multidisciplinary consensus document represents an important step to achieve uniform and consistent coronary CTA reporting using a standardized and simplified terminology. Similar data systems exist in breast, prostate and lung imaging, and studies have verified their ability of standardizing patient management in a practical way.[395-398] Both image interpretation and subsequent reporting can inflict errors in CAD assessment and thus lead to altered clinical decision making. Clinical experience and training of readers ensures the adequate assessment of lesion severity and high-risk plaque morphology and thus reduces interpretation inconsistency. The use of CAD-RADS could result in improved reproducibility for image interpretation although this has not yet been tested. Reporting inconsistency is associated with non-standardized reporting and inconsistent use of nomenclature and classification schemes. The implementation of CAD-RADS in the clinical routine requires proper training in coronary CTA and standardized clinical reporting.

Importantly, CAD-RADS classification might be influenced by reporting inconsistency despite proper image interpretation. Our study design provides a unique opportunity to assess this inconsistency. We have identified several potential pitfalls that could hinder the primary aim of CAD-RADS, namely, to provide consistent CTA reports in a standardized fashion. We demonstrated that approximately one fifth of the patients were misclassified by the readers during reporting. Total agreement between manual and automated classification was 80.2%. Lowest agreement was found for two high-risk feature positive plaques, denoted by modifier V. This could possibly alter patient management and also lead to lower data integrity for research purposes. In addition, we demonstrated that human error might influence further management and decision making up to 16% of the patients, including errors in plaque vulnerability assessment. Although clinicians should still evaluate the patient's individual risk status in addition to the CAD-RADS recommendation in clinical decision making. Structured reporting tools in cardiac imaging have been predominantly implemented to improve data integrity and to establish large databases for research purposes, education and patient care.[399-403] The implementation of automated CAD-RADS calculations in structured reporting platforms has been previously proposed by experts in the field.[242,404] Structured reporting algorithms that are capable of calculating CAD-RADS scores are needed to avoid simple mistakes in classification.

Our work suggests that structured reporting platforms could improve clinical workflow by assisting clinicians in reporting and at the same time significantly reducing errors due to human factors, such as inattention, clinical overload or lack in knowledge. Consequently,

effective communication of coronary CTA results and adequate clinical decision making can be established. Importantly, our study demonstrated that the misclassifications were not caused by the limitations of the common CAD-RADS lexicon, they can rather be attributed to human error. The results of our study could therefore help to develop training programs and software platforms to support the widespread adoption of CAD-RADS based coronary CTA interpretation.

We aimed to further elucidate the role of various factors that might be associated with CAD-RADS misclassification. Interestingly, more experienced readers had more errors in classifying the patients, which is also reflected in the higher number of non-existing CAD-RADS categories. This suggests that consistent CAD-RADS reporting is more influenced by factors that determine individual attention span rather than clinical experience. Nonetheless, we strongly encourage regular training of clinicians to ensure the proper use of CAD-RADS. We detected significant improvement in the agreement of modifier V as a result of training after the first half of the study (50 cases per reader). Importantly, the agreement for other modifiers (N, S and G) was similar throughout the whole study suggesting that these are not related to knowledge in classification but rather to inattention. Attention span is an important determinant of reader's performance and it might be influenced by the clinical workload or by the time of the day. Therefore, we also evaluated the effect of these factors on misclassification rates. However, we found that clinical load reflected by the number of reports or time of the day did not influence reader's performance. Even though automated CAD-RADS classification uses data filled in by the readers, it performs better in determining the CAD-RADS category than the clinical readers by preventing human errors. Structured reporting platforms with automated score calculations might improve data quality and support clinical decision making.

7 Summary of novel scientific findings

1. We showed that intravenous esmolol with a stepwise bolus administration protocol is at least as efficacious as the standard of care metoprolol to achieve the optimal heart rate during coronary CTA. Esmolol allows a safe heart rate control for coronary CTA examination even if it is administered in high doses with a dosage scheme independent of body weight.
2. We have developed a novel four-phasic contrast injection protocol, which resulted in a 65% reduction of the extravasation rate as compared to the conventionally used three-phasic CM injection-protocol in coronary CTA.
3. We demonstrated that the utilization of iterative model reconstruction leads to a significantly improved coronary CTA image quality with improved visualization of the distal vessel segments as compared to the conventional filtered back reconstruction techniques.
4. We showed that coronary CTA of heart transplant recipients is feasible and has a significantly better image quality as compared to a control group with similar heart rates. Our findings suggest that invasive coronary angiography could be replaced by coronary CTA in experienced centers to screen heart transplant recipients for cardiac allograft vasculopathy.
5. We have described a robust *ex vivo* experimental approach for data acquisition, co-registration, and systematic comparison of non-invasive and invasive imaging modalities with the standard of reference (histologic examination).
6. We have identified a novel coronary CTA imaging biomarker of high-risk atherosclerotic plaques and named it as ‘napkin-ring sign’.
7. We demonstrated that the napkin-ring sign has a high specificity and high positive predictive value for the presence of advanced lesions as defined by histology.
8. We showed that the qualitative assessment of the CT attenuation pattern of non-calcified plaque tissue improves diagnostic accuracy of coronary CTA to identify advanced atherosclerotic lesions and thin-cap fibroatheromas using histology as the reference standard.

9. We have demonstrated that various imaging features of plaques are associated with early plaque (normal cross section at coronary CTA and fibrous plaque at OFDI) and advanced plaque (partially calcified plaque at coronary CTA, any calcified plaque at IVUS, and lipid-rich plaque at OFDI).
10. We showed that the overall performance of OFDI for differentiating early from advanced plaque is significantly better than that of IVUS and coronary CT angiography.
11. In a prospective clinical study we have demonstrated that invasive coronary angiography identifies only half as many coronary segments with plaque and underestimates plaque sizes compared to coronary CTA. Therefore, ICA might underestimate patient risk because of the insufficient recognition of nonobstructive plaques.
12. We have developed a novel technique for radiomic analysis of coronary CTA images and demonstrated that coronary plaques consist of sufficient number of voxels to conduct radiomic analysis.
13. We showed that radiomic parameters have a higher diagnostic accuracy in identifying plaques with napkin-ring signs than conventional quantitative measures.
14. In our prospective two-center study we have demonstrated the feasibility of a rapid on-site FFR-CT approach to assess the hemodynamic significance of coronary artery plaque.
15. We have demonstrated that on-site FFR-CT algorithm has a good diagnostic accuracy when compared with the reference standard invasive FFR.
16. We showed that the diagnostic performance of on-site FFR-CT simulation algorithm is robust and does not depend on the readers who adjust the semiautomated lumen segmentation.
17. We showed that among the thoracic fat depots, pericoronary fat is associated with coronary atherosclerosis independently of the standard measures of obesity such as BMI.
18. We described that the association of pericoronary fat quantity with inflammatory biomarkers but not adiponectin (a marker of visceral fat) suggests that while systemic inflammation plays a role in the pathogenesis of coronary atherosclerosis, there are additional local effects that exist.

19. In a classical twin study we demonstrated that genetics have substantial, while environmental factors have only a modest influence on epicardial, subcutaneous and visceral adipose tissue volumes.
20. We showed that common and specific genetic effects may be involved in the heritability of all three adipose tissue quantities.
21. We have developed a structured reporting platform for clinical coronary CTA interpretation that is used in clinical practice at the Heart and Vascular Center of the Semmelweis University.
22. We have demonstrated that the use of structured reporting platforms in reporting coronary CTA findings allows the implementation of automatic classification into medical reporting, which substantially reduces human error and thus improves data integrity

8 References

1. Benjamin EJ, Virani SS, Callaway CW, et al. Heart Disease and Stroke Statistics-2018 Update: A Report From the American Heart Association. *Circulation* 2018; **137**(12): e67-e492.
2. Libby P. Mechanisms of acute coronary syndromes and their implications for therapy. *The New England journal of medicine* 2013; **368**(21): 2004-13.
3. Mathers CD, Loncar D. Projections of global mortality and burden of disease from 2002 to 2030. *PLoS medicine* 2006; **3**(11): e442.
4. Timmis A, Townsend N, Gale C, et al. European Society of Cardiology: Cardiovascular Disease Statistics 2017. *Eur Heart J* 2018; **39**(7): 508-79.
5. Virmani R, Burke AP, Farb A, Kolodgie FD. Pathology of the vulnerable plaque. *J Am Coll Cardiol* 2006; **47**(8 Suppl): C13-8.
6. Virmani R, Kolodgie FD, Burke AP, Farb A, Schwartz SM. Lessons from sudden coronary death: a comprehensive morphological classification scheme for atherosclerotic lesions. *Arterioscler Thromb Vasc Biol* 2000; **20**(5): 1262-75.
7. Arbab-Zadeh A, Fuster V. The Myth of the "Vulnerable Plaque": Transitioning From a Focus on Individual Lesions to Atherosclerotic Disease Burden for Coronary Artery Disease Risk Assessment. *J Am Coll Cardiol* 2015; **65**(8): 846-55.
8. Maurovich-Horvat P. Vulnerábilis koszorúér-plakkok vizsgálata: genomikától a képi markerekig. *Orvosképzés* 2013; **88**(2): 275-7.
9. Schwartz RB, Jones KM, Chernoff DM, et al. Common carotid artery bifurcation: evaluation with spiral CT. Work in progress. *Radiology* 1992; **185**(2): 513-9.
10. Napel S, Marks MP, Rubin GD, et al. CT angiography with spiral CT and maximum intensity projection. *Radiology* 1992; **185**(2): 607-10.
11. Rubin GD, Shiau MC, Schmidt AJ, et al. Computed tomographic angiography: historical perspective and new state-of-the-art using multi detector-row helical computed tomography. *J Comput Assist Tomogr* 1999; **23 Suppl 1**: S83-90.
12. Rubin GD, Shiau MC, Leung AN, Kee ST, Logan LJ, Sofilos MC. Aorta and iliac arteries: single versus multiple detector-row helical CT angiography. *Radiology* 2000; **215**(3): 670-6.
13. Achenbach S, Ulzheimer S, Baum U, et al. Noninvasive coronary angiography by retrospectively ECG-gated multislice spiral CT. *Circulation* 2000; **102**(23): 2823-8.
14. Hu XH, Zheng WL, Wang D, Xie SS, Wu R, Zhang SZ. Accuracy of high-pitch

prospectively ECG-triggering CT coronary angiography for assessment of stenosis in 103 patients: comparison with invasive coronary angiography. *Clin Radiol* 2012; **67**(11): 1083-8.

15. Budoff MJ, Dowe D, Jollis JG, et al. Diagnostic performance of 64-multidetector row coronary computed tomographic angiography for evaluation of coronary artery stenosis in individuals without known coronary artery disease: results from the prospective multicenter ACCURACY (Assessment by Coronary Computed Tomographic Angiography of Individuals Undergoing Invasive Coronary Angiography) trial. *J Am Coll Cardiol* 2008; **52**(21): 1724-32.

16. de Graaf FR, van Velzen JE, de Boer SM, et al. Non-invasive computed tomography coronary angiography as a gatekeeper for invasive coronary angiography. *Int J Cardiovasc Imaging* 2013; **29**(1): 221-8.

17. Shaw LJ, Hausleiter J, Achenbach S, et al. Coronary computed tomographic angiography as a gatekeeper to invasive diagnostic and surgical procedures: results from the multicenter CONFIRM (Coronary CT Angiography Evaluation for Clinical Outcomes: an International Multicenter) registry. *J Am Coll Cardiol* 2012; **60**(20): 2103-14.

18. Achenbach S, Boehmer K, Pflederer T, et al. Influence of slice thickness and reconstruction kernel on the computed tomographic attenuation of coronary atherosclerotic plaque. *J Cardiovasc Comput Tomogr* 2010; **4**(2): 110-5.

19. Achenbach S, Friedrich MG, Nagel E, et al. CV Imaging: What Was New in 2012? *JACC Cardiovascular imaging* 2013; **6**(6): 714-34.

20. Schroeder S, Achenbach S, Bengel F, et al. Cardiac computed tomography: indications, applications, limitations, and training requirements: report of a Writing Group deployed by the Working Group Nuclear Cardiology and Cardiac CT of the European Society of Cardiology and the European Council of Nuclear Cardiology. *Eur Heart J* 2008; **29**(4): 531-56.

21. Stolzmann P, Goetti RP, Maurovich-Horvat P, et al. Predictors of image quality in high-pitch coronary CT angiography. *AJR Am J Roentgenol* 2011; **197**(4): 851-8.

22. Matt D, Scheffel H, Leschka S, et al. Dual-source CT coronary angiography: image quality, mean heart rate, and heart rate variability. *AJR Am J Roentgenol* 2007; **189**(3): 567-73.

23. Abbara S, Blanke P, Maroules CD, et al. SCCT guidelines for the performance and acquisition of coronary computed tomographic angiography: A report of the society of Cardiovascular Computed Tomography Guidelines Committee: Endorsed by the North American Society for Cardiovascular Imaging (NASCI). *J Cardiovasc Comput Tomogr* 2016; **10**(6): 435-49.

24. Mahabadi AA, Achenbach S, Burgstahler C, et al. Safety, efficacy, and indications of beta-adrenergic receptor blockade to reduce heart rate prior to coronary CT angiography.

Radiology 2010; **257**(3): 614-23.

25. Johnson PT, Eng J, Pannu HK, Fishman EK. 64-MDCT angiography of the coronary arteries: nationwide survey of patient preparation practice. *AJR Am J Roentgenol* 2008; **190**(3): 743-7.

26. Wiest D. Esmolol. A review of its therapeutic efficacy and pharmacokinetic characteristics. *Clin Pharmacokinet* 1995; **28**(3): 190-202.

27. Wiest DB, Haney JS. Clinical pharmacokinetics and therapeutic efficacy of esmolol. *Clin Pharmacokinet* 2012; **51**(6): 347-56.

28. Moreno CC, Pinho D, Nelson RC, et al. Lessons learned from 118,970 multidetector computed tomographic intravenous contrast material administrations: impact of catheter dwell time and gauge, catheter location, rate of contrast material administration, and patient age and sex on volume of extravasate. *J Comput Assist Tomogr* 2013; **37**(2): 286-8.

29. Cohan RH, Ellis JH, Garner WL. Extravasation of radiographic contrast material: recognition, prevention, and treatment. *Radiology* 1996; **200**(3): 593-604.

30. Federle MP, Chang PJ, Confer S, Ozgun B. Frequency and effects of extravasation of ionic and nonionic CT contrast media during rapid bolus injection. *Radiology* 1998; **206**(3): 637-40.

31. Wienbeck S, Fischbach R, Kloska SP, et al. Prospective study of access site complications of automated contrast injection with peripheral venous access in MDCT. *AJR Am J Roentgenol* 2010; **195**(4): 825-9.

32. Wang CL, Cohan RH, Ellis JH, Adusumilli S, Dunnick NR. Frequency, management, and outcome of extravasation of nonionic iodinated contrast medium in 69,657 intravenous injections. *Radiology* 2007; **243**(1): 80-7.

33. Shuman WP, Adam JL, Schoenecker SA, Tazioli PR, Moss AA. Use of a power injector during dynamic computed tomography. *J Comput Assist Tomogr* 1986; **10**(6): 1000-2.

34. Behrendt FF, Bruners P, Keil S, et al. Impact of different vein catheter sizes for mechanical power injection in CT: in vitro evaluation with use of a circulation phantom. *Cardiovasc Intervent Radiol* 2009; **32**(1): 25-31.

35. Cademartiri F, de Monye C, Pugliese F, et al. High iodine concentration contrast material for noninvasive multislice computed tomography coronary angiography: iopromide 370 versus iomeprol 400. *Invest Radiol* 2006; **41**(3): 349-53.

36. Dykes TM, Bhargavan-Chatfield M, Dyer RB. Intravenous contrast extravasation during CT: a national data registry and practice quality improvement initiative. *J Am Coll Radiol* 2015; **12**(2): 183-91.

37. Wilson BG. Contrast media-induced compartment syndrome. *Radiol Technol* 2011; **83**(1): 63-77.

38. Shaqdan K, Aran S, Thrall J, Abujudeh H. Incidence of contrast medium extravasation for CT and MRI in a large academic medical centre: a report on 502,391 injections. *Clin Radiol* 2014; **69**(12): 1264-72.

39. Bellin MF, Jakobsen JA, Tomassin I, et al. Contrast medium extravasation injury: guidelines for prevention and management. *Eur Radiol* 2002; **12**(11): 2807-12.

40. Litmanovich D, Zamboni GA, Hauser TH, Lin PJ, Clouse ME, Raptopoulos V. ECG-gated chest CT angiography with 64-MDCT and tri-phasic IV contrast administration regimen in patients with acute non-specific chest pain. *Eur Radiol* 2008; **18**(2): 308-17.

41. Lu JG, Lv B, Chen XB, Tang X, Jiang SL, Dai RP. What is the best contrast injection protocol for 64-row multi-detector cardiac computed tomography? *Eur J Radiol* 2010; **75**(2): 159-65.

42. Lee MS, Chun EJ, Kim KJ, Kim JA, Vembar M, Choi SI. Reproducibility in the assessment of noncalcified coronary plaque with 256-slice multi-detector CT and automated plaque analysis software. *Int J Cardiovasc Imaging* 2010; **26**(Suppl 2): 237-44.

43. Schuhbaeck A, Dey D, Otaki Y, et al. Interscan reproducibility of quantitative coronary plaque volume and composition from CT coronary angiography using an automated method. *Eur Radiol* 2014; **24**(9): 2300-8.

44. Nakazato R, Shalev A, Doh JH, et al. Quantification and characterisation of coronary artery plaque volume and adverse plaque features by coronary computed tomographic angiography: a direct comparison to intravascular ultrasound. *Eur Radiol* 2013; **23**(8): 2109-17.

45. Korn A, Fenchel M, Bender B, et al. Iterative reconstruction in head CT: image quality of routine and low-dose protocols in comparison with standard filtered back-projection. *AJNR Am J Neuroradiol* 2012; **33**(2): 218-24.

46. Noel PB, Fingerle AA, Renger B, Munzel D, Rummeny EJ, Dobritz M. Initial performance characterization of a clinical noise-suppressing reconstruction algorithm for MDCT. *AJR Am J Roentgenol* 2011; **197**(6): 1404-9.

47. Hara AK, Paden RG, Silva AC, Kujak JL, Lawder HJ, Pavlicek W. Iterative reconstruction technique for reducing body radiation dose at CT: feasibility study. *AJR Am J Roentgenol* 2009; **193**(3): 764-71.

48. Gervaise A, Osemont B, Lecocq S, et al. CT image quality improvement using Adaptive Iterative Dose Reduction with wide-volume acquisition on 320-detector CT. *Eur Radiol* 2012;

22(2): 295-301.

49. Hou Y, Liu X, Xv S, Guo W, Guo Q. Comparisons of image quality and radiation dose between iterative reconstruction and filtered back projection reconstruction algorithms in 256-MDCT coronary angiography. *AJR Am J Roentgenol* 2012; **199**(3): 588-94.

50. Takx RA, Willemink MJ, Nathoe HM, et al. The effect of iterative reconstruction on quantitative computed tomography assessment of coronary plaque composition. *Int J Cardiovasc Imaging* 2014; **30**(1): 155-63.

51. Fuchs TA, Fiechter M, Gebhard C, et al. CT coronary angiography: impact of adapted statistical iterative reconstruction (ASIR) on coronary stenosis and plaque composition analysis. *Int J Cardiovasc Imaging* 2013; **29**(3): 719-24.

52. Willemink MJ, de Jong PA, Leiner T, et al. Iterative reconstruction techniques for computed tomography Part 1: technical principles. *Eur Radiol* 2013; **23**(6): 1623-31.

53. Fuchs TA, Stehli J, Bull S, et al. Coronary computed tomography angiography with model-based iterative reconstruction using a radiation exposure similar to chest X-ray examination. *Eur Heart J* 2014; **35**(17): 1131-6.

54. Oda S, Utsunomiya D, Funama Y, et al. A knowledge-based iterative model reconstruction algorithm: can super-low-dose cardiac CT be applicable in clinical settings? *Academic radiology* 2014; **21**(1): 104-10.

55. Szilveszter B, Elzomor H, Karolyi M, et al. The effect of iterative model reconstruction on coronary artery calcium quantification. *Int J Cardiovasc Imaging* 2016; **32**(1): 153-60.

56. Lund LH, Edwards LB, Kucheryavaya AY, et al. The registry of the International Society for Heart and Lung Transplantation: thirty-first official adult heart transplant report--2014; focus theme: retransplantation. *J Heart Lung Transplant* 2014; **33**(10): 996-1008.

57. Park KH, Kwon TG, Matsuzawa Y, et al. Association between the vasa vasorum and the atherosclerotic changes in cardiac allograft vasculopathy: volumetric analysis. *Eur Heart J Cardiovasc Imaging* 2016; **17**(3): 272-9.

58. Mehra MR, Crespo-Leiro MG, Dipchand A, et al. International Society for Heart and Lung Transplantation working formulation of a standardized nomenclature for cardiac allograft vasculopathy-2010. *J Heart Lung Transplant* 2010; **29**(7): 717-27.

59. Costanzo MR, Dipchand A, Starling R, et al. The International Society of Heart and Lung Transplantation Guidelines for the care of heart transplant recipients. *J Heart Lung Transplant* 2010; **29**(8): 914-56.

60. Kolossvary M, Szilveszter B, Edes IF, et al. Comparison of Quantity of Coronary Atherosclerotic Plaques Detected by Computed Tomography Versus Angiography. *Am J*

Cardiol 2016; **117**(12): 1863-7.

61. Badano LP, Miglioranza MH, Edvardsen T, et al. European Association of Cardiovascular Imaging/Cardiovascular Imaging Department of the Brazilian Society of Cardiology recommendations for the use of cardiac imaging to assess and follow patients after heart transplantation. *Eur Heart J Cardiovasc Imaging* 2015.

62. Braunwald E. Epilogue: what do clinicians expect from imagers? *J Am Coll Cardiol* 2006; **47**(8 Suppl): C101-3.

63. Heidenreich PA, Trogdon JG, Khavjou OA, et al. Forecasting the future of cardiovascular disease in the United States: a policy statement from the American Heart Association. *Circulation* 2011; **123**(8): 933-44.

64. Waxman S, Ishibashi F, Muller JE. Detection and treatment of vulnerable plaques and vulnerable patients: novel approaches to prevention of coronary events. *Circulation* 2006; **114**(22): 2390-411.

65. Drobni ZD, Karady J, Maurovich-Horvat P. Szív-CT szerepe a cardiovascularis rizikóbecslésben. *Magyar Családorvosok Lapja* 2015; **5**: 40-2.

66. Burke AP, Farb A, Malcom GT, Liang YH, Smialek J, Virmani R. Coronary risk factors and plaque morphology in men with coronary disease who died suddenly. *N Engl J Med* 1997; **336**(18): 1276-82.

67. Falk E, Nakano M, Bentzon JF, Finn AV, Virmani R. Update on acute coronary syndromes: the pathologists' view. *European heart journal* 2013; **34**(10): 719-28.

68. Finn AV, Nakano M, Narula J, Kolodgie FD, Virmani R. Concept of vulnerable/unstable plaque. *Arterioscler Thromb Vasc Biol* 2010; **30**(7): 1282-92.

69. Narula J, Garg P, Achenbach S, Motoyama S, Virmani R, Strauss HW. Arithmetic of vulnerable plaques for noninvasive imaging. *Nat Clin Pract Cardiovasc Med* 2008; **5 Suppl 2**: S2-10.

70. Ferencik M, Schlett CL, Ghoshhajra BB, et al. A computed tomography-based coronary lesion score to predict acute coronary syndrome among patients with acute chest pain and significant coronary stenosis on coronary computed tomographic angiogram. *The American journal of cardiology* 2012; **110**(2): 183-9.

71. Narula J, Nakano M, Virmani R, et al. Histopathologic characteristics of atherosclerotic coronary disease and implications of the findings for the invasive and noninvasive detection of vulnerable plaques. *Journal of the American College of Cardiology* 2013; **61**(10): 1041-51.

72. Maurovich-Horvat P, Ferencik M, Voros S, Merkely B, Hoffmann U. Comprehensive plaque assessment by coronary CT angiography. *Nature reviews Cardiology* 2014; **11**(7): 390-

402.

73. Achenbach S. Can CT detect the vulnerable coronary plaque? *Int J Cardiovasc Imaging* 2008; **24**(3): 311-2.

74. Kolodgie FD, Burke AP, Farb A, et al. The thin-cap fibroatheroma: a type of vulnerable plaque: the major precursor lesion to acute coronary syndromes. *Current opinion in cardiology* 2001; **16**(5): 285-92.

75. van der Giessen AG, Toepker MH, Donelly PM, et al. Reproducibility, accuracy, and predictors of accuracy for the detection of coronary atherosclerotic plaque composition by computed tomography: an ex vivo comparison to intravascular ultrasound. *Invest Radiol* 2010; **45**(11): 693-701.

76. Hoffmann U, Ferencik M, Cury RC, Pena AJ. Coronary CT angiography. *J Nucl Med* 2006; **47**(5): 797-806.

77. Achenbach S, Moselewski F, Ropers D, et al. Detection of calcified and noncalcified coronary atherosclerotic plaque by contrast-enhanced, submillimeter multidetector spiral computed tomography: a segment-based comparison with intravascular ultrasound. *Circulation* 2004; **109**(1): 14-7.

78. Becker CR, Knez A, Ohnesorge B, Schoepf UJ, Reiser MF. Imaging of noncalcified coronary plaques using helical CT with retrospective ECG gating. *AJR Am J Roentgenol* 2000; **175**(2): 423-4.

79. Pohle K, Achenbach S, Macneill B, et al. Characterization of non-calcified coronary atherosclerotic plaque by multi-detector row CT: comparison to IVUS. *Atherosclerosis* 2007; **190**(1): 174-80.

80. Voros S, Rinehart S, Qian Z, et al. Coronary atherosclerosis imaging by coronary CT angiography: current status, correlation with intravascular interrogation and meta-analysis. *JACC Cardiovasc Imaging* 2011; **4**(5): 537-48.

81. Marwan M, Taher MA, El Meniawy K, et al. In vivo CT detection of lipid-rich coronary artery atherosclerotic plaques using quantitative histogram analysis: a head to head comparison with IVUS. *Atherosclerosis* 2011; **215**(1): 110-5.

82. Schlett CL, Ferencik M, Celeng C, et al. How to assess non-calcified plaque in CT angiography: delineation methods affect diagnostic accuracy of low-attenuation plaque by CT for lipid-core plaque in histology. *Eur Heart J Cardiovasc Imaging* 2013; **14**(11): 1099-105.

83. Ito T, Terashima M, Kaneda H, et al. Comparison of in vivo assessment of vulnerable plaque by 64-slice multislice computed tomography versus optical coherence tomography. *Am J Cardiol* 2011; **107**(9): 1270-7.

84. Kashiwagi M, Tanaka A, Kitabata H, et al. Feasibility of noninvasive assessment of thin-cap fibroatheroma by multidetector computed tomography. *JACC Cardiovasc Imaging* 2009; **2**(12): 1412-9.

85. Cademartiri F, Mollet NR, Runza G, et al. Influence of intracoronary attenuation on coronary plaque measurements using multislice computed tomography: observations in an ex vivo model of coronary computed tomography angiography. *Eur Radiol* 2005; **15**(7): 1426-31.

86. Ferencik M, Chan RC, Achenbach S, et al. Arterial wall imaging: evaluation with 16-section multidetector CT in blood vessel phantoms and ex vivo coronary arteries. *Radiology* 2006; **240**(3): 708-16.

87. Suzuki S, Furui S, Kuwahara S, et al. Accuracy of attenuation measurement of vascular wall in vitro on computed tomography angiography: Effect of wall thickness, density of contrast medium, and measurement point. *Invest Radiol* 2006; **41**(6): 510-5.

88. Boogers MJ, Broersen A, van Velzen JE, et al. Automated quantification of coronary plaque with computed tomography: comparison with intravascular ultrasound using a dedicated registration algorithm for fusion-based quantification. *Eur Heart J* 2012; **33**(8): 1007-16.

89. Dey D, Schepis T, Marwan M, Slomka PJ, Berman DS, Achenbach S. Automated three-dimensional quantification of noncalcified coronary plaque from coronary CT angiography: comparison with intravascular US. *Radiology* 2010; **257**(2): 516-22.

90. Motoyama S, Kondo T, Sarai M, et al. Multislice computed tomographic characteristics of coronary lesions in acute coronary syndromes. *J Am Coll Cardiol* 2007; **50**(4): 319-26.

91. Ozaki Y, Okumura M, Ismail TF, et al. Coronary CT angiographic characteristics of culprit lesions in acute coronary syndromes not related to plaque rupture as defined by optical coherence tomography and angioscopy. *Eur Heart J* 2011; **32**(22): 2814-23.

92. Pflederer T, Marwan M, Schepis T, et al. Characterization of culprit lesions in acute coronary syndromes using coronary dual-source CT angiography. *Atherosclerosis* 2010; **211**(2): 437-44.

93. Kim SY, Kim KS, Seung MJ, et al. The culprit lesion score on multi-detector computed tomography can detect vulnerable coronary artery plaque. *Int J Cardiovasc Imaging* 2010; **26**(Suppl 2): 245-52.

94. Kitagawa T, Yamamoto H, Horiguchi J, et al. Characterization of noncalcified coronary plaques and identification of culprit lesions in patients with acute coronary syndrome by 64-slice computed tomography. *JACC Cardiovasc Imaging* 2009; **2**(2): 153-60.

95. Narula J, Strauss HW. The popcorn plaques. *Nat Med* 2007; **13**(5): 532-4.

96. Glagov S, Weisenberg E, Zarins CK, Stankunavicius R, Kolettis GJ. Compensatory

enlargement of human atherosclerotic coronary arteries. *N Engl J Med* 1987; **316**(22): 1371-5.

97. Varnava AM, Mills PG, Davies MJ. Relationship between coronary artery remodeling and plaque vulnerability. *Circulation* 2002; **105**(8): 939-43.

98. Moselewski F, Ropers D, Pohle K, et al. Comparison of measurement of cross-sectional coronary atherosclerotic plaque and vessel areas by 16-slice multidetector computed tomography versus intravascular ultrasound. *Am J Cardiol* 2004; **94**(10): 1294-7.

99. Gauss S, Achenbach S, Pflederer T, Schuhback A, Daniel WG, Marwan M. Assessment of coronary artery remodelling by dual-source CT: a head-to-head comparison with intravascular ultrasound. *Heart* 2011; **97**(12): 991-7.

100. Kroner ES, van Velzen JE, Boogers MJ, et al. Positive remodeling on coronary computed tomography as a marker for plaque vulnerability on virtual histology intravascular ultrasound. *Am J Cardiol* 2011; **107**(12): 1725-9.

101. Hoffmann U, Moselewski F, Nieman K, et al. Noninvasive assessment of plaque morphology and composition in culprit and stable lesions in acute coronary syndrome and stable lesions in stable angina by multidetector computed tomography. *J Am Coll Cardiol* 2006; **47**(8): 1655-62.

102. Motoyama S, Sarai M, Harigaya H, et al. Computed tomographic angiography characteristics of atherosclerotic plaques subsequently resulting in acute coronary syndrome. *J Am Coll Cardiol* 2009; **54**(1): 49-57.

103. Stone GW, Maehara A, Lansky AJ, et al. A prospective natural-history study of coronary atherosclerosis. *The New England journal of medicine* 2011; **364**(3): 226-35.

104. Otsuka F, Finn AV, Virmani R. Do vulnerable and ruptured plaques hide in heavily calcified arteries? *Atherosclerosis* 2013; **229**(1): 34-7.

105. Greenland P, LaBree L, Azen SP, Doherty TM, Detrano RC. Coronary artery calcium score combined with Framingham score for risk prediction in asymptomatic individuals. *JAMA* 2004; **291**(2): 210-5.

106. Taylor AJ, Bindeman J, Feuerstein I, Cao F, Brazaitis M, O'Malley PG. Coronary calcium independently predicts incident premature coronary heart disease over measured cardiovascular risk factors: mean three-year outcomes in the Prospective Army Coronary Calcium (PACC) project. *J Am Coll Cardiol* 2005; **46**(5): 807-14.

107. Maurovich-Horvat P. The left main stem: The barometer of coronary artery disease severity? *J Cardiovasc Comput Tomogr* 2018; **12**(3): 238-9.

108. Huang H, Virmani R, Younis H, Burke AP, Kamm RD, Lee RT. The impact of calcification on the biomechanical stability of atherosclerotic plaques. *Circulation* 2001;

103(8): 1051-6.

109. Maldonado N, Kelly-Arnold A, Vengrenyuk Y, et al. A mechanistic analysis of the role of microcalcifications in atherosclerotic plaque stability: potential implications for plaque rupture. *American journal of physiology Heart and circulatory physiology* 2012; **303**(5): H619-28.

110. Mauriello A, Servadei F, Zoccai GB, et al. Coronary calcification identifies the vulnerable patient rather than the vulnerable Plaque. *Atherosclerosis* 2013; **229**(1): 124-9.

111. Burke AP, Weber DK, Kolodgie FD, Farb A, Taylor AJ, Virmani R. Pathophysiology of calcium deposition in coronary arteries. *Herz* 2001; **26**(4): 239-44.

112. Kataoka Y, Wolski K, Uno K, et al. Spotty calcification as a marker of accelerated progression of coronary atherosclerosis: insights from serial intravascular ultrasound. *J Am Coll Cardiol* 2012; **59**(18): 1592-7.

113. Ehara S, Kobayashi Y, Yoshiyama M, et al. Spotty calcification typifies the culprit plaque in patients with acute myocardial infarction: an intravascular ultrasound study. *Circulation* 2004; **110**(22): 3424-9.

114. van Velzen JE, de Graaf FR, de Graaf MA, et al. Comprehensive assessment of spotty calcifications on computed tomography angiography: comparison to plaque characteristics on intravascular ultrasound with radiofrequency backscatter analysis. *Journal of nuclear cardiology : official publication of the American Society of Nuclear Cardiology* 2011; **18**(5): 893-903.

115. Joshi NV, Vesey AT, Williams MC, et al. F-fluoride positron emission tomography for identification of ruptured and high-risk coronary atherosclerotic plaques: a prospective clinical trial. *Lancet* 2013.

116. Mancini GB, Hartigan PM, Shaw LJ, et al. Predicting outcome in the COURAGE trial (Clinical Outcomes Utilizing Revascularization and Aggressive Drug Evaluation): coronary anatomy versus ischemia. *JACC Cardiovascular interventions* 2014; **7**(2): 195-201.

117. Bittencourt MS, Hulten E, Ghoshhajra B, et al. Prognostic value of nonobstructive and obstructive coronary artery disease detected by coronary computed tomography angiography to identify cardiovascular events. *Circ Cardiovasc Imaging* 2014; **7**(2): 282-91.

118. Min JK, Shaw LJ, Devereux RB, et al. Prognostic value of multidetector coronary computed tomographic angiography for prediction of all-cause mortality. *J Am Coll Cardiol* 2007; **50**(12): 1161-70.

119. Hadamitzky M, Achenbach S, Al-Mallah M, et al. Optimized prognostic score for coronary computed tomographic angiography: results from the CONFIRM registry (COronary

CT Angiography EvaluatioN For Clinical Outcomes: An InteRnational Multicenter Registry). *J Am Coll Cardiol* 2013; **62**(5): 468-76.

120. Andreini D, Pontone G, Mushtaq S, et al. A long-term prognostic value of coronary CT angiography in suspected coronary artery disease. *JACC Cardiovasc Imaging* 2012; **5**(7): 690-701.

121. Dougoud S, Fuchs TA, Stehli J, et al. Prognostic value of coronary CT angiography on long-term follow-up of 6.9 years. *Int J Cardiovasc Imaging* 2014; **30**(5): 969-76.

122. Hadamitzky M, Taubert S, Deseive S, et al. Prognostic value of coronary computed tomography angiography during 5 years of follow-up in patients with suspected coronary artery disease. *Eur Heart J* 2013; **34**(42): 3277-85.

123. Al-Mallah MH. Does coronary CT angiography improve risk stratification over coronary artery calcium scoring in symptomatic patients with a low pre-test probability of coronary artery disease and a CAC of zero? Reply. *Eur Heart J Cardiovasc Imaging* 2014; **15**(2): 232-3.

124. Min JK, Dunning A, Lin FY, et al. Age- and sex-related differences in all-cause mortality risk based on coronary computed tomography angiography findings results from the International Multicenter CONFIRM (Coronary CT Angiography Evaluation for Clinical Outcomes: An International Multicenter Registry) of 23,854 patients without known coronary artery disease. *J Am Coll Cardiol* 2011; **58**(8): 849-60.

125. Lin FY, Shaw LJ, Dunning AM, et al. Mortality risk in symptomatic patients with nonobstructive coronary artery disease: a prospective 2-center study of 2,583 patients undergoing 64-detector row coronary computed tomographic angiography. *J Am Coll Cardiol* 2011; **58**(5): 510-9.

126. Mark DB, Nelson CL, Califf RM, et al. Continuing evolution of therapy for coronary artery disease. Initial results from the era of coronary angioplasty. *Circulation* 1994; **89**(5): 2015-25.

127. Miller JM, Rochitte CE, Dewey M, et al. Diagnostic performance of coronary angiography by 64-row CT. *N Engl J Med* 2008; **359**(22): 2324-36.

128. Maurovich-Horvat P. The whole is more than the sum of its parts-Aristotle. *Eur Heart J Cardiovasc Imaging* 2017; **18**(3): 294-5.

129. Kolossvary M, Szilveszter B, Merkely B, Maurovich-Horvat P. Plaque imaging with CT-a comprehensive review on coronary CT angiography based risk assessment. *Cardiovascular diagnosis and therapy* 2017; **7**(5): 489-506.

130. Min JK, Dunning A, Lin FY, et al. Rationale and design of the CONFIRM (COronary

CT Angiography EvaluatioN For Clinical Outcomes: An InteRnational Multicenter) Registry. *J Cardiovasc Comput Tomogr* 2011; **5**(2): 84-92.

131. Expert Panel on Detection E, Treatment of High Blood Cholesterol in A. Executive Summary of The Third Report of The National Cholesterol Education Program (NCEP) Expert Panel on Detection, Evaluation, And Treatment of High Blood Cholesterol In Adults (Adult Treatment Panel III). *JAMA* 2001; **285**(19): 2486-97.

132. Wilson PW, D'Agostino RB, Levy D, Belanger AM, Silbershatz H, Kannel WB. Prediction of coronary heart disease using risk factor categories. *Circulation* 1998; **97**(18): 1837-47.

133. Morise AP, Jalisi F. Evaluation of pretest and exercise test scores to assess all-cause mortality in unselected patients presenting for exercise testing with symptoms of suspected coronary artery disease. *J Am Coll Cardiol* 2003; **42**(5): 842-50.

134. Austen WG, Edwards JE, Frye RL, et al. A reporting system on patients evaluated for coronary artery disease. Report of the Ad Hoc Committee for Grading of Coronary Artery Disease, Council on Cardiovascular Surgery, American Heart Association. *Circulation* 1975; **51**(4 Suppl): 5-40.

135. Genc Y, Gokmen D, Tuccar E, Yagmurlu B. Estimation of Sensitivity and Specificity for Clustered Data. *Turk J Med Sci* 2004; **35**: 21-4.

136. Kalbfleisch H, Hort W. Quantitative study on the size of coronary artery supplying areas postmortem. *Am Heart J* 1977; **94**(2): 183-8.

137. Leaman DM, Brower RW, Meester GT, Serruys P, van den Brand M. Coronary artery atherosclerosis: severity of the disease, severity of angina pectoris and compromised left ventricular function. *Circulation* 1981; **63**(2): 285-99.

138. de Araujo Goncalves P, Garcia-Garcia HM, Dores H, et al. Coronary computed tomography angiography-adapted Leaman score as a tool to noninvasively quantify total coronary atherosclerotic burden. *Int J Cardiovasc Imaging* 2013; **29**(7): 1575-84.

139. Chow BJ, Small G, Yam Y, et al. Incremental prognostic value of cardiac computed tomography in coronary artery disease using CONFIRM: COroNary computed tomography angiography evaluation for clinical outcomes: an InteRnational Multicenter registry. *Circ Cardiovasc Imaging* 2011; **4**(5): 463-72.

140. Mushtaq S, De Araujo Goncalves P, Garcia-Garcia HM, et al. Long-term prognostic effect of coronary atherosclerotic burden: validation of the computed tomography-Leaman score. *Circ Cardiovasc Imaging* 2015; **8**(2): e002332.

141. Serruys PW, Morice MC, Kappetein AP, et al. Percutaneous coronary intervention

versus coronary-artery bypass grafting for severe coronary artery disease. *N Engl J Med* 2009; **360**(10): 961-72.

142. Serruys PW, Unger F, van Hout BA, et al. The ARTS study (Arterial Revascularization Therapies Study). *Semin Interv Cardiol* 1999; **4**(4): 209-19.

143. Ryan TJ, Faxon DP, Gunnar RM, et al. Guidelines for percutaneous transluminal coronary angioplasty. A report of the American College of Cardiology/American Heart Association Task Force on Assessment of Diagnostic and Therapeutic Cardiovascular Procedures (Subcommittee on Percutaneous Transluminal Coronary Angioplasty). *Circulation* 1988; **78**(2): 486-502.

144. Hamburger JN, Serruys PW, Scabra-Gomes R, et al. Recanalization of total coronary occlusions using a laser guidewire (the European TOTAL Surveillance Study). *Am J Cardiol* 1997; **80**(11): 1419-23.

145. Topol EJ. Textbook of interventional cardiology. 4th ed. Philadelphia: Saunders; 2003.

146. Lefevre T, Louvard Y, Morice MC, et al. Stenting of bifurcation lesions: classification, treatments, and results. *Catheter Cardiovasc Interv* 2000; **49**(3): 274-83.

147. Suh YJ, Hong YJ, Lee HJ, et al. Prognostic value of SYNTAX score based on coronary computed tomography angiography. *Int J Cardiol* 2015; **199**: 460-6.

148. Farooq V, van Klaveren D, Steyerberg EW, et al. Anatomical and clinical characteristics to guide decision making between coronary artery bypass surgery and percutaneous coronary intervention for individual patients: development and validation of SYNTAX score II. *Lancet* 2013; **381**(9867): 639-50.

149. Bagyura Z, Kolossvary M, Merkely B, Maurovich-Horvat P. [Computer tomography examination of the coronary system - National Plaque Registry and Database, Hungary]. *Orv Hetil* 2017; **158**(3): 106-10.

150. Szilveszter B, Kolossvary M, Karady J, et al. Structured reporting platform improves CAD-RADS assessment. *J Cardiovasc Comput Tomogr* 2017; **11**(6): 449-54.

151. Blackmon KN, Streck J, Thilo C, Bastarrika G, Costello P, Schoepf UJ. Reproducibility of automated noncalcified coronary artery plaque burden assessment at coronary CT angiography. *Journal of thoracic imaging* 2009; **24**(2): 96-102.

152. Brodoefel H, Burgstahler C, Sabir A, et al. Coronary plaque quantification by voxel analysis: dual-source MDCT angiography versus intravascular sonography. *AJR Am J Roentgenol* 2009; **192**(3): W84-9.

153. Klass O, Kleinhans S, Walker MJ, et al. Coronary plaque imaging with 256-slice multidetector computed tomography: interobserver variability of volumetric lesion parameters

with semiautomatic plaque analysis software. *Int J Cardiovasc Imaging* 2010; **26**(6): 711-20.

154. Oberoi S, Meinel FG, Schoepf UJ, et al. Reproducibility of Noncalcified Coronary Artery Plaque Burden Quantification From Coronary CT Angiography Across Different Image Analysis Platforms. *AJR Am J Roentgenol* 2014; **202**(1): W43-9.

155. Madder RD, Chinnaiyan KM, Marandici AM, Goldstein JA. Features of disrupted plaques by coronary computed tomographic angiography: correlates with invasively proven complex lesions. *Circ Cardiovasc Imaging* 2011; **4**(2): 105-13.

156. Versteylen MO, Kietselaer BL, Dagnelie PC, et al. Additive value of semiautomated quantification of coronary artery disease using cardiac computed tomographic angiography to predict future acute coronary syndrome. *Journal of the American College of Cardiology* 2013; **61**(22): 2296-305.

157. Kristensen TS, Kofoed KF, Kuhl JT, Nielsen WB, Nielsen MB, Kelbaek H. Prognostic implications of nonobstructive coronary plaques in patients with non-ST-segment elevation myocardial infarction: a multidetector computed tomography study. *J Am Coll Cardiol* 2011; **58**(5): 502-9.

158. Papadopoulou SL, Neefjes LA, Garcia-Garcia HM, et al. Natural history of coronary atherosclerosis by multislice computed tomography. *JACC Cardiovasc Imaging* 2012; **5**(3 Suppl): S28-37.

159. Kolossvary M, Kellermayer M, Merkely B, Maurovich-Horvat P. Cardiac Computed Tomography Radiomics: A Comprehensive Review on Radiomic Techniques. *Journal of thoracic imaging* 2017.

160. Caro CG, Fitz-Gerald JM, Schroter RC. Arterial wall shear and distribution of early atheroma in man. *Nature* 1969; **223**(5211): 1159-60.

161. Friedman MH, Bargeron CB, Deters OJ, Hutchins GM, Mark FF. Correlation between wall shear and intimal thickness at a coronary artery branch. *Atherosclerosis* 1987; **68**(1-2): 27-33.

162. Koskinas KC, Feldman CL, Chatzizisis YS, et al. Natural history of experimental coronary atherosclerosis and vascular remodeling in relation to endothelial shear stress: a serial, in vivo intravascular ultrasound study. *Circulation* 2010; **121**(19): 2092-101.

163. Wentzel JJ, Chatzizisis YS, Gijsen FJ, Giannoglou GD, Feldman CL, Stone PH. Endothelial shear stress in the evolution of coronary atherosclerotic plaque and vascular remodelling: current understanding and remaining questions. *Cardiovasc Res* 2012; **96**(2): 234-43.

164. Chatzizisis YS, Coskun AU, Jonas M, Edelman ER, Feldman CL, Stone PH. Role of

endothelial shear stress in the natural history of coronary atherosclerosis and vascular remodeling: molecular, cellular, and vascular behavior. *J Am Coll Cardiol* 2007; **49**(25): 2379-93.

165. Fukumoto Y, Hiro T, Fujii T, et al. Localized elevation of shear stress is related to coronary plaque rupture: a 3-dimensional intravascular ultrasound study with in-vivo color mapping of shear stress distribution. *J Am Coll Cardiol* 2008; **51**(6): 645-50.

166. Samady H, Eshtehardi P, McDaniel MC, et al. Coronary artery wall shear stress is associated with progression and transformation of atherosclerotic plaque and arterial remodeling in patients with coronary artery disease. *Circulation* 2011; **124**(7): 779-88.

167. Slager CJ, Wentzel JJ, Gijsen FJ, et al. The role of shear stress in the destabilization of vulnerable plaques and related therapeutic implications. *Nat Clin Pract Cardiovasc Med* 2005; **2**(9): 456-64.

168. Falk E, Shah PK, Fuster V. Coronary plaque disruption. *Circulation* 1995; **92**(3): 657-71.

169. Puri R, Nicholls SJ, Ellis SG, Tuzcu EM, Kapadia SR. High-Risk Coronary Atheroma - The Interplay between Ischemia, Plaque Burden and Disease Progression. *J Am Coll Cardiol* 2013.

170. Hachamovitch R, Berman DS, Shaw LJ, et al. Incremental prognostic value of myocardial perfusion single photon emission computed tomography for the prediction of cardiac death: differential stratification for risk of cardiac death and myocardial infarction. *Circulation* 1998; **97**(6): 535-43.

171. Shaw LJ, Berman DS, Maron DJ, et al. Optimal medical therapy with or without percutaneous coronary intervention to reduce ischemic burden: results from the Clinical Outcomes Utilizing Revascularization and Aggressive Drug Evaluation (COURAGE) trial nuclear substudy. *Circulation* 2008; **117**(10): 1283-91.

172. Fearon WF. Is a myocardial infarction more likely to result from a mild coronary lesion or an ischemia-producing one? *Circulation Cardiovascular interventions* 2011; **4**(6): 539-41.

173. Fihn SD, Gardin JM, Abrams J, et al. 2012 ACCF/AHA/ACP/AATS/PCNA/SCAI/STS Guideline for the diagnosis and management of patients with stable ischemic heart disease: a report of the American College of Cardiology Foundation/American Heart Association Task Force on Practice Guidelines, and the American College of Physicians, American Association for Thoracic Surgery, Preventive Cardiovascular Nurses Association, Society for Cardiovascular Angiography and Interventions, and Society of Thoracic Surgeons. *J Am Coll Cardiol* 2012; **60**(24): e44-e164.

174. Giannopoulos AA, Mitsouras D, Bartykowszki A, et al. High-Risk Plaque Regression and Stabilization: Hybrid Noninvasive Morphological and Hemodynamic Assessment. *Circ Cardiovasc Imaging* 2018; **11**(7): e007888.

175. Kim HJ, Vignon-Clementel IE, Coogan JS, Figueroa CA, Jansen KE, Taylor CA. Patient-specific modeling of blood flow and pressure in human coronary arteries. *Annals of biomedical engineering* 2010; **38**(10): 3195-209.

176. Taylor CA, Fonte TA, Min JK. Computational fluid dynamics applied to cardiac computed tomography for noninvasive quantification of fractional flow reserve: scientific basis. *Journal of the American College of Cardiology* 2013; **61**(22): 2233-41.

177. Slager CJ, Wentzel JJ, Gijsen FJ, et al. The role of shear stress in the generation of rupture-prone vulnerable plaques. *Nat Clin Pract Cardiovasc Med* 2005; **2**(8): 401-7.

178. Brooks AR, Lelkes PI, Rubanyi GM. Gene expression profiling of human aortic endothelial cells exposed to disturbed flow and steady laminar flow. *Physiological genomics* 2002; **9**(1): 27-41.

179. Gimbrone MA, Jr., Topper JN, Nagel T, Anderson KR, Garcia-Cardena G. Endothelial dysfunction, hemodynamic forces, and atherogenesis. *Annals of the New York Academy of Sciences* 2000; **902**: 230-9; discussion 9-40.

180. Malek AM, Alper SL, Izumo S. Hemodynamic shear stress and its role in atherosclerosis. *JAMA : the journal of the American Medical Association* 1999; **282**(21): 2035-42.

181. Chatzizisis YS, Baker AB, Sukhova GK, et al. Augmented expression and activity of extracellular matrix-degrading enzymes in regions of low endothelial shear stress colocalize with coronary atheromata with thin fibrous caps in pigs. *Circulation* 2011; **123**(6): 621-30.

182. Koskinas KC, Chatzizisis YS, Papafaklis MI, et al. Synergistic effect of local endothelial shear stress and systemic hypercholesterolemia on coronary atherosclerotic plaque progression and composition in pigs. *Int J Cardiol* 2013; **169**(6): 394-401.

183. Stone PH, Saito S, Takahashi S, et al. Prediction of progression of coronary artery disease and clinical outcomes using vascular profiling of endothelial shear stress and arterial plaque characteristics: the PREDICTION Study. *Circulation* 2012; **126**(2): 172-81.

184. Ramkumar PG, Mitsouras D, Feldman CL, Stone PH, Rybicki FJ. New advances in cardiac computed tomography. *Current opinion in cardiology* 2009; **24**(6): 596-603.

185. Frauenfelder T, Boutsianis E, Schertler T, et al. In-vivo flow simulation in coronary arteries based on computed tomography datasets: feasibility and initial results. *Eur Radiol* 2007; **17**(5): 1291-300.

186. Jin S, Yang Y, Oshinski J, Tannenbaum A, Gruden J, Giddens D. Flow patterns and wall shear stress distributions at atherosclerotic-prone sites in a human left coronary artery--an exploration using combined methods of CT and computational fluid dynamics. *Conference proceedings : Annual International Conference of the IEEE Engineering in Medicine and Biology Society IEEE Engineering in Medicine and Biology Society Conference* 2004; **5**: 3789-91.

187. Borkin MA, Gajos KZ, Peters A, et al. Evaluation of artery visualizations for heart disease diagnosis. *IEEE transactions on visualization and computer graphics* 2011; **17**(12): 2479-88.

188. Gijsen FJ, Schuurbiers JC, van de Giessen AG, Schaap M, van der Steen AF, Wentzel JJ. 3D reconstruction techniques of human coronary bifurcations for shear stress computations. *Journal of biomechanics* 2014; **47**(1): 39-43.

189. Rikhtegar F, Knight JA, Olgac U, et al. Choosing the optimal wall shear parameter for the prediction of plaque location-A patient-specific computational study in human left coronary arteries. *Atherosclerosis* 2012; **221**(2): 432-7.

190. Bech GJ, De Bruyne B, Pijls NH, et al. Fractional flow reserve to determine the appropriateness of angioplasty in moderate coronary stenosis: a randomized trial. *Circulation* 2001; **103**(24): 2928-34.

191. Gijsen FJ, Wentzel JJ, Thury A, et al. Strain distribution over plaques in human coronary arteries relates to shear stress. *American journal of physiology Heart and circulatory physiology* 2008; **295**(4): H1608-14.

192. Yong AS, Pennings GJ, Chang M, et al. Intracoronary shear-related up-regulation of platelet P-selectin and platelet-monocyte aggregation despite the use of aspirin and clopidogrel. *Blood* 2011; **117**(1): 11-20.

193. Versteeg D, Hoefer IE, Schoneveld AH, et al. Monocyte toll-like receptor 2 and 4 responses and expression following percutaneous coronary intervention: association with lesion stenosis and fractional flow reserve. *Heart* 2008; **94**(6): 770-6.

194. Gaur S, Ovrehus KA, Dey D, et al. Coronary plaque quantification and fractional flow reserve by coronary computed tomography angiography identify ischaemia-causing lesions. *Eur Heart J* 2016; **37**(15): 1220-7.

195. Driessen RS, Stuijfzand WJ, Raijmakers PG, et al. Effect of Plaque Burden and Morphology on Myocardial Blood Flow and Fractional Flow Reserve. *J Am Coll Cardiol* 2018; **71**(5): 499-509.

196. Ahmadi A, Leipsic J, Ovrehus KA, et al. Lesion-Specific and Vessel-Related

Determinants of Fractional Flow Reserve Beyond Coronary Artery Stenosis. *JACC Cardiovasc Imaging* 2018; **11**(4): 521-30.

197. Tesche C, De Cecco CN, Caruso D, et al. Coronary CT angiography derived morphological and functional quantitative plaque markers correlated with invasive fractional flow reserve for detecting hemodynamically significant stenosis. *J Cardiovasc Comput Tomogr* 2016; **10**(3): 199-206.

198. Muller O, Mangiacapra F, Ntalianis A, et al. Long-term follow-up after fractional flow reserve-guided treatment strategy in patients with an isolated proximal left anterior descending coronary artery stenosis. *JACC Cardiovascular interventions* 2011; **4**(11): 1175-82.

199. Koo BK, Erglis A, Doh JH, et al. Diagnosis of ischemia-causing coronary stenoses by noninvasive fractional flow reserve computed from coronary computed tomographic angiograms. Results from the prospective multicenter DISCOVER-FLOW (Diagnosis of Ischemia-Causing Stenoses Obtained Via Noninvasive Fractional Flow Reserve) study. *J Am Coll Cardiol* 2011; **58**(19): 1989-97.

200. Min JK, Leipsic J, Pencina MJ, et al. Diagnostic accuracy of fractional flow reserve from anatomic CT angiography. *JAMA : the journal of the American Medical Association* 2012; **308**(12): 1237-45.

201. Norgaard BL, Leipsic J, Gaur S, et al. Diagnostic performance of noninvasive fractional flow reserve derived from coronary computed tomography angiography in suspected coronary artery disease: the NXT trial (Analysis of Coronary Blood Flow Using CT Angiography: Next Steps). *J Am Coll Cardiol* 2014; **63**(12): 1145-55.

202. Douglas PS, Pontone G, Hlatky MA, et al. Clinical outcomes of fractional flow reserve by computed tomographic angiography-guided diagnostic strategies vs. usual care in patients with suspected coronary artery disease: the prospective longitudinal trial of FFR(CT): outcome and resource impacts study. *Eur Heart J* 2015; **36**(47): 3359-67.

203. Hlatky MA, De Bruyne B, Pontone G, et al. Quality-of-Life and Economic Outcomes of Assessing Fractional Flow Reserve With Computed Tomography Angiography: PLATFORM. *J Am Coll Cardiol* 2015; **66**(21): 2315-23.

204. Douglas PS, De Bruyne B, Pontone G, et al. 1-Year Outcomes of FFRCT-Guided Care in Patients With Suspected Coronary Disease: The PLATFORM Study. *J Am Coll Cardiol* 2016; **68**(5): 435-45.

205. Coenen A, Lubbers MM, Kurata A, et al. Fractional flow reserve computed from noninvasive CT angiography data: diagnostic performance of an on-site clinician-operated computational fluid dynamics algorithm. *Radiology* 2015; **274**(3): 674-83.

206. De Geer J, Sandstedt M, Bjorkholm A, et al. Software-based on-site estimation of fractional flow reserve using standard coronary CT angiography data. *Acta Radiol* 2016; **57**(10): 1186-92.

207. Coenen A, Lubbers MM, Kurata A, et al. Coronary CT angiography derived fractional flow reserve: Methodology and evaluation of a point of care algorithm. *J Cardiovasc Comput Tomogr* 2016; **10**(2): 105-13.

208. Yang DH, Kim YH, Roh JH, et al. Diagnostic performance of on-site CT-derived fractional flow reserve versus CT perfusion. *Eur Heart J Cardiovasc Imaging* 2016.

209. Kim KH, Doh JH, Koo BK, et al. A Novel Noninvasive Technology for Treatment Planning Using Virtual Coronary Stenting and Computed Tomography-Derived Computed Fractional Flow Reserve. *JACC Cardiovascular interventions* 2013.

210. Van Gaal LF, Mertens IL, De Block CE. Mechanisms linking obesity with cardiovascular disease. *Nature* 2006; **444**(7121): 875-80.

211. Rocha VZ, Libby P. Obesity, inflammation, and atherosclerosis. *Nature reviews Cardiology* 2009; **6**(6): 399-409.

212. Kang SJ, Kim D, Park HE, et al. Visceral adipose tissue area is associated with coronary stenosis and noncalcified plaques. *Int J Obes (Lond)* 2014; **38**(2): 272-8.

213. Iacobellis G. Local and systemic effects of the multifaceted epicardial adipose tissue depot. *Nature reviews Endocrinology* 2015; **11**(6): 363-71.

214. Iacobellis G, Malavazos AE, Corsi MM. Epicardial fat: from the biomolecular aspects to the clinical practice. *Int J Biochem Cell Biol* 2011; **43**(12): 1651-4.

215. Nagy E, Jermendy AL, Merkely B, Maurovich-Horvat P. Clinical importance of epicardial adipose tissue. *Arch Med Sci* 2017; **13**(4): 864-74.

216. Drobni ZD, Kolossvary M, Karady J, et al. Van-e összefüggés az epikardiális zsírszövet és a koszorúér-betegség között? *Cardiologia Hungarica* 2017; **47**(1): 25-9.

217. Rabkin SW. Epicardial fat: properties, function and relationship to obesity. *Obes Rev* 2007; **8**(3): 253-61.

218. Sacks HS, Fain JN. Human epicardial adipose tissue: a review. *Am Heart J* 2007; **153**(6): 907-17.

219. Ishii T, Asuwa N, Masuda S, Ishikawa Y. The effects of a myocardial bridge on coronary atherosclerosis and ischaemia. *J Pathol* 1998; **185**(1): 4-9.

220. Wang TD, Lee WJ, Shih FY, et al. Association of epicardial adipose tissue with coronary atherosclerosis is region-specific and independent of conventional risk factors and intra-abdominal adiposity. *Atherosclerosis* 2010; **213**(1): 279-87.

221. Yerramasu A, Dey D, Venuraju S, et al. Increased volume of epicardial fat is an independent risk factor for accelerated progression of sub-clinical coronary atherosclerosis. *Atherosclerosis* 2012; **220**(1): 223-30.

222. Rosito GA, Massaro JM, Hoffmann U, et al. Pericardial fat, visceral abdominal fat, cardiovascular disease risk factors, and vascular calcification in a community-based sample: the Framingham Heart Study. *Circulation* 2008; **117**(5): 605-13.

223. Ding J, Hsu FC, Harris TB, et al. The association of pericardial fat with incident coronary heart disease: the Multi-Ethnic Study of Atherosclerosis (MESA). *Am J Clin Nutr* 2009; **90**(3): 499-504.

224. Wang CP, Hsu HL, Hung WC, et al. Increased epicardial adipose tissue (EAT) volume in type 2 diabetes mellitus and association with metabolic syndrome and severity of coronary atherosclerosis. *Clin Endocrinol (Oxf)* 2009; **70**(6): 876-82.

225. Alexopoulos N, McLean DS, Janik M, Arepalli CD, Stillman AE, Raggi P. Epicardial adipose tissue and coronary artery plaque characteristics. *Atherosclerosis* 2010; **210**(1): 150-4.

226. Ito T, Nasu K, Terashima M, et al. The impact of epicardial fat volume on coronary plaque vulnerability: insight from optical coherence tomography analysis. *Eur Heart J Cardiovasc Imaging* 2012; **13**(5): 408-15.

227. Schlett CL, Ferencik M, Kriegel MF, et al. Association of pericardial fat and coronary high-risk lesions as determined by cardiac CT. *Atherosclerosis* 2012; **222**(1): 129-34.

228. Wu FZ, Chou KJ, Huang YL, Wu MT. The relation of location-specific epicardial adipose tissue thickness and obstructive coronary artery disease: systemic review and meta-analysis of observational studies. *BMC Cardiovasc Disord* 2014; **14**: 62.

229. Despres JP. Body fat distribution and risk of cardiovascular disease: an update. *Circulation* 2012; **126**(10): 1301-13.

230. Ramachandrappa S, Farooqi IS. Genetic approaches to understanding human obesity. *J Clin Invest* 2011; **121**(6): 2080-6.

231. Tarnoki AD, Tarnoki DL, Medda E, et al. Bioimpedance analysis of body composition in an international twin cohort. *Obes Res Clin Pract* 2014; **8**(3): e201-98.

232. Segal NL, Feng R, McGuire SA, Allison DB, Miller S. Genetic and environmental contributions to body mass index: comparative analysis of monozygotic twins, dizygotic twins and same-age unrelated siblings. *Int J Obes (Lond)* 2009; **33**(1): 37-41.

233. Carey DG, Nguyen TV, Campbell LV, Chisholm DJ, Kelly P. Genetic influences on central abdominal fat: a twin study. *Int J Obes Relat Metab Disord* 1996; **20**(8): 722-6.

234. Samaras K, Kelly PJ, Chiano MN, Spector TD, Campbell LV. Genetic and

environmental influences on total-body and central abdominal fat: the effect of physical activity in female twins. *Ann Intern Med* 1999; **130**(11): 873-82.

235. Stillman AE, Rubin GD, Teague SD, White RD, Woodard PK, Larson PA. Structured reporting: coronary CT angiography: a white paper from the American College of Radiology and the North American Society for Cardiovascular Imaging. *J Am Coll Radiol* 2008; **5**(7): 796-800.

236. Liu D, Zucherman M, Tulloss WB, Jr. Six characteristics of effective structured reporting and the inevitable integration with speech recognition. *J Digit Imaging* 2006; **19**(1): 98-104.

237. Reiner BI, Knight N, Siegel EL. Radiology reporting, past, present, and future: the radiologist's perspective. *J Am Coll Radiol* 2007; **4**(5): 313-9.

238. Sistrom CL, Langlotz CP. A framework for improving radiology reporting. *J Am Coll Radiol* 2005; **2**(2): 159-67.

239. Sun Z, Choo GH, Ng KH. Coronary CT angiography: current status and continuing challenges. *Br J Radiol* 2012; **85**(1013): 495-510.

240. Maurovich-Horvat P, Bartykowszki A, Kerecsen G, et al. A koronária-CT-angiográfia leletezése. A Magyar Kardiológusok Társasága Szív-CT Munkacsoportjának és a Magyar Radiológusok Társasága Szív Képalkotó Diagnosztikai Szekciójának közös ajánlása. *Cardiologia Hungarica* 2013; **43**: 275-81.

241. Bartykowszki A, Toth L, Kerecsen G, et al. A koronária-CT-angiográfia értelmezése és leletezése. A Magyar Kardiológusok Társasága Kardiovaszkuláris Képalkotó Munkacsoportjának ajánlása. *Cardiologia Hungarica* 2017; **47**(1).

242. Dewey M. Structure or entropy in reporting cardiac CT findings. *Int J Cardiovasc Imaging* 2016; **32**(11): 1657-8.

243. Ghoshhajra BB, Lee AM, Ferencik M, et al. Interpreting the interpretations: the use of structured reporting improves referring clinicians' comprehension of coronary CT angiography reports. *J Am Coll Radiol* 2013; **10**(6): 432-8.

244. Cury RC, Abbara S, Achenbach S, et al. CAD-RADS(TM) Coronary Artery Disease - Reporting and Data System. An expert consensus document of the Society of Cardiovascular Computed Tomography (SCCT), the American College of Radiology (ACR) and the North American Society for Cardiovascular Imaging (NASCI). Endorsed by the American College of Cardiology. *J Cardiovasc Comput Tomogr* 2016; **10**(4): 269-81.

245. Maurovich-Horvat P, Karolyi M, Horvath T, et al. Esmolol is noninferior to metoprolol in achieving a target heart rate of 65 beats/min in patients referred to coronary CT angiography:

a randomized controlled clinical trial. *J Cardiovasc Comput Tomogr* 2015; **9**(2): 139-45.

246. Roberts WT, Wright AR, Timmis JB, Timmis AD. Safety and efficacy of a rate control protocol for cardiac CT. *Br J Radiol* 2009; **82**(976): 267-71.

247. Degertekin M, Gemici G, Kaya Z, et al. Safety and efficacy of patient preparation with intravenous esmolol before 64-slice computed tomography coronary angiography. *Coron Artery Dis* 2008; **19**(1): 33-6.

248. Wilcox RR. Introduction to robust estimation and hypothesis testing. 3rd ed. Amsterdam ; Boston: Academic Press; 2012.

249. Karady J, Panajotu A, Kolossvary M, et al. The effect of four-phasic versus three-phasic contrast media injection protocols on extravasation rate in coronary CT angiography: a randomized controlled trial. *Eur Radiol* 2017; **27**(11): 4538-43.

250. Karolyi M, Szilveszter B, Kolossvary M, et al. Iterative model reconstruction reduces calcified plaque volume in coronary CT angiography. *Eur J Radiol* 2017; **87**: 83-9.

251. Leipsic J, Abbara S, Achenbach S, et al. SCCT guidelines for the interpretation and reporting of coronary CT angiography: a report of the Society of Cardiovascular Computed Tomography Guidelines Committee. *J Cardiovasc Comput Tomogr* 2014; **8**(5): 342-58.

252. Scheffel H, Stolzmann P, Schlett CL, et al. Coronary artery plaques: cardiac CT with model-based and adaptive-statistical iterative reconstruction technique. *European journal of radiology* 2012; **81**(3): e363-9.

253. Ferencik M, Nomura CH, Maurovich-Horvat P, et al. Quantitative parameters of image quality in 64-slice computed tomography angiography of the coronary arteries. *Eur J Radiol* 2006; **57**(3): 373-9.

254. Altman DG. Practical statistics for medical research. Boca Raton, Fla.: Chapman & Hall/CRC; 1999.

255. Bartykowszki A, Kolossvary M, Jermendy AL, et al. Image Quality of Prospectively ECG-Triggered Coronary CT Angiography in Heart Transplant Recipients. *AJR Am J Roentgenol* 2018; **210**(2): 314-9.

256. Lee AM, Beaudoin J, Engel LC, et al. Assessment of image quality and radiation dose of prospectively ECG-triggered adaptive dual-source coronary computed tomography angiography (cCTA) with arrhythmia rejection algorithm in systole versus diastole: a retrospective cohort study. *Int J Cardiovasc Imaging* 2013; **29**(6): 1361-70.

257. Leschka S, Alkadhi H, Plass A, et al. Accuracy of MSCT coronary angiography with 64-slice technology: first experience. *Eur Heart J* 2005; **26**(15): 1482-7.

258. Shuman WP, Branch KR, May JM, et al. Prospective versus retrospective ECG gating

for 64-detector CT of the coronary arteries: comparison of image quality and patient radiation dose. *Radiology* 2008; **248**(2): 431-7.

259. Maurovich-Horvat P, Hoffmann U, Vorpahl M, Nakano M, Virmani R, Alkadhi H. The napkin-ring sign: CT signature of high risk coronary plaques? *JACC: Cardiovascular Imaging* 2010; **3**(4): 440-05.

260. Maurovich-Horvat P, Schlett CL, Alkadhi H, et al. The napkin-ring sign indicates advanced atherosclerotic lesions in coronary CT angiography. *JACC Cardiovascular imaging* 2012; **5**(12): 1243-52.

261. Stary HC, Chandler AB, Dinsmore RE, et al. A definition of advanced types of atherosclerotic lesions and a histological classification of atherosclerosis. A report from the Committee on Vascular Lesions of the Council on Arteriosclerosis, American Heart Association. *Arterioscler Thromb Vasc Biol* 1995; **15**(9): 1512-31.

262. Virmani R, Burke AP, Farb A. Plaque rupture and plaque erosion. *Thromb Haemost* 1999; **82 Suppl 1**: 1-3.

263. Landis JR, Koch GG. The measurement of observer agreement for categorical data. *Biometrics* 1977; **33**(1): 159-74.

264. Donner A, Klar N. Confidence interval construction for effect measures arising from cluster randomization trials. *J Clin Epidemiol* 1993; **46**(2): 123-31.

265. Hanley JA, McNeil BJ. The meaning and use of the area under a receiver operating characteristic (ROC) curve. *Radiology* 1982; **143**(1): 29-36.

266. DeLong ER, DeLong DM, Clarke-Pearson DL. Comparing the areas under two or more correlated receiver operating characteristic curves: a nonparametric approach. *Biometrics* 1988; **44**(3): 837-45.

267. Maurovich-Horvat P, Schlett CL, Alkadhi H, et al. Differentiation of early from advanced coronary atherosclerotic lesions: systematic comparison of CT, intravascular US, and optical frequency domain imaging with histopathologic examination in ex vivo human hearts. *Radiology* 2012; **265**(2): 393-401.

268. Yun SH, Tearney GJ, Vakoc BJ, et al. Comprehensive volumetric optical microscopy in vivo. *Nat Med* 2006; **12**(12): 1429-33.

269. Tearney GJ, Waxman S, Shishkov M, et al. Three-dimensional coronary artery microscopy by intracoronary optical frequency domain imaging. *JACC Cardiovasc Imaging* 2008; **1**(6): 752-61.

270. Voros S, Rinehart S, Vazquez-Figueroa JG, et al. Prospective, head-to-head comparison of quantitative coronary angiography, quantitative computed tomography angiography, and

intravascular ultrasound for the prediction of hemodynamic significance in intermediate and severe lesions, using fractional flow reserve as reference standard (from the ATLANTA I and II Study). *Am J Cardiol* 2014; **113**(1): 23-9.

271. Voros S, Maurovich-Horvat P, Marvasty IB, et al. Precision phenotyping, panomics, and system-level bioinformatics to delineate complex biologies of atherosclerosis: rationale and design of the "Genetic Loci and the Burden of Atherosclerotic Lesions" study. *J Cardiovasc Comput Tomogr* 2014; **8**(6): 442-51.

272. Wu FZ, Wu MT. 2014 SCCT guidelines for the interpretation and reporting of coronary CT angiography: a report of the Society of Cardiovascular Computed Tomography Guidelines Committee. *J Cardiovasc Comput Tomogr* 2015; **9**(2): e3.

273. Altman DG. Practical statistics for medical research. London ; New York: Chapman and Hall; 1991.

274. Kolossvary M, Karady J, Szilveszter B, et al. Radiomic Features Are Superior to Conventional Quantitative Computed Tomographic Metrics to Identify Coronary Plaques With Napkin-Ring Sign. *Circ Cardiovasc Imaging* 2017; **10**(12).

275. Boogers MJ, Schuijf JD, Kitslaar PH, et al. Automated quantification of stenosis severity on 64-slice CT: a comparison with quantitative coronary angiography. *JACC Cardiovasc Imaging* 2010; **3**(7): 699-709.

276. Kolossvary M. RIA: Radiomics Image Analysis Toolbox for Grayscale Images. 2017.

277. Shafiq-Ul-Hassan M, Zhang GG, Latifi K, et al. Intrinsic dependencies of CT radiomic features on voxel size and number of gray levels. *Med Phys* 2017; **44**(3): 1050-62.

278. Hothorn T, Hornik K, van de Wiel MA, Zeileis A. Implementing a Class of Permutation Tests: The coin Package. *2008* 2008; **28**(8): 23.

279. Robin X, Turck N, Hainard A, et al. pROC: an open-source package for R and S+ to analyze and compare ROC curves. *BMC Bioinformatics* 2011; **12**(1): 77.

280. Rousseeuw PJ. Silhouettes: A graphical aid to the interpretation and validation of cluster analysis. *Journal of Computational and Applied Mathematics* 1987; **20**: 53-65.

281. Dietterich TG. Approximate Statistical Tests for Comparing Supervised Classification Learning Algorithms. *Neural Comput* 1998; **10**(7): 1895-923.

282. Gao X, Starmer J, Martin ER. A multiple testing correction method for genetic association studies using correlated single nucleotide polymorphisms. *Genet Epidemiol* 2008; **32**(4): 361-9.

283. Johnson RC, Nelson GW, Troyer JL, et al. Accounting for multiple comparisons in a genome-wide association study (GWAS). *BMC Genomics* 2010; **11**: 724.

284. R Core Team. R: A language and environment for statistical computing. R Foundation for Statistical Computing. 3.3.2 ed: R Foundation for Statistical Computing; 2016.

285. Donnelly PM, Kolossvary M, Karady J, et al. Experience With an On-Site Coronary Computed Tomography-Derived Fractional Flow Reserve Algorithm for the Assessment of Intermediate Coronary Stenoses. *Am J Cardiol* 2018; **121**(1): 9-13.

286. Altman DG, Bland JM. Measurement in Medicine: The Analysis of Method Comparison Studies. *Journal of the Royal Statistical Society Series D (The Statistician)* 1983; **32**(3): 307-17.

287. DeLong ER, DeLong DM, Clarke-Pearson DL. Comparing the Areas under Two or More Correlated Receiver Operating Characteristic Curves: A Nonparametric Approach. *Biometrics* 1988; **44**(3): 837-45.

288. Hoffmann U, Bamberg F, Chae CU, et al. Coronary computed tomography angiography for early triage of patients with acute chest pain: the ROMICAT (Rule Out Myocardial Infarction using Computer Assisted Tomography) trial. *J Am Coll Cardiol* 2009; **53**(18): 1642-50.

289. Maurovich-Horvat P, Kallianos K, Engel LC, et al. Relationship of thoracic fat depots with coronary atherosclerosis and circulating inflammatory biomarkers. *Obesity (Silver Spring)* 2015; **23**(6): 1178-84.

290. Nichols JH, Samy B, Nasir K, et al. Volumetric measurement of pericardial adipose tissue from contrast-enhanced coronary computed tomography angiography: a reproducibility study. *Journal of cardiovascular computed tomography* 2008; **2**(5): 288-95.

291. Fox CS, Massaro JM, Schlett CL, et al. Periaortic fat deposition is associated with peripheral arterial disease: the Framingham heart study. *Circulation Cardiovascular imaging* 2010; **3**(5): 515-9.

292. Schlett CL, Massaro JM, Lehman SJ, et al. Novel measurements of periaortic adipose tissue in comparison to anthropometric measures of obesity, and abdominal adipose tissue. *Int J Obes (Lond)* 2009; **33**(2): 226-32.

293. Bamberg F, Dannemann N, Shapiro MD, et al. Association between cardiovascular risk profiles and the presence and extent of different types of coronary atherosclerotic plaque as detected by multidetector computed tomography. *Arteriosclerosis, thrombosis, and vascular biology* 2008; **28**(3): 568-74.

294. Jermendy AL, Kolossvary M, Drobni ZD, et al. Assessing genetic and environmental influences on epicardial and abdominal adipose tissue quantities: a classical twin study. *Int J Obes (Lond)* 2018; **42**(2): 163-8.

295. Chen MY, Shanbhag SM, Arai AE. Submillisievert median radiation dose for coronary angiography with a second-generation 320-detector row CT scanner in 107 consecutive patients. *Radiology* 2013; **267**(1): 76-85.

296. Cury RC, Abbara S, Achenbach S, et al. Coronary Artery Disease - Reporting and Data System (CAD-RADS): An Expert Consensus Document of SCCT, ACR and NASCI: Endorsed by the ACC. *JACC Cardiovasc Imaging* 2016; **9**(9): 1099-113.

297. Mekkaoui C, Huang S, Chen HH, et al. Fiber architecture in remodeled myocardium revealed with a quantitative diffusion CMR tractography framework and histological validation. *J Cardiovasc Magn Reson* 2012; **14**: 70.

298. Seifarth H, Schlett CL, Nakano M, et al. Histopathological correlates of the napkin-ring sign plaque in coronary CT angiography. *Atherosclerosis* 2012; **224**(1): 90-6.

299. Kassamali RH, Kim DH, Patel H, et al. Safety of an i.v. beta-adrenergic blockade protocol for heart rate optimization before coronary CT angiography. *AJR Am J Roentgenol* 2014; **203**(4): 759-62.

300. Reynolds RD, Gorczynski RJ, Quon CY. Pharmacology and pharmacokinetics of esmolol. *J Clin Pharmacol* 1986; **26**(S1): A3-A14.

301. Oxorn D, Knox JW, Hill J. Bolus doses of esmolol for the prevention of perioperative hypertension and tachycardia. *Can J Anaesth* 1990; **37**(2): 206-9.

302. Parnass SM, Rothenberg DM, Kerchberger JP, Ivankovich AD. A single bolus dose of esmolol in the prevention of intubation-induced tachycardia and hypertension in an ambulatory surgery unit. *J Clin Anesth* 1990; **2**(4): 232-7.

303. Sheppard D, DiStefano S, Byrd RC, et al. Effects of esmolol on airway function in patients with asthma. *J Clin Pharmacol* 1986; **26**(3): 169-74.

304. Jimenez-Juan L, Nguyen ET, Wintersperger BJ, et al. Failed heart rate control with oral metoprolol prior to coronary CT angiography: effect of additional intravenous metoprolol on heart rate, image quality and radiation dose. *Int J Cardiovasc Imaging* 2013; **29**(1): 199-206.

305. Davenport MS, Wang CL, Bashir MR, Neville AM, Paulson EK. Rate of contrast material extravasations and allergic-like reactions: effect of extrinsic warming of low-osmolality iodinated CT contrast material to 37 degrees C. *Radiology* 2012; **262**(2): 475-84.

306. Kim R, Park EA, Lee W, Chung JW. Feasibility of 320-row area detector CT coronary angiography using 40 mL of contrast material: assessment of image quality and diagnostic accuracy. *Eur Radiol* 2016; **26**(11): 3802-10.

307. Felmly LM, De Cecco CN, Schoepf UJ, et al. Low contrast medium-volume third-generation dual-source computed tomography angiography for transcatheter aortic valve

replacement planning. *Eur Radiol* 2017; **27**(5): 1944-53.

308. Mangold S, Wichmann JL, Schoepf UJ, et al. Coronary CT angiography in obese patients using 3(rd) generation dual-source CT: effect of body mass index on image quality. *Eur Radiol* 2016; **26**(9): 2937-46.

309. Yuki H, Utsunomiya D, Funama Y, et al. Value of knowledge-based iterative model reconstruction in low-kV 256-slice coronary CT angiography. *J Cardiovasc Comput Tomogr* 2014; **8**(2): 115-23.

310. Oda S, Weissman G, Vembar M, Weigold WG. Iterative model reconstruction: improved image quality of low-tube-voltage prospective ECG-gated coronary CT angiography images at 256-slice CT. *Eur J Radiol* 2014; **83**(8): 1408-15.

311. Halpern EJ, Gingold EL, White H, Read K. Evaluation of coronary artery image quality with knowledge-based iterative model reconstruction. *Academic radiology* 2014; **21**(6): 805-11.

312. Puchner SB, Ferencik M, Karolyi M, et al. The effect of iterative image reconstruction algorithms on the feasibility of automated plaque assessment in coronary CT angiography. *Int J Cardiovasc Imaging* 2013; **29**(8): 1879-88.

313. Patel J, Al Rifai M, Blaha MJ, et al. Coronary Artery Calcium Improves Risk Assessment in Adults With a Family History of Premature Coronary Heart Disease: Results From Multiethnic Study of Atherosclerosis. *Circ Cardiovasc Imaging* 2015; **8**(6): e003186.

314. Shaw LJ, Raggi P, Schisterman E, Berman DS, Callister TQ. Prognostic value of cardiac risk factors and coronary artery calcium screening for all-cause mortality. *Radiology* 2003; **228**(3): 826-33.

315. Kurata A, Dharampal A, Dedic A, et al. Impact of iterative reconstruction on CT coronary calcium quantification. *Eur Radiol* 2013; **23**(12): 3246-52.

316. van Osch JA, Mouden M, van Dalen JA, et al. Influence of iterative image reconstruction on CT-based calcium score measurements. *Int J Cardiovasc Imaging* 2014; **30**(5): 961-7.

317. Wellnhofer E, Stypmann J, Bara CL, et al. Angiographic assessment of cardiac allograft vasculopathy: results of a Consensus Conference of the Task Force for Thoracic Organ Transplantation of the German Cardiac Society. *Transpl Int* 2010; **23**(11): 1094-104.

318. Mittal TK, Panicker MG, Mitchell AG, Banner NR. Cardiac allograft vasculopathy after heart transplantation: electrocardiographically gated cardiac CT angiography for assessment. *Radiology* 2013; **268**(2): 374-81.

319. Gregory SA, Ferencik M, Achenbach S, et al. Comparison of sixty-four-slice

multidetector computed tomographic coronary angiography to coronary angiography with intravascular ultrasound for the detection of transplant vasculopathy. *Am J Cardiol* 2006; **98**(7): 877-84.

320. von Ziegler F, Leber AW, Becker A, et al. Detection of significant coronary artery stenosis with 64-slice computed tomography in heart transplant recipients: a comparative study with conventional coronary angiography. *Int J Cardiovasc Imaging* 2009; **25**(1): 91-100.

321. Nunoda S, Machida H, Sekikawa A, et al. Evaluation of cardiac allograft vasculopathy by multidetector computed tomography and whole-heart magnetic resonance coronary angiography. *Circ J* 2010; **74**(5): 946-53.

322. Wever-Pinzon O, Romero J, Kelesidis I, et al. Coronary computed tomography angiography for the detection of cardiac allograft vasculopathy: a meta-analysis of prospective trials. *J Am Coll Cardiol* 2014; **63**(19): 1992-2004.

323. Schepis T, Marwan M, Pflederer T, et al. Quantification of non-calcified coronary atherosclerotic plaques with dual-source computed tomography: comparison with intravascular ultrasound. *Heart* 2010; **96**(8): 610-5.

324. Sands KE, Appel ML, Lilly LS, Schoen FJ, Mudge GH, Jr., Cohen RJ. Power spectrum analysis of heart rate variability in human cardiac transplant recipients. *Circulation* 1989; **79**(1): 76-82.

325. Cornelissen VA, Vanhaecke J, Aubert AE, Fagard RH. Heart rate variability after heart transplantation: a 10-year longitudinal follow-up study. *Journal of cardiology* 2012; **59**(2): 220-4.

326. Stolzmann P, Leschka S, Scheffel H, et al. Dual-source CT in step-and-shoot mode: noninvasive coronary angiography with low radiation dose. *Radiology* 2008; **249**(1): 71-80.

327. Brodoefel H, Burgstahler C, Tsiflikas I, et al. Dual-source CT: effect of heart rate, heart rate variability, and calcification on image quality and diagnostic accuracy. *Radiology* 2008; **247**(2): 346-55.

328. Nakazawa G, Tanabe K, Onuma Y, et al. Efficacy of culprit plaque assessment by 64-slice multidetector computed tomography to predict transient no-reflow phenomenon during percutaneous coronary intervention. *Am Heart J* 2008; **155**(6): 1150-7.

329. Leber AW, Knez A, Becker A, et al. Accuracy of multidetector spiral computed tomography in identifying and differentiating the composition of coronary atherosclerotic plaques: a comparative study with intracoronary ultrasound. *J Am Coll Cardiol* 2004; **43**(7): 1241-7.

330. Leber AW, Becker A, Knez A, et al. Accuracy of 64-slice computed tomography to

classify and quantify plaque volumes in the proximal coronary system: a comparative study using intravascular ultrasound. *J Am Coll Cardiol* 2006; **47**(3): 672-7.

331. Tanaka A, Shimada K, Yoshida K, et al. Non-invasive assessment of plaque rupture by 64-slice multidetector computed tomography--comparison with intravascular ultrasound. *Circ J* 2008; **72**(8): 1276-81.

332. Sarwar A, Rieber J, Mooyaart EA, et al. Calcified plaque: measurement of area at thin-section flat-panel CT and 64-section multidetector CT and comparison with histopathologic findings. *Radiology* 2008; **249**(1): 301-6.

333. Leber AW, Knez A, White CW, et al. Composition of coronary atherosclerotic plaques in patients with acute myocardial infarction and stable angina pectoris determined by contrast-enhanced multislice computed tomography. *Am J Cardiol* 2003; **91**(6): 714-8.

334. Pundziute G, Schuijf JD, Jukema JW, et al. Noninvasive assessment of plaque characteristics with multislice computed tomography coronary angiography in symptomatic diabetic patients. *Diabetes Care* 2007; **30**(5): 1113-9.

335. Russo V, Zavalloni A, Bacchi Reggiani ML, et al. Incremental prognostic value of coronary CT angiography in patients with suspected coronary artery disease. *Circ Cardiovasc Imaging* 2010; **3**(4): 351-9.

336. van Werkhoven JM, Schuijf JD, Gaemperli O, et al. Incremental prognostic value of multi-slice computed tomography coronary angiography over coronary artery calcium scoring in patients with suspected coronary artery disease. *Eur Heart J* 2009; **30**(21): 2622-9.

337. Naghavi M, Libby P, Falk E, et al. From vulnerable plaque to vulnerable patient: a call for new definitions and risk assessment strategies: Part II. *Circulation* 2003; **108**(15): 1772-8.

338. Otsuka K, Fukuda S, Tanaka A, et al. Napkin-ring sign on coronary CT angiography for the prediction of acute coronary syndrome. *JACC Cardiovascular imaging* 2013; **6**(4): 448-57.

339. Puchner SB, Liu T, Mayrhofer T, et al. High-risk plaque detected on coronary CT angiography predicts acute coronary syndromes independent of significant stenosis in acute chest pain: results from the ROMICAT-II trial. *J Am Coll Cardiol* 2014; **64**(7): 684-92.

340. Jang IK, Tearney GJ, MacNeill B, et al. In vivo characterization of coronary atherosclerotic plaque by use of optical coherence tomography. *Circulation* 2005; **111**(12): 1551-5.

341. Kawasaki M, Bouma BE, Bressner J, et al. Diagnostic accuracy of optical coherence tomography and integrated backscatter intravascular ultrasound images for tissue characterization of human coronary plaques. *J Am Coll Cardiol* 2006; **48**(1): 81-8.

342. Tearney GJ, Jang IK, Bouma BE. Optical coherence tomography for imaging the vulnerable plaque. *J Biomed Opt* 2006; **11**(2): 021002.

343. Low AF, Kawase Y, Chan YH, Tearney GJ, Bouma BE, Jang IK. In vivo characterisation of coronary plaques with conventional grey-scale intravascular ultrasound: correlation with optical coherence tomography. *EuroIntervention* 2009; **4**(5): 626-32.

344. Carlier SG, Mintz GS, Stone GW. Imaging of atherosclerotic plaque using radiofrequency ultrasound signal processing. *Journal of nuclear cardiology : official publication of the American Society of Nuclear Cardiology* 2006; **13**(6): 831-40.

345. DeMaria AN, Narula J, Mahmud E, Tsimikas S. Imaging vulnerable plaque by ultrasound. *J Am Coll Cardiol* 2006; **47**(8 Suppl): C32-9.

346. Di Mario C, Gorge G, Peters R, et al. Clinical application and image interpretation in intracoronary ultrasound. Study Group on Intracoronary Imaging of the Working Group of Coronary Circulation and of the Subgroup on Intravascular Ultrasound of the Working Group of Echocardiography of the European Society of Cardiology. *Eur Heart J* 1998; **19**(2): 207-29.

347. Mintz GS, Nissen SE, Anderson WD, et al. American College of Cardiology Clinical Expert Consensus Document on Standards for Acquisition, Measurement and Reporting of Intravascular Ultrasound Studies (IVUS). A report of the American College of Cardiology Task Force on Clinical Expert Consensus Documents. *J Am Coll Cardiol* 2001; **37**(5): 1478-92.

348. Kaple RK, Maehara A, Sano K, et al. The axial distribution of lesion-site atherosclerotic plaque components: an in vivo volumetric intravascular ultrasound radio-frequency analysis of lumen stenosis, necrotic core and vessel remodeling. *Ultrasound Med Biol* 2009; **35**(4): 550-7.

349. Matsumoto N, Sato Y, Yoda S, et al. Prognostic value of non-obstructive CT low-dense coronary artery plaques detected by multislice computed tomography. *Circ J* 2007; **71**(12): 1898-903.

350. Motoyama S, Ito H, Sarai M, et al. Plaque Characterization by Coronary Computed Tomography Angiography and the Likelihood of Acute Coronary Events in Mid-Term Follow-Up. *J Am Coll Cardiol* 2015; **66**(4): 337-46.

351. Mowatt G, Cook JA, Hillis GS, et al. 64-Slice computed tomography angiography in the diagnosis and assessment of coronary artery disease: systematic review and meta-analysis. *Heart* 2008; **94**(11): 1386-93.

352. Chopard R, Boussel L, Motreff P, et al. How reliable are 40 MHz IVUS and 64-slice MDCT in characterizing coronary plaque composition? An ex vivo study with histopathological comparison. *Int J Cardiovasc Imaging* 2010; **26**(4): 373-83.

353. Becker CR, Nikolaou K, Muders M, et al. Ex vivo coronary atherosclerotic plaque

characterization with multi-detector-row CT. *Eur Radiol* 2003; **13**(9): 2094-8.

354. Knollmann F, Ducke F, Krist L, et al. Quantification of atherosclerotic coronary plaque components by submillimeter computed tomography. *Int J Cardiovasc Imaging* 2008; **24**(3): 301-10.

355. Butler J, Shapiro M, Reiber J, et al. Extent and distribution of coronary artery disease: a comparative study of invasive versus noninvasive angiography with computed angiography. *Am Heart J* 2007; **153**(3): 378-84.

356. Otsuka K, Fukuda S, Tanaka A, et al. Prognosis of vulnerable plaque on computed tomographic coronary angiography with normal myocardial perfusion image. *Eur Heart J Cardiovasc Imaging* 2014; **15**(3): 332-40.

357. Kubo T, Maehara A, Mintz GS, et al. The dynamic nature of coronary artery lesion morphology assessed by serial virtual histology intravascular ultrasound tissue characterization. *J Am Coll Cardiol* 2010; **55**(15): 1590-7.

358. Burrell HC, Pinder SE, Wilson AR, et al. The positive predictive value of mammographic signs: a review of 425 non-palpable breast lesions. *Clin Radiol* 1996; **51**(4): 277-81.

359. Orel SG, Kay N, Reynolds C, Sullivan DC. BI-RADS categorization as a predictor of malignancy. *Radiology* 1999; **211**(3): 845-50.

360. Grimm LJ, Anderson AL, Baker JA, et al. Interobserver Variability Between Breast Imagers Using the Fifth Edition of the BI-RADS MRI Lexicon. *AJR Am J Roentgenol* 2015; **204**(5): 1120-4.

361. Bickelhaupt S, Paech D, Kickingereder P, et al. Prediction of malignancy by a radiomic signature from contrast agent-free diffusion MRI in suspicious breast lesions found on screening mammography. *J Magn Reson Imaging* 2017; **46**(2): 604-16.

362. Coroller TP, Agrawal V, Huynh E, et al. Radiomic-Based Pathological Response Prediction from Primary Tumors and Lymph Nodes in NSCLC. *J Thorac Oncol* 2017; **12**(3): 467-76.

363. Huang Y, Liu Z, He L, et al. Radiomics Signature: A Potential Biomarker for the Prediction of Disease-Free Survival in Early-Stage (I or II) Non-Small Cell Lung Cancer. *Radiology* 2016; **281**(3): 947-57.

364. Altazi BA, Zhang GG, Fernandez DC, et al. Reproducibility of F18-FDG PET radiomic features for different cervical tumor segmentation methods, gray-level discretization, and reconstruction algorithms. *J Appl Clin Med Phys* 2017; **18**(6): 32-48.

365. Hu P, Wang J, Zhong H, et al. Reproducibility with repeat CT in radiomics study for

rectal cancer. *Oncotarget* 2016; **7**(44): 71440-6.

366. Mackin D, Fave X, Zhang L, et al. Measuring Computed Tomography Scanner Variability of Radiomics Features. *Invest Radiol* 2015; **50**(11): 757-65.

367. Yang DH, Kim YH, Roh JH, et al. Diagnostic performance of on-site CT-derived fractional flow reserve versus CT perfusion. *Eur Heart J Cardiovasc Imaging* 2017; **18**(4): 432-40.

368. Coenen A, Kim YH, Kruk M, et al. Diagnostic Accuracy of a Machine-Learning Approach to Coronary Computed Tomographic Angiography-Based Fractional Flow Reserve: Result From the MACHINE Consortium. *Circ Cardiovasc Imaging* 2018; **11**(6): e007217.

369. Freiman M, Nickisch H, Prevrhal S, et al. Improving CCTA-based lesions' hemodynamic significance assessment by accounting for partial volume modeling in automatic coronary lumen segmentation. *Med Phys* 2017; **44**(3): 1040-9.

370. van der Horst A, Boogaard FL, van't Veer M, Rutten MC, Pijls NH, van de Vosse FN. Towards patient-specific modeling of coronary hemodynamics in healthy and diseased state. *Comput Math Methods Med* 2013; **2013**: 393792.

371. Huo Y, Kassab GS. Intraspecific scaling laws of vascular trees. *J R Soc Interface* 2012; **9**(66): 190-200.

372. Lamon-Fava S, Wilson PW, Schaefer EJ. Impact of body mass index on coronary heart disease risk factors in men and women. The Framingham Offspring Study. *Arterioscler Thromb Vasc Biol* 1996; **16**(12): 1509-15.

373. Mahabadi AA, Reinsch N, Lehmann N, et al. Association of pericoronary fat volume with atherosclerotic plaque burden in the underlying coronary artery: a segment analysis. *Atherosclerosis* 2010; **211**(1): 195-9.

374. Darvall KA, Sam RC, Silverman SH, Bradbury AW, Adam DJ. Obesity and thrombosis. *Eur J Vasc Endovasc Surg* 2007; **33**(2): 223-33.

375. Sattar N, Wannamethee G, Sarwar N, et al. Adiponectin and coronary heart disease: a prospective study and meta-analysis. *Circulation* 2006; **114**(7): 623-9.

376. Greenstein AS, Khavandi K, Withers SB, et al. Local inflammation and hypoxia abolish the protective anticontractile properties of perivascular fat in obese patients. *Circulation* 2009; **119**(12): 1661-70.

377. Montani JP, Carroll JF, Dwyer TM, Antic V, Yang Z, Dulloo AG. Ectopic fat storage in heart, blood vessels and kidneys in the pathogenesis of cardiovascular diseases. *Int J Obes Relat Metab Disord* 2004; **28 Suppl 4**: S58-65.

378. Ouchi N, Kihara S, Funahashi T, et al. Reciprocal association of C-reactive protein with

adiponectin in blood stream and adipose tissue. *Circulation* 2003; **107**(5): 671-4.

379. Baker AR, Silva NF, Quinn DW, et al. Human epicardial adipose tissue expresses a pathogenic profile of adipocytokines in patients with cardiovascular disease. *Cardiovasc Diabetol* 2006; **5**: 1.

380. Kremen J, Dolinkova M, Krajickova J, et al. Increased subcutaneous and epicardial adipose tissue production of proinflammatory cytokines in cardiac surgery patients: possible role in postoperative insulin resistance. *J Clin Endocrinol Metab* 2006; **91**(11): 4620-7.

381. Thalmann S, Meier CA. Local adipose tissue depots as cardiovascular risk factors. *Cardiovasc Res* 2007; **75**(4): 690-701.

382. Fox CS, White CC, Lohman K, et al. Genome-wide association of pericardial fat identifies a unique locus for ectopic fat. *PLoS Genet* 2012; **8**(5): e1002705.

383. Tayo BO, Harders R, Luke A, Zhu X, Cooper RS. Latent common genetic components of obesity traits. *Int J Obes (Lond)* 2008; **32**(12): 1799-806.

384. Li F, Zhao J, Yuan Z, Zhang X, Ji J, Xue F. A powerful latent variable method for detecting and characterizing gene-based gene-gene interaction on multiple quantitative traits. *BMC Genet* 2013; **14**: 89.

385. Barsh GS, Farooqi IS, O'Rahilly S. Genetics of body-weight regulation. *Nature* 2000; **404**(6778): 644-51.

386. Malis C, Rasmussen EL, Poulsen P, et al. Total and regional fat distribution is strongly influenced by genetic factors in young and elderly twins. *Obes Res* 2005; **13**(12): 2139-45.

387. Jermendy G, Horvath T, Littvay L, et al. Effect of genetic and environmental influences on cardiometabolic risk factors: a twin study. *Cardiovasc Diabetol* 2011; **10**: 96.

388. Tarnoki AD, Tarnoki DL, Bata P, et al. Heritability of non-alcoholic fatty liver disease and association with abnormal vascular parameters: a twin study. *Liver Int* 2012; **32**(8): 1287-93.

389. Orio F, Tafuri D, Ascione A, et al. Lifestyle changes in the management of adulthood and childhood obesity. *Minerva Endocrinol* 2016; **41**(4): 509-15.

390. Colquitt JL, Loveman E, O'Malley C, et al. Diet, physical activity, and behavioural interventions for the treatment of overweight or obesity in preschool children up to the age of 6 years. *Cochrane Database Syst Rev* 2016; **3**: CD012105.

391. Iacobellis G, Singh N, Wharton S, Sharma AM. Substantial changes in epicardial fat thickness after weight loss in severely obese subjects. *Obesity (Silver Spring)* 2008; **16**(7): 1693-7.

392. Kim MK, Tomita T, Kim MJ, Sasai H, Maeda S, Tanaka K. Aerobic exercise training

reduces epicardial fat in obese men. *J Appl Physiol (1985)* 2009; **106**(1): 5-11.

393. Saura D, Oliva MJ, Rodriguez D, et al. Reproducibility of echocardiographic measurements of epicardial fat thickness. *Int J Cardiol* 2010; **141**(3): 311-3.

394. Sicari R, Sironi AM, Petz R, et al. Pericardial rather than epicardial fat is a cardiometabolic risk marker: an MRI vs echo study. *J Am Soc Echocardiogr* 2011; **24**(10): 1156-62.

395. Thomassin-Naggara I, Tardivon A, Chopier J. Standardized diagnosis and reporting of breast cancer. *Diagn Interv Imaging* 2014; **95**(7-8): 759-66.

396. Santillan CS, Tang A, Cruite I, Shah A, Sirlin CB. Understanding LI-RADS: a primer for practical use. *Magn Reson Imaging Clin N Am* 2014; **22**(3): 337-52.

397. Tewes S, Mokov N, Hartung D, et al. Standardized Reporting of Prostate MRI: Comparison of the Prostate Imaging Reporting and Data System (PI-RADS) Version 1 and Version 2. *PLoS One* 2016; **11**(9): e0162879.

398. Xiao X, Jiang Q, Wu H, Guan X, Qin W, Luo B. Diagnosis of sub-centimetre breast lesions: combining BI-RADS-US with strain elastography and contrast-enhanced ultrasound-a preliminary study in China. *Eur Radiol* 2017; **27**(6): 2443-50.

399. Douglas PS, Hendel RC, Cummings JE, et al. ACCF/ACR/AHA/ASE/ASNC/HRS/NASCI/RSNA/SAIP/SCAI/SCCT/SCMR 2008 Health Policy Statement on Structured Reporting in Cardiovascular Imaging. *J Am Coll Cardiol* 2009; **53**(1): 76-90.

400. Larson DB, Towbin AJ, Pryor RM, Donnelly LF. Improving consistency in radiology reporting through the use of department-wide standardized structured reporting. *Radiology* 2013; **267**(1): 240-50.

401. Powell DK, Silberzweig JE. State of structured reporting in radiology, a survey. *Academic radiology* 2015; **22**(2): 226-33.

402. Faggioni L, Coppola F, Ferrari R, Neri E, Regge D. Usage of structured reporting in radiological practice: results from an Italian online survey. *Eur Radiol* 2017; **27**(5): 1934-43.

403. Gassenmaier S, Armbruster M, Haasters F, et al. Structured reporting of MRI of the shoulder - improvement of report quality? *Eur Radiol* 2017; **27**(10): 4110-9.

404. Chandrashekhar Y, Min JK, Hecht H, Narula J. CAD-RADS: A Giant First Step Toward a Common Lexicon? *JACC Cardiovasc Imaging* 2016; **9**(9): 1125-9.

9 List of publications of the applicant

9.1 International publications related to the present thesis

Manuscripts published before the PhD degree defence (before 2011)

1. Ferencik M, Nomura CH, **Maurovich-Horvat P**, Hoffmann U, Pena AJ, Cury RC, Abbar S, Nieman K, Fatima U, Achenbach S, Brady TJ
Quantitative parameters of image quality in 64-slice computed tomography angiography of the coronary arteries
EUROPEAN JOURNAL OF RADIOLOGY 57:(3) pp. 373-379. (2006)
Independent citations: 78 Dependent citations: 16 Total: 94
IF:1.332

2. **Maurovich-Horvat P**, Hoffmann U, Vorpahl M, Nakano M, Virmani R, Alkadhi H
The napkin-ring sign: CT signature of high-risk coronary plaques?
JACC-CARDIOVASCULAR IMAGING 3:(4) pp. 440-444. (2010)
Independent citations: 66 Dependent citations: 25 Total: 91
IF: 5.528

3. van der Giessen AG, Toepker MH, Donelly PM, Bamberg F, Schlett CL, Raffle C, Irlbeck T, Lee H, van Walsum T, **Maurovich-Horvat P**, Gijsen FJ, Wentzel JJ, Hoffmann U
Reproducibility, accuracy, and predictors of accuracy for the detection of coronary atherosclerotic plaque composition by computed tomography: an ex vivo comparison to intravascular ultrasound
INVESTIGATIVE RADIOLOGY 45:(11) pp. 693-701. (2010)
Independent citations: 17 Dependent citations: 18 Total: 35
IF: 4.670

4. Stolzmann P, Goetti RP, **Maurovich-Horvat P**, Hoffmann U, Flohr TG, Leschka S, Alkadhi H
Predictors of Image Quality in High-Pitch Coronary CT Angiography.
AMERICAN JOURNAL OF ROENTGENOLOGY 197:(4) pp. 851-858. (2011)
Independent citations: 17 Dependent citations: 3 Total: 20
IF: 2.775

Manuscripts published after PhD degree defence (after 2011)

5. **Maurovich-Horvat P**, Schlett CL, Alkadhi H, Nakano M, Otsuka F, Stolzmann P, Scheffel H, Ferencik M, Kriegel MF, Seifarth H, Virmani R, Hoffmann U
The Napkin-Ring Sign Indicates Advanced Atherosclerotic Lesions in Coronary CT Angiography
JACC-CARDIOVASCULAR IMAGING 5:(12) pp. 1243-1252. (2012)
Independent citations: 43 Dependent citations: 16 Total: 59

IF: 6.164

6. Scheffel H, Stolzmann P, Schlett CL, Engel LC, Major GP, Karolyi M, Do S, **Maurovich-Horvat P**, Hoffmann U
Coronary artery plaques: Cardiac CT with model-based and adaptive-statistical iterative reconstruction technique.
EUROPEAN JOURNAL OF RADIOLOGY 81:(3) pp. e363-e369. (2012)
Independent citations: 80 Dependent citations: 8 Total: 88
IF: 2.512

7. **Maurovich-Horvat P**, Schlett CL, Alkadhi H, Nakano M, Stolzmann P, Vorpahl M, Scheffel H, Tanaka A, Warger WC nd, Maehara A, Ma S, Kriegel MF, Kaple RK, Seifarth H, Bamberg F, Mintz GS, Tearney GJ, Virmani R, Hoffmann U
Differentiation of early from advanced coronary atherosclerotic lesions: systematic comparison of CT, intravascular US, and optical frequency domain imaging with histopathologic examination in ex vivo human hearts.
RADIOLOGY 265:(2) pp. 393-401. (2012)
Independent citations: 11 Dependent citations: 11 Total: 22
IF: 6.339

8. Puchner SB, Ferencik M, Karolyi M, Do S, **Maurovich-Horvat P**, Kauczor HU, Hoffmann U, Schlett CL
The effect of iterative image reconstruction algorithms on the feasibility of automated plaque assessment in coronary CT angiography.
INTERNATIONAL JOURNAL OF CARDIOVASCULAR IMAGING 29:(8) pp. 1879-1888. (2013)
Independent citations: 5 Dependent citations: 5 Total: 10
IF: 2.322

9. Schlett CL, **Maurovich-Horvat P**, Ferencik M, Alkadhi H, Stolzmann P, Scheffel H, Seifarth H, Nakano M, Do S, Vorpahl M, Kauczor HU, Bamberg F, Tearney GJ, Virmani R, Hoffmann U
Histogram Analysis of Lipid-Core Plaques in Coronary Computed Tomographic Angiography: Ex Vivo Validation Against Histology.
INVESTIGATIVE RADIOLOGY 48:(9) pp. 646-653. (2013)
Independent citations: 8 Dependent citations: 9 Total: 17
IF: 4.453

10. **Maurovich-Horvat P**, Ferencik M, Voros S, Merkely B, Hoffmann U
Comprehensive plaque assessment by coronary CT angiography.
NATURE REVIEWS CARDIOLOGY 11:(7) pp. 390-402. (2014)
Independent citations: 84 Dependent citations: 25 Total: 109
IF: 9.183

11. Ferencik M, Schlett CL, Ghoshhajra BB, Kriegel MF, Joshi SB, **Maurovich-Horvat P**, Rogers IS, Banerji D, Bamberg F, Truong QA, Brady TJ, Nagurney JT, Hoffmann U
A Computed Tomography-Based Coronary Lesion Score to Predict Acute Coronary Syndrome Among Patients With Acute Chest Pain and Significant Coronary Stenosis on Coronary Computed Tomographic Angiogram.

AMERICAN JOURNAL OF CARDIOLOGY 110:(2) pp. 183-189. (2012)
Independent citations: 26 Dependent citations: 15 Total: 41
IF: 3.209

12. Szilard Voros, **Pal Maurovich-Horvat**, Idean B Marvasty, Aruna T Bansal, Michael R Barnes, Gustavo Vazquez, Sarah S Murray, Viktor Voros, Bela Merkely, Bradley O Brown, G Russell Warnick
Precision phenotyping, panomics, and system-level bioinformatics to delineate complex biologies of atherosclerosis: Rationale and design of the "Genetic Loci and the Burden of Atherosclerotic Lesions" study
JOURNAL OF CARDIOVASCULAR COMPUTED TOMOGRAPHY 8:(6) pp. 442-451. (2014)
Independent citations: 6 Dependent citations: 3 Total: 9
IF: 2.289

13. **Maurovich-Horvat P**, Karolyi M, Horvath T, Szilveszter B, Bartykowszki A, Jermendy AL, Panajotu A, Celeng C, Suhai FI, Major GP, Csobay-Novak C, Huttl K, Merkely B
Esmolol is noninferior to metoprolol in achieving a target heart rate of 65 beats/min in patients referred to coronary CT angiography: A randomized controlled clinical trial.
JOURNAL OF CARDIOVASC COMPUTED TOMOGRAPHY 9:(2) pp. 139-145. (2015)
Independent citations: 4 Dependent citations: 1 Total: 5
IF: 2.472

14. **Maurovich-Horvat P**, Kallianos K, Engel LC, Szymonifka J, Schlett CL, Koenig W, Hoffmann U, Truong QA
Relationship of thoracic fat depots with coronary atherosclerosis and circulating inflammatory biomarkers.
OBESITY 23:(6) pp. 1178-1184. (2015)
Independent citations: 11 Dependent citations: 1 Total: 12
IF: 3.614

15. Szilveszter B, Elzomor H, Karolyi M, Kolossvary M, Raaijmakers R, Benke K, Celeng C, Bartykowszki A, Bagyura Z, Lux A, Merkely B, **Maurovich-Horvat P**
The effect of iterative model reconstruction on coronary artery calcium quantification.
INTERNATIONAL JOURNAL OF CARDIOVASCULAR IMAGING 32:(1) pp. 153-160. (2016)
Independent citations: 19 Dependent citations: 2 Total: 21
IF 1.896

16. Kolossvary M, Szilveszter B, Edes IF, Nardai S, Voros V, Hartyanszky I, Merkely B, Voros S, **Maurovich-Horvat P**
Comparison of Quantity of Coronary Atherosclerotic Plaques Detected by Computed Tomography Versus Angiography
AMERICAN JOURNAL OF CARDIOLOGY 117:(12) pp. 1863-1867. (2016)
Independent citations: 3 Dependent citations: 5 Total: 8
IF: 3.398

17. Szilveszter B, Kolossvary M, Karady J, Jermendy AL, Karolyi M, Panajotu A, Bagyura

Z, Vecsey-Nagy M, Cury RC, Leipsic JA, Merkely B, **Maurovich-Horvat P**
Structured reporting platform improves CAD-RADS assessment.
JOURNAL OF CARDIOVASCULAR COMPUTED TOMOGRAPHY 11:(6) pp. 449-454. (2017)
IF: 3.095

18. Nagy E, Jermendy ÁL, Merkely B, **Maurovich-Horvat P**
Clinical importance of epicardial adipose tissue
ARCHIVES OF MEDICAL SCIENCE 13:(4) pp. 864-874. (2017)
Independent citations: 3 Dependent citations: 1 Total: 4
IF: 2.344

19. Kolossvary M, Karady J, Szilveszter B, Kitslaar P, Hoffmann U, Merkely B, **Maurovich-Horvat P**
Radiomic Features Are Superior to Conventional Quantitative Computed Tomographic Metrics to Identify Coronary Plaques With Napkin-Ring Sign
CIRCULATION-CARDIOVASCULAR IMAGING 10:(12) Paper e006843. 9 p. (2017)
Independent citations: 1 Total: 1
IF: 6.221

20. Kolossváry Márton, Szilveszter Bálint, Merkely Béla, **Maurovich-Horvat Pál**
Plaque imaging with CT—a comprehensive review on coronary CT angiography based risk assessment
CARDIOVASCULAR DIAGNOSIS AND THERAPY 7:(5) pp. 489-506. (2017)
Independent citations: 1 Dependent citations: 1 Total: 2
IF: -

21. Karolyi M, Szilveszter B, Kolossvary M, Takx RA, Celeng C, Bartykowszki A, Jermendy AL, Panajotu A, Karady J, Raaijmakers R, Giepmans W, Merkely B, **Maurovich-Horvat P**
Iterative model reconstruction reduces calcified plaque volume in coronary CT angiography.
EUROPEAN JOURNAL OF RADIOLOGY 87: pp. 83-89. (2017)
Independent citations: 3 Total: 3
IF: 2.843

22. Freiman M, Nickisch H, Prevrhal S, Schmitt H, Vembar M, **Maurovich-Horvat P**, Donnelly P, Goshen L
Improving CCTA-based lesions' hemodynamic significance assessment by accounting for partial volume modeling in automatic coronary lumen segmentation.
MEDICAL PHYSICS 44:(3) pp. 1040-1049. (2017)
Independent citations: 3 Dependent citations: 2 Total: 5
IF: 2.884

23. Karady J, Panajotu A, Kolossvary M, Szilveszter B, Jermendy AL, Bartykowszki A, Karolyi M, Celeng C, Merkely B, **Maurovich-Horvat P**
The effect of four-phasic versus three-phasic contrast media injection protocols on extravasation rate in coronary CT angiography: a randomized controlled trial.

EUROPEAN RADIOLOGY 27:(11) pp. 4538-4543. (2017)
Dependent citations: 2 Total: 2
IF: 4.027

24. Kolossvary M, Kellermayer M, Merkely B, **Maurovich-Horvat P**
Cardiac Computed Tomography Radiomics: A Comprehensive Review on Radiomic Techniques
JOURNAL OF THORACIC IMAGING 33:(1) pp. 26-34. (2018)
Independent citations: 5 Dependent citations: 2 Total: 7
IF: 1.624

25. Jermendy AL, Kolossvary M, Drobni ZD, Tarnoki AD, Tarnoki DL, Karady J, Voros S, Lamb HJ, Merkely B, Jermendy G, **Maurovich-Horvat P**
Assessing genetic and environmental influences on epicardial and abdominal adipose tissue quantities: A classical twin study.
INTERNATIONAL JOURNAL OF OBESITY 42: pp. 163-168. (2018)
IF: 5.151

26. Donnelly PM, Kolossvary M, Karady J, Ball PA, Kelly S, Fitzsimons D, Spence MS, Celeng C, Horvath T, Szilveszter B, van Es HW, Swaans MJ, Merkely B, **Maurovich-Horvat P**
Experience With an On-Site Coronary Computed Tomography-Derived Fractional Flow Reserve Algorithm for the Assessment of Intermediate Coronary Stenoses.
AMERICAN JOURNAL OF CARDIOLOGY 121:(1) pp. 9-13. (2018)
Independent citations: 2 Total: 2
IF: 3.171

27. Bartykowszki A, Kolossvary M, Jermendy AL, Karady J, Szilveszter B, Karolyi M, Balogh O, Sax B, Merkely B, **Maurovich-Horvat P**
Image Quality of Prospectively ECG-Triggered Coronary CT Angiography in Heart Transplant Recipients
AMERICAN JOURNAL OF ROENTGENOLOGY 210:(2) pp. 314-329. (2018)
Independent citations: 1 Total: 1
IF: 3.125

28. Giannopoulos AA, Mitsouras D, Bartykowszki A, Merkely B, Chatzizisis YS, Buechel RR, Kaufmann PA, Gaemperli O, **Maurovich-Horvat P**
High-Risk Plaque Regression and Stabilization: Hybrid Noninvasive Morphological and Hemodynamic Assessment.
CIRCULATION-CARDIOVASCULAR IMAGING 11:(7) Paper e007888. (2018)
IF: 6.221

9.2 Publications in Hungarian language related to the present thesis

29. **Maurovich-Horvat P**, Bartykowszki A, Kerecsen G, Thury A, Károlyi M, Balázs G, Várady E, Tóth L, Pintér N, Szukits S, Kolozsvári R, Hoffer K, Király I, Nagy L, Hüttl K, Préda I, Palkó A, Kiss RG, Battyány I, Merkely B
A koronária-CT-angiográfia leletezése. A Magyar Kardiológusok Társasága Szív-CT Munkacsoportjának és a Magyar Radiológusok Társasága Szív Képalkotó

Diagnosztikai Szekciójának közös ajánlása.
CARDIOLOGIA HUNGARICA 43:(5) pp. 275-281. (2013)

30. Maurovich-Horvat P
Vulnerábilis koszorúér-plakkok vizsgálata: genomikától a képi markerekig.
ORVOSKÉPZÉS 88:(2) pp. 275-277. (2013)

31. Drobni Zs, Karády J, **Maurovich-Horvat P**
Szív-CT szerepe a cardiovascularis rizikóbecslésben
MAGYAR CSALÁDORVOSOK LAPJA 2015:(5) pp. 40-42. (2015)

32. Bartykowszki A, Tóth L, Kerecsen G, Jermendy ÁL, Kolossváry M, Karády J, Szilveszter B, Károlyi M, Suhai FI, Panajotu A, Kolozsvári R, Balázs Gy, Hüttl K, Thury A, Batthyány I, Kiss RG, Merkely B, **Maurovich-Horvat P**
A koronária-CT-angiográfia értelmezése és leletezése. A Magyar Kardiológusok Társasága Kardiovaszkuláris Képalkotó Munkacsoportjának ajánlása.
CARDIOLOGIA HUNGARICA 47:(1) pp. 2-9. (2017)

33. Drobni Zs D, Kolossváry M, Karády J, Jermendy ÁL, Littvay L, Tárnoki Á D , Tárnoki D L , Voros Sz, Jermendy Gy, Merkely B, **Maurovich-Horvat P**
Van-e összefüggés az epikardiális zsírszövet és a koszorúér-betegség között?
CARDIOLOGIA HUNGARICA 47:(1) pp. 25-29. (2017)

34. Bagyura Z, Kolossvary M, Merkely B, **Maurovich-Horvat P**
A coronariarendszer komputertomográfiás vizsgálata - Országos Plakk Regiszter és Adatbázis (OPeRA)
ORVOSI HETILAP 158:(3) pp. 106-110. (2017)
IF: 0.322

9.3 Editorials related to the present thesis

35. Maurovich-Horvat P
The whole is more than the sum of its parts-Aristotle.
EUROPEAN HEART JOURNAL-CARDIOVASC IMAGING 18:(3) pp. 294-295. (2017)

36. Maurovich-Horvat P
The left main stem: The barometer of coronary artery disease severity?
JOURNAL OF CARDIOVASC COMPUTED TOMOGRAPHY 12:(3) pp. 238-239. (2018)

9.4 Book chapters not related to the present thesis

37. Préda I, Balogh I, Édes I, Forster T, Kerecsen G, Kiss RG, Maurovich-Horvat P, Merkely B, Simor T, Thury A
Irányelvek a szív sokszeletes CT-vizsgálatának szakmai feltételrendszeréhez -

Másodközlés magyar nyelven
In: Kardiológiai Szakmai Kollégium (szerk.)
Kardiológiai útmutató: klinikai irányelvek kézikönyve. Budapest: Medition Kiadó, 2008. pp. 8-20.

38. Préda I, Balogh I, Édes I, Forster T, Kerecsen G, Kiss RG, **Maurovich-Horvat P**, Merkely B, Simor T, Thury A
Irányelvek a szív sokszeletes CT – vizsgálatának szakmai feltételrendszeréhez.
In: Kardiológiai Szakmai Kollégium (szerk.)
Kardiológiai útmutató 2009/2. 184 p.
Budapest: Medition Kiadó, 2009. pp. 37-49.
(Klinikai irányelvek kézikönyve)

39. Osztheimer I, **Maurovich-Horvat P**
Control of Cardiac Output and Arterial Blood Pressure Regulation
In: Splinter R (szerk.)
Handbook of Physics in Medicine and Biology. Charlotte (NC): CRC Press, 2010. pp. 15-1-15-6.
(ISBN:978-1-4200-7524-3)

40. Mahabadi A, **Maurovich-Horvat P**, Hoffmann U
Antropometry of Abdominal Subcutaneous and Visceral Adipose Tissue with Computed Tomography
In: Preedy VR
The Handbook of Anthropometry: Physical Measures of Human Form in Health and Disease. New York: Springer-Verlag London Ltd, 2012. pp. 869-880.

41. Maurovich-Horvat P
Komputertomográfia (CT)
In: Tulassay Zsolt (szerk.)
A belgyógyászat alapjai. Budapest: Medicina Könyvkiadó, 2016. pp. 541-542.
(ISBN:978 963 226 554 4)
5., átdolgozott kiadás

42. Maurovich-Horvat P
Kóreredet. Az ischaemiás szívbetegség megjelenési formái
In: Tulassay Zsolt (szerk.)
A belgyógyászat alapjai. Budapest: Medicina Könyvkiadó, 2016. pp. 580-581.
(ISBN:978 963 226 554 4)
5., átdolgozott kiadás

43. Maurovich-Horvat P
Stabil koszorúér-betegség
In: Tulassay Zsolt (szerk.)
A belgyógyászat alapjai. Budapest: Medicina Könyvkiadó, 2016. pp. 581-586.
5., átdolgozott kiadás

44. Maurovich-Horvat P

Stabil koszorúér-betegség
In: Tulassay Zsolt, Békési Gábor, Rácz Károly (szerk.)
A belgyógyászat alapjai fogorvosok számára. 544 p.
Budapest: Medicina Könyvkiadó Zrt., 2014. pp. 91-93.
(ISBN:978-963-226-467-7)

45. Maurovich-Horvat P
Coronary computed tomography angiography: imaging of coronary atherosclerotic plaque
In: Camm AJ, Lüscher TF, Maurer G, Serruys PW (szerk.)
ESC CardioMed. Oxford: Oxford University Press, 2018. p. online.
(ISBN:978-019-878-490-6)
3. kiadás

9.5 International and Hungarian publications not related to the present

46. Celeng C, Leiner T, **Maurovich-Horvat P**, Merkely B, de Jong P, Dankbaar JW, van Es HW, Ghoshhajra BB, Hoffmann U, Takx RAP
Anatomical and Functional Computed Tomography for Diagnosing Hemodynamically Significant Coronary Artery Disease: A Meta-Analysis.
JACC-CARDIOVASCULAR IMAGING (In Press) (2018)
IF: 10.247

47. Foldyna B, Szilveszter B, Scholtz JE, Banerji D, **Maurovich-Horvat P**, Hoffmann U
CAD-RADS - a new clinical decision support tool for coronary computed tomography angiography.
EUROPEAN RADIOLOGY 28:(4) pp. 1365-1372. (2018)
IF: 4.027

48. Freiman M, Nickisch H, Schmitt H, **Maurovich-Horvat P**, Donnelly PM, Vembar M, Goshen L
A Functionally-Personalized Boundary Condition Model to Improve Estimates of Fractional Flow Reserve with CT (CT-FFR).
MEDICAL PHYSICS 45:(3) pp. 1170-1177. (2018)
IF: 2.884

49. Karady J, Ntalas I, Prendergast B, Blauth C, Niederer S, **Maurovich-Horvat P**, Rajani R
Transcatheter mitral valve replacement in mitral annulus calcification - "The art of computer simulation".
JOURNAL OF CARDIOVASCULAR COMPUTED TOMOGRAPHY 12:(2) pp. 153-157. (2018)
IF: 3.095

50. Kovacs A, Molnar AA, Kolossvary M, Szilveszter B, Panajotu A, Lakatos BK, Littvay L, Tarnoki AD, Tarnoki DL, Voros S, Jermendy G, Sengupta PP, Merkely B, **Maurovich-Horvat P**
Genetically determined pattern of left ventricular function in normal and hypertensive hearts.

JOURNAL OF CLINICAL HYPERTENSION 20:(5) pp. 949-958. (2018)
IF: 2.629

51. Liu T, **Maurovich-Horvat P**, Mayrhofer T, Puchner SB, Lu MT, Ghemigian K, Kitslaar PH, Broersen A, Pursnani A, Hoffmann U, Ferencik M
Quantitative coronary plaque analysis predicts high-risk plaque morphology on coronary computed tomography angiography: results from the ROMICAT II trial.
INTERNATIONAL JOURNAL OF CARDIOVASCULAR IMAGING 34:(2) pp. 311-319. (2018)
Independent citations: 1 Total: 1
IF: 2.036

52. Lucatelli P, Fagnani C, Tarnoki AD, Tarnoki DL, Sacconi B, Fejer B, Stazi MA, Salemi M, Cirelli C, d'Adamo A, Fanelli F, Catalano C, **Maurovich-Horvat P**, Jermendy AL, Jermendy G, Merkely B, Molnar AA, Pucci G, Schillaci G, Farina F, Meneghetti G, Baracchini C, Medda E
Genetic influence on femoral plaque and its relationship with carotid plaque: an international twin study.
INTERNATIONAL JOURNAL OF CARDIOVASCULAR IMAGING 34:(4) pp. 531-541. (2018)
IF: 2.036

53. Maroules CD, Hamilton-Craig C, Branch K, Lee J, Cury RC, **Maurovich-Horvat P**, Rubinshtein R, Thomas D, Williams M, Guo Y, Cury RC
Coronary artery disease reporting and data system (CAD-RADS(TM)): Inter-observer agreement for assessment categories and modifiers.
JOURNAL OF CARDIOVASCULAR COMPUTED TOMOGRAPHY 12:(2) pp. 125-130. (2018)
IF: 3.095

54. Szilveszter B, Maurovich-Horvat P
Myocardial computed tomography perfusion: a synergy of form and function
EUROPEAN HEART JOURNAL-CARDIOVASCULAR IMAGING *in press* (2018)
IF: 8.336

55. Puchner SB, Mayrhofer T, Park J, Lu MT, Liu T, **Maurovich-Horvat P**, Ghemigian K, Bittner DO, Fleg JL, Udelson JE, Truong QA, Hoffmann U, Ferencik M
Differences in the association of total versus local coronary artery calcium with acute coronary syndrome and culprit lesions in patients with acute chest pain: The coronary calcium paradox.
ATHEROSCLEROSIS 274: pp. 251-257. (2018)
IF: 4.467

56. Stocker TJ, Deseive S, Chen M, Leipsic J, Hadamitzky M, Rubinshtein R, Grove EL, Fang XM, Lesser J, **Maurovich-Horvat P**, Marques H, Andreini D, Tabbalat R, Kang JW, Eckert J, Dickson P, Forsdahl SH, Lambrechtsen J, Cury RC, Hausleiter J
Rationale and design of the worldwide prospective multicenter registry on radiation dose estimates of cardiac CT angiography in daily practice in 2017 (PROTECTION VI).
JOURNAL OF CARDIOVASCULAR COMPUTED TOMOGRAPHY 12:(1) pp.

81-85. (2018)
Independent citations: 1 Total: 1
IF: 3.095

57. Stocker TJ, Deseive S, Leipsic J, Hadamitzky M, Chen MY, Rubinshtein R, Heckner M, Bax JJ, Fang XM, Grove E, Lesser J, **Maurovich-Horvat P**, Otton J, Shin S, Pontone G, Marques H, Chow B, Nomura CH, Tabbalat R, Schmermund A, Kang JW, Naoum C, Atkins M, Martuscelli E, Massberg S, Hausleiter J
Reduction in radiation exposure in cardiovascular computed tomography imaging: results from the Prospective Multicenter Registry on RadiaTion Dose Estimates of Cardiac CT AngIOgraphy IN Daily Practice in 2017 (PROTECTION VI).
EUROPEAN HEART JOURNAL 2018: pp. 1-9. (2018)
IF: 23.425

58. Varga A, Di Leo G, Banga PV, Csobay-Novak C, Kolossvary M, **Maurovich-Horvat P**, Huttl K
Multidetector CT angiography of the Circle of Willis: association of its variants with carotid artery disease and brain ischemia
EUROPEAN RADIOLOGY 2018: Paper DOI:0.1007/s00330-018-5577-x. 11 p. (2018)
IF: 4.027

59. de Vecchi A, Niederer S, Karady J, Ntalas I, **Maurovich-Horvat P**, Rajani R
Computational fluid dynamic modelling to determine the hemodynamic effects of implanting a transcatheter mitral valve within the left ventricle.
INTERNATIONAL JOURNAL OF CARDIOVASCULAR IMAGING 34:(5) pp. 803-805. (2018)
IF: 2.036

60. Celeng C, Kolossvary M, Kovacs A, Molnar AA, Szilveszter B, Horvath T, Karolyi M, Jermendy AL, Tarnoki AD, Tarnoki DL, Karady J, Voros S, Jermendy G, Merkely B, **Maurovich-Horvat P**
Aortic root dimensions are predominantly determined by genetic factors: a classical twin study
EUROPEAN RADIOLOGY 27:(6) pp. 2419-2425. (2017)
IF: 4.027

61. Csobay-Novak C, Fontanini DM, Szilagyi B, Szeberin Z, Kolossvary M, **Maurovich-Horvat P**, Huttl K, Sotonyi P
Thoracic Aortic Strain is Irrelevant Regarding Endograft Sizing in Most Young Patients
ANNALS OF VASCULAR SURGERY 38: pp. 227-232. (2017)
IF: 1.363

62. Czimbalmos C, Csecs I, Polos M, Bartha E, Szucs N, Toth A, **Maurovich-Horvat P**, Becker D, Sapi Z, Szabolcs Z, Merkely B, Vago H
Uncommon presentation of a rare tumour - incidental finding in an asymptomatic patient: case report and comprehensive review of the literature on intrapericardial solitary fibrous tumours.
BMC CANCER 17:(1) Paper 612. 8 p. (2017)
IF: 3.288

63. Engel LC, Thai WE, Medina-Zuluaga H, Karolyi M, Sidhu MS, **Maurovich-Horvat P**, Margey R, Pomerantsev E, Abbara S, Ghoshhajra BB, Hoffmann U, Liew GY
Non-diagnostic coronary artery calcification and stenosis: a correlation of coronary computed tomography angiography and invasive coronary angiography.
ACTA RADIOLOGICA 58:(5) pp. 528-536. (2017)
Independent citations: 1 Total: 1
IF: 1.823

64. Fejer B, Tarnoki AD, Tarnoki DL, Lucatelli P, Littvay L, **Maurovich-Horvat P**, Jermendy AL, Kovacs A, Godor E, Fagnani C, Stazi MA, Molnar AA, Fanelli F, Cirelli C, Farina F, Baracchini C, Meneghetti G, Pucci G, Jermendy G, Merkely B, Schillaci G, Medda E
Heritability of the femoral intima media thickness
EUROPEAN JOURNAL OF INTERNAL MEDICINE 41: pp. 44-48. (2017)
IF: 3.282

65. Nemcsik J, Vecsey-Nagy M, Szilveszter B, Kolossváry M, Karády J, László A, Kőrösi B, Nemcsik-Bencze Z, Gonda X, Merkely B, Rihmer Z, **Maurovich-Horvat P**
Inverse association between hyperthymic affective temperament and coronary atherosclerosis: A coronary computed tomography angiography study
JOURNAL OF PSYCHOSOMATIC RESEARCH 103: pp. 108-112. (2017)
IF 2.947

66. Kolossvary M, Szekely AD, Gerber G, Merkely B, **Maurovich-Horvat P**
CT Images Are Noninferior to Anatomic Specimens in Teaching Cardiac Anatomy-A Randomized Quantitative Study
JOURNAL OF THE AMERICAN COLLEGE OF RADIOLOGY 14:(3) pp. 409-415.e2. (2017)
IF: 3.383

67. **Maurovich-Horvat P**, Suhai FI, Czimbalmos C, Toth A, Becker D, Kiss E, Ferencik M, Hoffmann U, Vago H, Merkely B
Coronary Artery Manifestation of Ormond Disease: The "Mistletoe Sign".
RADIOLOGY 282:(2) pp. 356-360. (2017)
IF: 7.469

68. Napp AE, Haase R, Laule M, Schuetz GM, Rief M, Dreger H, Feuchtner G, Friedrich G, Špaček M, Suchánek V, Fuglsang Kofoed K, Engstroem T, Schroeder S, Drosch T, Gutberlet M, Woinke M, **Maurovich-Horvat P**, Merkely B, Donnelly P, Ball P, Dodd JD, Quinn M, Saba L, Porcu M, Francone M, Mancone M, Erglis A, Zvaigzne L, Jankauskas A, Sakalyte G, Harań T, Ilnicka-Suckiel M, Bettencourt N, Gama-Ribeiro V, Condrea S, Benedek I, Čemerlić Adjić N, Adjić O, Rodriguez-Palomares J, Garcia Del Blanco B, Roditi G, Berry C, Davis G, Thwaite E, Knuuti J, Pietilä M, Kępka C, Kruk M, Vidakovic R, Neskovic AN, Díez I, Lecumberri I, Geleijns J, Kubiak C, Strenge-Hesse A, Do TH, Frömel F, Gutiérrez-Ibarluzea I, Benguria-Arrate G, Keiding H, Katzer C, Müller-Nordhorn J, Rieckmann N, Walther M, Schlattmann P, Dewey M
Computed tomography versus invasive coronary angiography: design and methods of the pragmatic randomised multicentre DISCHARGE trial.
EUROPEAN RADIOLOGY 27:(7) pp. 2957-2968. (2017)

Independent citations: 1 Dependent citations: 1 Total: 2
IF: 4.027

69. Varga-Szemes A, van der Geest RJ, Schoepf UJ, Spottiswoode BS, De Cecco CN, Muscogiuri G, Wichmann JL, Mangold S, Fuller SR, **Maurovich-Horvat P**, Merkely B, Litwin SE, Vliegenthart R, Suranyi P
Effect of inversion time on the precision of myocardial late gadolinium enhancement quantification evaluated with synthetic inversion recovery MR imaging.
EUROPEAN RADIOLOGY 27:(8) pp. 3235-3243. (2017)
Dependent citations: 2 Total: 2
IF: 4.027

70. Vereckei A, Katona G, Szelenyi Z, Takacs E, **Maurovich-Horvat P**, Becker D
ECG stress test induced atrial ischemia in a patient with old inferior myocardial infarction due to a distal coronary artery lesion
JOURNAL OF GERIATRIC CARDIOLOGY 14:(1) pp. 73-77. (2017)
IF: 1.581

71. Benke K, Agg B, Szabo L, Szilveszter B, Odler B, Polos M, Cao C, **Maurovich-Horvat P**, Radovits T, Merkely B, Szabolcs Z
Bentall procedure: quarter century of clinical experiences of a single surgeon
JOURNAL OF CARDIOTHORACIC SURGERY 11:(1) Paper 19. 9 p. (2016)
Dependent citations: 3 Total: 3
IF: 1.101

72. Benke K, Sayour AA, Ágg B, Radovits T, Szilveszter B, Odler B, Németh BT, Pólos M, Oláh A, Mátyás Cs, Ruppert M, Hartyánszky I, **Maurovich-Horvat P**, Merkely B, Szabolcs Z
Génpolimorfizmusok, mint rizikófaktorok a Marfan-szindróma kardiovaszkuláris manifesztációinak előrejelzésében
CARDIOLOGIA HUNGARICA 46:(2) pp. 76-81. (2016)

73. Celeng C, Vadvala H, Puchner S, Pursnani A, Sharma U, Kovacs A, **Maurovich-Horvat P**, Hoffmann U, Ghoshhajra B
Defining the optimal systolic phase targets using absolute delay time for reconstructions in dual-source coronary CT angiography.
INTERNATIONAL JOURNAL OF CARDIOVASCULAR IMAGING 32:(1) pp. 91-100. (2016)
Independent citations: 1 Dependent citations: 1 Total: 2
IF: 1.896

74. Celeng C, **Maurovich-Horvat P**, Ghoshhajra BB, Merkely B, Leiner T, Takx RA
Prognostic Value of Coronary Computed Tomography Angiography in Patients With Diabetes: A Meta-analysis.
DIABETES CARE 39:(7) pp. 1274-1280. (2016)
Independent citations: 5 Total: 5
IF: 11.857

75. den Harder AM, de Heer LM, **Maurovich-Horvat P**, Merkely B, de Jong PA, Das M, de Wit GA, Leiner T, Budde RP, on behalf of the CRICKET Investigators

Ultra low-dose chest ct with iterative reconstructions as an alternative to conventional chest x-ray prior to heart surgery (CRICKET study): Rationale and design of a multicenter randomized trial.
JOURNAL OF CARDIOVASCULAR COMPUTED TOMOGRAPHY 10:(3) pp. 242-245. (2016)
Independent citations: 5 Dependent citations: 1 Total: 6
IF: 3.185

76. Giannopoulos AA, Chatzizisis YS, **Maurovich-Horvat P**, Antoniadis AP, Hoffmann U, Steigner ML, Rybicki FJ, Mitsouras D
Quantifying the effect of side branches in endothelial shear stress estimates.
ATHEROSCLEROSIS 251: pp. 213-218. (2016)
Independent citations: 2 Dependent citations: 3 Total: 5
IF: 4.239

77. Kovacs A, Molnar AA, Celeng C, Toth A, Vago H, Apor A, Tarnoki AD, Tarnoki DL, Kosa J, Lakatos P, Voros S, Jermendy G, Merkely B, Maurovich-Horvat P
Hypertrophic Cardiomyopathy in a Monozygotic Twin Pair: Similarly Different
CIRCULATION-CARDIOVASCULAR IMAGING 9:(6) Paper e004794. 2 p. (2016)
IF: 6.803

78. Singh P, Emami H, Subramanian S, Maurovich-Horvat P, Marincheva-Savcheva G, Medina HM, Abdelbaky A, Alon A, Shankar SS, Rudd JH, Fayad ZA, Hoffmann U, Tawakol A
Coronary Plaque Morphology and the Anti-Inflammatory Impact of Atorvastatin: A Multicenter 18F-Fluorodeoxyglucose Positron Emission Tomographic/Computed Tomographic Study.
CIRCULATION-CARDIOVASCULAR IMAGING 9:(12) Paper e004195. 9 p. (2016)
Independent citations: 6 Dependent citations: 3 Total: 9
IF: 6.803

79. Széplaki G, Gellér L, Özcan EE, Tahin T, Kovács OM, Parázs N, Karády J, **Maurovich-Horvat P**, Szilágyi S, Osztheimer I, Tóth A, Merkely B
Respiratory gating algorithm helps to reconstruct more accurate electroanatomical maps during atrial fibrillation ablation performed under spontaneous respiration
JOURNAL OF INTERVENTIONAL CARDIAC ELECTROPHYSIOLOGY 46:(2) pp. 153-159. (2016)
Dependent citations: 1 Total: 1
IF: 1.826

80. Bagyura Zs, Kolossváry M, Merkely B, **Maurovich-Horvat P**
Személyre szabott kardiovaszkuláris rizikóbecslés koronária CT-vel Strukturált leletezés és az OPeRA (Országos Plaque Regiszter és Adatbázis) Projekt.
IME: INTERDISZCIPLINÁRIS MAGYAR EGÉSZSÉGÜGY / INFORMATIKA ÉS MENEDZSMENT AZ EGÉSZSÉGÜGYBEN 14:(4) pp. 19-23. (2015)

81. Bencsik P, Sasi V, Kiss K, Kupai K, Kolossvary M, **Maurovich-Horvat P**, Csont T, Ungi I, Merkely B, Ferdinandy P

Serum lipids and cardiac function correlate with nitrotyrosine and MMP activity in coronary artery disease patients
EUROPEAN JOURNAL OF CLINICAL INVESTIGATION 45:(7) pp. 692-701. (2015)
Independent citations: 7 Dependent citations: 6 Total: 13
IF: 2.687

82. Benke K, Agg B, Matyas G, Szokolai V, Harsanyi G, Szilveszter B, Odler B, Polos M, **Maurovich-Horvat P**, Radovits T, Merkely B, Nagy ZB, Szabolcs Z
Gene polymorphisms as risk factors for predicting the cardiovascular manifestations in Marfan syndrome. Role of folic acid metabolism enzyme gene polymorphisms in Marfan syndrome.
THROMBOSIS AND HAEMOSTASIS 114:(4) pp. 748-756. (2015)
Independent citations: 3 Dependent citations: 2 Total: 5
IF: 5.255

83. Celeng C, Szekely L, Toth A, Denes M, Csobay-Novak C, Bartykowszki A, Karolyi M, Vago H, Szoke S, Coelho Filho OR, Andreka P, Merkely B, **Maurovich-Horvat P**
Multimodality Imaging of Giant Right Coronary Aneurysm and Postsurgical Coronary Artery Inflammation.
CIRCULATION 132:(1) pp. e1-e5. (2015)
Independent citations: 1 Total: 1
IF 17,202

84. Ferencik M, Mayrhofer T, Puchner SB, Lu MT, **Maurovich-Horvat P**, Liu T, Ghemigian K, Kitslaar P, Broersen A, Bamberg F, Truong QA, Schlett CL, Hoffmann U
Computed tomography-based high-risk coronary plaque score to predict acute coronary syndrome among patients with acute chest pain - Results from the ROMICAT II trial.
JOURNAL OF CARDIOVASCULAR COMPUTED TOMOGRAPHY 9:(6) pp. 538-545. (2015)
Independent citations: 11 Dependent citations: 8 Total: 19
IF: 2.472

85. Ferencik M, Liu T, Mayrhofer T, Puchner SB, Lu MT, **Maurovich-Horvat P**, Pope JH, Truong QA, Udelson JE, Peacock WF, White CS, Woodard PK, Fleg JL, Nagurney JT, Januzzi JL, Hoffmann U
hs-Troponin I Followed by CT Angiography Improves Acute Coronary Syndrome Risk Stratification Accuracy and Work-Up in Acute Chest Pain Patients: Results From ROMICAT II Trial.
JACC-CARDIOVASCULAR IMAGING 8:(11) pp. 1272-1281. (2015)
Independent citations: 7 Dependent citations: 7 Total: 14
IF: 7.815

86. Gitsioudis G, Schussler A, Nagy E, **Maurovich-Horvat P**, Buss SJ, Voss A, Hosch W, Hofmann N, Kauczor HU, Giannitsis E, Katus HA, Korosoglou G
Combined Assessment of High-Sensitivity Troponin T and Noninvasive Coronary Plaque Composition for the Prediction of Cardiac Outcomes.
RADIOLOGY 276:(1) pp. 73-81. (2015)
Independent citations: 3 Dependent citations: 5 Total: 8

IF: 6.798

87. **Maurovich-Horvat P**, Tarnoki DL, Tarnoki AD, Horvath T, Jermendy AL, Kolossvary M, Szilveszter B, Voros V, Kovacs A, Molnar AA, Littvay L, Lamb HJ, Voros S, Jermendy G, Merkely B
Rationale, Design, and Methodological Aspects of the BUDAPEST-GLOBAL Study (Burden of Atherosclerotic Plaques Study in Twins-Genetic Loci and the Burden of Atherosclerotic Lesions).
CLINICAL CARDIOLOGY 38:(12) pp. 699-707. (2015)
Dependent citations: 6 Total: 6
IF: 2.431

88. Puchner SB, Ferencik M, **Maurovich-Horvat P**, Nakano M, Otsuka F, Kauczor H-U, Virmani R, Hoffmann U, Schlett CL
Iterative image reconstruction algorithms in coronary CT angiography improve the detection of lipid-core plaque - a comparison with histology
EUROPEAN RADIOLOGY 25:(1) pp. 15-23. (2015)
Independent citations: 14 Dependent citations: 1 Total: 15
IF: 3.640

89. Szelid Z, Lux A, Kolossvary M, Toth A, Vago H, Lendvai Z, Kiss L, **Maurovich-Horvat P**, Bagyura Z, Merkely B
Right Ventricular Adaptation Is Associated with the Glu298Asp Variant of the NOS3 Gene in Elite Athletes.
PLOS ONE 10:(10) Paper e0141680. 12 p. (2015)
Independent citations: 2 Dependent citations: 1 Total: 3
IF: 3.057

90. Becker D, Móri A, Bárczi Gy, Vágó H, Szenczi O, Berta B, Heltai K, Zima E, **Maurovich-Horvat P**, Merkely B
The magnitude of percutaneous coronary intervention treatment in high and medium risk non-ST elevation acute coronary syndrome
COR ET VASA 56:(4) pp. e333-e336. (2014)

91. Molnar AA, Kovacs A, Apor A, Tarnoki AD, Tarnoki DL, Horvath T, **Maurovich-Horvat P**, Kiss RG, Jermendy G, Merkely B
Case Report of Multiple Valve Disease Found in Triplets
TWIN RESEARCH AND HUMAN GENETICS 17:(5) pp. 383-389. (2014)
Dependent citations: 1 Total: 1
IF: 2.297

92. Ozcan EE, Szeplaki G, Tahin T, Osztheimer I, Szilagyi S, Apor A, **Maurovich-Horvat P**, Vago H, Merkely B, Geller L
Impact of respiration gating on image integration guided atrial fibrillation ablation.
CLINICAL RESEARCH IN CARDIOLOGY 103:(9) pp. 727-731. (2014)
Independent citations: 6 Dependent citations: 1 Total: 7
IF: 4.560

93. Karolyi M, Seifarth H, Liew G, Schlett CL, **Maurovich-Horvat P**, Stolzmann P, Dai G, Huang S, Goergen CJ, Nakano M, Otsuka F, Virmani R, Hoffmann U, Sosnovik DE

Classification of coronary atherosclerotic plaques ex vivo with T1, T2, and ultrashort echo time CMR
JACC-CARDIOVASCULAR IMAGING 6:(4) pp. 466-474. (2013)
Independent citations: 8 Dependent citations: 4 Total: 12
IF: 6.986

94. Schlett CL, **Maurovich-Horvat P**, Ferencik M, Alkadhi H, Stolzmann P, Scheffel H, Seifarth H, Nakano M, Do S, Vorpahl M, Kauczor HU, Bamberg F, Tearney GJ, Virmani R, Hoffmann U
Histogram Analysis of Lipid-Core Plaques in Coronary Computed Tomographic Angiography: Ex Vivo Validation Against Histology
INVESTIGATIVE RADIOLOGY 48:(9) pp. 646-653. (2013)
Independent citations: 8 Dependent citations: 9 Total: 17
IF: 4.453

95. Schlett CL, Ferencik M, Celeng C, **Maurovich-Horvat P**, Scheffel H, Stolzmann P, Do S, Kauczor HU, Alkadhi H, Bamberg F, Hoffmann U
How to assess non-calcified plaque in CT angiography: delineation methods affect diagnostic accuracy of low-attenuation plaque by CT for lipid-core plaque in histology.
EUROPEAN HEART JOURNAL-CARDIOVASCULAR IMAGING 14:(11) pp. 1099-1105. (2013)
Independent citations: 6 Dependent citations: 5 Total: 11
IF: 3.669

96. Bagyura Zs, Szelid Zs, Soós P, Szenczi O, **Maurovich-Horvat P**, Édes E, Lux Á, Polgár L, Andrási Z, Tátrai A, Józan P, Merkely B
Magyarországi primer prevenciós populációs felmérés: Budakalász Epidemiológiai Vizsgálat előzetes eredmények.
ORVOSKÉPZÉS 87:(2) pp. 102-108. (2012)

97. Ferencik M, Schlett CL, Ghoshhajra BB, Kriegel MF, Joshi SB, **Maurovich-Horvat P**, Rogers IS, Banerji D, Bamberg F, Truong QA, Brady TJ, Nagurney JT, Hoffmann U
A Computed Tomography-Based Coronary Lesion Score to Predict Acute Coronary Syndrome Among Patients With Acute Chest Pain and Significant Coronary Stenosis on Coronary Computed Tomographic Angiogram.
AMERICAN JOURNAL OF CARDIOLOGY 110:(2) pp. 183-189. (2012)
Independent citations: 26 Dependent citations: 15 Total: 41
IF: 3.209

98. Genders TS, Steyerberg EW, Hunink MG, Nieman K, Galema TW, Mollet NR, de Feyter PJ, Krestin GP, Alkadhi H, Leschka S, Desbiolles L, Meijs MF, Cramer MJ, Knuuti J, Kajander S, Bogaert J, Goetschalckx K, Cademartiri F, Maffei E, Martini C, Seitun S, Aldrovandi A, Wildermuth S, Stinn B, Fornaro J, Feuchtner G, De Zordo T, Auer T, Plank F, Friedrich G, Pugliese F, Petersen SE, Davies LC, Schoepf UJ, Rowe GW, van Mieghem CA, van Driessche L, Sinitsyn V, Gopalan D, Nikolaou K, Bamberg F, Cury RC, Battle J, **Maurovich-Horvat P**, Bartykowszki A, Merkely B, Becker D, Hadamitzky M, Hausleiter J, Dewey M, Zimmermann E, Laule M Prediction model to estimate presence of coronary artery disease: retrospective pooled analysis of existing cohorts
BRITISH MEDICAL JOURNAL (BMJ) 344:(7862) Paper e3485. 13 p. (2012)

Independent citations: 60 Dependent citations: 12 Total: 72
IF: 17.215

99. Ghoshhajra BB, **Maurovich-Horvat P**, Techasith T, Medina HM, Verdini D, Sidhu MS, Blankstein R, Brady TJ, Cury RC
Infarct detection with a comprehensive cardiac CT protocol
JOURNAL OF CARDIOVASCULAR COMPUTED TOMOGRAPHY 6:(1) pp. 14-23. (2012)
Independent citations: 8 Dependent citations: 2 Total: 10
IF: 2.552

100. Jensen JK, Medina H, Norgaard BL, Ovrehus KA, Jensen JM, Nielsen LH, **Maurovich-Horvat P**, Engel LC, Januzzi JL, Hoffmann U, Truong QA
Association of ischemic stroke to coronary artery disease using computed tomography coronary angiography
INTERNATIONAL JOURNAL OF CARDIOLOGY 160:(3) pp. 171-174. (2012)
Independent citations: 9 Total: 9
IF: 5.509

101. Mekkaoui C, Huang S, Chen HH, Dai G, Reese TG, Kostis WJ, Thiagalingam A, Maurovich-Horvat P, Ruskin JN, Hoffmann U, Jackowski MP, Sosnovik DE
Fiber architecture in remodeled myocardium revealed with a quantitative diffusion CMR tractography framework and histological validation.
JOURNAL OF CARDIOVASCULAR MAGNETIC RESONANCE 14: Paper 70. 11 p. (2012)
Independent citations: 29 Dependent citations: 6 Total: 35
IF: 4.435

102. Seifarth H, Schlett CL, Nakano M, Otsuka F, Károlyi M, Liew G, Maurovich-Horvat P, Alkadhi H, Virmani R, Hoffmann U
Histopathological correlates of the napkin-ring sign plaque in coronary CT angiography
ATHEROSCLEROSIS 224:(1) pp. 90-96. (2012)
Independent citations: 28 Dependent citations: 8 Total: 36
IF: 3.706

103. Stolzmann P, Schlett CL, **Maurovich-Horvat P**, Maehara A, Ma S, Scheffel H, Engel LC, Karolyi M, Mintz GS, Hoffmann U
Variability and accuracy of coronary CT angiography including use of iterative reconstruction algorithms for plaque burden assessment as compared with intravascular ultrasound-an ex vivo study.
EUROPEAN RADIOLOGY 22:(10) pp. 2067-2075. (2012)
Independent citations: 12 Dependent citations: 3 Total: 15
IF: 3.548

104. Ghoshhajra BB, Rogers IS, **Maurovich-Horvat P**, Techasith T, Verdini D, Sidhu MS, Drzezga NK, Medina HM, Blankstein R, Brady TJ, Cury RC
A comparison of reconstruction and viewing parameters on image quality and accuracy of stress myocardial CT perfusion.
JOURNAL OF CARDIOVASCULAR COMPUTED TOMOGRAPHY 5:(6) pp. 459-466. (2011)

Independent citations: 7 Dependent citations: 3 Total: 10

105. **Maurovich-Horvat P**, Kallianos K, Engel LC, Szymonifka J, Fox CS, Hoffmann U, Truong QA
Influence of pericoronary adipose tissue on local coronary atherosclerosis as assessed by a novel MDCT volumetric method
ATHEROSCLEROSIS 219:(1) pp. 151-157. (2011)
Independent citations: 18 Dependent citations: 4 Total: 22
IF: 3.794

106. Donnelly P, **Maurovich-Horvat P**, Vorpahl M, Nakano M, Kaple RK, Warger W, Tanaka A, Tearney G, Virmani R, Hoffmann U
Multimodality imaging atlas of coronary atherosclerosis.
JACC-CARDIOVASCULAR IMAGING 3:(8) pp. 876-880. (2010)
Independent citations: 6 Dependent citations: 3 Total: 9
IF: 5.528

107. Kárpáti K, Brodszky V, Boncz I, Merkely B, **Maurovich-Horvat P**, Gulácsi L
Az első akut miokardiális infarktuson átesett, hospitalizált betegek halálozása Magyarországon 2003-2005
EGÉSZSÉGÜGYI GAZDASÁGI SZEMLE 48:(1) pp. 6-10. (2010)

108. **Maurovich-Horvat P**, Mori T, Kerecsen G, Fovenyi J, Sallai T, Soos P, Preda I, Merkely B, Jermendy G
Assessment of coronary artery calcification using dual-source computed tomography in adult asymptomatic patients with type 1 diabetes mellitus.
MEDICAL SCIENCE MONITOR 16:(7) pp. MT59-MT64. (2010)
Independent citations: 2 Total: 2
IF: 1.699

109. Szelid Zs, Kerecsen G, Maurovich-Horvát P, Lux Á, Marosi E, Kovács A, Kiss RG, Préda I, Merkely B
Determination of coronary in-stent restenosis using dual source computed tomography angiography
INTERVENTIONAL MEDICINE AND APPLIED SCIENCE 2:(1) pp. 5-9. (2010)
Independent citations: 1 Total: 1

110. Truong QA, Yared K, **Maurovich-Horvat P**, Siegel E, Cubeddu RJ, King ME, Heist EK, Mansour M, Holmvang G
Images in cardiovascular medicine. Double-chambered right ventricle and situs inversus with dextrocardia
CIRCULATION 121:(9) pp. e229-e232. (2010)
Independent citations: 2 Total: 2
IF: 14.432

111. Vago H, Toth A, Apor A, **Maurovich-Horvat P**, Toth M, Merkely B
Cardiac contusion in a professional soccer player: visualization of acute and late pathological changes in the myocardium with magnetic resonance imaging
CIRCULATION 121:(22) pp. 2456-2461. (2010)
Independent citations: 17 Dependent citations: 2 Total: 19

IF: 14.432

112. Becker D, **Maurovich-Horvat P**, Barczi G, Szabo G, Fulop G, Nagy A, Molnar L, Apor A, Belicza E, Merkely B
Life after coronary stent thrombosis.
MEDICAL SCIENCE MONITOR 15:(5) pp. CR236-CR241. (2009)
Independent citations: 3 Total: 3
IF: 1.543

113. **Maurovich-Horvat P**, Kerecsen G, Móri TJ, Fövényi J, Sallai T, Soós P, Préda I, Merkely B, Jermendy Gy
A coronariakalcifikáció vizsgálata kettős sugárforrású, sokszeletes komputertomográfiával 1-es típusú diabetes mellitusban szenvedők körében.
LEGE ARTIS MEDICINAE 19:(8-9) pp. 501-507. (2009)

114. **Maurovich-Horvat P**, Kerecsen G, Préda I, Merkely B, Jermendy Gy
Nem-invazív koronarográfia és "Ca-scoring"-vizsgálat 2-es típusú cukorbetegségben
DIABETOLOGIA HUNGARICA 16:(2) pp. 165-167. (2008)

115. Abbara S, Pena AJ, **Maurovich-Horvat P**, Butler J, Sosnovik DE, Lembcke A, Cury RC, Hoffmann U, Ferencik M, Brady TJ
Feasibility and optimization of aortic valve planimetry with MDCT
AMERICAN JOURNAL OF ROENTGENOLOGY 188:(2) pp. 356-360. (2007)
Independent citations: 32 Dependent citations: 5 Total: 37
IF: 2.470

116. Fox CS, Massaro JM, Hoffmann U, Pou KM, **Maurovich-Horvat P**, Liu CY, Vasan RS, Murabito JM, Meigs JB, Cupples LA, D Agostino RB Sr, O Donnell CJ
Abdominal visceral and subcutaneous adipose tissue compartments: association with metabolic risk factors in the Framingham Heart Study
CIRCULATION 116:(1) pp. 39-48. (2007)
Independent citations: 1174 Dependent citations: 91 Total: 1265
IF: 12.755

117. Pou KM, Massaro JM, Hoffmann U, Vasan RS, **Maurovich-Horvat P**, Larson MG, Keaney JF Jr, Meigs JB, Lipinska I, Kathiresan S, Murabito JM, O Donnell CJ, Benjamin EJ, Fox CS
Visceral and subcutaneous adipose tissue volumes are cross-sectionally related to markers of inflammation and oxidative stress: the Framingham Heart Study
CIRCULATION 116:(11) pp. 1234-1241. (2007)
Independent citations: 462 Dependent citations: 27 Total: 489
IF:12.755

118. Gulácsi L, Májer I, Boncz I, Brodszky V, Merkely B, **Maurovich-Horvat P**, Kárpáti K
Az akut myocardiális infarctus betegségterhe Magyarországon, 2003-2005
ORVOSI HETILAP 148:(27) pp. 1259-1266. (2007)
Independent citations: 4 Dependent citations: 2 Total: 6

119. Kerecsen G, **Maurovich-Horvat P**, Kiss RG, Préda I
A szív koszorúereinek non-invazív ábrázolása multidetektoros CT-vel.

PRAXIS 16:(9) pp. 693-699. (2007)

120. **Maurovich-Horvat P**, Massaro J, Fox CS, Moselewski F, O Donnell CJ, Hoffmann U
Comparison of anthropometric, area- and volume-based assessment of abdominal subcutaneous and visceral adipose tissue volumes using multi-detector computed tomography
INTERNATIONAL JOURNAL OF OBESITY 31:(3) pp. 500-506. (2007)
Independent citations: 92 Dependent citations: 69 Total: 161
IF: 3.560

121. **Maurovich-Horvat P**, Schauerte P, Soós P, Zima E, Acsády Gy, Merkely B
Nem-gyógyszeres kamrai frekvenciakontroll pitvarfibrilláció alatt: a pitvar-kamrai (AV) csomóra ható paraszimpatikus plexus ingerlése
CARDIOLOGIA HUNGARICA 35:(4) pp. 210-217. (2005)

122. Soos P, Merkely B, **Maurovich-Horvat P**, Zima E, Schauerte P
Determinants and effects of electrical stimulation of the inferior interatrial parasympathetic plexus during atrial fibrillation
JOURNAL OF CARDIOVASCULAR ELECTROPHYSIOLOGY 16:(12) pp. 1362-1367. (2005)
Independent citations: 7 Dependent citations: 6 Total: 13
IF: 3.285

9.6 Review articles

123. Préda I, Kerecsen G, **Maurovich-Horvat P**
Nem invazív coronaria-angiográfia sokszeletes komputertomográfiával
LEGE ARTIS MEDICINAE 17:(8-9) pp. 555-563. (2007)
Dependent citations: 5 Total: 5

124. **Maurovich-Horvat P**, Kerecsen G, Kiss RG, Merkely B, Préda I
A szív koszorúereinek non-invazív ábrázolása dual-source CT-vel.
PRAXIS: A MINŐSÉGI GYÓGYÍTÁS ELMÉLETE ÉS GYAKORLATA 17:(6) pp. 409-415. (2008)

125. Préda I, Balogh I, Édes I, Forster T, Kerecsen G, Kiss RG, **Maurovich-Horvat P**, Merkely B, Simor T, Thury A
Irányelvek a szív sokszeletes CT-vizsgálatának szakmai feltételrendszeréhez.
CARDIOLOGIA HUNGARICA 38:(4) pp. 368-375. (2008)

126. **Maurovich-Horvat P**, Kerecsen G, Préda I, Kiss RG, Kovács A, Merkely B
A coronaria-CT technikai háttere és klinikai alkalmazása
ORVOSKÉPZÉS 84:(2) pp. 107-113. (2009)
Dependent citations: 3 Total: 3

127. Préda I, **Maurovich-Horvat P**, Kerecsen G, Kiss RG, Kovács A, Merkely B
A sokszeletes CT jelentősége a kardiovaszkuláris prevencióban.
KARDIOVASZKULÁRIS PREVENCIÓ ÉS REHABILITÁCIÓ 2:(3) pp. 5-8. (2009)

128. **Maurovich-Horvat P**, Ferencik M, Bamberg F, Hoffmann U
Methods of plaque quantification and characterization by cardiac computed tomography
JOURNAL OF CARDIOVASCULAR COMPUTED TOMOGRAPHY 3:(Suppl 2) pp. S91- S98. (2009)
Independent citations: 4 Dependent citations: 2 Total: 6

129. Bárczi Gy, **Maurovich-Horvat P**, Merkely B
Fókuszban a vulnerábilis plakk - a jelen és a közeljövő.
METABOLIZMUS 8:(3) pp. 143-146. (2010)

130. **Maurovich-Horvat P**, Ghoshhajra B, Ferencik M
Coronary CT Angiography for the Detection of Obstructive Coronary Artery Disease
CURRENT CARDIOVASCULAR IMAGING REPORTS 3:(6) pp. 355-365. (2010)
Dependent citations: 1 Total: 1

131. Stolzmann P, Subramanian S, Abdelbaky A, **Maurovich-Horvat P**, Scheffel H, Tawakol A, Hoffmann U
Complementary Value of Cardiac FDG PET and CT for the Characterization of Atherosclerotic Disease
RADIOGRAPHICS 31:(5) pp. 1255-1269. (2011)
Independent citations: 9 Dependent citations: 3 Total: 12
IF: 2.854

132. Bartykowszki A, **Maurovich-Horvat P**
A szív-CT vizsgálat és indikációja.
MAGYAR CSALÁDORVOSOK LAPJA 2012:(1) pp. 47-51. (2012)

133. Bartykowszki A, Celeng C, Károlyi M, **Maurovich-Horvat P**
High Risk Plaque Features on Coronary CT Angiography
CURRENT CARDIOVASCULAR IMAGING REPORTS 7:(8) p. Article Number: 9279. 12 p. (2014)
Independent citations: 1 Total: 1

134. **Maurovich-Horvat P**, Bartykowszki A, Kerecsen G, Thury A, Károlyi M, Balázs G, Várady E, Tóth L, Pintér N, Szukits S, Kolozsvári R, Hoffer K, Király I, Nagy L, Hüttl K, Préda I, Palkó A, Kiss RG, Battyány I, Merkely B
A coronariák CT-angiográfiás vizsgálatának leletezése.
MAGYAR RADIOLÓGIA ONLINE 4:(11) Paper a_coronariak.html. 11 p. (2013)

135. Nagy E, **Maurovich-Horvat P**, Jermendy ÁL, Merkely B, Jermendy Gy
Az epicardialis zsírszövet klinikai jelentősége
DIABETOLOGIA HUNGARICA 22:(4) pp. 225-234. (2014)

136. Júlia Karády, Zsófia D Drobni, Márton Kolossváry, **Pál Maurovich-Horvat**
Non-invasive Assessment of Coronary Plaque Morphology
CURRENT RADIOLOGY REPORTS 3: Paper 36. 10 p. (2015)

137. Celeng C, Takx RA, Ferencik M, **Maurovich-Horvat P**
Non-invasive and invasive imaging of vulnerable coronary plaque

TRENDS IN CARDIOVASCULAR MEDICINE 26:(6) pp. 538-547. (2016)
IF: 4.964
Independent citations: 8 Dependent citations: 1 Total: 9

138. Benedek T, **Maurovich-Horvat P**, Ferdinandy P, Merkely B
The Use of Biomarkers for the Early Detection of Vulnerable Atherosclerotic Plaques and Vulnerable Patients. A Review
JOURNAL OF CARDIOVASCULAR EMERGENCIES 2:(3) pp. 106-113. (2016)
Independent citations: 1 Dependent citations: 1 Total: 2

139. Karády Júlia, Whitaker John, Rajani Ronak, **Maurovich-Horvat Pál**
State-of-the-Art CT Imaging of the Left Atrium
CURRENT RADIOLOGY REPORTS 4:(8) Paper 45. 11 p. (2016)

140. Szilveszter B, Celeng C, **Maurovich-Horvat P**
Plaque assessment by coronary CT
INTERNATIONAL JOURNAL OF CARDIOVASCULAR IMAGING 32:(1) pp. 161-172. (2016)
IF: 1.896
Independent citations: 10 Dependent citations: 2 Total: 12

141. Willemink MJ, Leiner T, **Maurovich-Horvat P**
Cardiac CT Imaging of Plaque Vulnerability: Hype or Hope?
CURRENT CARDIOLOGY REPORTS 18:(4) Paper 37. 10 p. (2016)
IF: 2.058

142. Edvardsen T, Donal E, Bucciarelli-Ducci C, **Maurovich-Horvat P**, Maurer G, Popescu BA
The years 2015-2016 in the European Heart Journal-Cardiovascular Imaging. Part I
EUROPEAN HEART JOURNAL-CARDIOVASCULAR IMAGING 18:(10) pp. 1092-1098.(2017)
Dependent citations: 1 Total: 1
IF: 8.336

143. Edvardsen T, Gerber B, Donal E, **Maurovich-Horvat P**, Maurer G, Popescu BA
The year 2015-16 in the European Heart Journal-Cardiovascular Imaging. Part II
EUROPEAN HEART JOURNAL-CARDIOVASCULAR IMAGING 18:(12) pp. 1322-1330. (2017)
IF: 8.336

144. Edvardsen T, Haugaa KH, Gerber BL, **Maurovich-Horvat P**, Donal E, Maurer G, Popescu BA
The year 2017 in the European Heart Journal-Cardiovascular Imaging: Part II.
EUROPEAN HEART JOURNAL-CARDIOVASCULAR IMAGING
10.1093/ehjci/jey110. 8 p. (2018)
IF: 8.336

145. Popescu BA, Petersen SE, Maurovich-Horvat P, Haugaa KH, Donal E, Maurer G, Edvardsen T
The year 2017 in the European Heart Journal-Cardiovascular Imaging: Part I.

EUROPEAN HEART JOURNAL-CARDIOVASCULAR IMAGING 19:(10) pp. 1099-1106. (2018)
IF: 8.336

9.7 Editorials, case reports, short communications, position papers

146. Becker D, **Maurovich-Horvat P**, Merkely B
Coronary plaque rupture triggered by electrical cardioversion
INTERVENTIONAL MEDICINE AND APPLIED SCIENCE 4:(2) p. 186. (2010)
Independent citations: 1 Total: 1

147. **Maurovich-Horvat P**
Coronaria CT angiográfia és iszkémia provokációs tesztek költséghatékonysága a koszorúér-betegség diagnosztikájában.
MOTESZ MAGAZIN 19:(3-4) pp. 24-25. (2011)

148. Becker D, **Maurovich-Horvat P**, Jambrik Z, Barczi G, Merkely B
Metallic taste after coronary artery stent implantation.
INTERNATIONAL JOURNAL OF CARDIOLOGY 158:(2) pp. e30-e31. (2012)
Independent citations: 1 Total: 1

149. **Maurovich-Horvat P**, Schlett CL, Hoffmann U
Response
RADIOLOGY 268:(1) pp. 304-305. (2013)

150. Drobni ZsD, Károlyi M, Heltai K, Simon A, Merkely B, **Maurovich-Horvat P**
Wellens' Syndrome Depicted by Coronary CT Angiography
JOURNAL OF CARDIOVASCULAR EMERGENCIES 2:(4) pp. 185-187. (2016)

151. Janjua SA, Pursnani A, Mayrhofer T, Puchner SB, Liu T, Lu MT, **Maurovich-Horvat P**, Woodard PK, Chou E, Fleg JL, Truong QA, Ferencik M, Hoffmann U
Statin Use Is Associated With Fewer High-Risk Plaques on Coronary CT Angiography
JACC-CARDIOVASCULAR IMAGING 10:(2) pp. 208-210. (2017)

152. Papp S, Édes IF, Merkely B, **Maurovich Horvat P**, Károlyi M
Symptomatic Coronary-Pulmonary Fistula Revealed with Coronary CT Angiography
JOURNAL OF CARDIOVASCULAR EMERGENCIES 3:(2) pp. 89-92. (2017)

153. Karady J, **Maurovich-Horvat P**
The Closer We Get, The Further Apart We Become
JOURNAL OF CARDIOVASCULAR EMERGENCIES 3:(3) pp. 111-112. (2017)

154. Pontone G, Moharem-Elgamal S, **Maurovich-Horvat P**, Gaemperli O, Pugliese F, Westwood M, Stefanidis A, Fox KF, Popescu BA
Training in cardiac computed tomography: EACVI certification process.
EUROPEAN HEART JOURNAL-CARDIOVASCULAR IMAGING 19:(2) pp. 123-126. (2018)

9.8 Scientometric data

Total impact factors: **488.411**

The impact factor of first and last author publications: **183.28**

Total number of citations: **3100**

Independent citations: **2601**

Hirsch index: **19**

The impact factor of publications part of the current thesis: **103.184**

First and last author publications: **76.738**

The total and independent citation numbers of publications part of the current thesis: **668 / 497**

Maurovich-Horvat Pál tudományos és oktatási munkásságának összefoglalása
MTA V. Orvostudományi Osztály (2018.10.18.)

Tudományos és oktatási közlemények	Száma		Hivatkozások[1]	
	Összesen	Részletezve	Független	Összes
I. Folyóiratcikk[2]	125	---	---	---
szakcikk, nemzetközi folyóiratban, idegen nyelvű	---	75	2307	2707
szakcikk, hazai idegen nyelvű	---	1	1	1
szakcikk, magyar nyelvű	---	10	4	6
szakcikk, sokszerzős, érdemi szerzőként[3]	---	4	66	80
összefoglaló közlemény	---	22	125	172
rövid közlemény	---	13	92	123
II. Könyv	0	---	---	---
a) Szakkönyv, kézikönyv	0	---	---	---
idegen nyelvű	---	0	0	0
magyar nyelvű	---	0	0	0
aa) Felsőoktatási tankönyv	---	0	0	0
b) Szakkönyv, tankönyv szerkesztőként	0	---	---	---
idegen nyelvű	---	0	---	---
magyar nyelvű	---	0	---	---
bb) Felsőoktatási tankönyv	---	0	---	---
III. Könyvrészlet	8	---	---	---
idegen nyelvű	---	3	0	0
magyar nyelvű	---	1	0	0
cc) Felsőoktatási tankönyvfejezet	---	4	0	0
IV. Konferenciaközlemény[4]	2	---	0	0
Oktatási közlemények összesen (II.aa,bb-III.cc)		**4**	**0**	**0**
Tudományos közlemények összesen (I.-IV.)	---	**131**	**2595**	**3089**
Tudományos és oktatási közlemények összesen (I-IV.)	135	---	2595	3089

V. További tudományos művek	21	---	---	---
További tudományos művek, ide értve a nem teljes folyóiratcikkeket és a nem ismert lektoráltságú folyóiratokban megjelent teljes folyóiratcikkeket is	---	14	2	3
Szerkesztőségi levelezés, hozzászólások, válaszok	---	7	1	1

VI. Idézett absztraktok[5]	4	---	3	7

Idézettség száma[1]	---	---	2601	3100

Hirsch index[6]	19	---	---	---
g index[6]	56	---	---	---

Speciális tudománymetriai adatok	Száma	Összes hivatkozás
Első szerzős folyóiratcikkek száma[2]*	19	499
Utolsó szerzős folyóiratcikkek száma[2]*	30	79
Az utolsó tudományos fokozat (PhD) elnyerése utáni (2011 -) teljes tudományos folyóiratcikkek	95	783
Az utolsó 10 év (2008-2018) tudományos, teljes, lektorált folyóiratcikkeinek száma	115	1019
A legmagasabb idézettségű közlemény idézettsége (az összes idézettség százalékában)	1265	40,81%
További, az MTMT-ben nyilvántartott idézetek száma, amelyek nem szerepelnek a WOS és/vagy Scopus rendszerben	151	
Jelentés, guideline	4	0
Csoportos (multicentrikus) közleményben kollaborációs közreműködő[7]	0	0

*Az MTMT nem tudja szolgáltatni a megosztott első és megosztott utolsó szerzőség adatokat. Ezeket a kérelmezőnek a doktori eljárás folyamán a 3. sz. adatlapon kell feltüntetnie.

Megjegyzések:

[1] kizárólag a WOS és/vagy Scopus rendszerben nyilvántartott idézetek száma az egyéb adatbázisokból, egyéb típusú idézőkből, valamint disszertációkból az MTMT-be feltöltött, azonosítószámmal rendelkező idézők nélkül

[2] lektorált, tudományos folyóiratban

[3] a szerző írásban nyilatkozik, hogy érdemi szerzői hozzájárulásával készültek szerzőként jegyzett közleményei, és az érdemi hozzájárulást dokumentálni tudja

[4] konferenciaközlemény folyóiratban, könyvben vagy egyéb konferenciakötetben

[5] nem idézett absztrakt itt nem kerül az összesítésbe

[6] a disszertáció és egyéb típusú idéző nélküli összes idézővel számolva

[7] közreműködés esetén a csoportos szerzőségű közlemények idézettsége külön értékelendő, és nem számítható be az összesített idézetek közé

Acknowledgements

First and foremost, I would like to express my gratitude to **Professor Béla Merkely**, my mentor during the past 20 years. Professor Merkely's support and guidance was instrumental for me throughout my entire clinical and scientific career. Professor Merkely's trust and positive attitude towards me as a medical student and later PhD student was a decisive factor to return back to Hungary after my studies and research fellowships at foreign universities. It was due to his visionary thinking that the Heart and Vascular Center of the Semmelweis University is equipped with the latest generation cardiac CT scanner, which allowed me to continue my research work after I have returned back from Boston.

I would like to gratefully thank the support of **Professor Udo Hoffmann**, whom I consider not only a mentor but a good friend of mine. I have had the privilege to spent three years in Professor Hoffmann's research group at the Massachusetts General Hospital and Harvard University. Under his guidance I have learnt image interpretation and the cornerstones of clinical research and cardiovascular epidemiology. With his support, I was able to graduate at the School of Public Health of Harvard University, which was truly a life changing experience.

My third mentor was **Professor György Jermendy**, from whom I have learnt patients, persistence, discipline and that hard work always pays off.

I also thank to my former and current colleagues for their support throughout my career as medical student, PhD student and clinician at the Heart and Vascular Center. I would like to thank to **Pál Soós** and **Violetta Kékesi** and who helped and supported me early of my work as student researcher and PhD student.

I had the chance to collaborate with extraordinary researchers worldwide. I am especially grateful to **Maros Ferencik, Koen Nieman, Brian Ghoshharja** and **Szilard Voros** for their insights, support and friendship.

Of course, I could not have done all these research projects described in this thesis without an amazing team of students, fellows and co-workers. First and foremost, I would like to express my gratitude to my current enthusiastic and hardworking team of PhD students and fellows: **Márton Kolossváry, Bálint Szilveszter, Júlia Karády, Zsófia Drobni, Ádám Jermendy, Andrea Bartykowszki and Judit Simon**. I am also grateful to my former PhD students and teammates: **Mihály Károlyi, Csilla Celeng, Tamás Horváth** and **Zsolt Bagyura**. The co-workers our imaging department enabled the successful completion of research projects. I would like to thank to **Alexisz Panajotu, Ferenc Suhai, Csaba Csobay-Novák, György Balázs, Professor Kalman Hüttl and to the devoted assistants and radiographers.**

The funding and support is essential for a successful research program. I would like to express my gratitude to the NKFIH and to the Hungarian Academy of Sciences. The 'Lendület' grant provided security and independence and allowed us to establish the Cardiovascular Imaging Research Group. I would like to thank to **Ildikó Haranginé, Ilona Berzéné Pénzes** and **Miklós Idei** for their constant help and support. In addition, I would like to thank to **Rozina Cselovszky** my assistant who provided essential administrative support.

Finally, I am thankful to my family, to my parents, sister and brother and to my mother in law. My wife **Ágnes** and our two beautiful sons **Benedek** and **Domonkos** kept me going throughout the years and supported even my wildest ideas, I am eternally thankful to them.